LOCKHEED MARTIN ENERGY RESEARCH LIBRARIES

3 4456 0441361 3

ORNL-5019

4,88

Theoretical and Experimental Stress Analyses of ORNL Thin-Shell Cylinder-To-Cylinder Model 4

R. C. Gwaltney S. E. Bolt
J. W. Bryson

OAK RIDGE NATIONAL LABORATORY
CENTRAL RESEARCH LIBRARY
DOCUMENT COLLECTION
LIBRARY LOAN COPY
DO NOT TRANSFER TO ANOTHER PERSON
If you wish someone else to see this document, send in name with document and the library will arrange a loan.

OAK RIDGE NATIONAL LABORATORY
OPERATED BY UNION CARBIDE CORPORATION • FOR THE U.S. ATOMIC ENERGY COMMISSION

Printed in the United States of America. Available from
National Technical Information Service
U.S. Department of Commerce
5285 Port Royal Road, Springfield, Virginia 22161
Price: Printed Copy $7.60; Microfiche $2.25

This report was prepared as an account of work sponsored by the United States Government. Neither the United States nor the Energy Research and Development Administration, nor any of their employees, nor any of their contractors, subcontractors, or their employees, makes any warranty, express or implied, or assumes any legal liability or responsibility for the accuracy, completeness or usefulness of any information, apparatus, product or process disclosed, or represents that its use would not infringe privately owned rights.

ORNL-5019
UC-79, -79h, -79k

Contract No. W-7405-eng-26

Reactor Division

THEORETICAL AND EXPERIMENTAL STRESS ANALYSES OF ORNL THIN-SHELL CYLINDER-TO-CYLINDER MODEL 4

R. C. Gwaltney S. E. Bolt
J. W. Bryson

JUNE 1975

OAK RIDGE NATIONAL LABORATORY
Oak Ridge, Tennessee 37830
operated by
UNION CARBIDE CORPORATION
for the
U.S. ENERGY RESEARCH AND DEVELOPMENT ADMINISTRATION

LOCKHEED MARTIN ENERGY RESEARCH LIBRARIES
3 4456 0441361 3

CONTENTS

	Page
ABSTRACT	1
1. INTRODUCTION	1
2. EXPERIMENTAL ANALYSIS	4
2.1 Model Construction	5
2.2 Strain-Gage Layout	5
2.3 Test Description	8
2.4 Data Acquisition and Reduction	13
2.5 Variations of Maximum Measured Stresses Around Nozzle-Cylinder Junction	14
3. FINITE-ELEMENT ANALYSIS	23
3.1 Background	23
3.2 Finite-Element Method	24
3.3 Finite-Element Idealization of Model	30
4. COMPARISON OF THEORY AND EXPERIMENT	32
4.1 Internal Pressure	32
4.2 Out-of-Plane Moment Loading, M_{XN}, on Nozzle	34
4.3 Torsional Moment Loading, M_{YN}, on Nozzle	34
4.4 In-Plane Moment Loading, M_{ZN}, on Nozzle	35
4.5 In-Plane Force, F_{XN}, on Nozzle	35
4.6 Axial Force, F_{YN}, on Nozzle	36
4.7 Out-of-Plane Force, F_{ZN}, on Nozzle	36
4.8 Torsional Moment Loading, M_{XC}, on Cylinder	37
4.9 Out-of-Plane Moment Loading, M_{YC}, on Cylinder	37
4.10 In-Plane Moment Loading, M_{ZC}, on Cylinder	38
4.11 Axial Force, F_{XC}, on Cylinder	38
4.12 In-Plane Force, F_{YC}, on Cylinder	38
4.13 Out-of-Plane Force, F_{ZC}, on Cylinder	39
5. CONCLUSIONS	39
ACKNOWLEDGMENTS	42
REFERENCES	108
APPENDIX. TABULATION OF EXPERIMENTAL DATA	111

THEORETICAL AND EXPERIMENTAL STRESS ANALYSES OF ORNL THIN-SHELL CYLINDER-TO-CYLINDER MODEL 4

R. C. Gwaltney S. E. Bolt
J. W. Bryson

ABSTRACT

The last in a series of four thin-shell cylinder-to-cylinder models was tested, and the experimentally determined elastic stress distributions were compared with theoretical predictions obtained from a thin-shell finite-element analysis. The models in the series are idealized thin-shell structures consisting of two circular cylindrical shells that intersect at right angles. There are no transitions, reinforcements, or fillets in the junction region. This series of model tests serves two basic purposes: (1) the experimental data provide design information directly applicable to nozzles in cylindrical vessels, and (2) the idealized models provide test results for use in developing and evaluating theoretical analyses applicable to nozzles in cylindrical vessels and to thin piping tees.

The cylinder of model 4 had an outside diameter of 10 in., and the nozzle had an outside diameter of 1.29 in., giving a d_o/D_o ratio of 0.129. The OD/thickness ratios were 50 and 20.2 for the cylinder and nozzle respectively. Thirteen separate loading cases were analyzed. For each loading condition one end of the cylinder was rigidly held. In addition to an internal pressure loading, three mutually perpendicular force components and three mutually perpendicular moment components were individually applied at the free end of the cylinder and at the end of the nozzle. The experimental stress distributions for each of the 13 loadings were obtained using 157 three-gage strain rosettes located on the inner and outer surfaces.

Each of the 13 loading cases was also analyzed theoretically using a finite-element shell analysis developed at the University of California, Berkeley. The analysis used flat-plate elements and considered five degrees of freedom per node in the final assembled equations. The comparisons between theory and experiment show reasonably good agreement for this model.

1. INTRODUCTION

Intersecting cylindrical shells are common configurations in structural components for nuclear reactor systems. Piping tees and nozzles in cylindrical vessels are specific examples. However, despite their common

occurrence, proven elastic stress analysis methods for such configurations have not been generally available, and only recently have potential analyses been developed. This is true even for the case of an idealized configuration consisting of two thin-shell normally intersecting cylinders with no transitions, reinforcements, or fillets in the junction region.

To meet the need for experimental data obtained from carefully machined models, Oak Ridge National Laboratory (ORNL) has tested a series of four thin-shell cylinder-to-cylinder models. In addition to providing test results for use in developing and evaluating potential analytical techniques, the models will provide design information directly applicable to nozzles in cylindrical vessels and to a class of thin piping tees as well. The test results will be particularly applicable to liquid-metal-cooled fast breeder reactor components in which relatively low internal pressures and high thermal transients dictate the use of thin-walled structures.

The four models have been tested, and the experimentally determined stress distributions have been compared with the predictions of a thin-shell finite-element analysis. This report describes the tests and analyses of model 4 and presents comparisons of theory and experiment. The tests and analyses for models 1 and 3 are described in Refs. 1 to 3.

Model 4 is shown in Fig. 1 along with a listing of the significant dimensions of all four models in the series. As indicated by the figure, these models are truly idealized shell structures. There are no transitions, fillets, or reinforcing in the junction region. The outside diameter D_o of the cylinder of the fourth model was 10 in., and the outside diameter d_o of the nozzle was 1.29 in., giving a d_o/D_o ratio of 0.129. The cylinder thickness T was 0.2 in., and the nozzle thickness t was 0.064 in. Thus the OD/thickness ratios of the cylinder and nozzle were 50 and 20.2 respectively. The fourth model was obtained from the third by boring out the nozzle to provide a thinner wall thickness.

Model 4 is shown schematically in Fig. 2, together with the applied forces and moments to which it was subjected and the major dimensions. One end of the model was rigidly fixed, or "built-in," as shown, while external loads were applied to the free end of the cylinder and to the end of the nozzle. Three mutually perpendicular force components and three

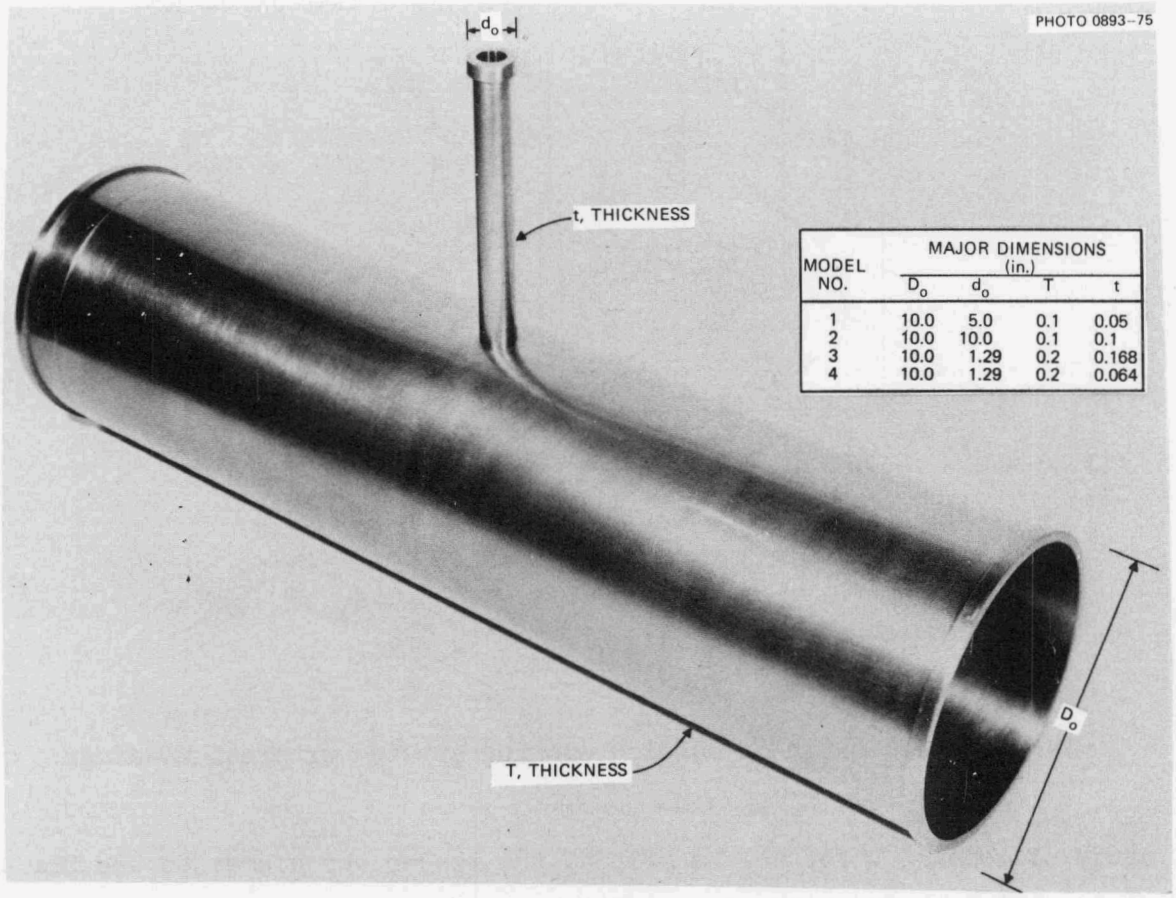

MODEL NO.	MAJOR DIMENSIONS (in.)			
	D_o	d_o	T	t
1	10.0	5.0	0.1	0.05
2	10.0	10.0	0.1	0.1
3	10.0	1.29	0.2	0.168
4	10.0	1.29	0.2	0.064

Fig. 1. Thin-shell cylinder-to-cylinder model 4 and table of dimensions for all four models in test series.

mutually perpendicular moment components were applied individually at each location. Thus, including internal pressure, there was a total of 13 loading cases. These loading cases were examined both experimentally and analytically, and the results were compared for each loading case.

Chapter 2 of this report describes the testing aspects of the experimental analysis and also the strain-gage data-acquisition and reduction techniques used. Representative experimental results, in the form of maximum measured stress distributions around the nozzle-cylinder junction, are presented for each loading. The finite-element analysis, discussed in Chap. 3, includes a brief description of the formulation used and the specific element layout for the model. Complete comparisons of theory and experiment for all 13 loading cases are presented and discussed in Chap. 4, and Chap. 5 contains a concise summary of the conclusions drawn from the

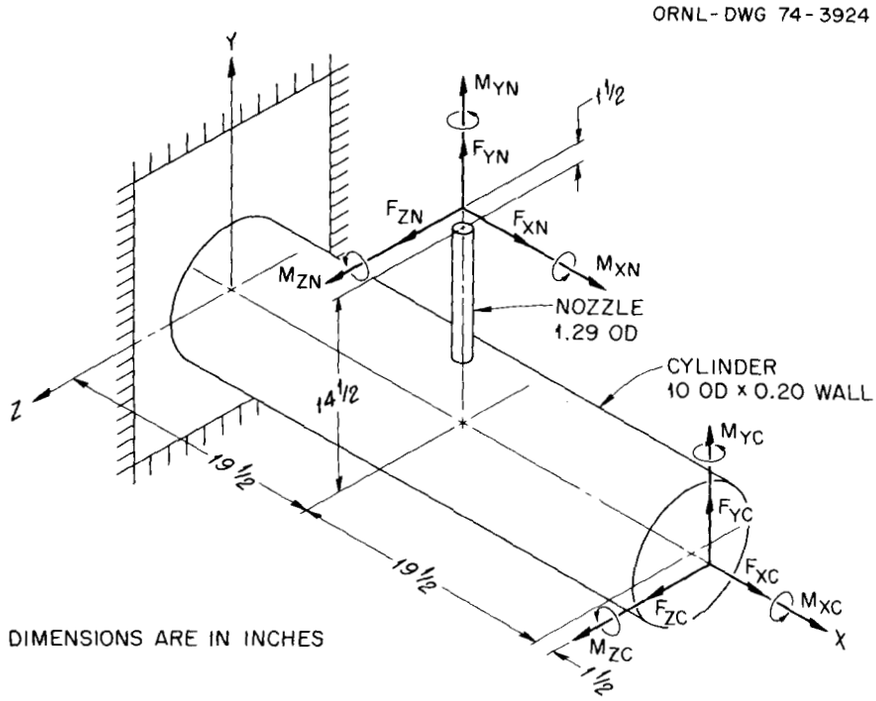

Fig. 2. Schematic of model 4 showing applied external loadings.

study of model 4. For the benefit of the reader who wishes to use the experimental data for comparisons with his own analyses, an appendix is included that gives a complete set of experimental data for each of the 13 loading cases.

2. EXPERIMENTAL ANALYSIS

In experimental investigations of thin-shell cylinder-to-cylinder pressure vessel configurations, both strain-gage metal models and photoelastic models have been used. Strain-gage studies for internal pressure and for external nozzle loadings have been carried out by Hardenbergh, Zamrik, and Edmondson;[4] by Hardenbergh and Zamrik;[5] and by Riley.[6] Contoured and reinforced outlets were used in the first two studies; in the third, the model was fabricated from hot rolled sheet steel by welding. In photoelastic studies carried out by Taylor and Lind[7] and by Leven,[8] reinforced openings were examined. Thus, of the previous studies, only that of Riley[6] used a thin-shell idealized cylinder-to-cylinder metal model, and it was of welded construction rather than being carefully machined.

2.1 Model Construction

One of the primary objectives of the experimental analysis described in this report was to obtain experimental data on a carefully machined cylinder-to-cylinder model so that the effects of geometrical imperfections would be minimized.

The basic configuration was obtained by forging. A carbon steel billet was formed into the shape of a tee and then annealed. The forging was then bored out to the rough inside dimensions, and the outside was rough machined. The structure was annealed a second time. To maintain the correct dimensions during annealing, a tight-fitting graphite mandrel was machined and inserted in both the nozzle and cylinder. The inside surfaces were then machined to the final dimensions by boring. The final machining on the outside surface was done on a tracing-type milling machine using a carefully constructed mahogany wood pattern. The above description describes the manufacture of model 3; model 4 was obtained by boring out the nozzle of model 3.

2.2 Strain-Gage Layout

The model was instrumented with electric resistance strain gages on both the outside and inside surfaces. Actually only the inside surface of the nozzle had to be strain gaged, since model 4 was made from model 3 by boring out the nozzle. A sufficient number of gages was used on this model to provide a good description of the stress distributions for comparisons with predictions and for identifying the high-stress regions.

The strain-gage layouts for the outer and inner surfaces are shown in Figs. 3 and 4 respectively. A total of 157 three-gage strain-gage rosettes was used, a total of 471 individual strain gages. There were 84 rosettes on the outer surface and 73 on the inner surface. These were, in most cases, located "back to back" at the locations shown in Figs. 3 and 4.

The gages were arranged in two opposite quadrants along lines running from the junction of the nozzle and cylinder. In one quadrant there are three lines of gages at 45° intervals, while in the other quadrant there are two lines of gages at 90° intervals with only six rosettes in a line on each surface.

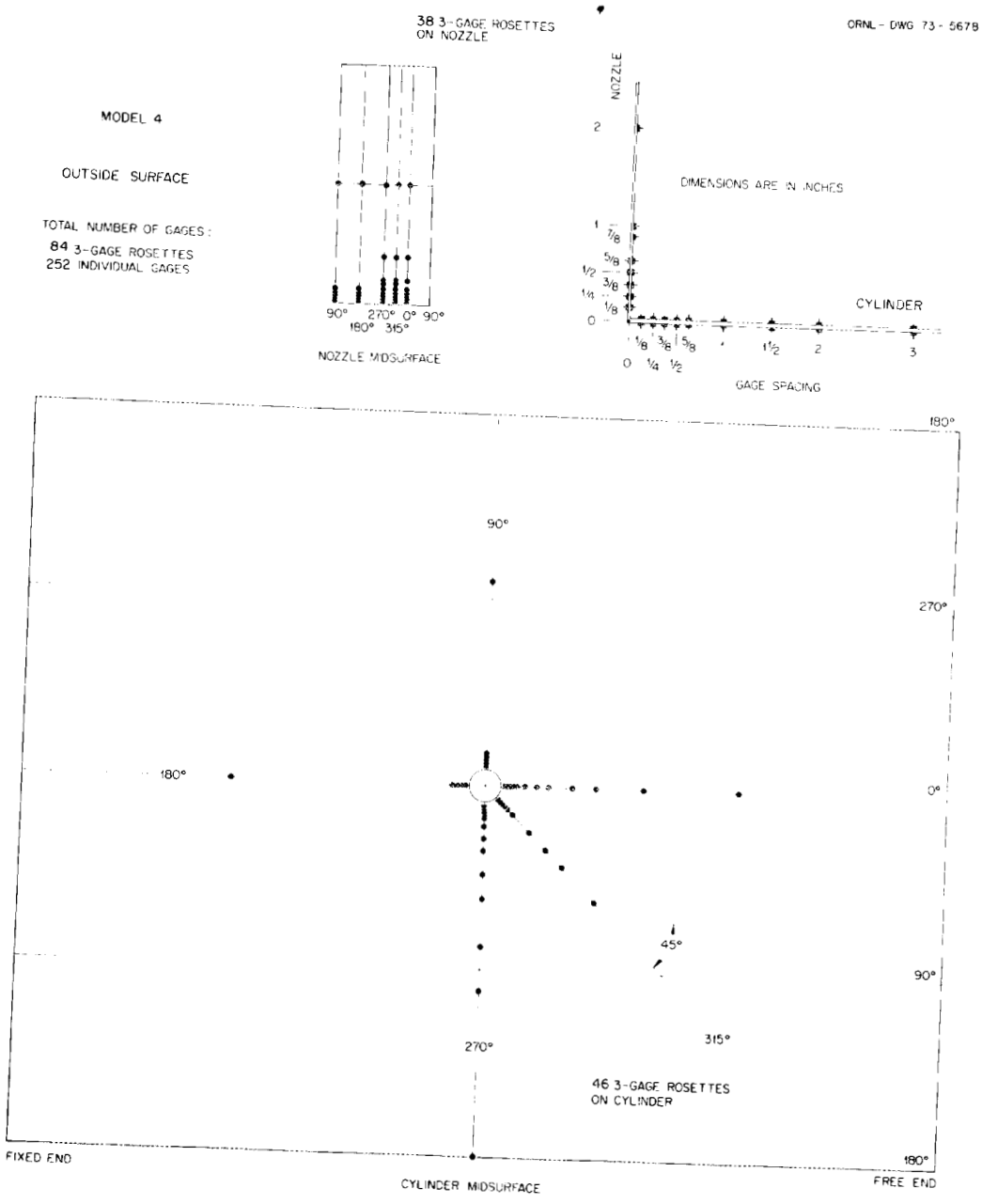

Fig. 3. Strain-gage layout on the outer surface.

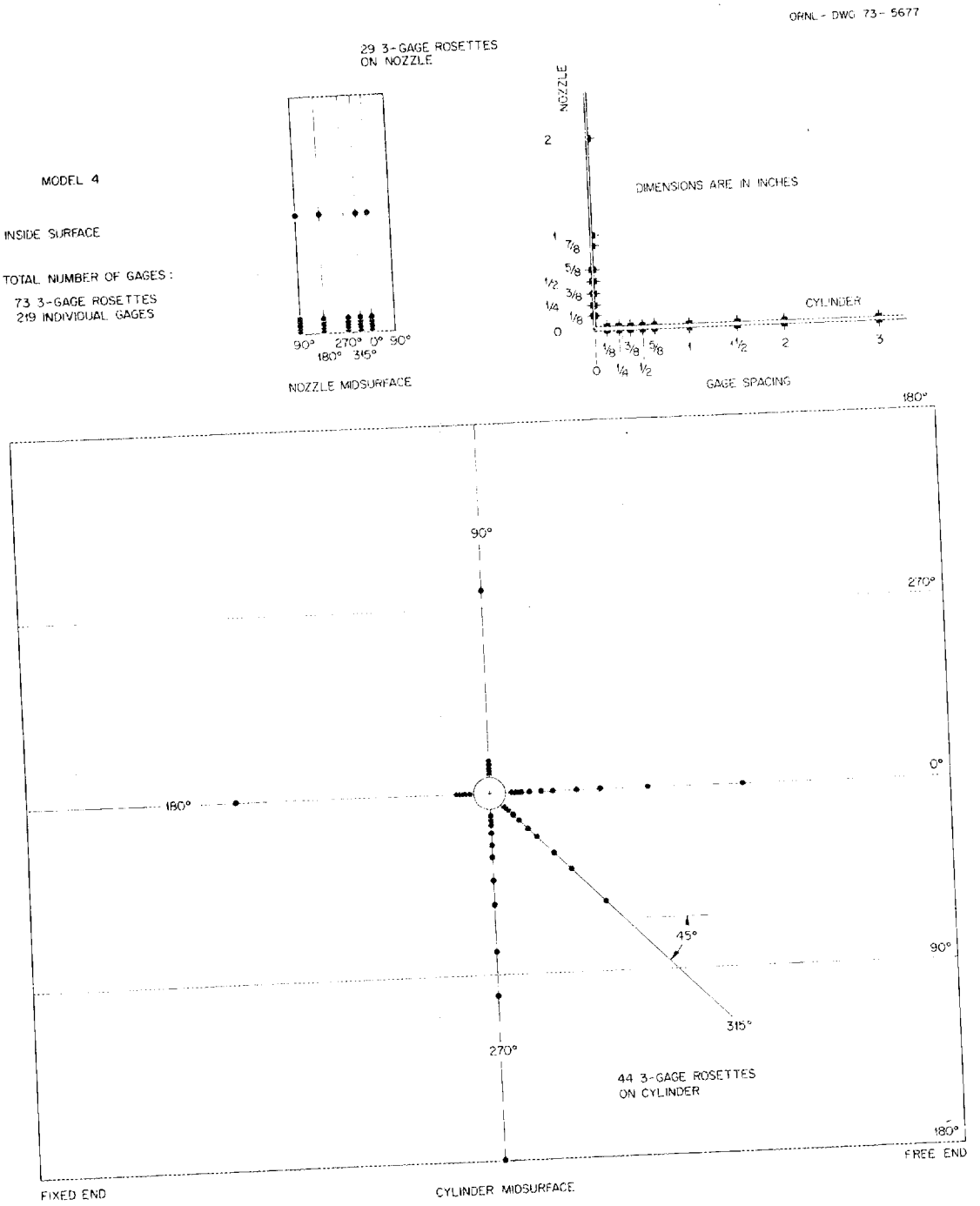

Fig. 4. Strain-gage layout on the inner surface.

There were two principal reasons for gaging two opposite quadrants. First, for the majority of the 13 loadings the behavior in the two quadrants was expected to be different. Second, for loadings such as internal pressure, where the behavior should be identical, experimental data from two supposedly identical quadrants allow a check of the data and provide some indication of the effects of geometrical imperfections in the model.

The three-gage rosettes used were Micro-Measurements type EA-06-030YB-120, option SE, which is a very compact three-gage foil rosette. The three individual gages are arranged in a "Y" pattern and have an individual gage length of 0.030 in. As can be seen in the inset in the upper right-hand corner of Fig. 3, five complete rosettes were located along each gage line within the first 5/8 in. from the junction. These first five rosettes were supplied mounted on a common backing by the gage manufacturer. These assemblies have the same designation as the single rosettes except that the option becomes B27. One of the five-rosette assemblies is shown in Fig. 5.

The rosettes were applied with an epoxy adhesive, BR-610, which is available from W. T. Bean, Inc. Curing times and temperatures ranged from 10 hr at 250°F to 24 hr at 200°F. Uninsulated 4-mil-diam wire was used to connect the gages to terminal tabs to which larger lead wires were connected. The strain-gage data were recorded by a Datum Computer-Controlled Data-Acquisition System (Sect. 2.4).

The model is shown in Fig. 6 with the strain gages applied but not completely wired. The three lines of gages in the fourth quadrant can be clearly seen. They are in the longitudinal plane at 0°, 45° from the longitudinal plane, and in the transverse plane at 90° from the longitudinal plane. A closeup of the rosettes in the junction region is shown in Fig. 7.

2.3 Test Description

Figure 8 shows the instrumented model in a loading frame being subjected to an in-plane moment loading on the nozzle. The right end of the cylinder was rigidly clamped to the heavy flat plate using a split ring

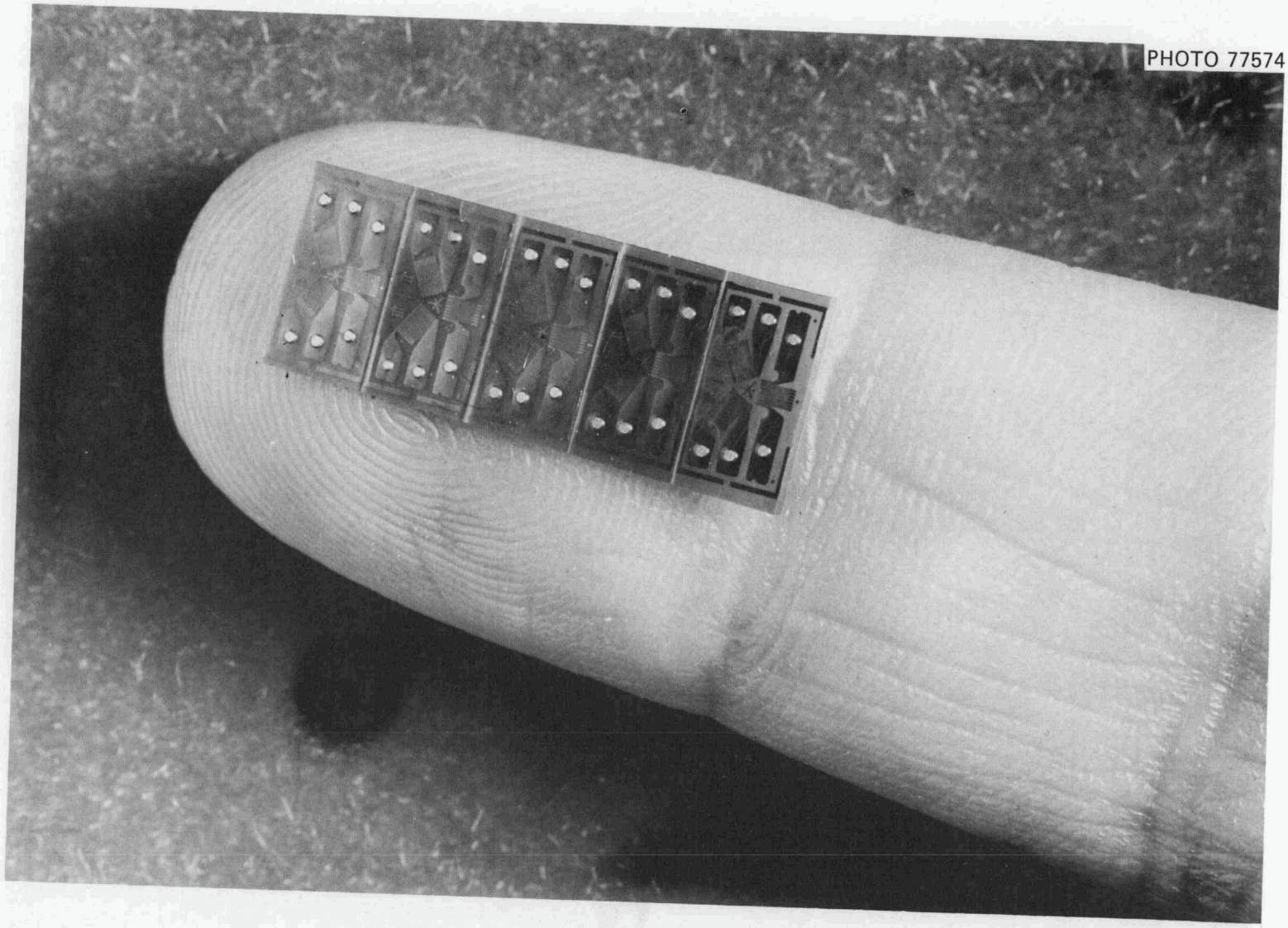

Fig. 5. Closeup of assembly of five strain-gage rosettes on a common foil backing.

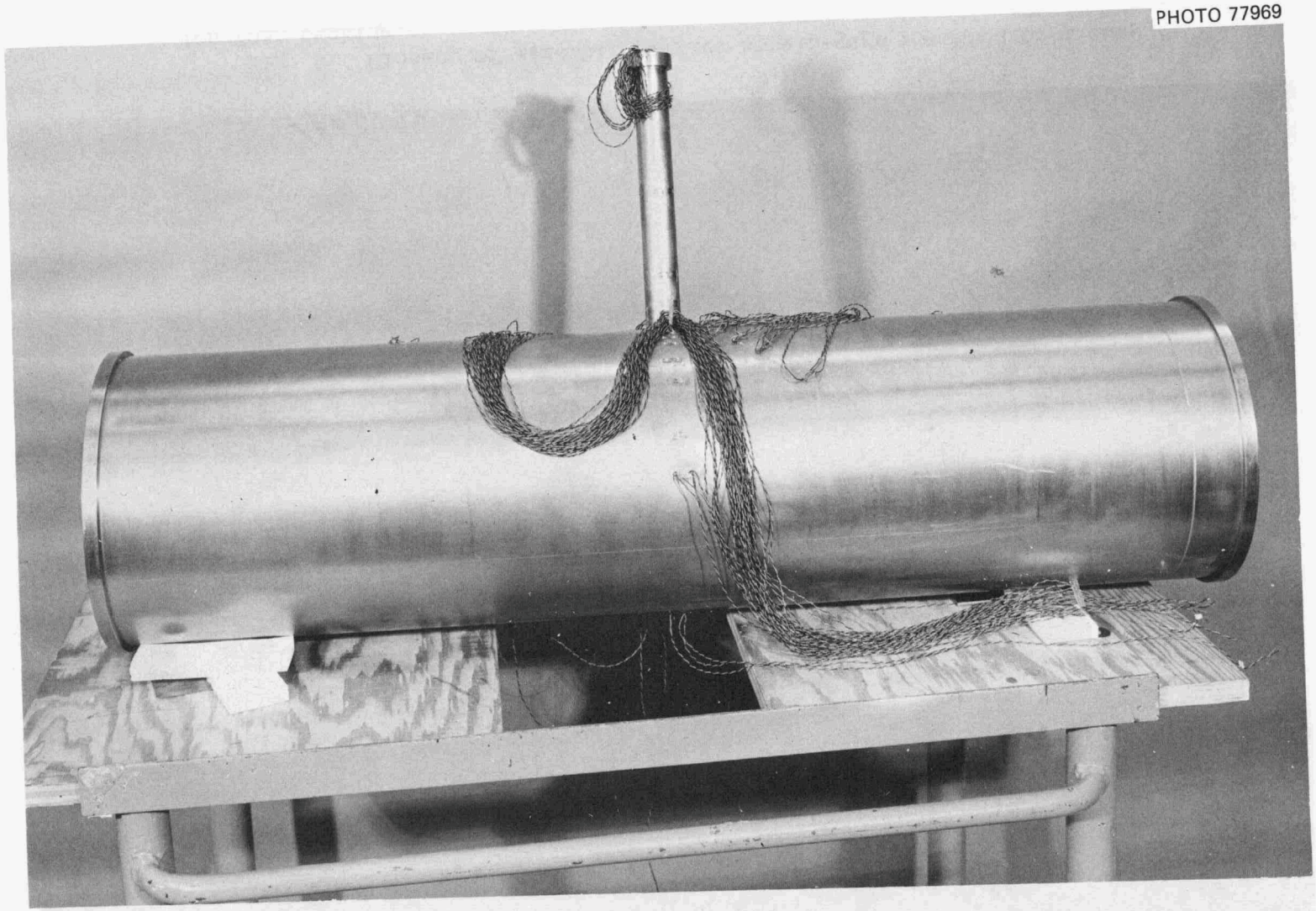

Fig. 6. Model during instrumentation.

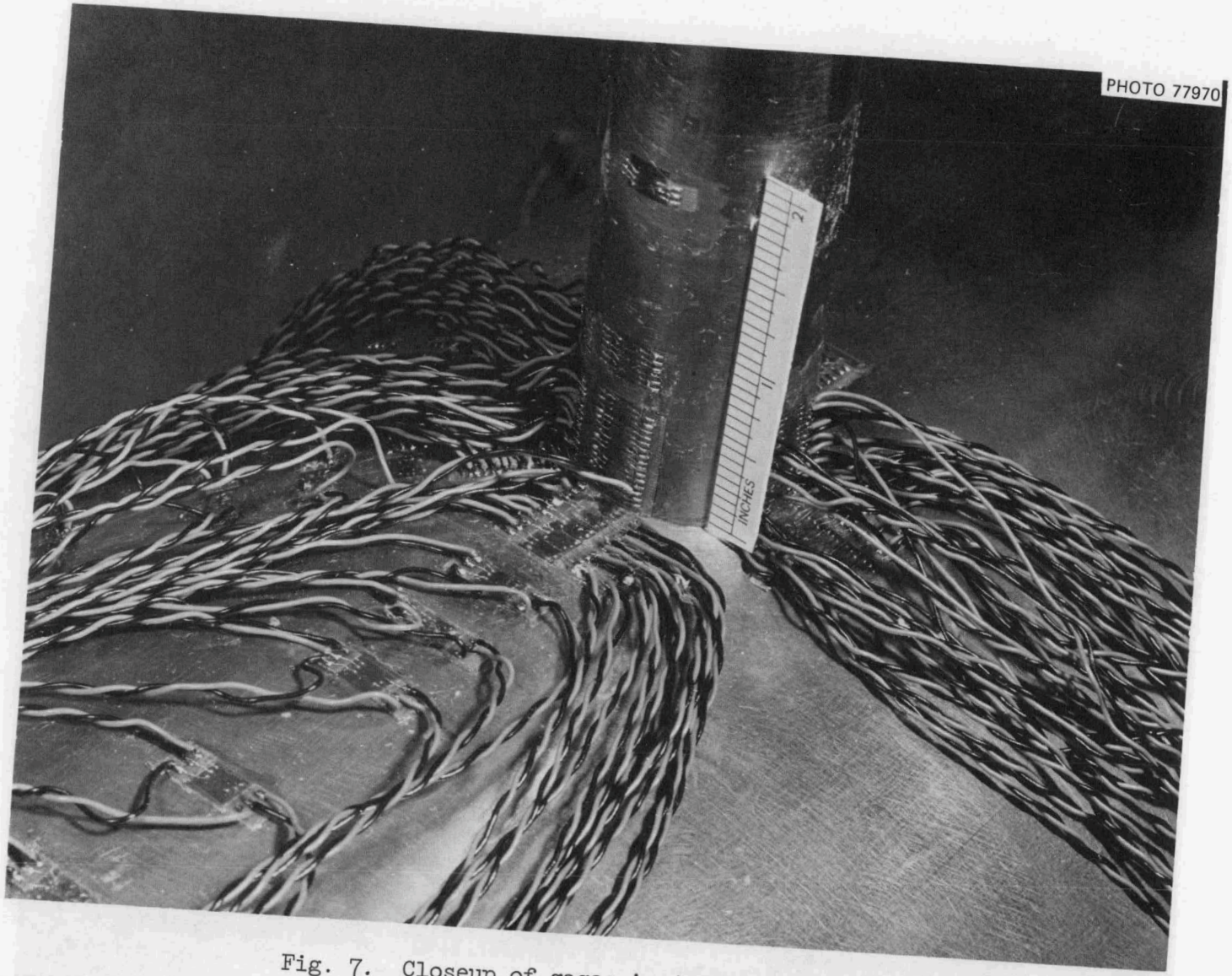

Fig. 7. Closeup of gages in junction region.

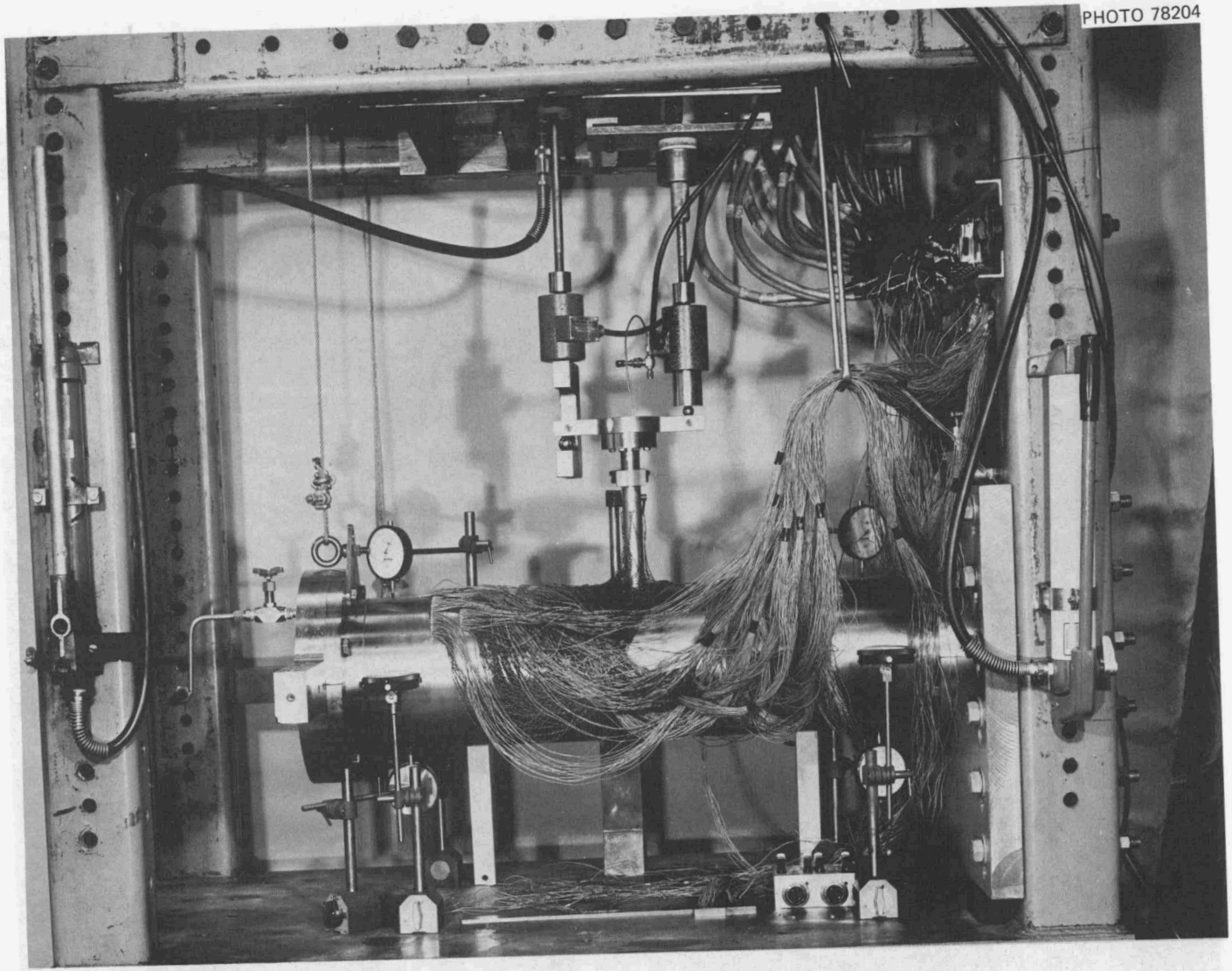

Fig. 8. Instrumented model in test frame being subjected to an in-plane moment loading on the nozzle.

arrangement acting over the flange on the end of the cylinder. The loading fixtures on the other end of the cylinder and on the end of the nozzle were attached in a similar manner. These heavy fixtures in effect constrained the end circles of the shell to remain plane circles. The end fixtures were counterbalanced by weights attached to the cables (Fig. 8).

The external loads were applied by hydraulic rams acting through load cells, and the loads were controlled by the load cell indications. The pressure loading was applied using a hydraulic fluid. To avoid undue straining of the model, weights were used to counterbalance the weight of the pressurizing fluid in the model.

For all 13 loading cases, data were taken in eight steps. In most cases the data were taken at 0, 25, 50, 75, 100, 100, 50, 0% of full load. The procedure was then repeated, so that two complete sets of data were taken for each gage every loading.

2.4 Data Acquisition and Reduction

The strain-gage data were recorded by a Datum Computer-Controlled Data-Acquisition System. The system consists of a data-acquisition unit composed of a data-acquisition control module controlled by a PDP-8/I computer with the following capabilities: (1) magnetic tape input/output system, (2) in-core calculation ability, and (3) teletypewriter input and output.

The system records the strain data in millivolt readings on magnetic tape. The PDP-8/I computer converts the millivolt reading on the tape into engineering units (strains in this case) and stores them on a second tape which is compatible with the ORNL IBM 360-91 computer. This second tape is sent to the ORNL 360-91 computer, and stresses are calculated for each rosette by stripping the strains off the second tape.

The experimental results presented later in this report and tabulated in the appendix are generally based on the strain-gage readings at maximum load and on the first of the two sets of data taken from each gage and loading. If the first set of data was questionable for some reason, the second set was used. The strain-gage readings at fractional values of the maximum load were used to check linearity and drift of the gages. In cases

where nonlinearity or drift was excessive or where an individual gage or circuit was otherwise obviously malfunctioning, the rosette of which the gage was a part was not used in the final results for the specific loading case under consideration. In some instances, a gage that behaved erratically during one loading behaved normally during others. Thus, in the final plots showing the experimental stresses, results from a given rosette may be included for some loadings but not for others.

Stresses were calculated from the experimental strains by using a modulus of elasticity value of 30×10^6 psi and a Poisson ratio of 0.3.

2.5 Variations of Maximum Measured Stresses Around Nozzle-Cylinder Junction

In all cases, the maximum measured stresses occurred at the nozzle-to-cylinder junction. Consequently, in this section representative experimental results, in the form of maximum measured stress distributions around the nozzle-cylinder junction, are presented and discussed for each loading. Plots of all the experimental points along each gage line are presented in Chap. 4 for each loading and compared with theoretical predictions.

To examine the maximum stresses, stress ratios were considered. These ratios were determined by dividing the maximum absolute principal stress value at a point by a nominal membrane stress value. The membrane hoop stress in the cylinder and in the nozzle was used as the nominal stress level for the pressure loading. For the moment loadings on the nozzle or cylinder, the maximum membrane bending stresses (computed by Mc/I) or the membrane shear stress (computed by Tc/J and equal to the maximum normal stress) in the nozzle or cylinder were used as the nominal stresses. For the axial forces on the nozzle and cylinder, the axial membrane stress (calculated by P/A) was used. For the in-plane and out-of-plane forces on the nozzle, the nominal stress was somewhat arbitrarily chosen as the maximum bending stress in the nozzle (calculated by Mc/I) at the level of the top of the cylinder. For the in-plane and out-of-plane forces on the cylinder, the nominal stress was arbitrarily chosen as the maximum bending stress in the cylinder at its midlength (at the center line of the nozzle).

The applied loads used in the experimental analyses are given in Table 1, together with the nominal membrane stress levels calculated by the above procedures.

Table 1. Applied loads and nominal stress levels

Loading case	Load level	Nominal membrane stress (psi)
Internal pressure	300 psi	7,350
Out-of-plane moment, M_{XN}	400 in.-lb	5,300
Torsional moment, M_{YN}	1600 in.-lb	10,590
In-plane moment, M_{ZN}	400 in.-lb	5,300
In-plane force, F_{XN}	80 lb	10,060
Axial force, F_{YN}	400 lb	1,620
Out-of-plane force, F_{ZN}	60 lb	7,540
Torsional moment, M_{XC}	30,000 in.-lb	990
Out-of-plane moment, M_{YC}	80,000 in.-lb	5,300
In-plane moment, M_{ZC}	80,000 in.-lb	5,300
Axial force, F_{XC}	10,000 lb	1,620
In-plane force, F_{YC}	3000 lb	3,880
Out-of-plane force, F_{ZC}	3000 lb	3,880

The variations in the experimentally determined maximum stresses around the nozzle-cylinder junction are shown in Figs. 9 through 21 for each of the 13 individual loading cases. In each case, the stresses shown were determined from the strain-gage rosettes immediately adjacent to the junction, and of the four possible maximum stress distributions — cylinder inside and outside and nozzle inside and outside — those shown produced the largest stresses in each case.

The points labeled "extrapolated maximum" in the figures are estimated maximum stress ratios at the junction obtained by extrapolating the experimentally determined principal stress distributions along each gage line

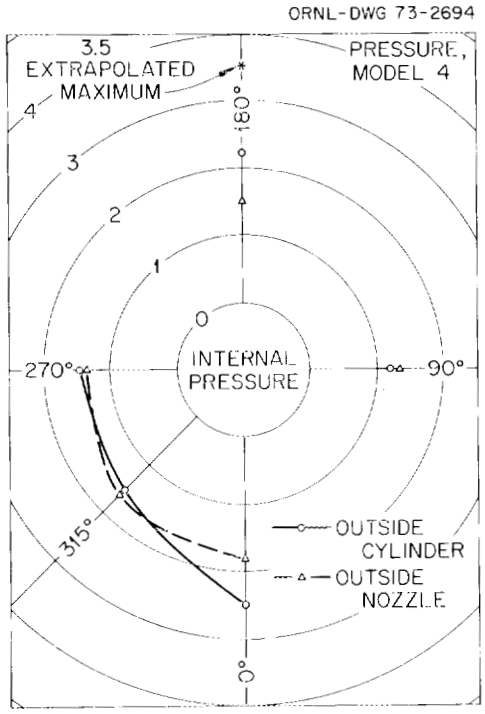

Fig. 9. Variation of maximum principal stress ratios around the nozzle-cylinder junction for internal pressure.

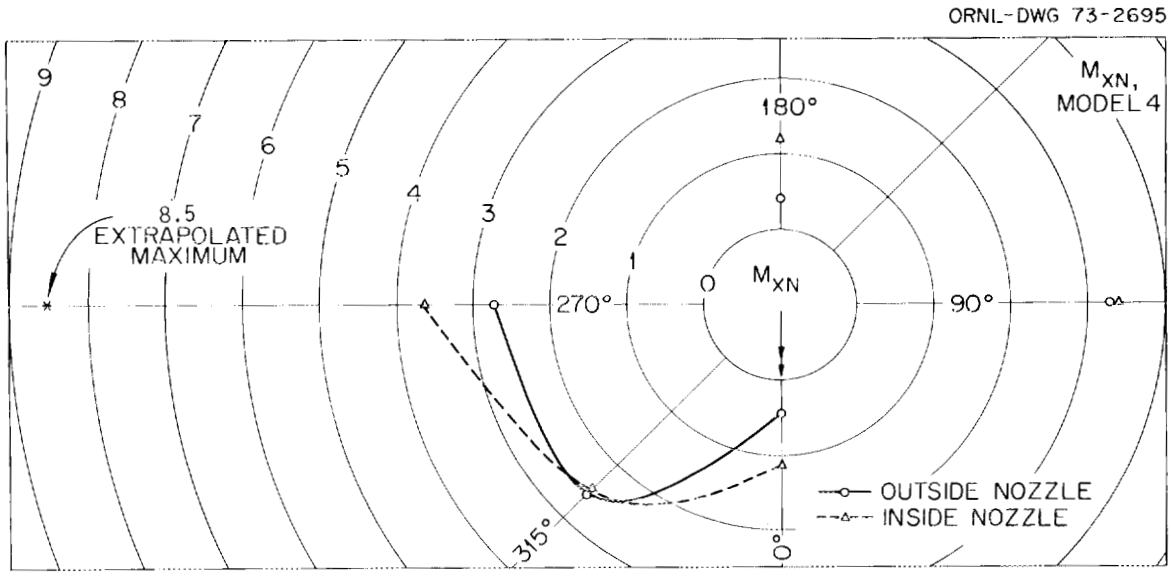

Fig. 10. Variation of maximum principal stress ratios around the nozzle-cylinder junction for out-of-plane moment, M_{XN}, on nozzle.

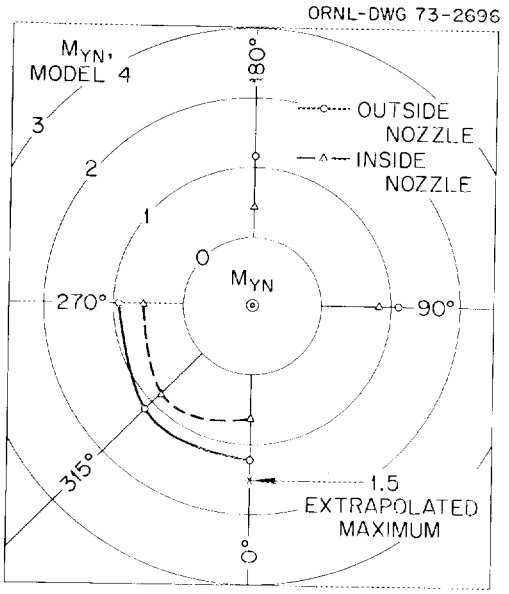

Fig. 11. Variation of maximum principal stress ratios around the nozzle-cylinder junction for torsional moment, M_{YN}, on nozzle.

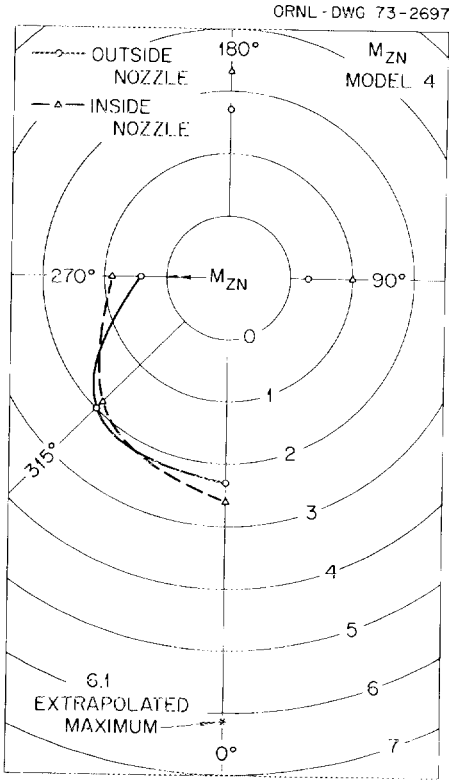

Fig. 12. Variation of maximum principal stress ratios around the nozzle-cylinder junction for in-plane moment, M_{ZN}, on nozzle.

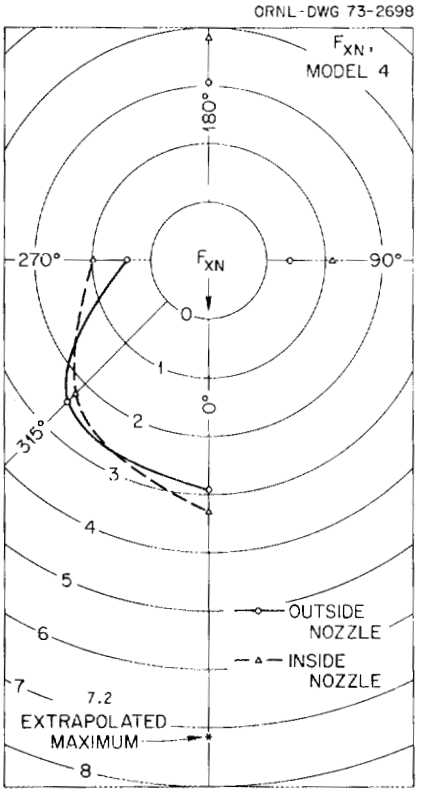

Fig. 13. Variation of maximum principal stress ratios around the nozzle-cylinder junction for in-plane force, F_{XN}, on nozzle.

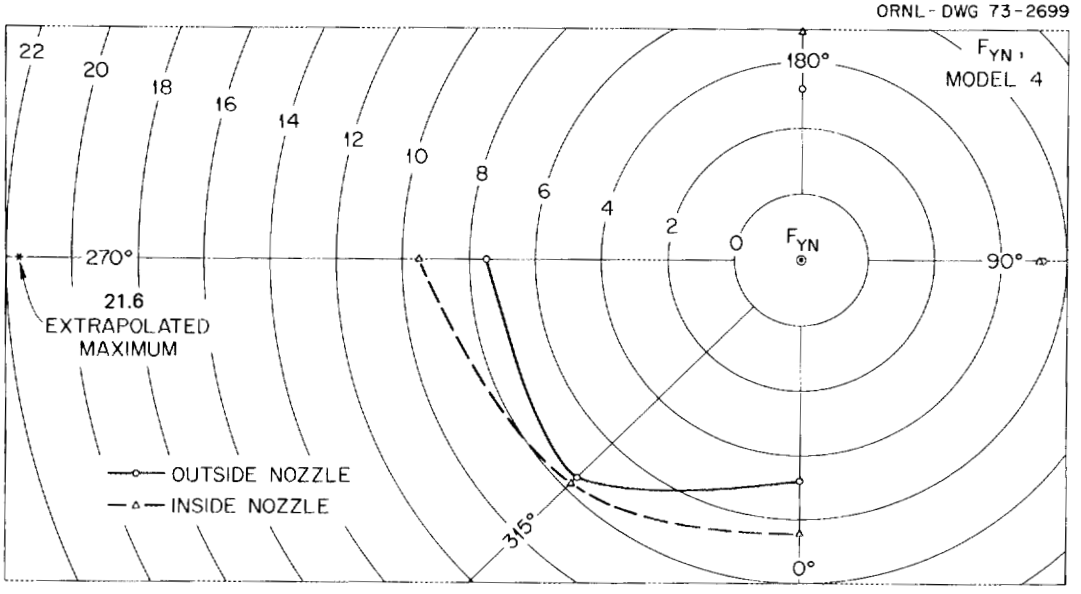

Fig. 14. Variation of maximum principal stress ratios around the nozzle-cylinder junction for axial force, F_{YN}, on nozzle.

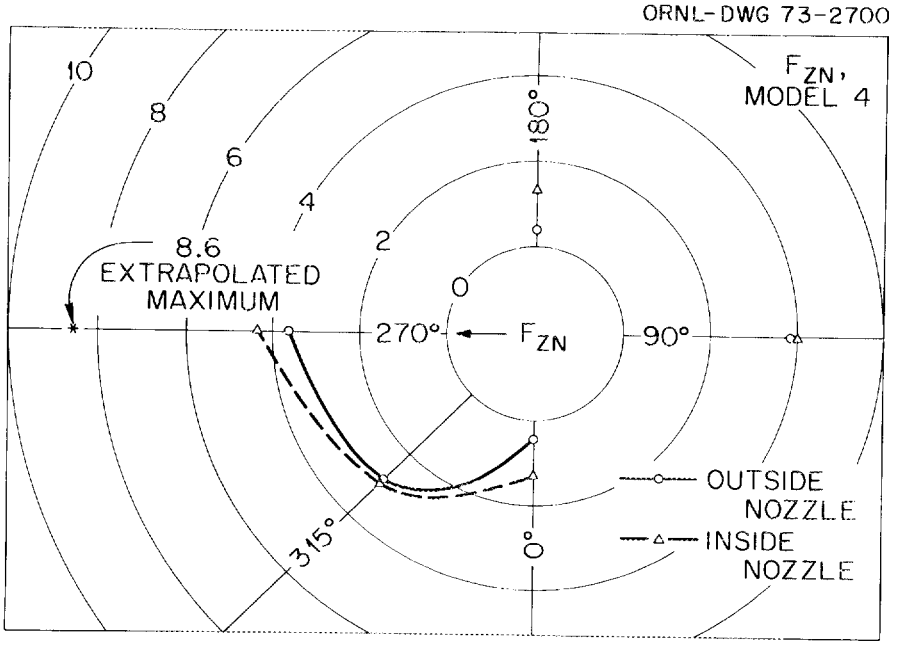

Fig. 15. Variation of maximum principal stress ratios around the nozzle-cylinder junction for out-of-plane force, F_{ZN}, on nozzle.

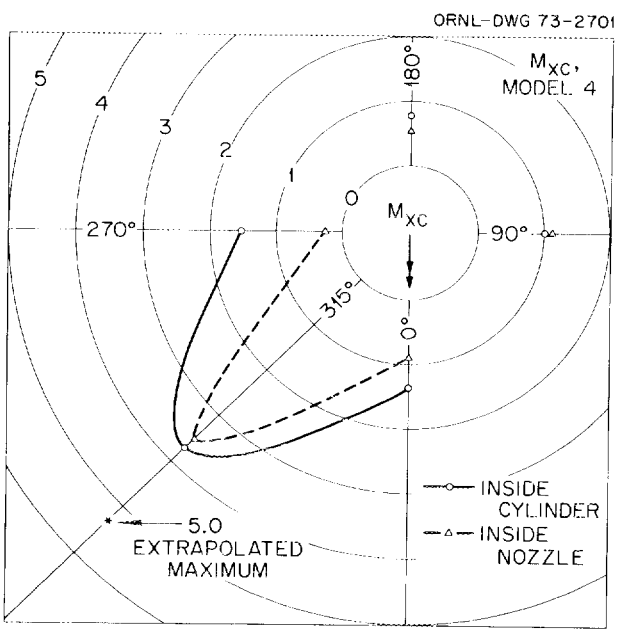

Fig. 16. Variation of maximum principal stress ratios around the nozzle-cylinder junction for torsional moment, M_{XC}, on cylinder.

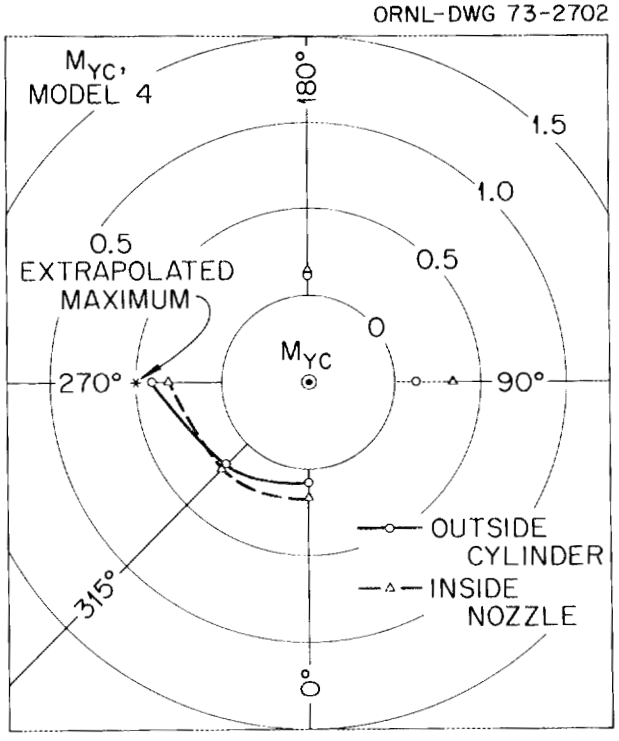

Fig. 17. Variation of maximum principal stress ratios around the nozzle-cylinder junction for out-of-plane moment, M_{YC}, on cylinder.

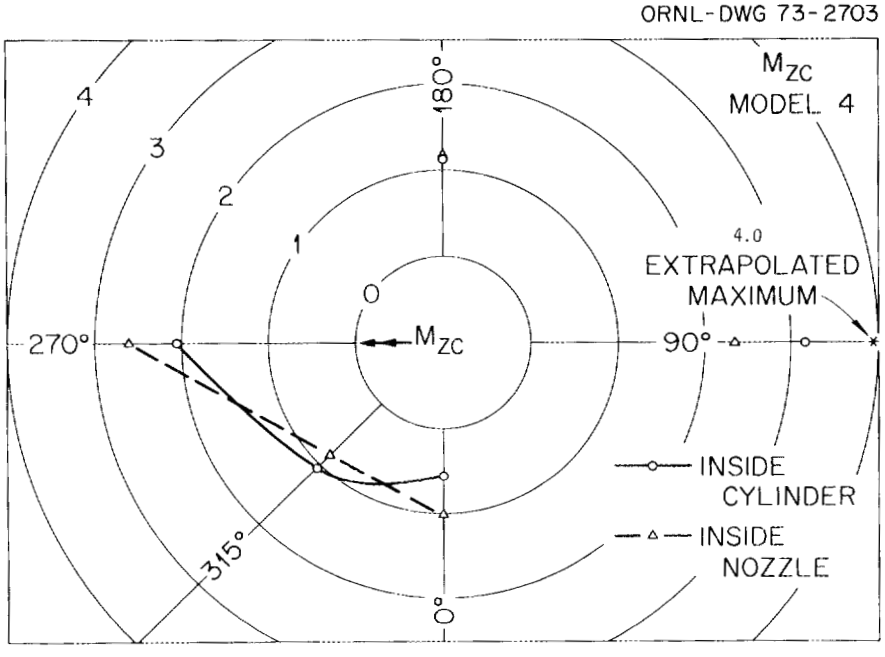

Fig. 18. Variation of maximum principal stress ratios around the nozzle-cylinder junction for in-plane moment, M_{ZC}, on cylinder.

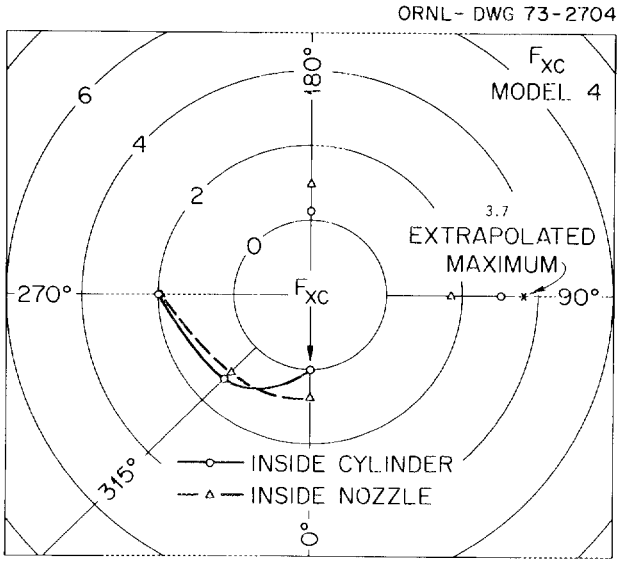

Fig. 19. Variation of maximum principal stress ratios around the nozzle-cylinder junction for axial force, F_{XC}, on cylinder.

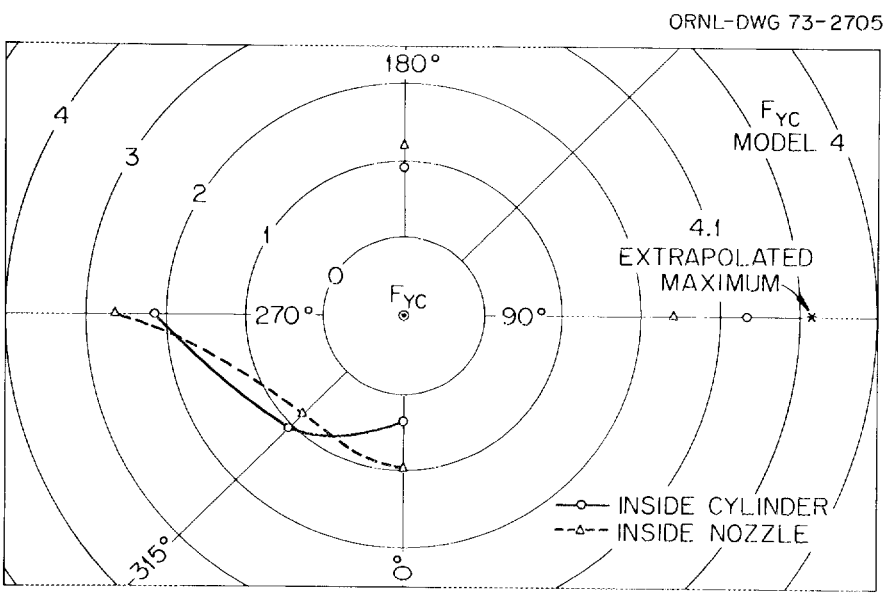

Fig. 20. Variation of maximum principal stress ratios around the nozzle-cylinder junction for in-plane force, F_{YC}, on cylinder.

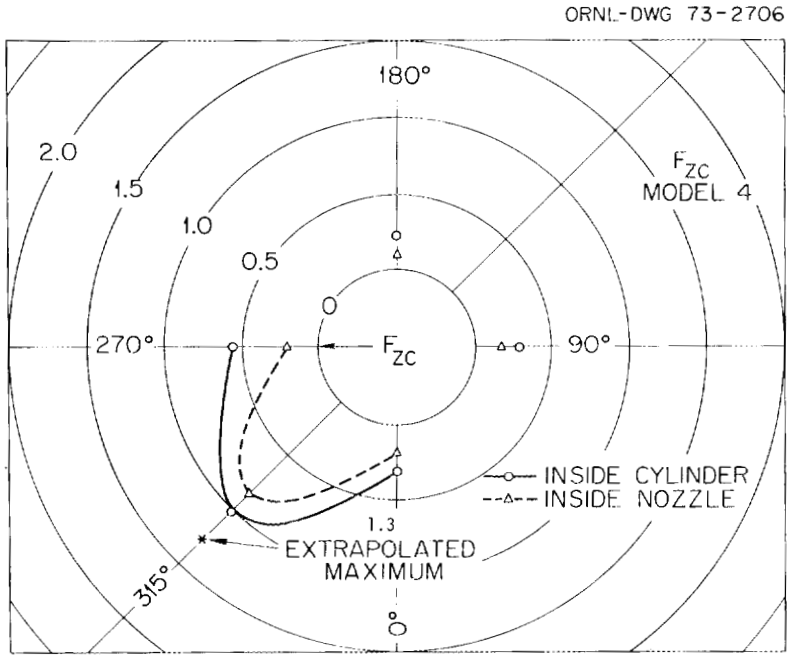

Fig. 21. Variation of maximum principal stress ratios around the nozzle-cylinder junction for out-of-plane force, F_{ZC}, on cylinder.

to the peak stresses at the junction. It should be emphasized that the maximum stress estimates are based on a consideration of the stresses along gage lines only; this does not preclude the existence of slightly higher stresses at locations between gage lines. The maximum stress ratios and the locations of the maximum stresses based on both the experimental and the finite-element analyses are tabulated and compared in Chap. 5.

Figures 9 through 21 indicate that, in general, the maximum measured stresses varied in a reasonably smooth and consistent manner around the nozzle-cylinder junction. It is particularly significant to note that the maximum stress occurred in the longitudinal plane of symmetry only for the internal pressure case, in-plane force and moment, and torsional moment on the nozzle. For all other loadings, the maximum occurred in the transverse plane of symmetry or at an intermediate position between the two planes of symmetry.

3. FINITE-ELEMENT ANALYSIS

3.1 Background

Thin-shell cylinder-to-cylinder intersection problems have, in recent years, been a favorite with the stress analyst. Their popularity stems not only from the common occurrence of such configurations in practical design, but also from the challenge that they present as complex shell analysis problems. In addition to their use in piping and pressure vessel configurations, thin-shell cylinder-to-cylinder intersections occur in the petroleum industry, which uses tubular structural members extensively in off-shore oil-drilling towers. Much of the cylinder-to-cylinder intersection research, both experimental and theoretical, that has been done was motivated by the off-shore oil-drilling tower application.[9]

Both analytical and numerical analyses have been developed and applied to thin-shell cylinder-to-cylinder intersection problems. In 1961, Reidelbach[10] developed the first analytical solution for two perpendicularly intersecting cylindrical shells subjected to internal pressure. Eringen[11-14] and his co-workers corrected some errors and approximations in Reidelbach's solutions and formulated a solution in which the intersection curve was approximated by a circle. These solutions consisted of products of Krylov functions and Hankel functions of the first kind. A collocation method was used whereby the boundary conditions were satisfied in a least-squares sense at selected boundary points.

In 1969, Hansberry and Jones[15] used the method developed by Reidelbach and Eringen et al. to develop a solution for an in-plane bending moment applied to the nozzle of a nozzle-to-cylinder configuration. In 1970, Maye and Eringen[16] developed a solution using Fourier series involving Bessel functions in place of the Krylov functions. In 1973, Hansberry and Jones[17] expanded their solution to include the case of an axial force applied to the nozzle. As in the case of earlier solutions, however, the nozzle diameter was limited relative to the cylinder diameter.

In 1967, Bijlaard, Dohrmann, and Wang[18] formulated the problem to include the case where the nozzle and cylinder are of equal diameter. They indicated a solution in the form given by Flügge for closed cylindrical

shells. In 1969, Pan[19] developed a numerical solution to the differential equations of Flügge and Donnell that is applicable to the equal-diameter case. He compared his predictions with the experimental results obtained by Riley[6] for a nozzle-diameter/cylinder-diameter ratio of 1/2. By careful choice of some of the factors used in the solution, he obtained predictions that agreed reasonably well with experiment.

In 1968, Herrmann and Campbell[20] presented a finite-element shell analysis formulation using flat-plate elements, and as a sample problem they used the 1/2 diameter ratio model tested by Riley.[6] The limited comparisons shown were for internal pressure and indicated reasonably good agreement between theory and experiment. In 1969, Prince and Rashid[21] also presented a flat-plate finite-element shell analysis and used the cylinder-to-cylinder intersection as a sample problem. Their shell analysis program was developed under subcontract to ORNL as a part of the ORNL Prestressed Concrete Reactor Vessel Program.

3.2 Finite-Element Method

The finite-element program used for the analysis of this model was chosen as being reasonably representative of currently available and widely used finite-element shell formulations. The program was developed at the University of California, Berkeley, under the direction of Professor R. W. Clough. The original program was written for general shell analysis by Johnson[22,23] and was later modified and adopted by Greste[9,24] for treating the "K" joints of cylindrical shells found in off-shore oil-drilling towers.

The basic elements used in the program, shown in Fig. 22, are non-planar quadrilaterals that are built up of an assemblage of four component triangles as shown. Within each component triangle, the in-plane displacements u and v are assumed to vary quadratically over the plane of the triangle, except that they are constrained to vary linearly along the one exterior edge. The resulting membrane element, referred to as a constrained linear strain triangle (CLST), has two degrees of freedom (u and v) at each of the five nodes.

ORNL-DWG 70-422R

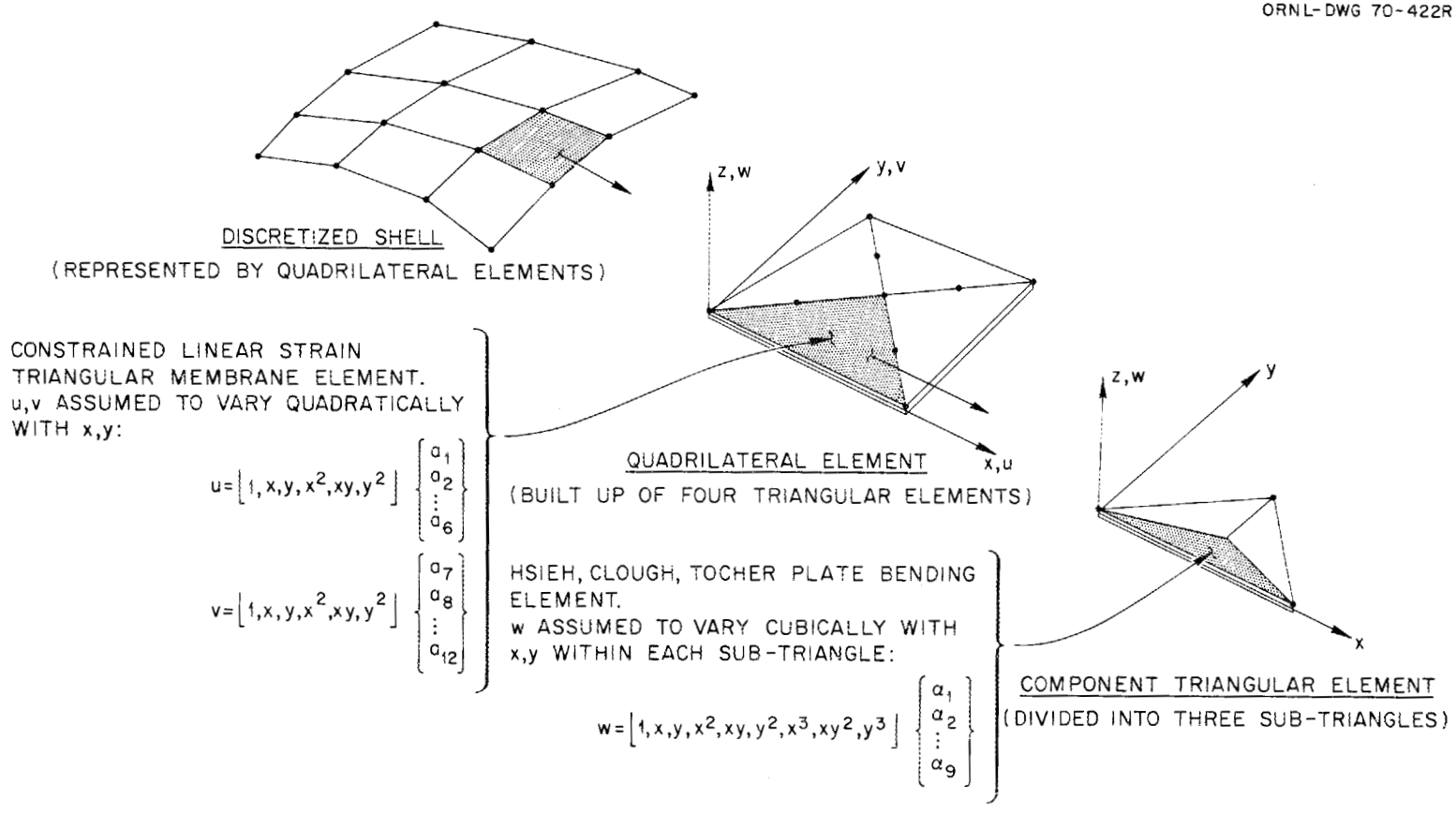

Fig. 22. Quadrilateral element and component triangles.

The plate bending portion of the component triangle elements has three degrees of freedom at each of the three corner nodes – two rotations about axes in the plane of the element and the transverse, or normal, displacement w. The displacement expansion for this element is due to Hsieh, Clough, and Tocher,[25] and the element is referred to as the HCT triangle. Full compatibility of displacements and slopes between triangular element boundaries is achieved by dividing the element into three subtriangles and assuming an independent cubic variation for w within each subtriangle. One of the ten terms of the general cubic is neglected in each subtriangle, so that in the final assembled component triangle the normal slope varies linearly along each exterior edge. It is this feature that ensures slope compatibility in the resulting element system for plate bending problems. The 27 constants in the three cubic expressions for w within the triangular element are reduced to 9 (and related to the 9 nodal degrees of freedom) by internal compatibility considerations. With w varying as a cubic polynomial within each subtriangle, the three components of curvature, and hence the bending and twisting moments, vary linearly.

The total stiffness (membrane plus bending) of the triangular elements that form the components of the quadrilateral is obtained by superposition of the plate bending element and the membrane element. The membrane plus bending stresses vary piecewise linearly over the surface of the resulting triangular element.

The quadrilateral element stiffness is obtained from that of the four component triangles. In general, due to the curvature of the shell that is being discretized, an arbitrary quadrilateral will be nonplanar. This introduces a complication in the transformation of the triangular element stiffness, because on the element level only two bending rotations per node are defined. When transformed from the element coordinates to some other coordinate system, a third bending rotation quantity is introduced, and in the transformed system three rotational degrees of freedom should be considered at each node. This consideration regarding the third rotational degree of freedom also arises in the subsequent assembly of the quadrilateral elements into the total structural stiffness, since adjacent elements are generally not coplanar. In his formulation, Johnson[22] chose to retain only two rotations per node in the total element assemblage. He argued

that since the element plane in a sufficiently fine mesh lies close to the shell tangent plane at each node, the rotations could be transformed from the element coordinates (in the plane of the element) to coordinates in the shell tangent plane and the small transformed component of bending rotation about the normal to the shell could be neglected. This is perhaps a reasonable assumption everywhere except at the junction of intersecting shells.

The stiffness formulation for the quadrilateral element, as well as for the CLST membrane element and the HCT plate bending element, is summarized by Greste.[9] The quadrilateral element has five degrees of freedom at each node: u, v, w, and the two rotations. In the final assembled structure, the five degrees of freedom per node are u, v, w, and the two rotations about the shell tangent coordinates at each node.

The task of the finite-element method is to determine the unknown coefficients of the assumed element displacement functions for u, v, and w. This is done by connecting the quadrilateral elements at discrete points, the corner nodes, and requiring compatibility of displacements and rotations and equilibrium of forces and moments at these nodes. Unfortunately, when the elements are assembled into a curved-shell structure, compatibility and equilibrium are not completely achieved along the element interfaces. Thus there are inherent small errors involved. However, studies by Johnson[22] have shown that these errors are not too significant provided a sufficiently fine element mesh is used.

There is an error in intersecting shell problems which is not diminished by mesh refinement. This error arises from the aforementioned neglect of the rotation about the shell normal. At the junction nodes in the cylinder-to-cylinder intersection problem, there are three nonzero rotational components, but only two of these can be retained as nodal degrees of freedom. Greste[9] chose to define the tangent plane, and hence the two rotational degrees of freedom, at the junction nodes as the cylinder tangent plane. The manner in which he treated the junction nodes thus constrained the normal rotation about the cylindrical shell normal to be zero at the junction. This rotational constraint unrealistically constrains the bending deformation of the adjacent nozzle elements.

This constraint did not greatly affect the analysis of model 1, but its effect was significant in the analysis of model 4. A problem arose in the analysis of model 4, with its small slender nozzle, that was not encountered in the analysis of model 1 or in similar models with relatively large nozzles. In the cases of the in-plane and out-of-plane forces and moments applied to the end of the nozzle, it was found that the membrane-type axial bending stresses, which should have been constant along the nozzle, were dissipated with distance from the end of the nozzle. This dissipation was traced to the neglect of the rotational degree of freedom about normals to the nozzle surface and occurred in model 4 because of the relatively large deformations of the small slender nozzle. This problem was overcome by redefining the neglected sixth degree of freedom for these loading cases.

The difficulty is illustrated by the example problem shown in Fig. 23, in which the nozzle of model 3 was analyzed by fixing a row of nodes near the junction.[2] The mesh shown in Fig. 24 for the nozzle was used, and the nozzle was subjected to a bending moment at the free end. The distribution of normalized bending stress in the outer wall of the nozzle is shown for three different analyses. Also shown is the predicted stress based on simple beam theory with $I = \pi a^3 h$ and $c = a$, where a is the radius of the midsurface and h is the nozzle thickness.

The middle curve in Fig. 23 was obtained with the component of bending rotation about normals to the nozzle surface neglected. These neglected rotations are small and are in effect set to zero in the assembled set of equations. Overall equilibrium implicitly requires that small moments be imposed at each node to maintain zero bending rotation. These small constraints combine to counteract a portion of the applied moment and result in the decrease in membrane bending stress depicted in Fig. 23.

To illustrate that these nodal constraints depend on the deflection of the nozzle, the problem was reexamined using a reduced elastic modulus for a section near the fixed end. The nozzle deflection produced by the applied moment was thus increased, and the bending moment was dissipated more rapidly as shown by the left-hand curve in Fig. 23.

The problem was overcome by redefining the neglected degree of freedom in the nozzle.[2] Rather than setting the rotations about normals equal

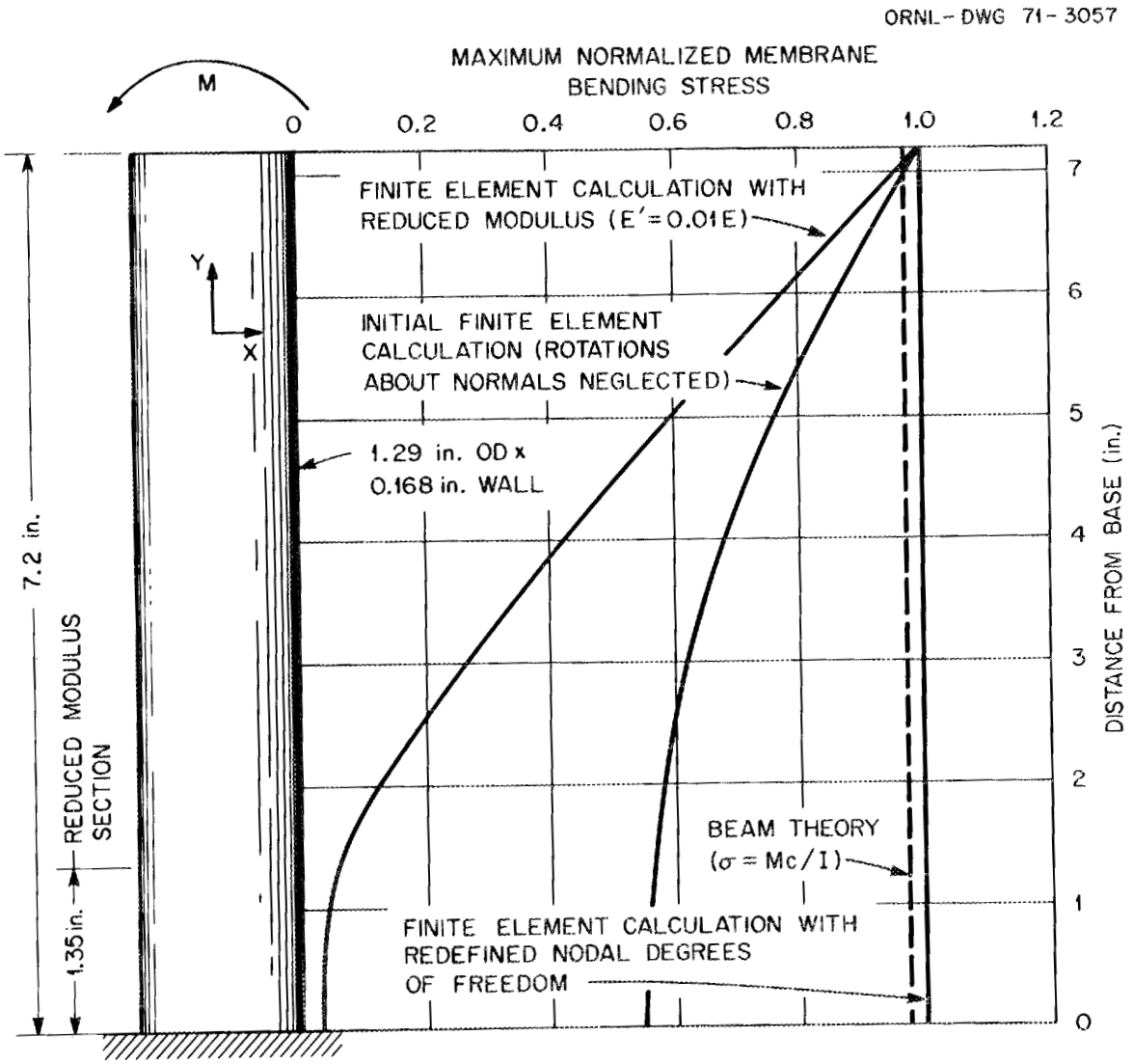

Fig. 23. Example problem demonstrating effects of neglecting the component of bending rotation about normals to the surface of a small slender nozzle.

to zero, the rotations about lines parallel to the nozzle axis were set equal to zero in the final assembled set of equations. The assumption of zero bending rotation about lines parallel to the nozzle axis is a reasonable one and is equivalent to the assumption, often made in analyzing the local bending in cylindrical shells, that changes in curvature in the hoop direction are negligible compared with those in the axial direction. Bailey and Hicks,[26] for example, made the latter assumption in examining

the effects of a bending moment applied to the nozzle of a nozzle-to-spherical-shell attachment. With this modification, the membrane bending moment remained constant, as shown by the right-hand curve in Fig. 23. This modification was used in the analysis of the in-plane and out-of-plane forces and moments on the nozzle.

In conclusion, two significant points should be made. First, even though a computer program may be checked for some geometries and conditions, there can be other cases for which it does not function properly. Thus, structural analysis programs must be thoroughly validated for the range of parameters over which they are expected to apply. Second, the problems introduced by considering only five degrees of freedom per node could be eliminated by retaining six degrees of freedom in the final assembled equations. However, for large systems, the five degrees of freedom per node has a distinct advantage from the standpoint of economy of computer time.

3.3 Finite-Element Idealization of Model

The finite-element representation chosen for model 4 is depicted in Fig. 24, which shows developed views of one-half of the nozzle, cylinder, and end plates. It was necessary to consider only one-half of the structure because of symmetry considerations. This mesh layout was developed manually and was arranged so that lines of nodes corresponded to the lines of strain gages in the experimental model. There were 993 nodes, resulting in approximately 4500 linear algebraic simultaneous equations to be solved for the unknown displacement parameters. There were 25 nodes along the (half) junction line between the nozzle and cylinder. All 13 loading cases considered experimentally were analyzed using this mesh, and the theoretical predictions were compared with the experimentally determined stresses (Chap. 4).

Seven of the 13 loadings – pressure, axial forces on cylinder and nozzle, and in-plane moments and forces on cylinder and nozzle – produce behavior that is theoretically symmetric about the longitudinal plane of symmetry of the model. For these symmetric loadings, it is correct to consider just one-half of the model in the finite-element representation. The

ORNL-DWG 71-3058

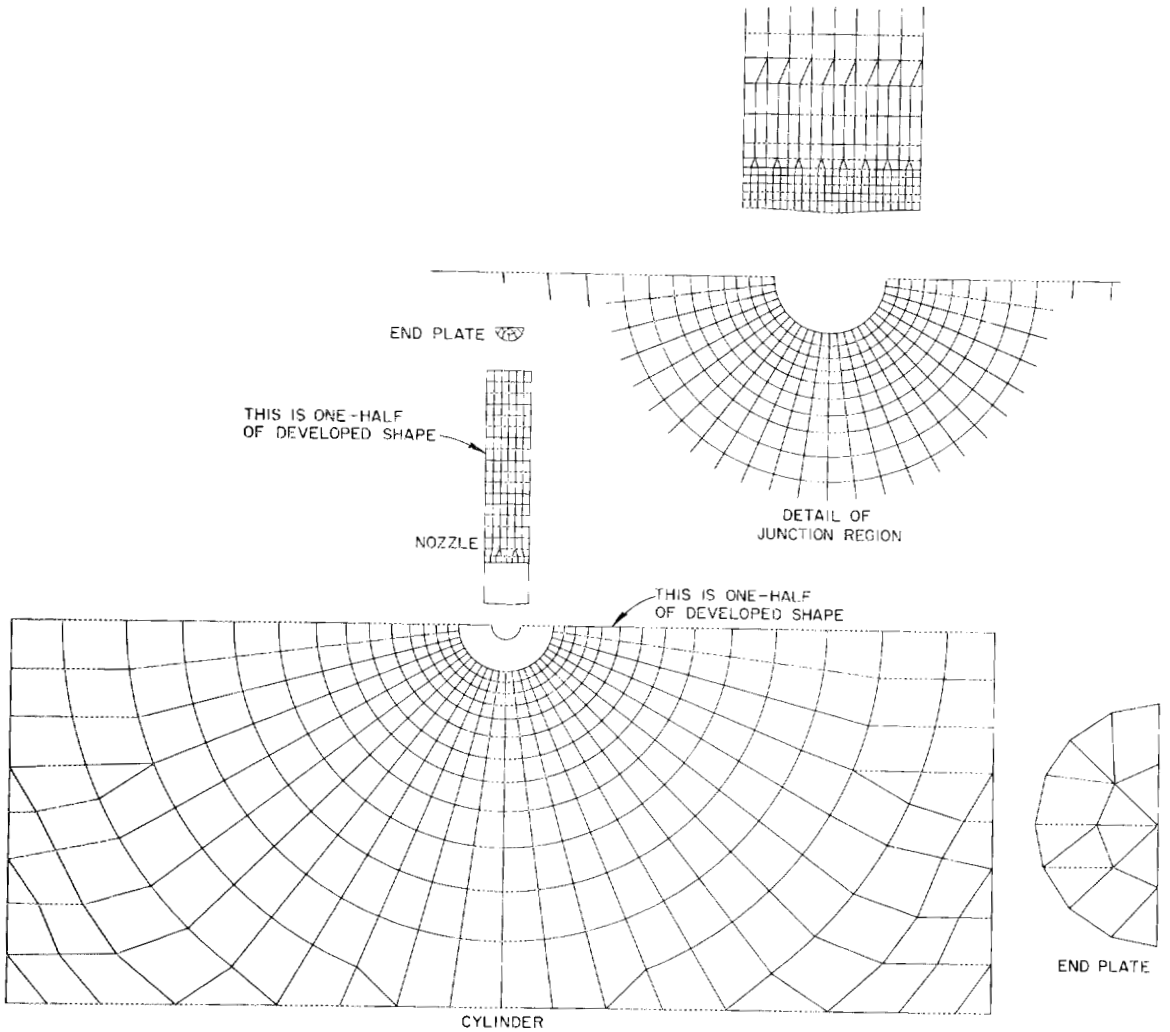

Fig. 24. Finite-element idealization of model 4.

boundary conditions on nodal displacements and rotations are those commonly associated with symmetry conditions.

For the remaining six loadings – out-of-plane moments and forces on cylinder and nozzle and torsional moments on cylinder and nozzle – asymmetric conditions exist, and to consider just one-half of the model in the finite-element representation requires assumptions or approximations in establishing nodal displacement and rotational boundary conditions. Basically, the boundary conditions used were based on the assumption that the projection on the X-Y plane (see Fig. 2) of the boundary remained fixed in

the X-Y plane. In other words, the displacements in the X and Y directions and the rotation about the Z axis were assumed to be zero for the nodes along the boundary in the X-Y plane. Although these conditions are obviously not strictly correct, they nonetheless seem to be reasonable assumptions that are useful for reducing the size of the problem to be solved.

4. COMPARISON OF THEORY AND EXPERIMENT

The theoretical predictions, based on the finite-element layout shown in Fig. 24, are compared in this chapter with experimentally determined distributions for all 13 loading cases. For each loading, the theoretical and experimental stress distributions along the five gage lines on the cylinder and nozzle (see Figs. 3 and 4) are presented. The stresses shown are always those parallel (longitudinal) to the gage lines and those perpendicular (transverse) to the gage lines.

4.1 Internal Pressure

The measured and predicted stress distributions determined for an internal pressure of 300 psi applied to the model are shown in Figs. 25 through 29. Figure 25 shows the measured and predicted stress distributions on the outside and inside surfaces of the cylinder and on the outside and inside surfaces of the nozzle along the 0° gage line, which is the longitudinal plane of symmetry (see Figs. 3 and 4). The stresses are shown as a function of distance from the junction of nozzle and cylinder midsurfaces. The heavy lines are the predicted stresses, while the fine lines through the experimental points show the measured distributions. The solid lines in each case represent the transverse stresses, which are perpendicular to the gage lines. The dashed lines represent the longitudinal stresses, which are parallel to the gage lines. Thus, we can compare the solid lines with each other and the dashed lines with each other.

The agreement between theory and experiment is good in Fig. 25, except that the stresses at the junction, which is where the maximum occurs, are at times underestimated somewhat by the finite-element predictions.

However, the general shape and distributions of the stresses are well predicted by the theory.

Figures 26 through 29 are arranged to facilitate ready comparison of comparable results. Figure 26 shows the stresses along the 180° gage line, which is opposite the 0° gage line in the longitudinal plane of symmetry. Because of symmetry, the stresses along the 180° gage line are almost the same as those along the 0° gage line shown in Fig. 25. Comparison of the two figures shows excellent agreement between results for opposite sides of the nozzle in the longitudinal plane of symmetry.

The results for a gage line 45° from the longitudinal plane of symmetry (see Figs. 3 and 4) are shown in Fig. 27. Figure 27 shows the results for the 315° gage line, which is in the fourth quadrant. Agreement between theory and experiment is not as good here as for the previous two figures. Note in particular the large disagreement in the shape of the measured and predicted stresses on the inner surface of the cylinder.

The internal pressure results for the 270 and 90° gage lines, in the transverse plane of symmetry, are shown in Figs. 28 and 29 respectively. Here the agreement between theory and experiment is not as good on the transverse plane as along the longitudinal plane; however, since the stresses are low, the disagreement is perhaps not too significant. The overall agreement between theory and experiment is generally good.

The method used to determine the estimated maximum experimental stresses and stress ratios was described in Sect. 2.5. The maximum theoretically predicted stresses were obtained in the same manner; that is, they were taken as the largest absolute values of the principal stresses. To match the experimental maximums, the search for the theoretical maximums was limited to gage lines only.

The maximum experimentally determined stress occurred on the inside surface of the cylinder at 180°, and the maximum stress ratio was 3.5. The theoretical maximum stress was on the outer surface of the nozzle at 0°; the maximum stress ratio was 3.1.

4.2 Out-of-Plane Moment Loading, M_{XN}, on Nozzle

The measured and predicted stress distributions for an out-of-plane moment loading of 400 in.-lb applied to the nozzle of the model are shown in Figs. 30 through 34. Results for the five gage lines are arranged in the same manner as for the internal pressure case, although the fourth and second quadrant results are not, in this case, theoretically the same.

The results in Figs. 30 and 31 are for 0 and 180°, respectively, in the longitudinal plane of symmetry. As expected, the stresses are small, since these locations are somewhat analogous to the neutral axis of a beam in bending. The results for the 315° gage line, which is 45° from the longitudinal plane of symmetry, are shown in Fig. 32. At this location the stresses are larger, and the agreement between theory and experiment is very good.

The results for the 270 and 90° gage lines, which are located in the transverse plane of symmetry, are shown in Figs. 33 and 34 respectively. Here, the stresses are a maximum on the transverse plane, and the agreement between theory and experiment is very good. The maximum experimental stress is on the inner surface of the nozzle and is closely predicted by the analysis.

The maximum experimentally determined principal stress ratio was 8.5, with the maximum stress occurring on the inner surface of the nozzle at the junction on the 270° gage line. The theoretical maximum was on the outer surface of the nozzle at the junction on the 270° gage line, and the maximum stress ratio was 7.6.

4.3 Torsional Moment Loading, M_{YN}, on Nozzle

The measured and predicted stress distributions for a torsional moment loading of 1600 in.-lb applied to the nozzle of the model are shown in Figs. 35 through 39. As in the previous case, the fourth and second quadrant results are not theoretically the same. Here the stresses in the longitudinal and transverse planes of symmetry are low and rise to their maximum levels on the intermediate gage line. The distribution of stresses along the intermediate gage line is shown in Fig. 37, which is 45° from

the longitudinal plane of symmetry. Here the agreement is very poor. In general, the stresses are very low, and therefore the distributions show very poor quantitative agreement between theory and experimental results.

The maximum experimentally determined stress ratio was 1.5, with the maximum stress located on the outer surface of the nozzle at the junction on the 0° gage line. The maximum theoretical stress was also on the outer surface of the nozzle at the same location. The maximum theoretical stress ratio was 1.0.

4.4 In-Plane Moment Loading, M_{ZN}, on Nozzle

The measured and predicted stress distributions for an in-plane moment loading of 400 in.-lb applied to the nozzle are shown in Figs. 40 through 44. Here the stresses are large in the longitudinal plane of symmetry, as shown in Figs. 40 and 41. The agreement between theory and experiment is very good for the gage lines in the longitudinal plane of symmetry.

The stresses are lower along the gage line 45° from the longitudinal plane of symmetry; in the transverse plane of symmetry, the stresses are very low (Figs. 43 and 44). For this loading, the transverse plane is somewhat similar to the neutral axis of a beam.

The maximum experimentally determined stress ratio was 6.1, with the maximum stress occurring on the outer surface of the nozzle at the junction along the 0° gage line. The maximum theoretical stress also occurred on the outer surface of the nozzle at the junction along the 0° gage line. The stress ratio was 7.2.

4.5 In-Plane Force, F_{XN}, on Nozzle

The in-plane force applied to the nozzle had a value of 80 lb. The comparisons of theory and experiment for the eight gage lines are shown in Figs. 45 through 49. The results here are very similar to the previous case of the in-plane bending moment on the nozzle, and the overall agreement is very good.

The maximum experimentally determined stress occurred on the inner surface of the nozzle at the junction along the 0° gage line; the ratio was 7.2. The maximum theoretical stress occurred on the outer surface of the nozzle at the junction along the 0° gage line; the maximum theoretical stress ratio was 8.1.

4.6 Axial Force, F_{YN}, on Nozzle

The comparisons of theory and experiment for an axial force of 400 lb applied to the nozzle are presented in Figs. 50 through 54. The agreement between theory and experiment is very good, except for the inside surface of the cylinder on the 315° gage line, which is 45° from the longitudinal plane of symmetry. The agreement is very good, particularly as the larger stress levels are approached on the transverse plane of symmetry (Figs. 53 and 54).

The experimentally determined maximum stress occurred on the inner surface of the nozzle on the 270° plane at the junction; the ratio was 21.6. The theoretically determined maximum stress occurred on the outer surface of the nozzle on the 270° gage line at the junction; the ratio was 13.9.

4.7 Out-of-Plane Force, F_{ZN}, on Nozzle

The comparisons of theory and experimental data for an out-of-plane force of 60 lb applied to the nozzle are presented in Figs. 55 through 59. These results are very similar to the case of out-of-plane moment on the nozzle, and the overall agreement between theory and experiment is again very good, except on the inside surface of the cylinder along the 315° gage line (Fig. 57). Since the stresses are very small on the 0 and 180° gage lines, the agreement does not look as good as along other gage lines.

The experimentally determined maximum stress (ratio of 8.6) occurred on the inner surface of the nozzle along the 270° gage line at the junction. The theoretically determined maximum stress (ratio of 8.5) occurred on the outer surface at the same location.

4.8 Torsional Moment Loading, M_{XC}, on Cylinder

The comparisons of theory and experiment for a torsional moment of 30,000 in.-lb applied to the cylinder are presented in Figs. 60 through 64. The experimental stresses are low in the longitudinal and transverse planes of symmetry and rise to their maximum levels on the intermediate gage line. The agreement between theory and experiment is satisfactory on the intermediate line. However, the maximum theoretical stress is located on the 0° plane on the nozzle.

The experimentally determined maximum stress occurred on the inner surface of the cylinder along the 315° gage line at the junction, and the maximum stress ratio was 5.0. The theoretically determined maximum stress occurred on the outer surface of the nozzle along the 0° gage line at the junction, and the maximum stress ratio was 5.1.

4.9 Out-of-Plane Moment Loading, M_{YC}, on Cylinder

The out-of-plane moment loading applied to the cylinder had a value of 80,000 in.-lb. The comparisons of theory and experiment are presented in Figs. 65 through 69. The 0 and 180° gage lines on the longitudinal plane of symmetry are analogous to the neutral axis of a beam in bending, and the stresses are thus low. However, the stresses are not very large anywhere in the model. A peculiarity of the finite-element analysis calculates a large stress at the junction on the 0 and 180° planes of symmetry which is obviously not correct. The maximum stress ratios for this case were the lowest of all 13 loading cases. As a result of the relatively low stress levels, the stress distributions are not too well defined on the 0, 180, and 315° gage lines, and the agreement between theory and experiment appears to be relatively poor. However, on the gage lines of maximum stress (270 and 90°), the agreement between theory and experiment is fair.

Both the experimentally determined and the theoretical maximum stresses occurred on the outside surface of the cylinder on the 90° gage line. The experimental maximum stress ratio was 1.3, and the theoretical was 1.0.

4.10 In-Plane Moment Loading, M_{ZC}, on Cylinder

The comparisons of theory and experiment for the in-plane moment loading of 80,000 in.-lb applied to the cylinder are presented in Figs. 70 through 74. The stress levels are a maximum in the transverse plane of symmetry, as shown in Figs. 73 and 74, and agreement between experimental and analytical results is reasonably good. Where the stress levels are lower along other gage lines, the apparent agreement between theory and experiment is poorer.

The experimentally determined and the theoretical maximum stresses occurred on the inside surface of the cylinder at the junction. The experimental maximum was on the 90° gage line, while the theoretical maximum occurred both on the 90 and 270° gage lines. The maximum experimental stress ratio was 4.0, and the maximum theoretical ratio was 3.1.

4.11 Axial Force, F_{XC}, on Cylinder

The axial force applied to the cylinder had a value of 10,000 lb. The comparisons of theory and experiment for the five gage lines are presented in Figs. 75 through 79. Considering the relatively low stresses, the agreement between theory and experiment is reasonably good throughout. The agreement between theory and experiment is good for the 270 and 90° gage lines on the nozzle, as shown in Figs. 78 and 79.

The experimentally determined and the theoretically predicted maximum stresses occurred on the inner surface of the cylinder at the junction. The experimental maximum was on the 90° gage line, while the theoretical value was on both the 270 and 90° gage lines. The experimental maximum stress ratio was 3.7; the theoretical stress ratio was 3.0.

4.12 In-Plane Force, F_{YC}, on Cylinder

The comparisons of theory and experiment for the in-plane force of 3000 lb applied to the cylinder are shown in Figs. 80 through 84. The agreement between theory and experiment is very good for this loading case.

Both the experimentally determined and the theoretical maximum stresses occurred on the inside surface of the cylinder at the junction. The experimental maximum was on the 90° gage line, while the theoretical maximum was on both the 270 and 90° gage lines. The maximum experimental stress ratio was 4.1, and the maximum theoretical ratio was 3.2.

4.13 Out-of-Plane Force, F_{ZC}, on Cylinder

The comparisons of theory and experiment for the out-of-plane force of 3000 lb applied to the cylinder are shown in Figs. 85 through 89. The 0 and 180° gage lines, in the longitudinal plane of symmetry, are analogous to the neutral axis of a beam, so that the stresses are low along these gage lines. However, the stresses build up for the other gage lines, and the agreement between theory and experiment is very good. A peculiarity of the finite-element analysis calculates a large stress at the junction on the 0 and 180° planes of symmetry on the nozzle which is obviously not correct. These points were neglected.

Both the experimentally determined maximum and the theoretical maximum stresses occurred on the inner surface of the cylinder at the junction along the 315° gage line. The maximum experimental stress ratio was 1.3, while the maximum theoretical ratio was 1.2.

5. CONCLUSIONS

Table 2 represents an attempt to concisely summarize the principal findings of this study in terms of maximum principal stress ratios, locations of maximum principal stresses, and the relative overall agreement between theory and experiment for each loading case. The maximum stress ratios are based on the stresses, either measured or predicted, along the five lines of strain gages only and were determined by dividing the maximum absolute principal stress value by a nominal membrane stress value. The maximum experimental principal stresses were determined by extrapolating the experimentally determined stress distributions to peak stresses at the junction in all but one case.

Table 2. Summary of maximum stress ratios and maximum stress locations

Loading case	Experimentally determined maximum stress[a]		Theoretical maximum stress		Overall agreement between theory and experiment
	Stress ratio[b]	Location[c]	Stress ratio[b]	Location[c]	
Internal pressure	3.5	Inside cylinder, 180°	3.1	Outside nozzle, 0°	Good, poor
M_{XN}, out-of-plane moment on nozzle	8.5	Inside nozzle, 270°	7.6	Outside nozzle, 270°	Excellent
M_{YN}, torsional moment on nozzle	1.5	Outside nozzle, 0°	1.0	Outside nozzle, 0°	Poor
M_{ZN}, in-plane moment on nozzle	6.1	Outside nozzle, 0°	7.2	Outside nozzle, 0°	Excellent
F_{XN}, in-plane force on nozzle	7.2	Inside nozzle, 0°	8.1	Outside nozzle, 0°	Excellent
F_{YN}, axial force on nozzle	21.6	Inside nozzle, 270°	13.9	Outside nozzle, 270°	Good
F_{ZN}, out-of-plane force on nozzle	8.6	Inside nozzle, 270°	8.5	Outside nozzle, 270°	Good
M_{XC}, torsional moment on cylinder	5.0	Inside cylinder, 315°	5.1	Outside nozzle, 0°	Good
M_{YC}, out-of-plane moment on cylinder	1.3	Outside cylinder,[d] 90°	1.0	Outside cylinder,[d] 90°	Fair
M_{ZC}, in-plane moment on cylinder	4.0	Inside cylinder, 90°	3.1	Inside cylinder, 90°	Fair
F_{XC}, axial force on cylinder	3.7	Inside cylinder, 90°	3.0	Inside cylinder, 90°	Good, poor
F_{YC}, in-plane force on cylinder	4.1	Inside cylinder, 90°	3.2	Inside cylinder, 90°	Excellent
F_{ZC}, out-of-plane force on cylinder	1.3	Inside cylinder, 315°	1.2	Inside cylinder, 315°	Fair

[a]Based on extrapolation of experimental distributions to a maximum at the junction.

[b]Ratio of maximum absolute principal stress value to nominal stress value.

[c]Maximums all occurred at the junction.

[d]Maximum not at junction, at approximately 90° around on the transverse plane.

The relative overall agreement between the finite-element predictions and the experimental results is rated in the table as excellent, good, fair, or poor. These ratings are, of course, a matter of opinion, but an attempt was made to make an unbiased evaluation by basing them on both the overall qualitative agreement along the gage lines and on the quantitative agreement in areas where the stresses were relatively high. For the internal pressure case and the case of an axial loading on the cylinder, the relative rating is listed as good, poor; that is, the agreement was good in regions where the stress levels were relatively high but poor in regions where they were relatively low.

Table 2 indicates that generally the experimentally determined maximum stress ratios and those based on finite-element predictions are in good agreement. Furthermore, the degree of agreement between the stress ratios generally correlates well with the relative ratings of the overall agreement between theory and experiment. Generally, the agreement was best for cases involving loadings on the nozzle. However, the torsional moment on the nozzle was an exception; there the agreement was poor qualitatively and quantitatively.

In every loading case except one, the maximum stress occurred at the junction of the nozzle and cylinder. In the one exception, which was the case of an out-of-plane moment, M_{YC}, on the cylinder, the maximum occurred on the outside surface of the cylinder at approximately 90° around on the transverse plane (around at the side of the cylinder). The stresses on the inside surface of the cylinder were, however, almost as high as those on the outer surface.

In 7 of the 13 cases, the maximum values occurred in the transverse plane of symmetry. The torsional moment on the cylinder and the out-of-plane force on the cylinder produced maximum stresses at points intermediate to the two planes of symmetry. The other four cases produced maximum stresses in the longitudinal plane of symmetry.

Finally, it should be pointed out that, as would be expected, the out-of-plane moment and force loadings on the nozzle produced quite similar results, and the in-plane moment and force loadings on the nozzle produced similar results. The stress distributions were very similar for each pair, and the maximum stress ratios were very close.

In conclusion, the comparison of these particular finite-element predictions with the experimental results shows reasonably good agreement. It is felt that this analysis would be satisfactory for most engineering purposes.

However, there is room for improvement, particularly in the out-of-plane moment and force loadings on the cylinder. The finite-element analysis for these cases calculated a large stress at the junction on the longitudinal plane of symmetry which obviously is not correct. The inclusion of the sixth degree of freedom, at least in the junction region, might improve the predictions.

ACKNOWLEDGMENTS

The planning and execution of the analytical and experimental study reported here would not have been possible without the assistance and cooperation of many individuals, both within ORNL and outside. The authors are deeply indebted to these people for their contributions.

Special thanks are due J. P. Rudd for the instrumentation of the model, which was a very painstaking task. The finite-element computer program used in the analysis was developed at the University of California, Berkeley, by C. P. Johnson under the direction of Professor R. W. Clough.

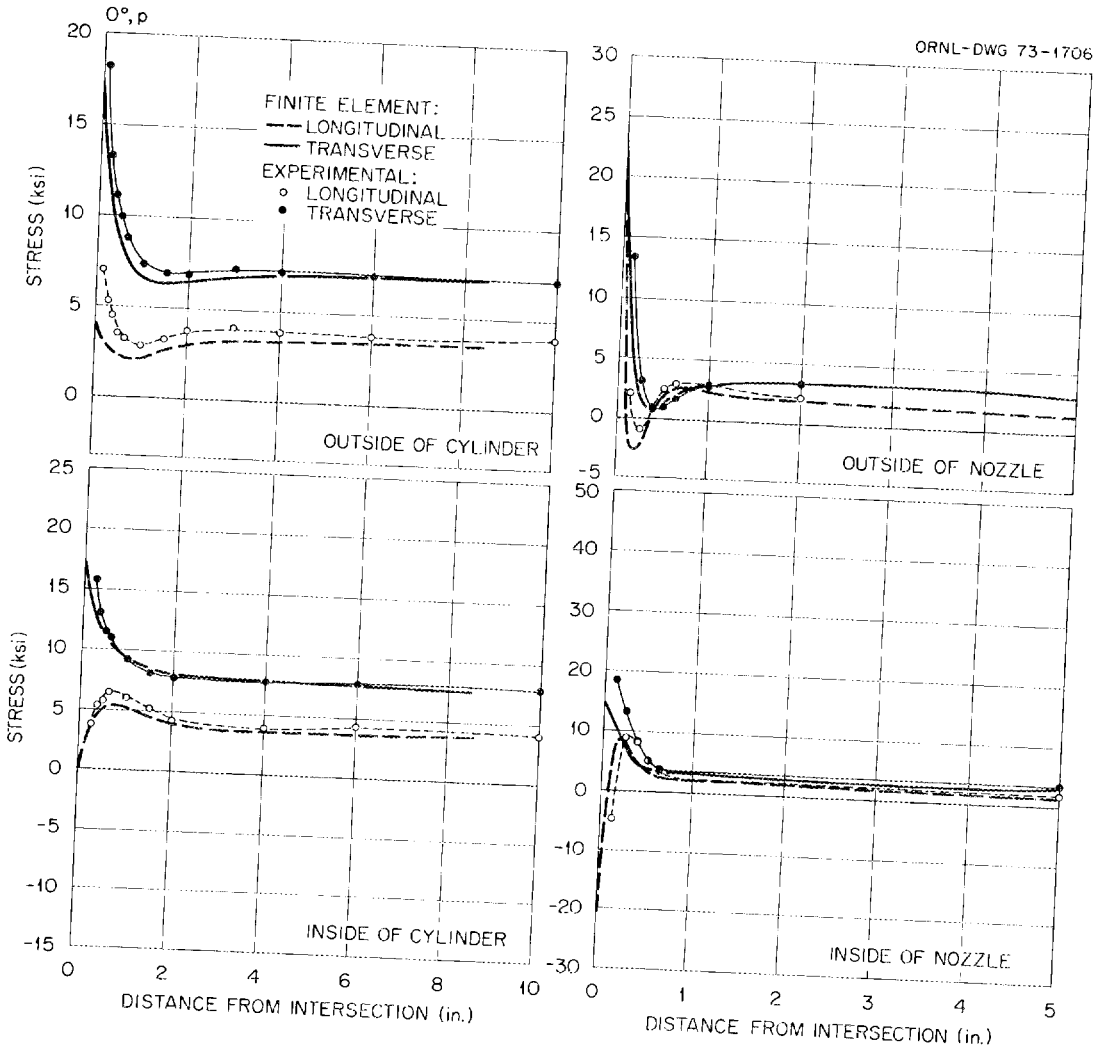

Fig. 25. Measured and predicted stress distributions at 0° for internal pressure of 300 psi.

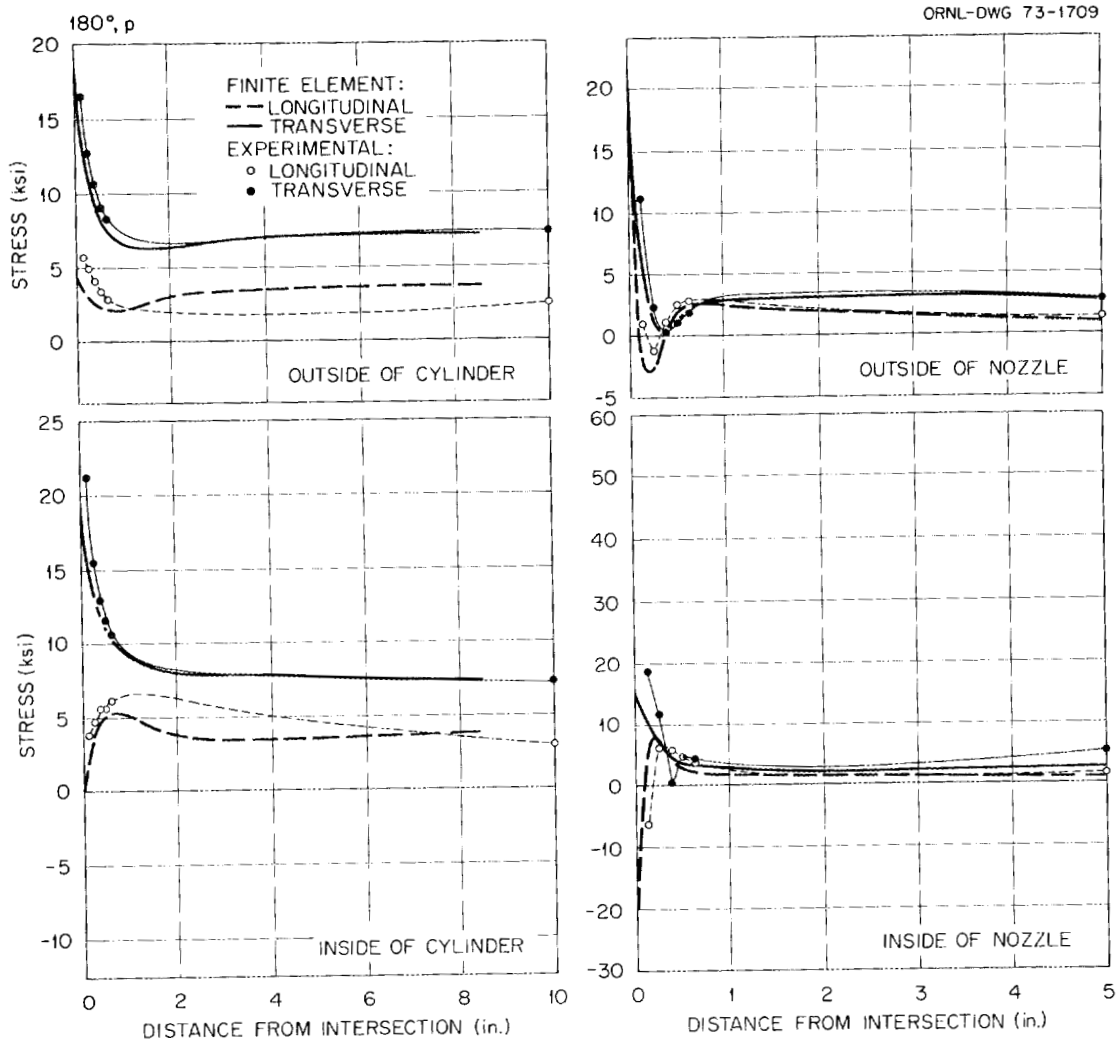

Fig. 26. Measured and predicted stress distributions at 180° for internal pressure of 300 psi.

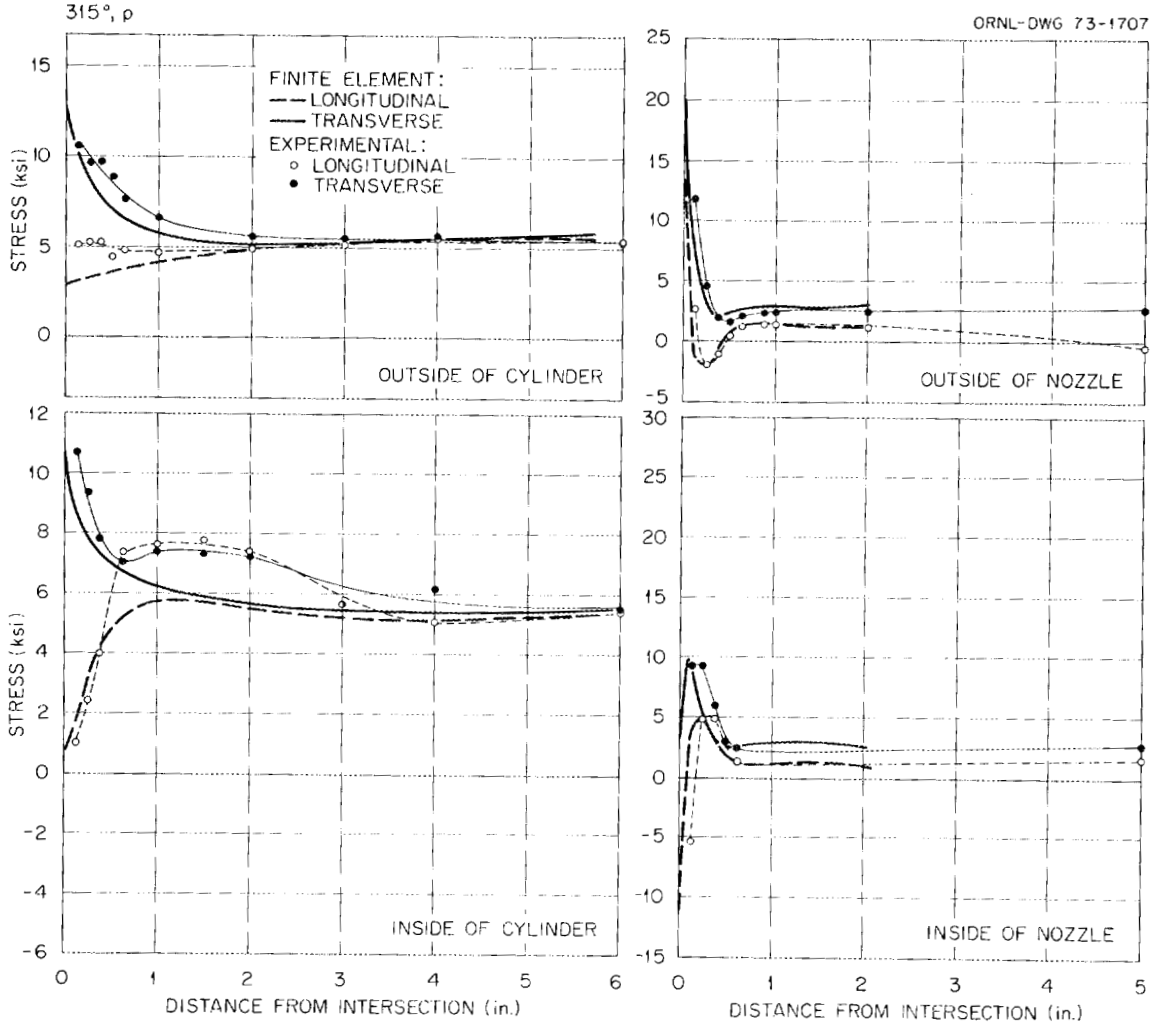

Fig. 27. Measured and predicted stress distributions at 315° for internal pressure of 300 psi.

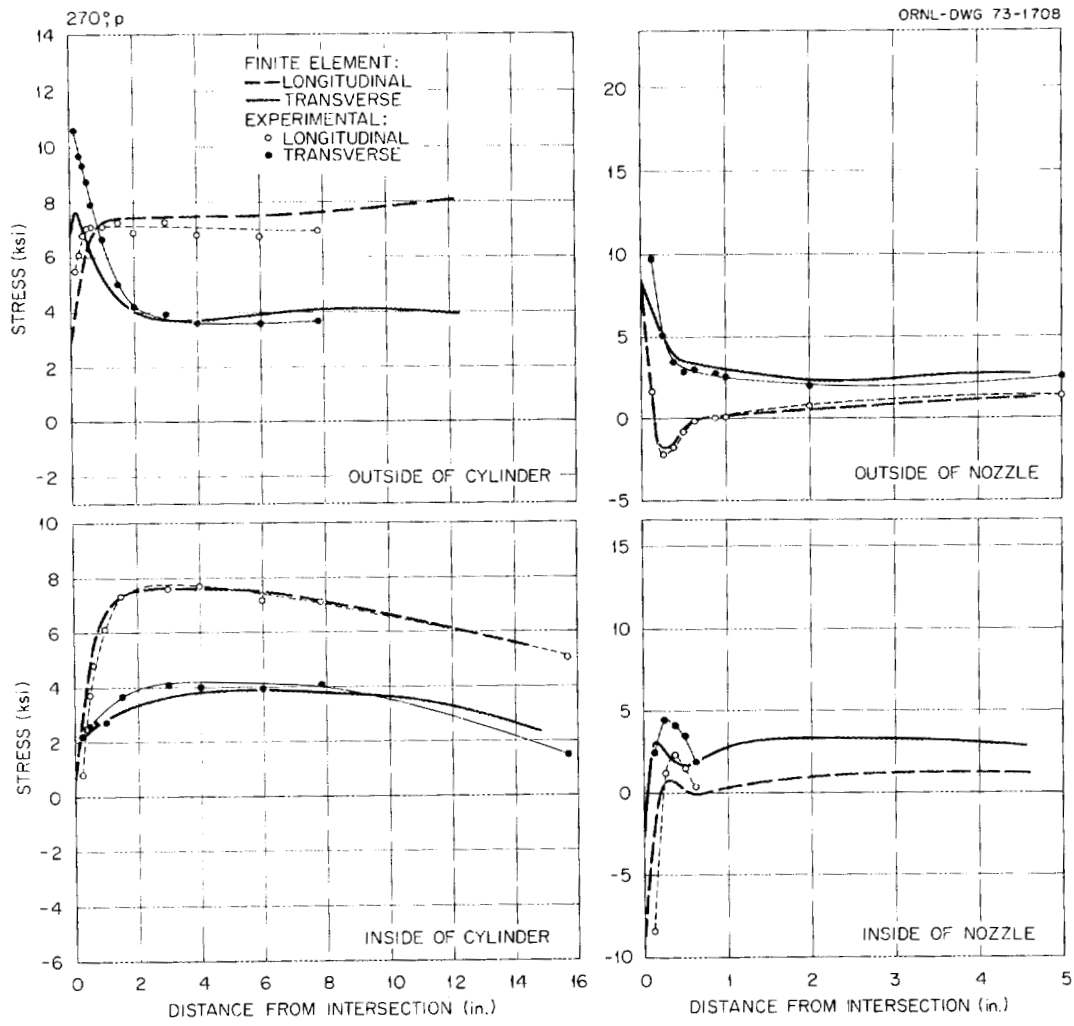

Fig. 28. Measured and predicted stress distributions at 270° for internal pressure of 300 psi.

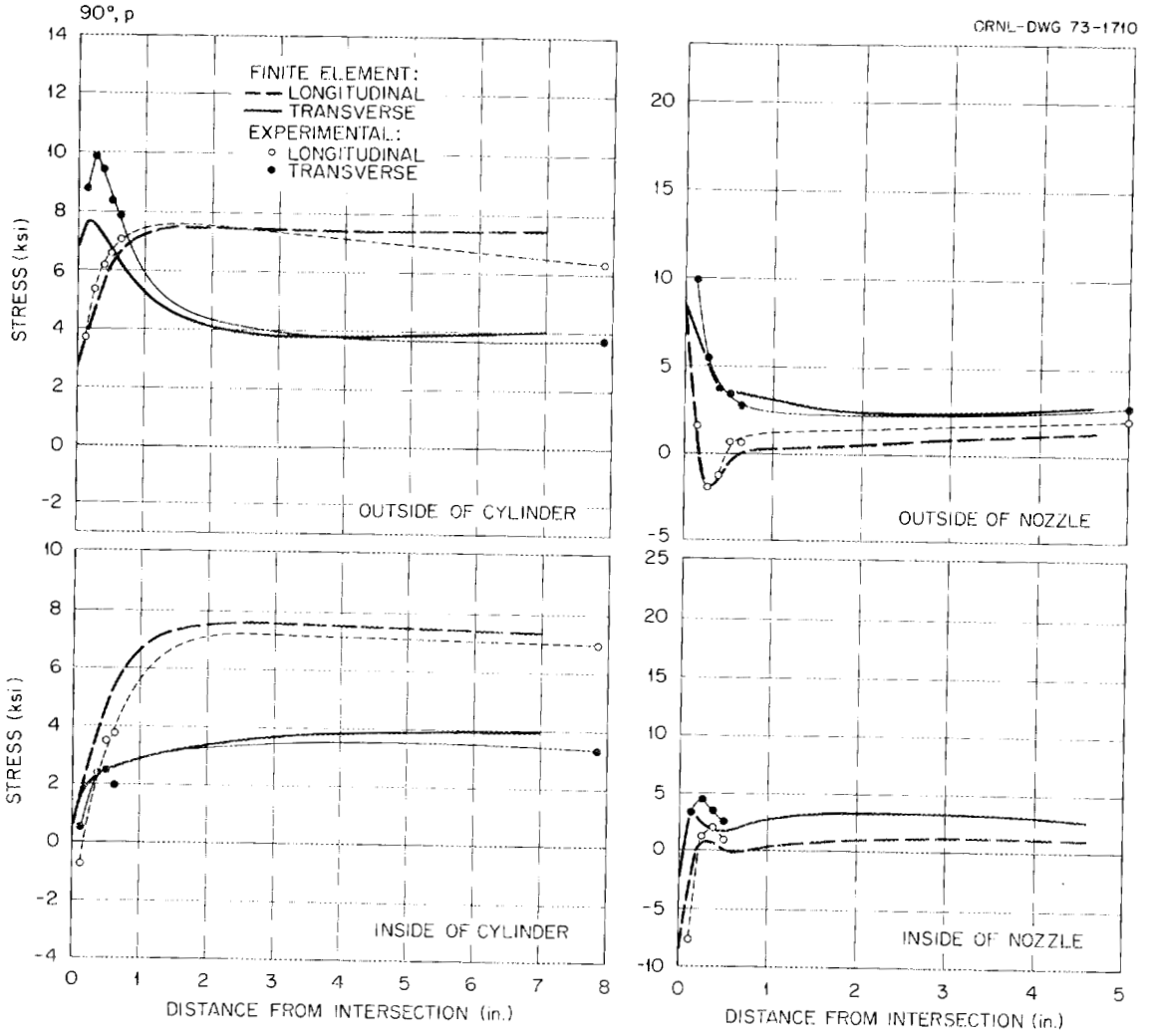

Fig. 29. Measured and predicted stress distributions at 90° for internal pressure of 300 psi.

ORNL-DWG 73-1877

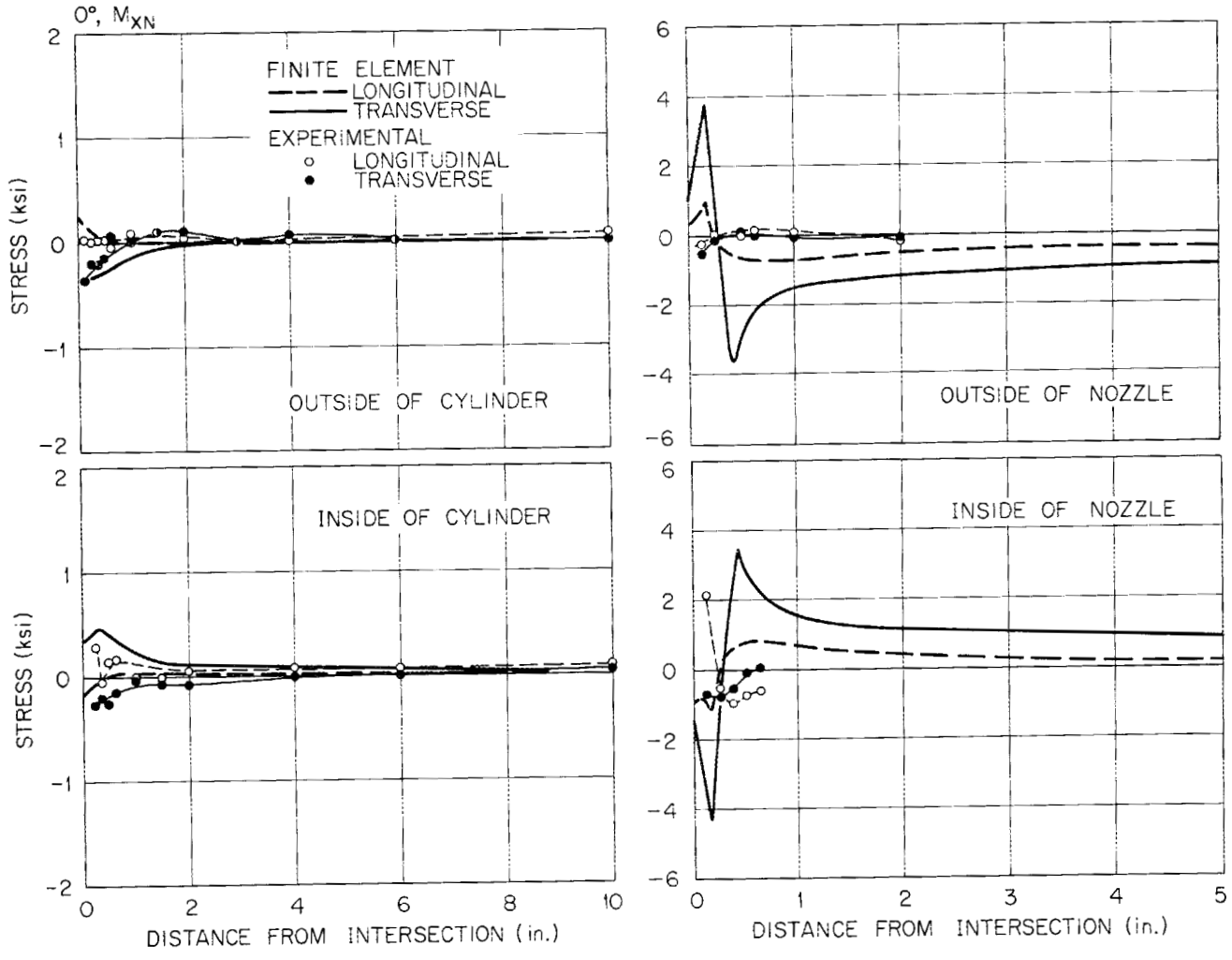

Fig. 30. Measured and predicted stress distributions at 0° for out-of-plane moment, M_{XN}, on nozzle.

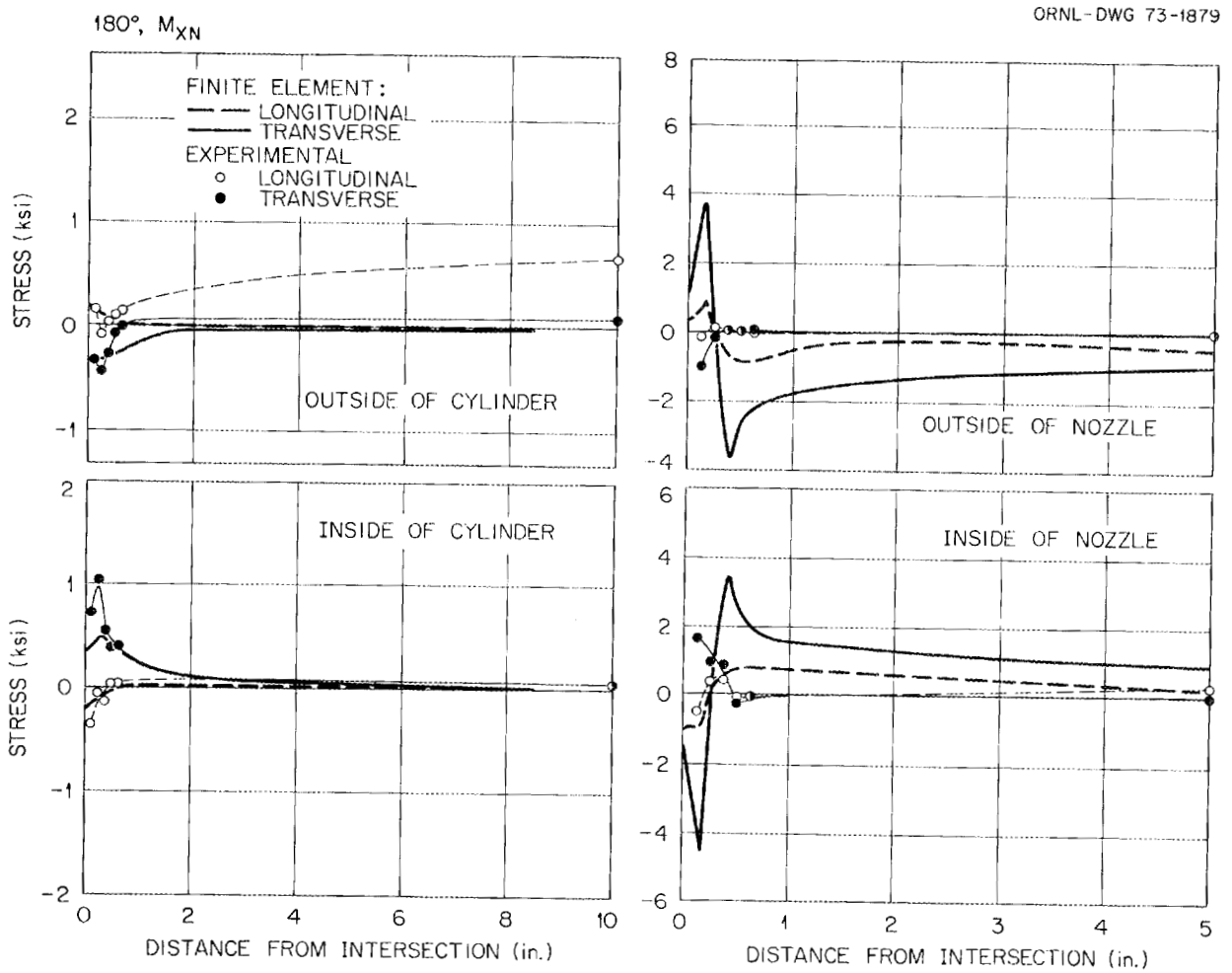

Fig. 31. Measured and predicted stress distributions at 180° for out-of-plane moment, M_{XN}, on nozzle.

ORNL-DWG 73-1881

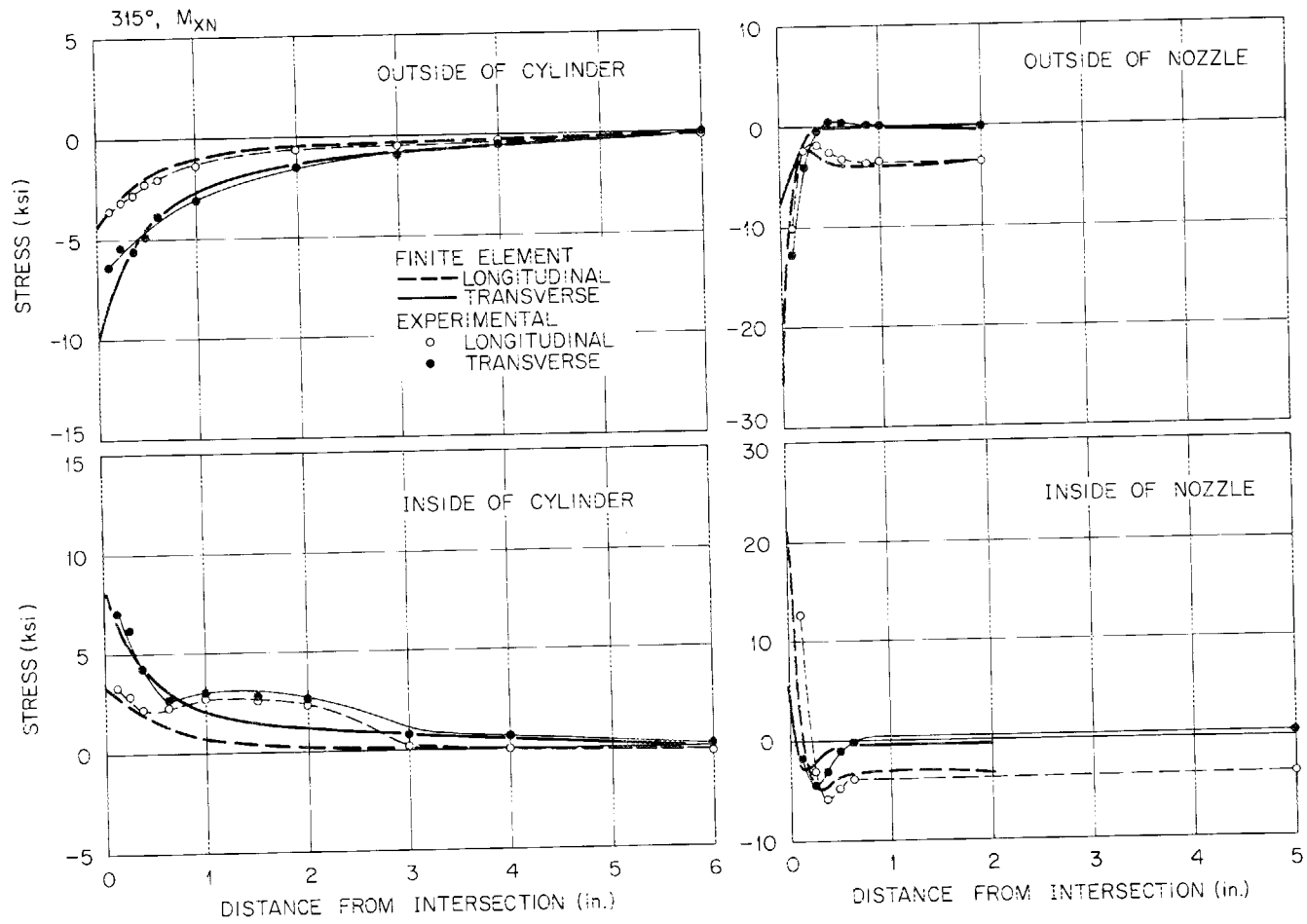

Fig. 32. Measured and predicted stress distributions at 315° for out-of-plane moment, M_{XN}, on nozzle.

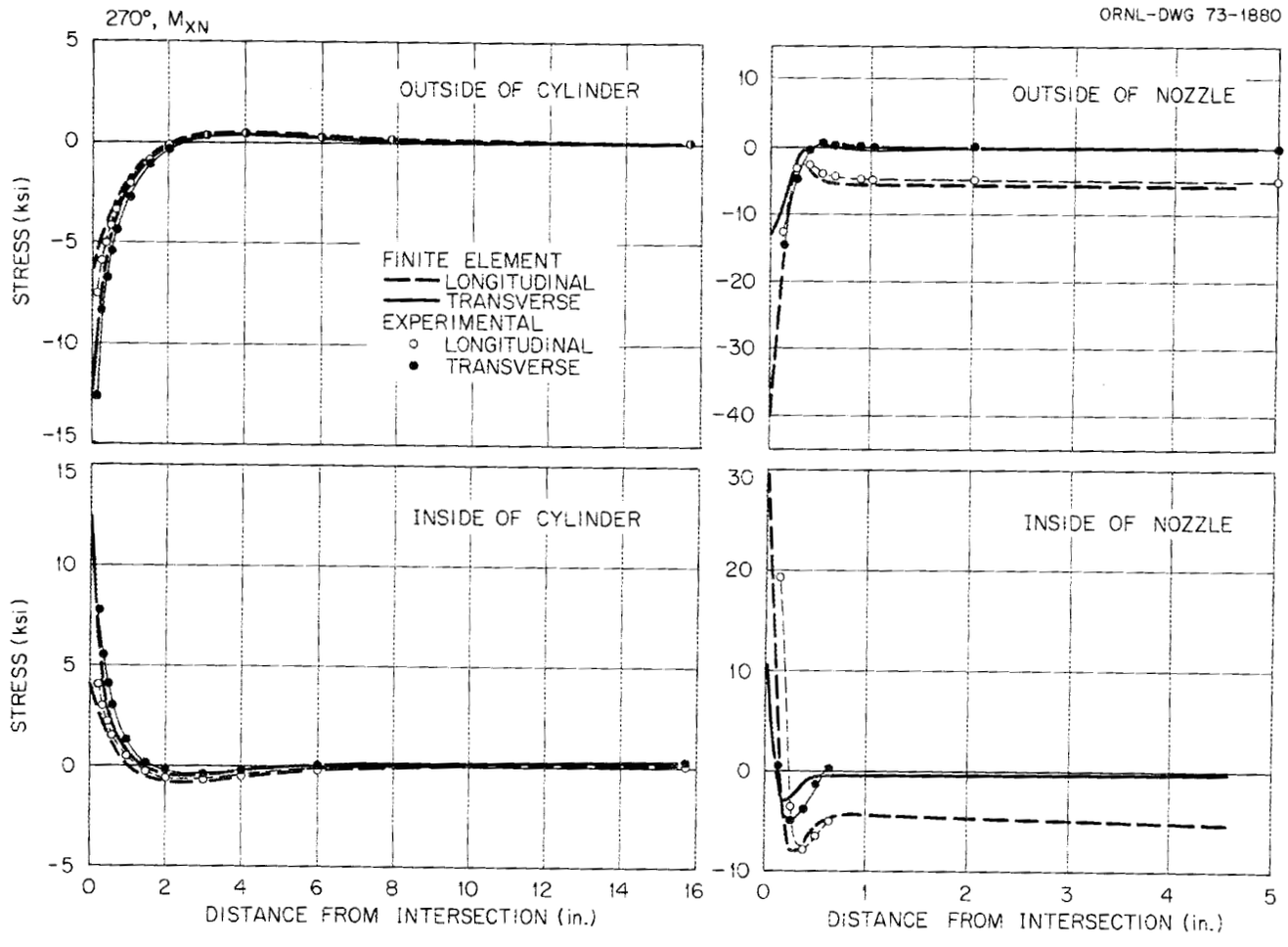

Fig. 33. Measured and predicted stress distributions at 270° for out-of-plane moment, M_{XN}, on nozzle.

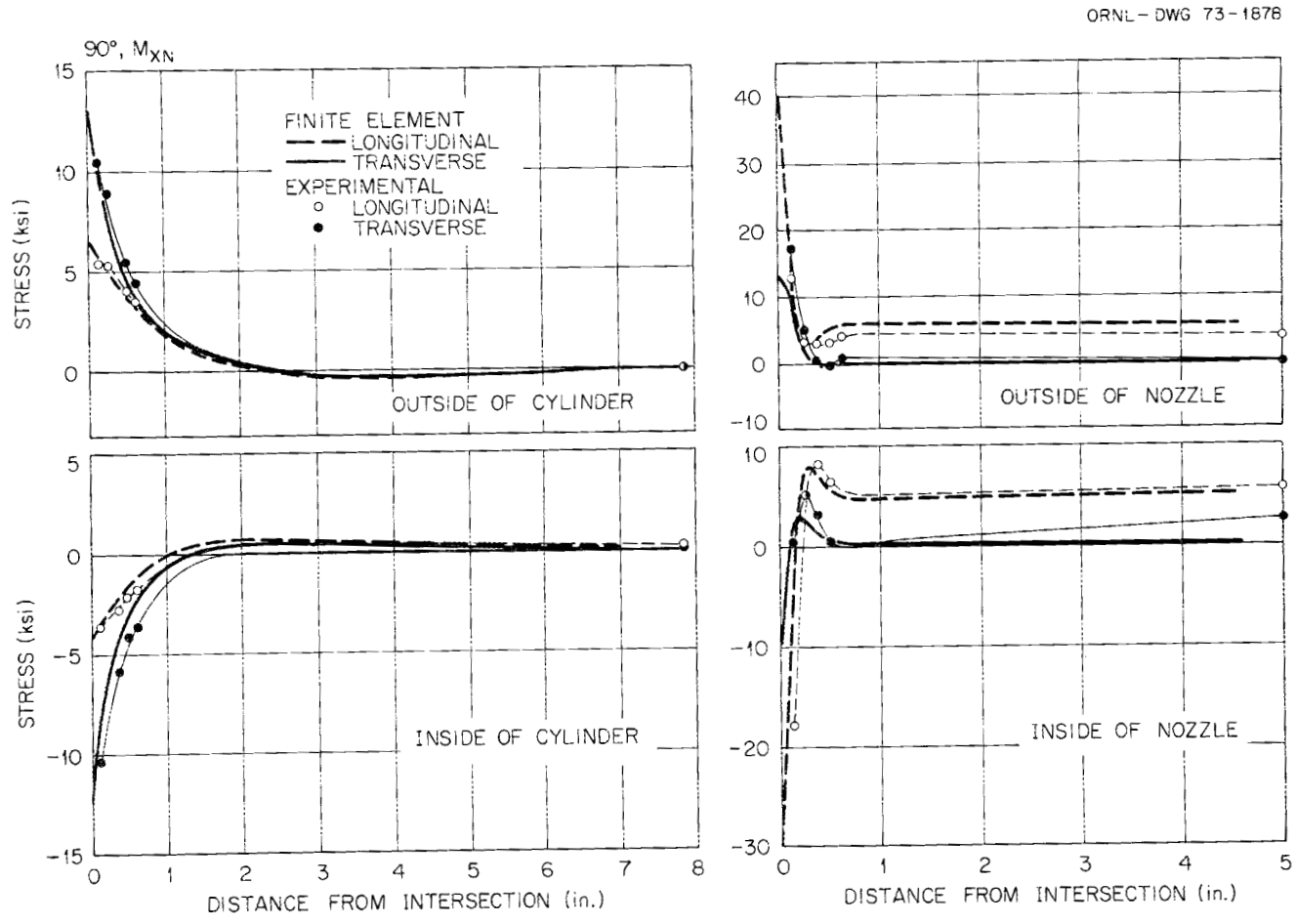

Fig. 34. Measured and predicted stress distributions at 90° for out-of-plane moment, M_{XN}, on nozzle.

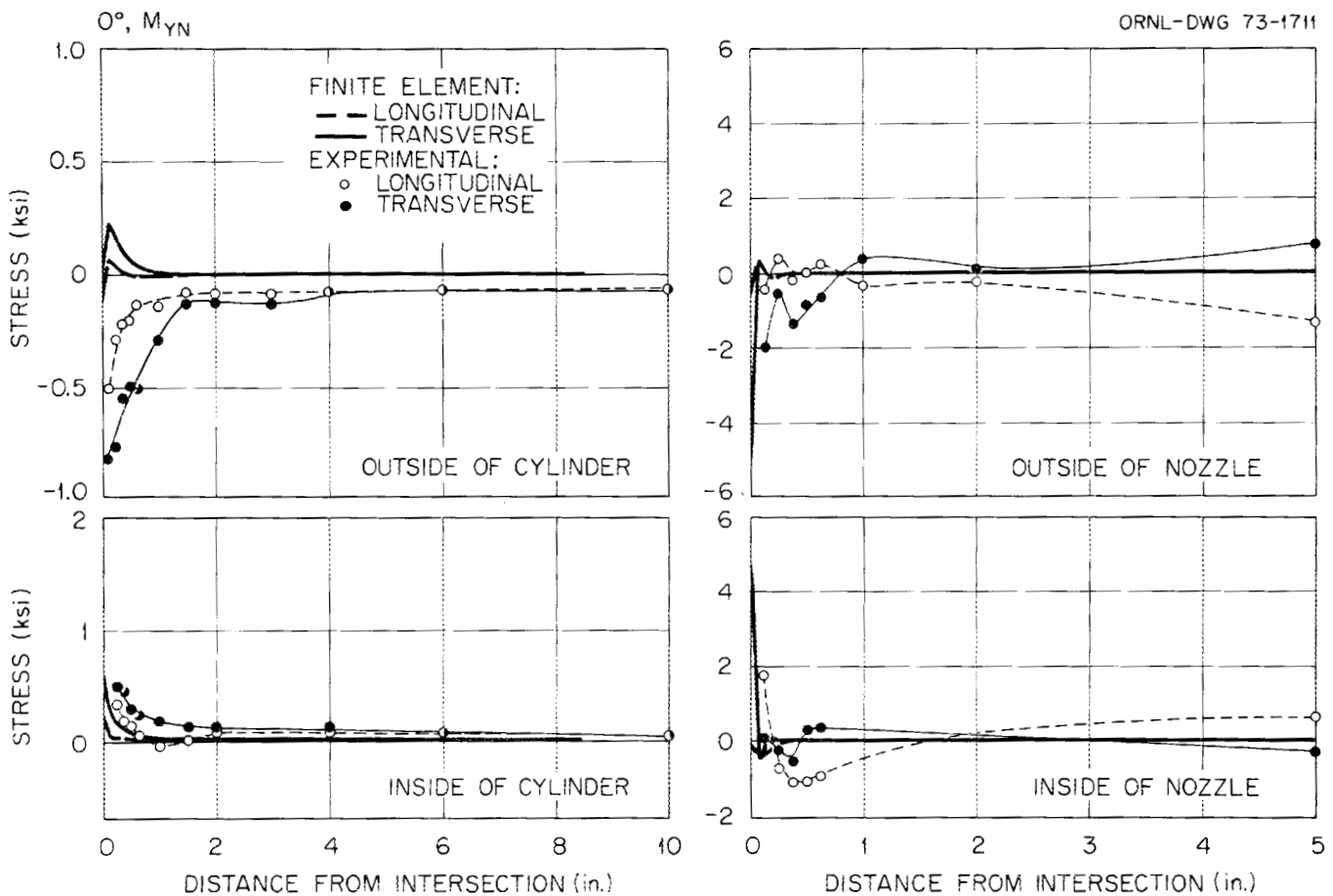

Fig. 35. Measured and predicted stress distributions at 0° for torsional moment, M_{YN}, on nozzle.

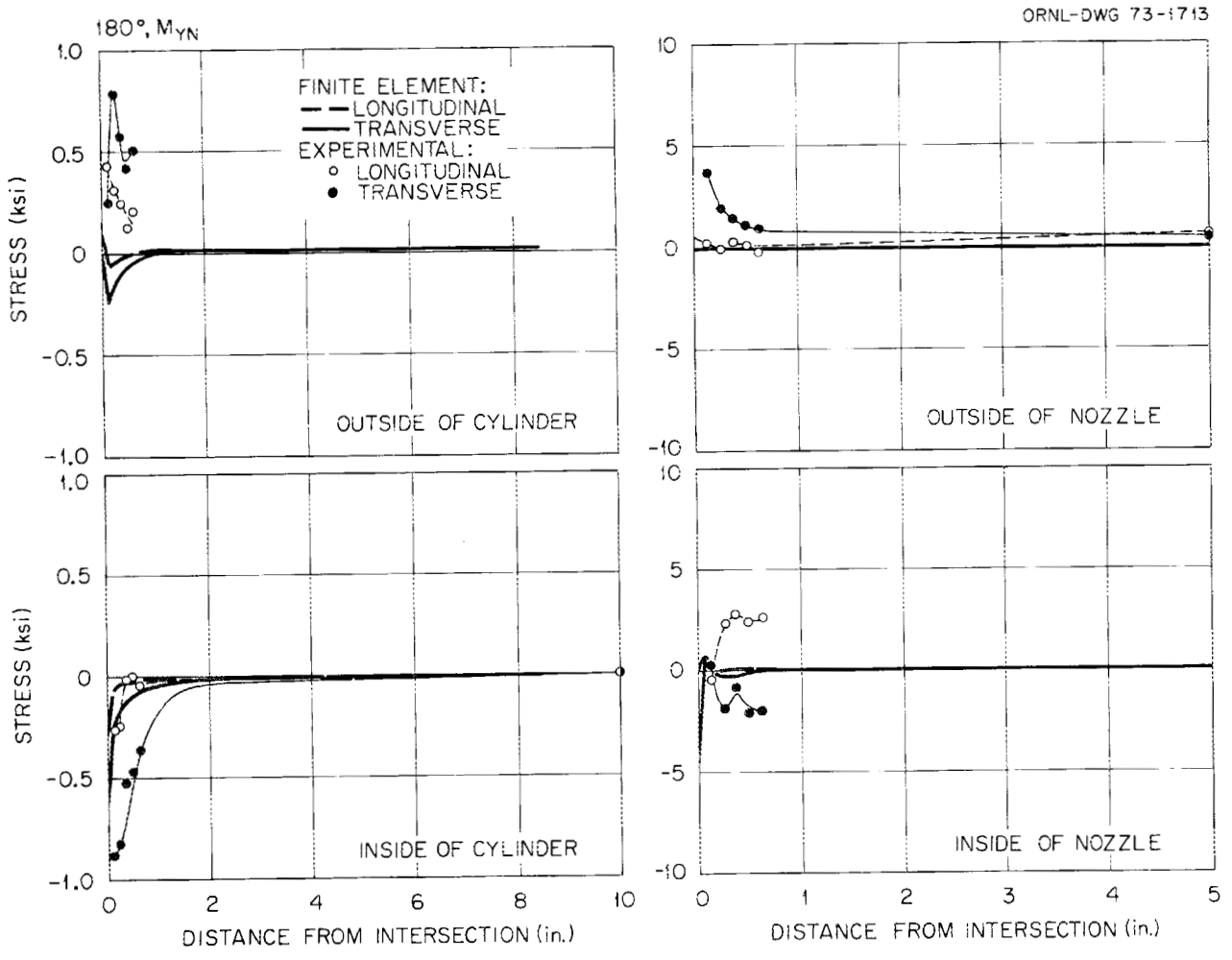

Fig. 36. Measured and predicted stress distributions at 180° for torsional moment, M_{YN}, on nozzle.

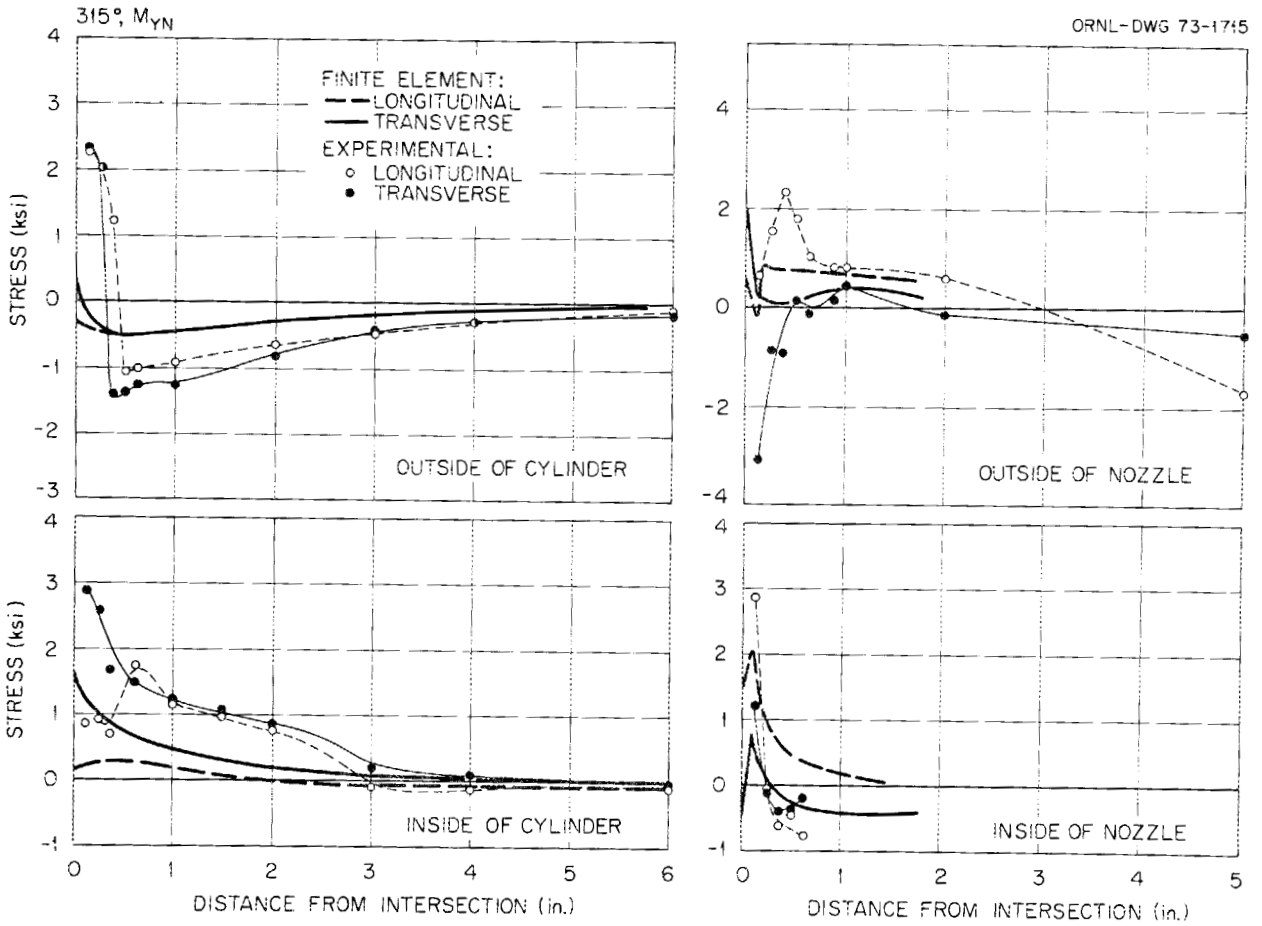

Fig. 37. Measured and predicted stress distributions at 315° for torsional moment, M_{YN}, on nozzle.

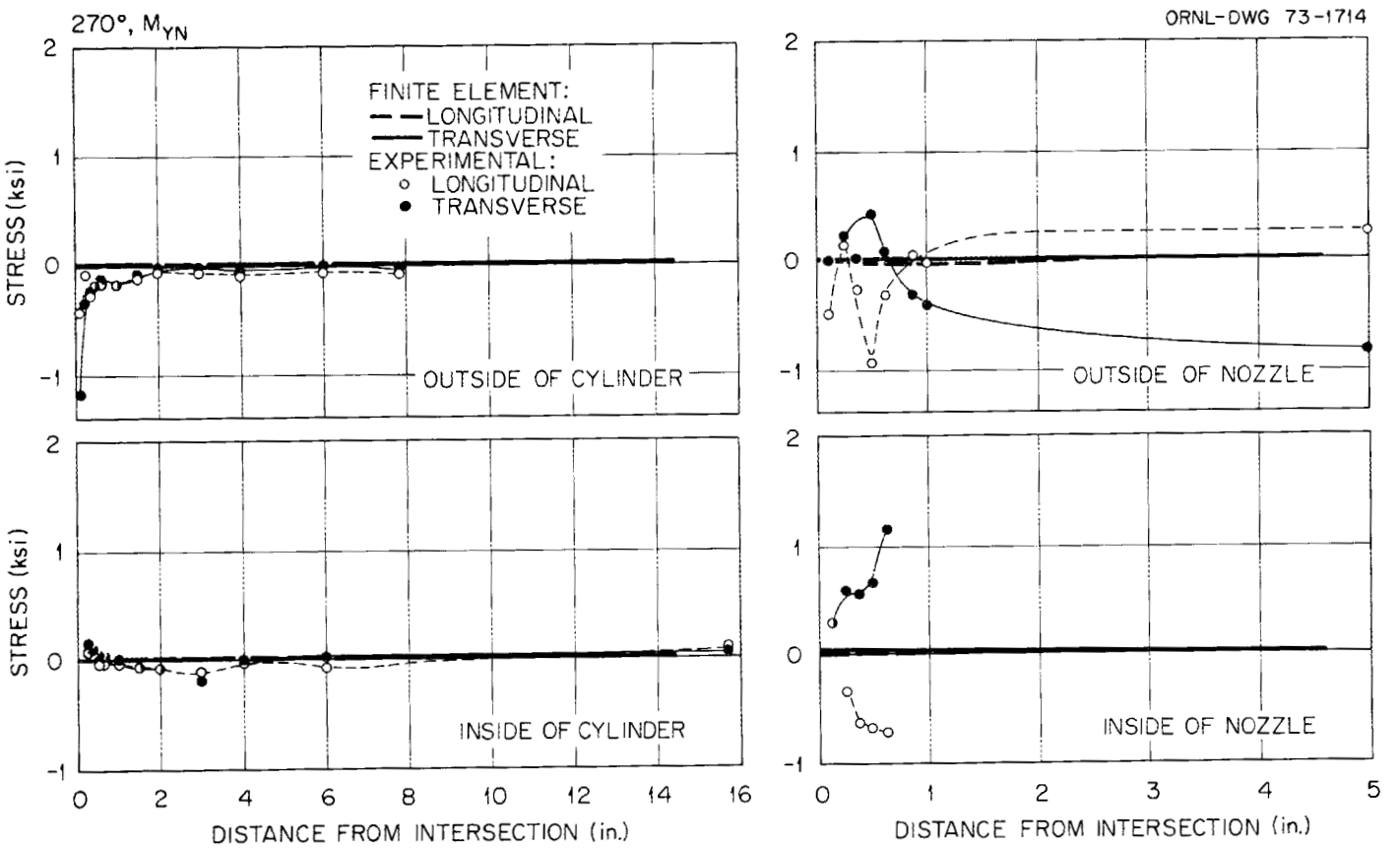

Fig. 38. Measured and predicted stress distributions at 270° for torsional moment, M_{YN}, on nozzle.

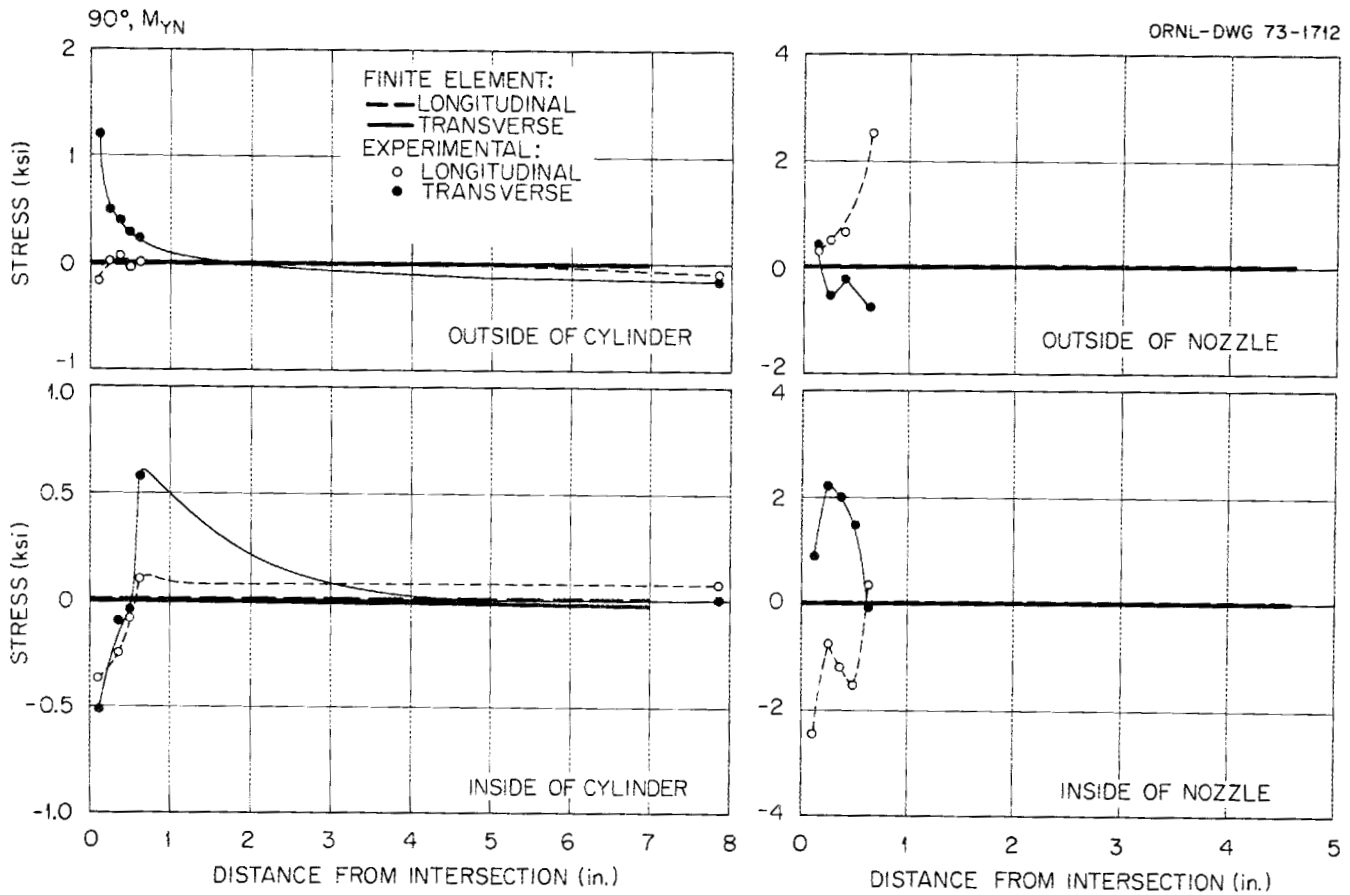

Fig. 39. Measured and predicted stress distributions at 90° for torsional moment, M_{YN}, on nozzle.

ORNL-DWG 73-1716

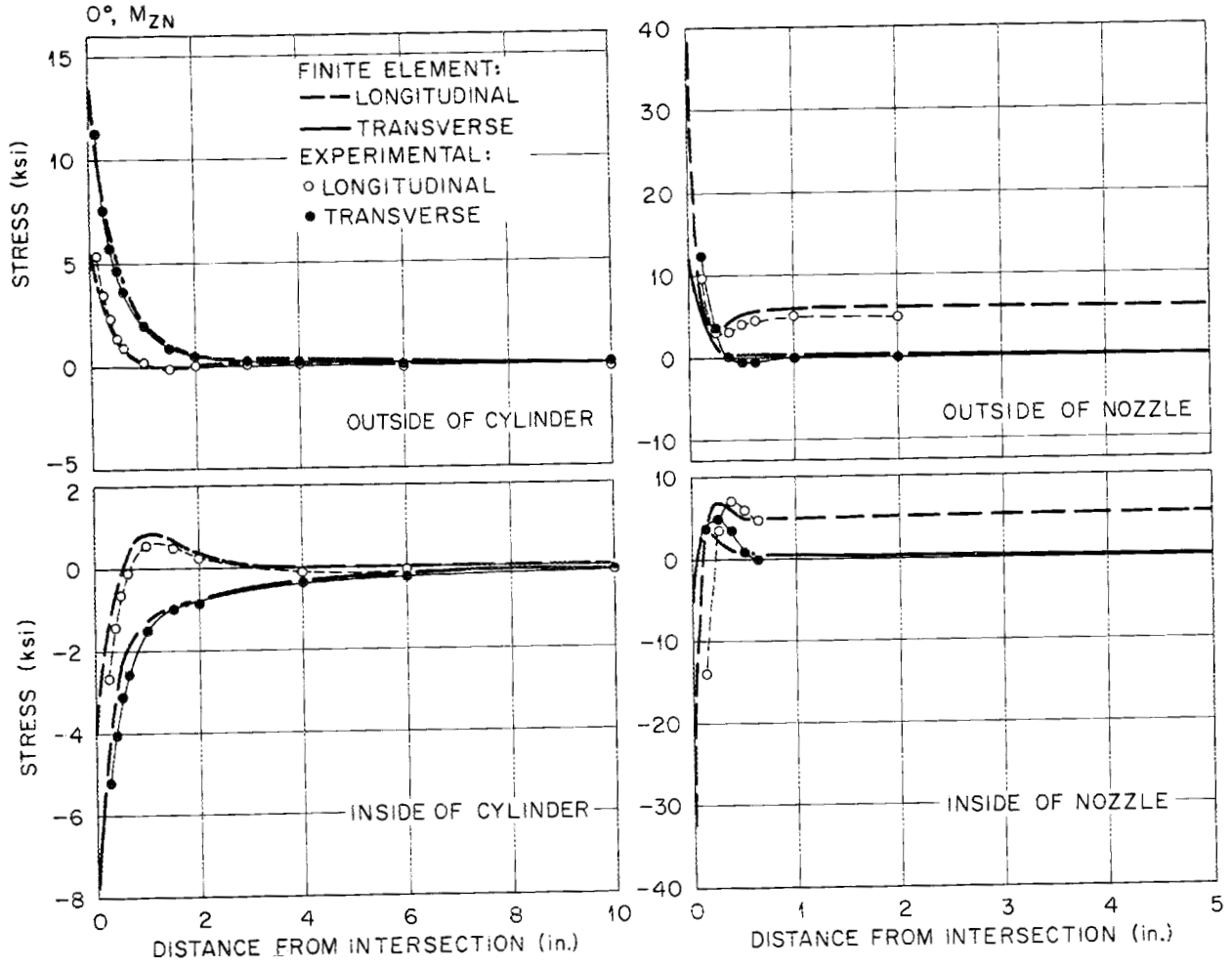

Fig. 40. Measured and predicted stress distributions at 0° for in-plane moment, M_{ZN}, on nozzle.

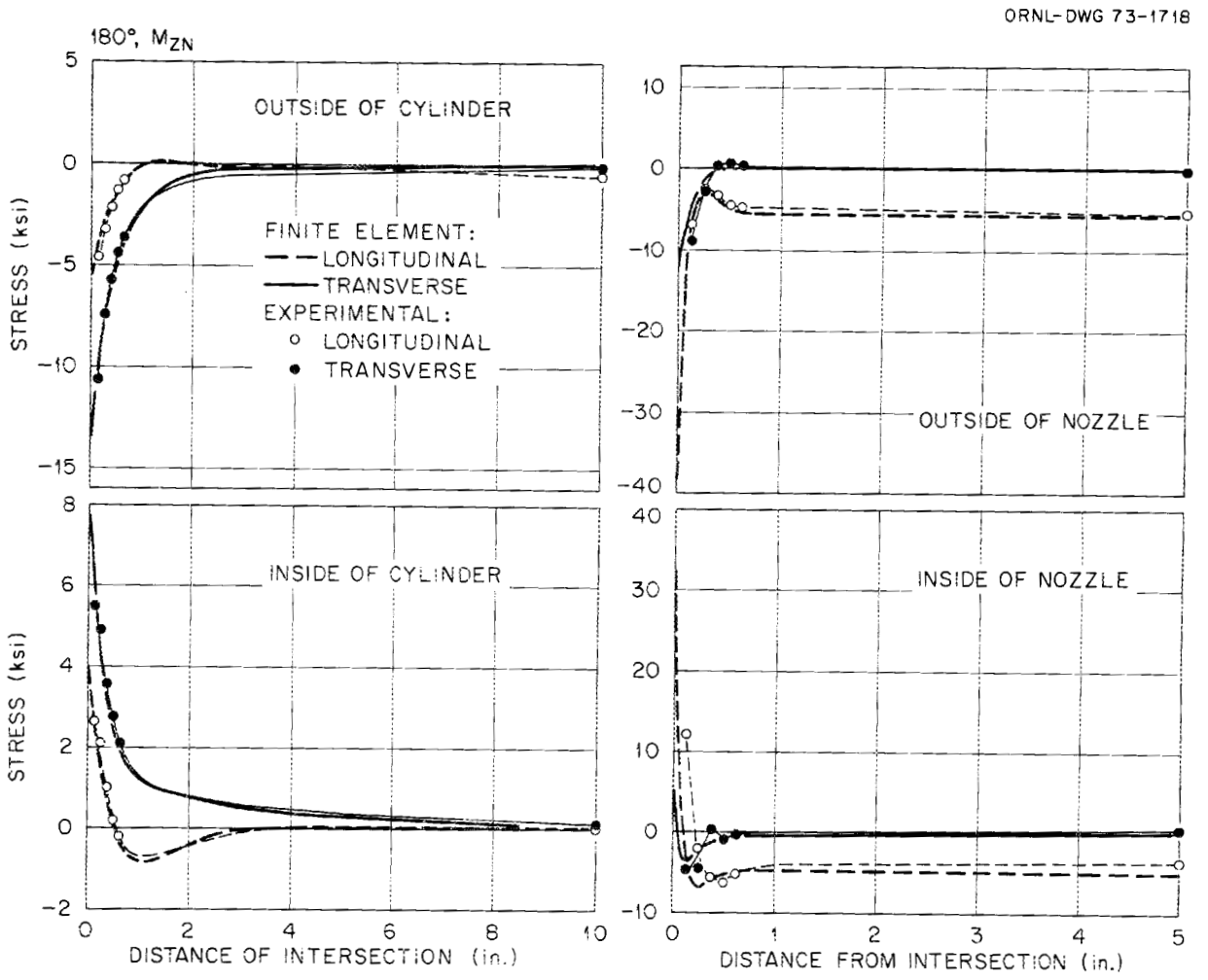

Fig. 41. Measured and predicted stress distributions at 180° for in-plane moment, M_{ZN}, on nozzle.

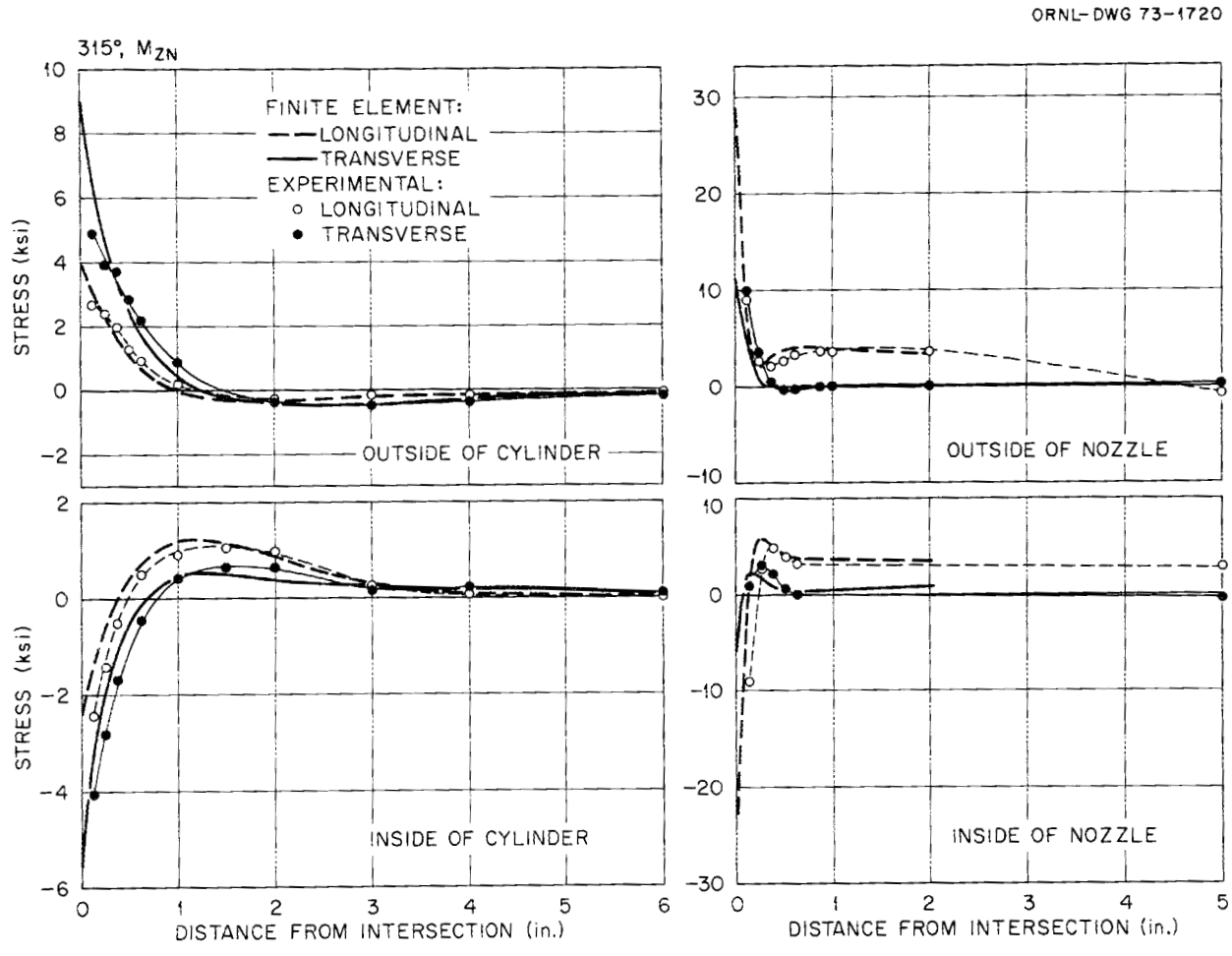

Fig. 42. Measured and predicted stress distributions at 315° for in-plane moment, M_{ZN}, on nozzle.

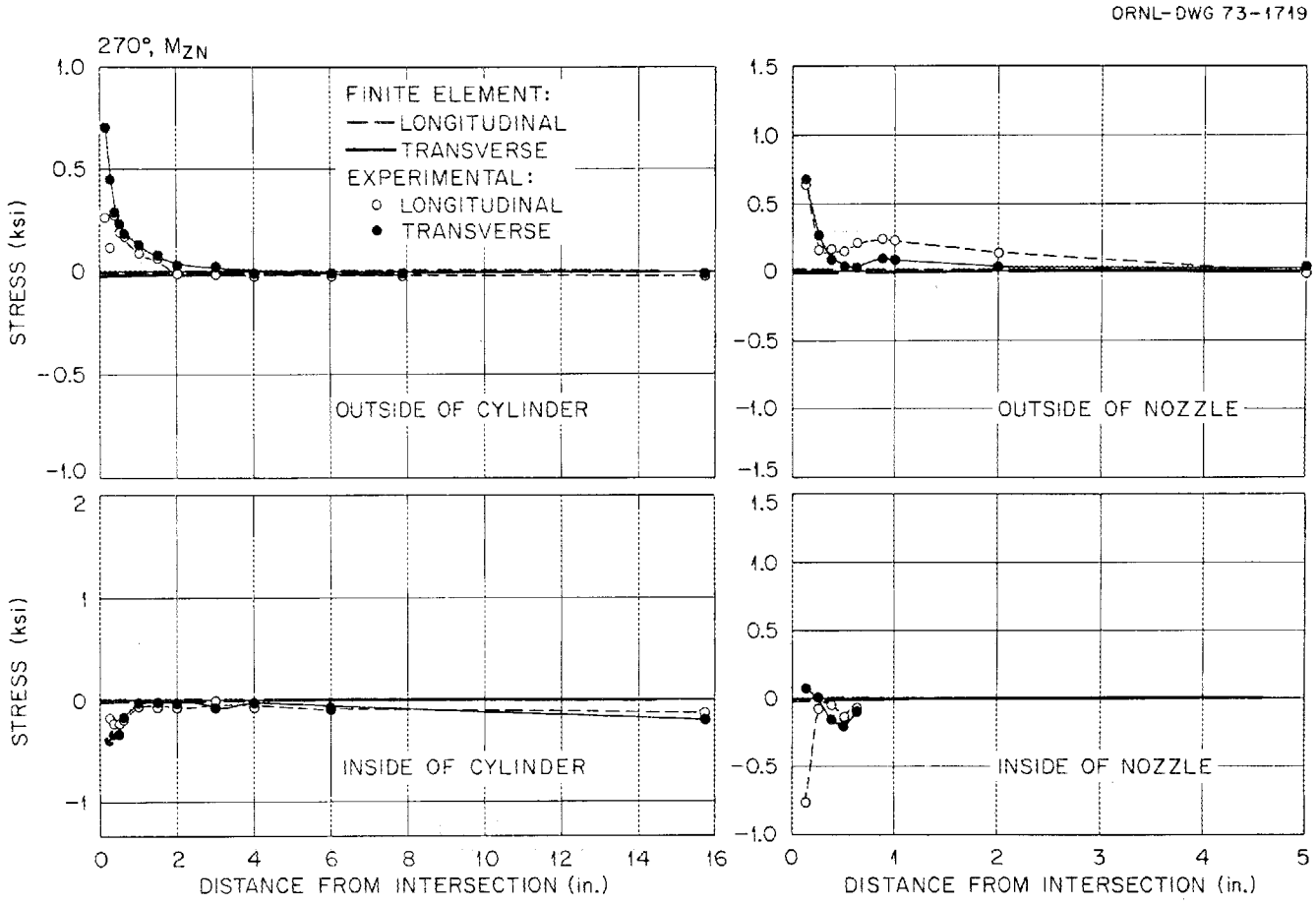

Fig. 43. Measured and predicted stress distributions at 270° for in-plane moment, M_{ZN}, on nozzle.

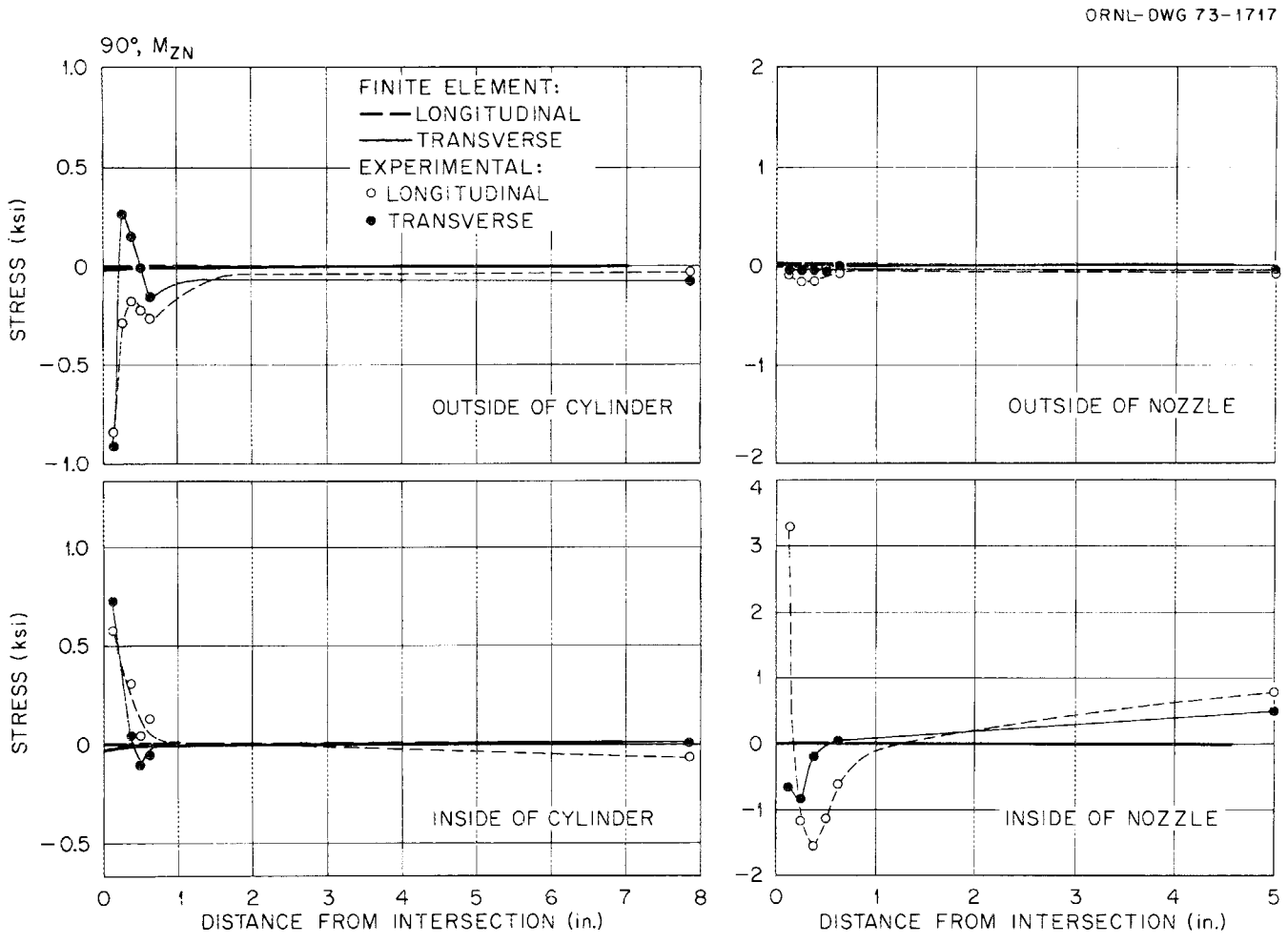

Fig. 44. Measured and predicted stress distributions at 90° for in-plane moment, M_{ZN}, on nozzle.

ORNL-DWG 73-1756

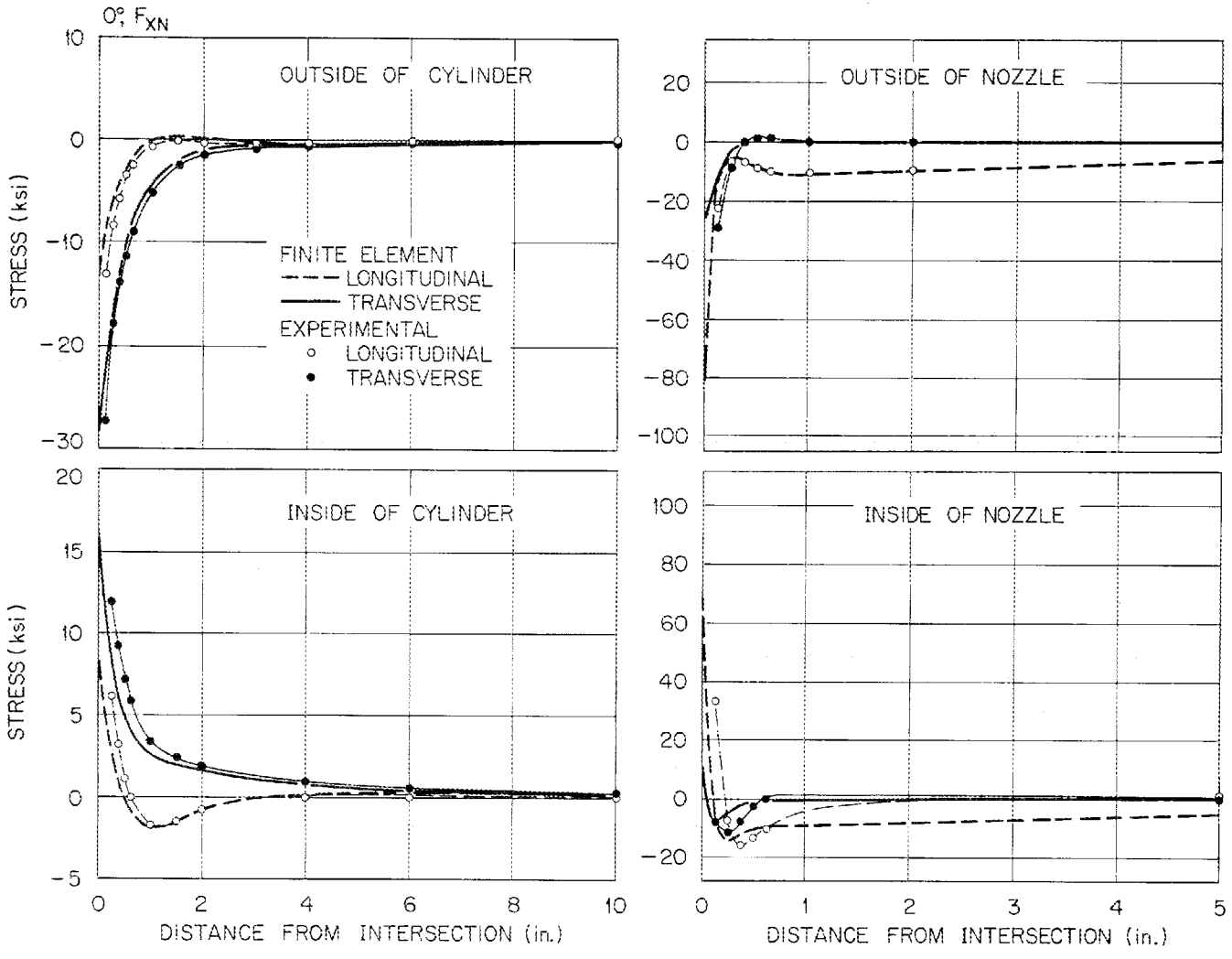

Fig. 45. Measured and predicted stress distributions at 0° for in-plane force, F_{XN}, on nozzle.

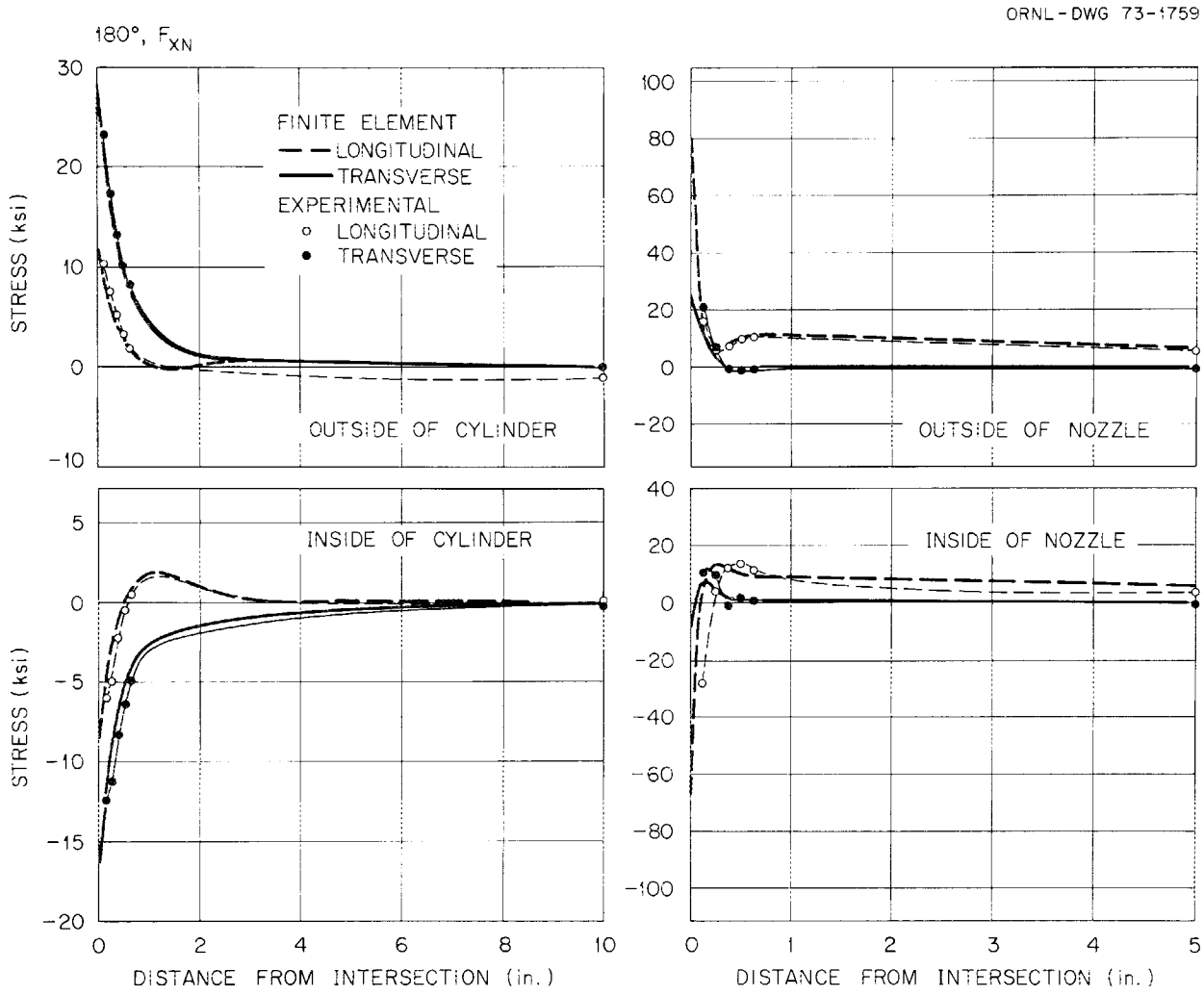

Fig. 46. Measured and predicted stress distributions at 180° for in-plane force, F_{XN}, on nozzle.

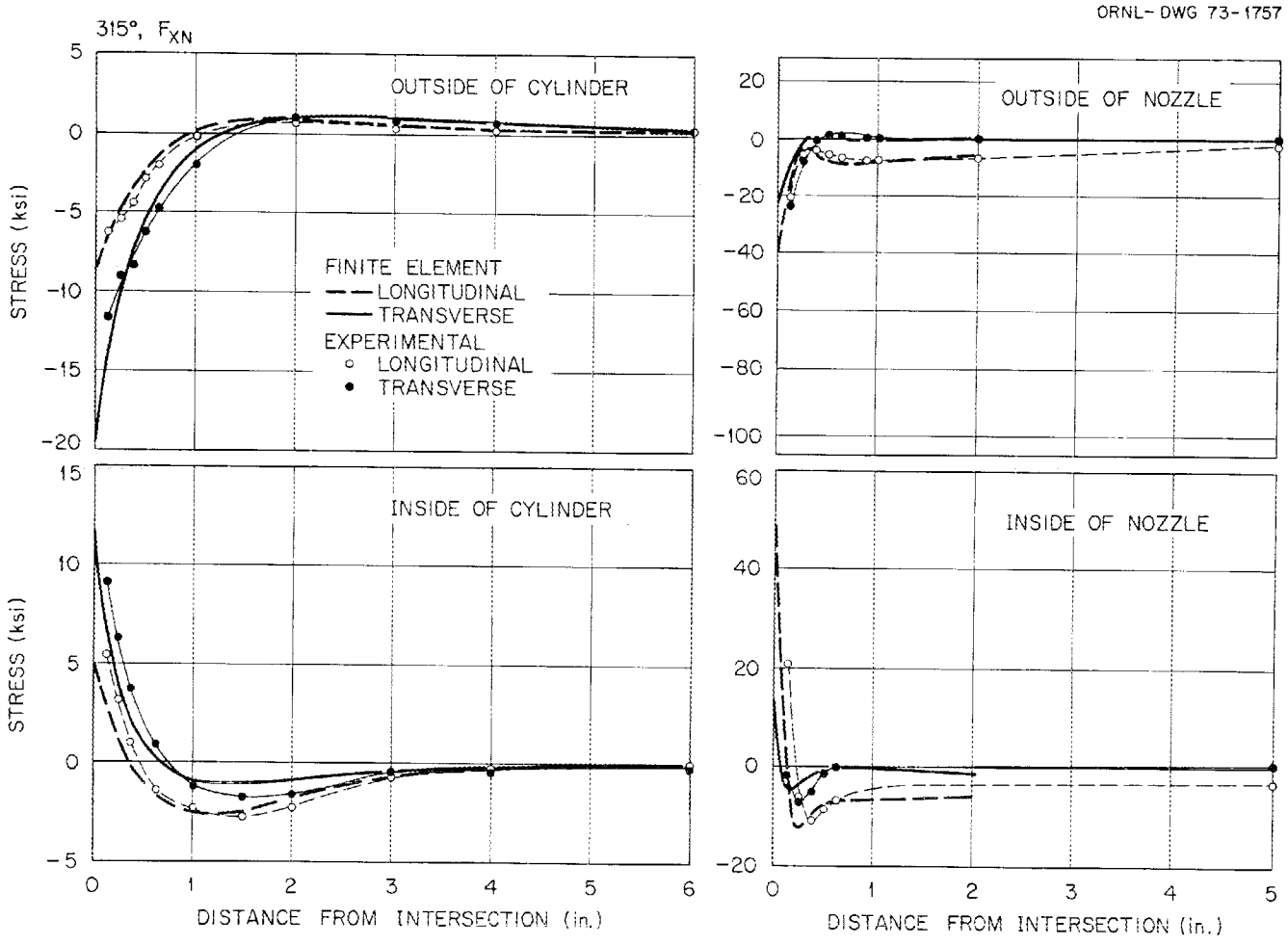

Fig. 47. Measured and predicted stress distributions at 315° for in-plane force, F_{XN}, on nozzle.

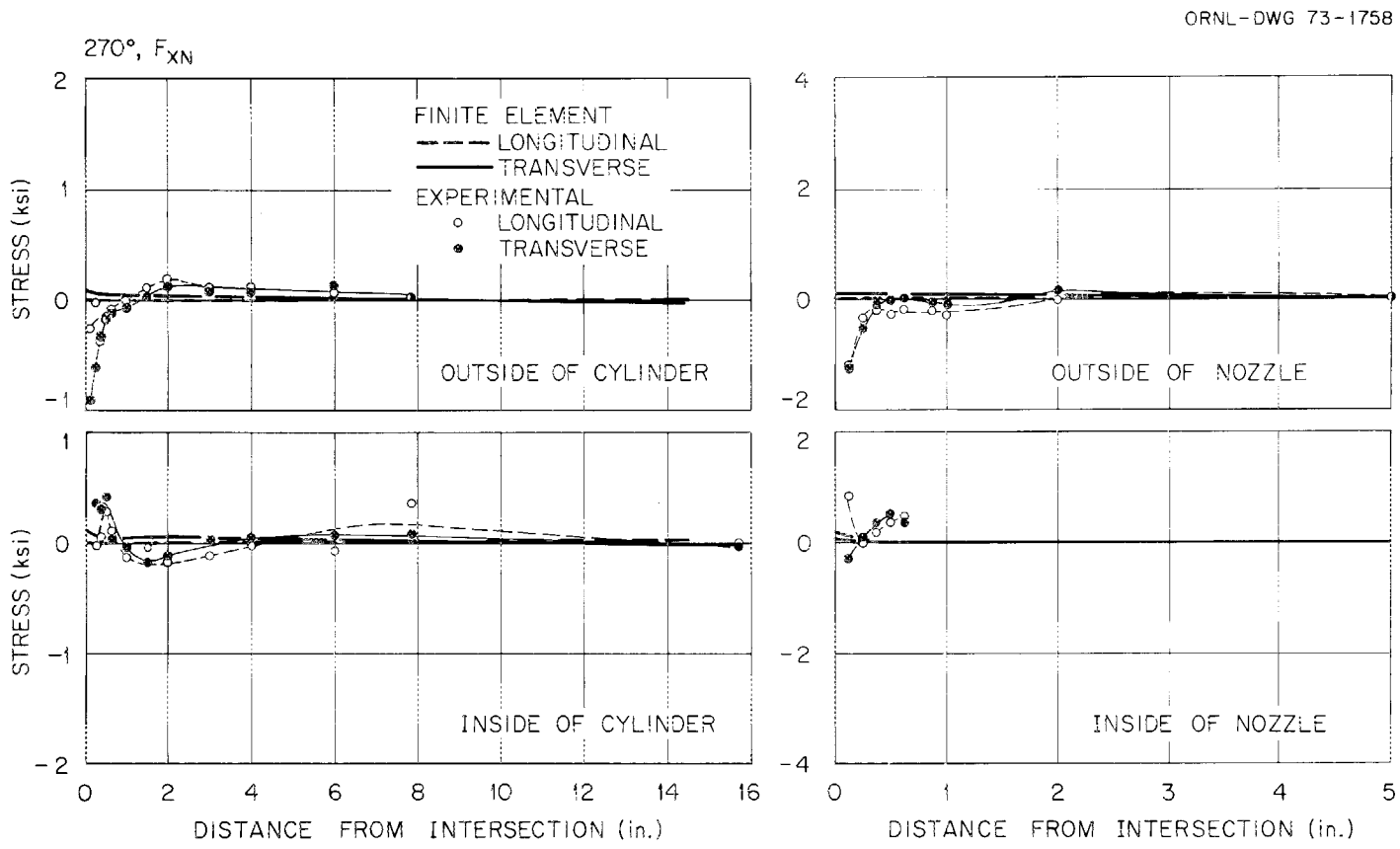

Fig. 48. Measured and predicted stress distributions at 270° for in-plane force, F_{XN}, on nozzle.

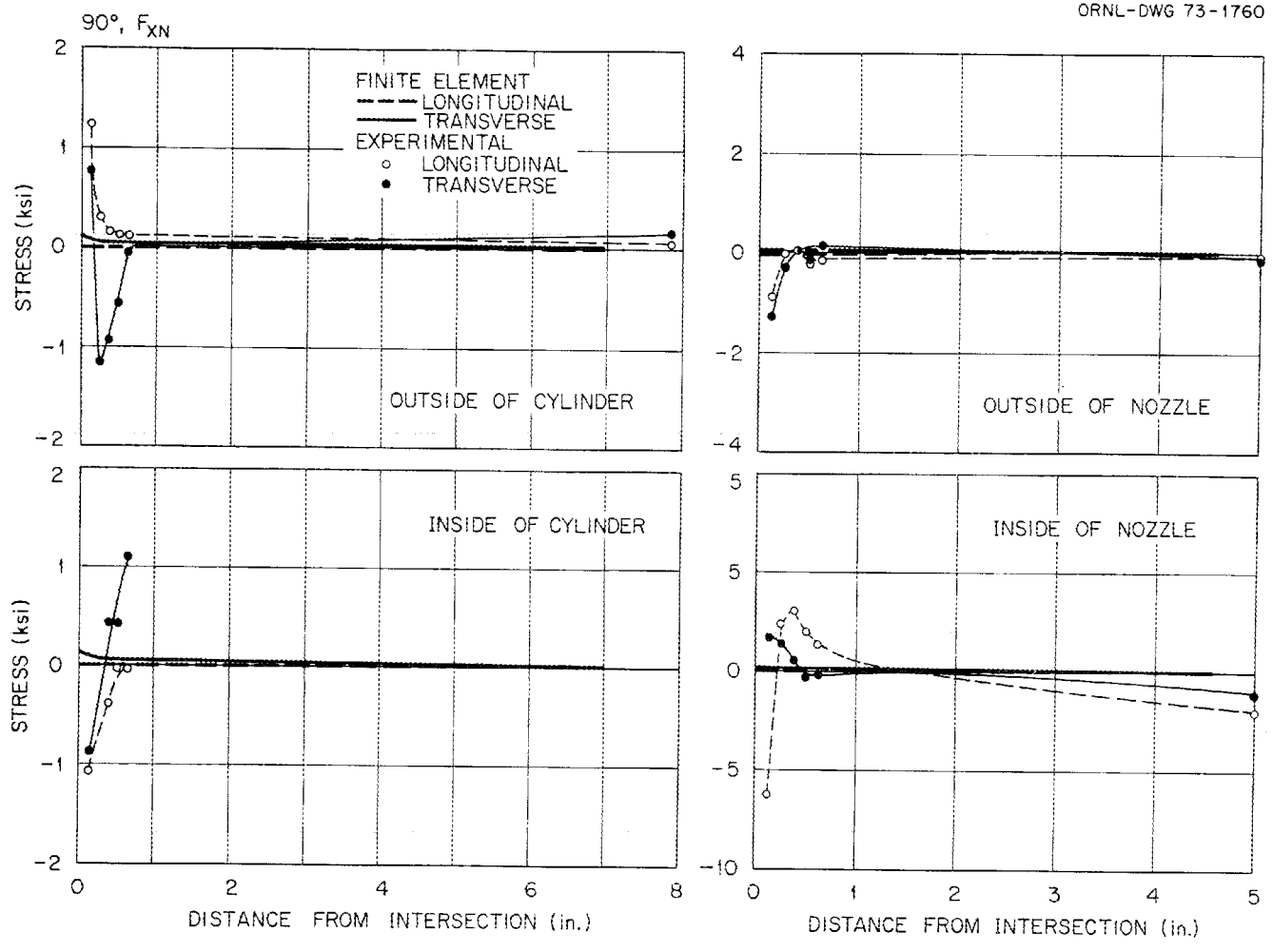

Fig. 49. Measured and predicted stress distributions at 90° for in-plane force, F_{XN}, on nozzle.

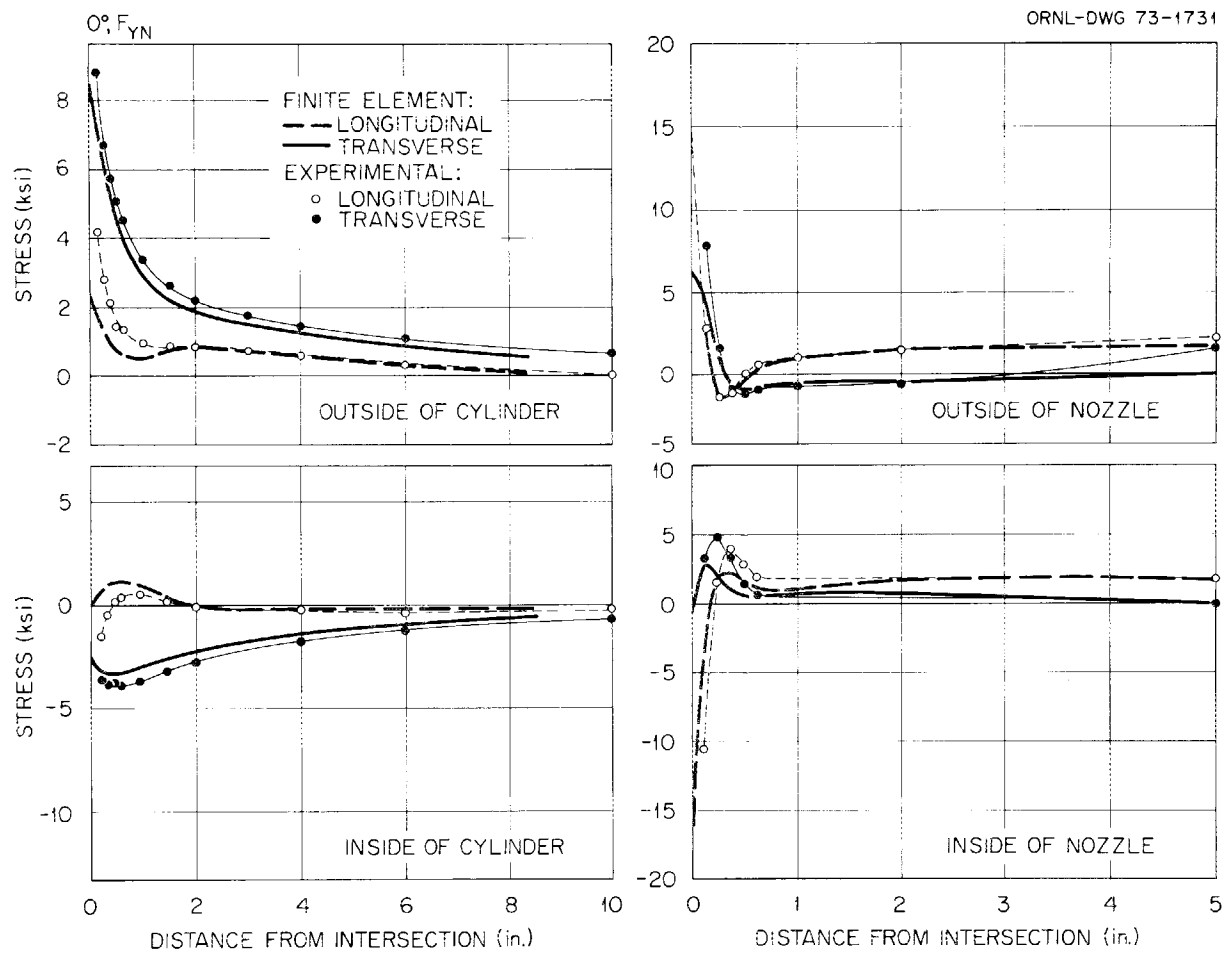

Fig. 50. Measured and predicted stress distributions at 0° for axial force, F_{YN}, on nozzle.

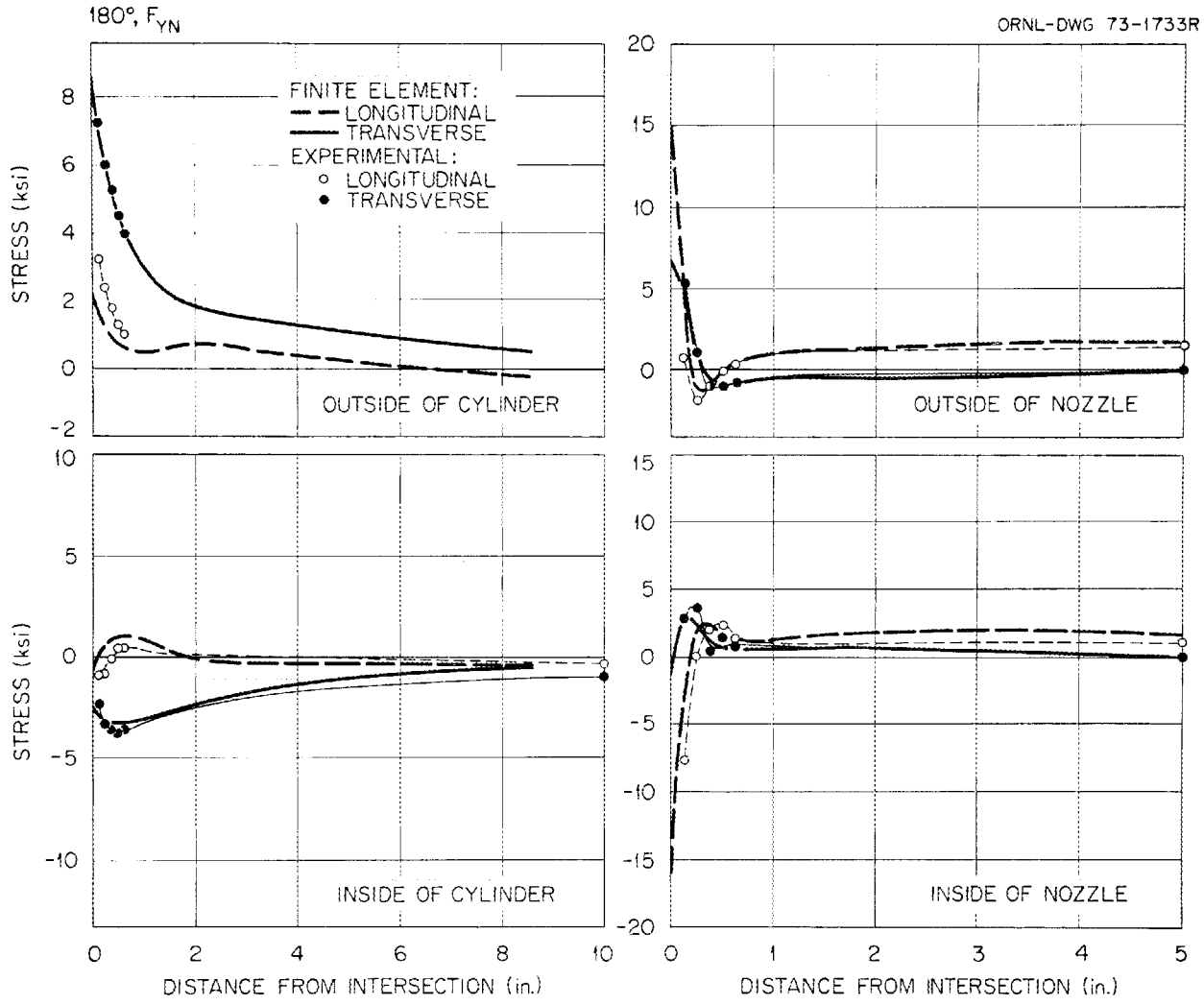

Fig. 51. Measured and predicted stress distributions at 180° for axial force, F_{YN}, on nozzle.

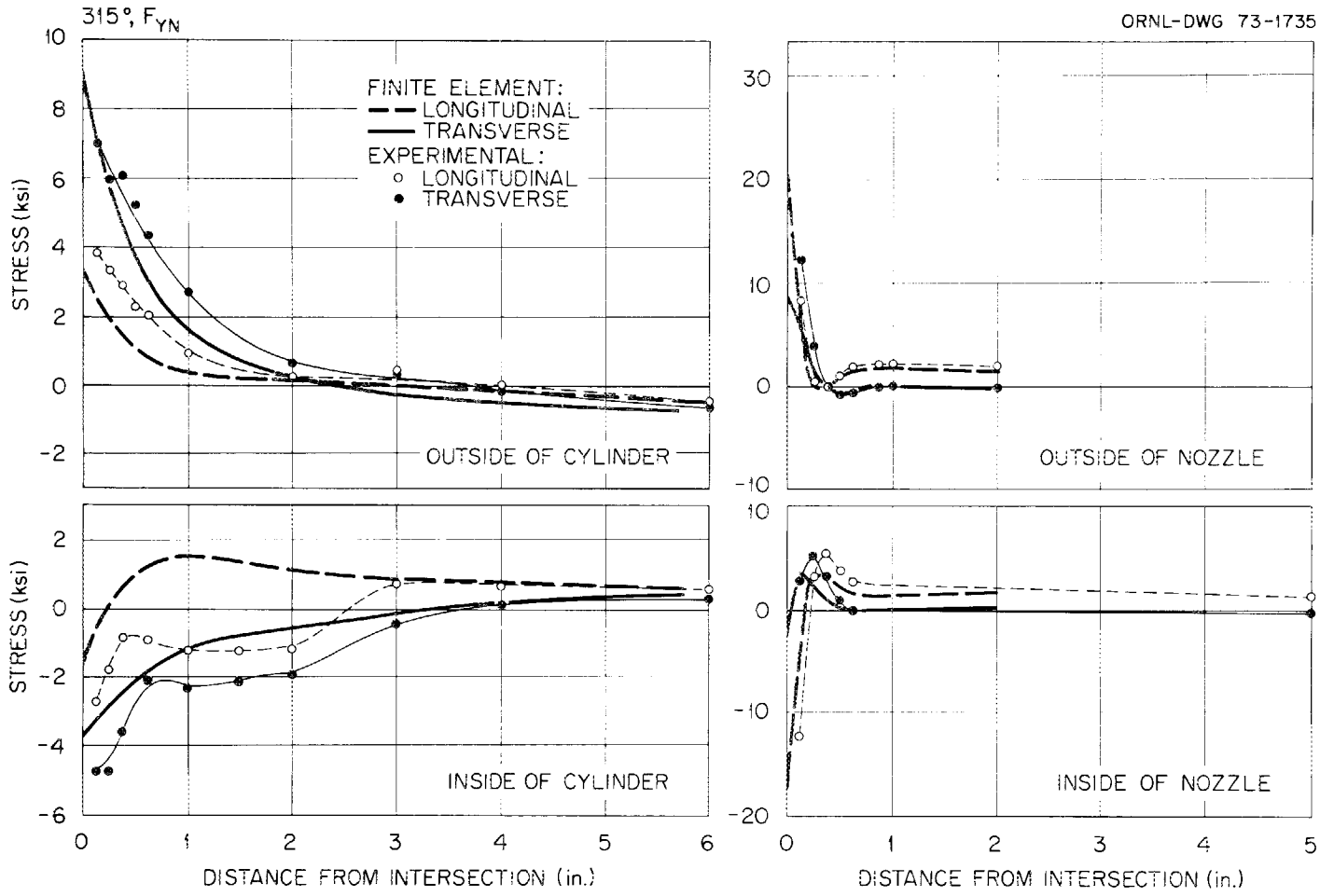

Fig. 52. Measured and predicted stress distributions at 315° for axial force, F_{YN}, on nozzle.

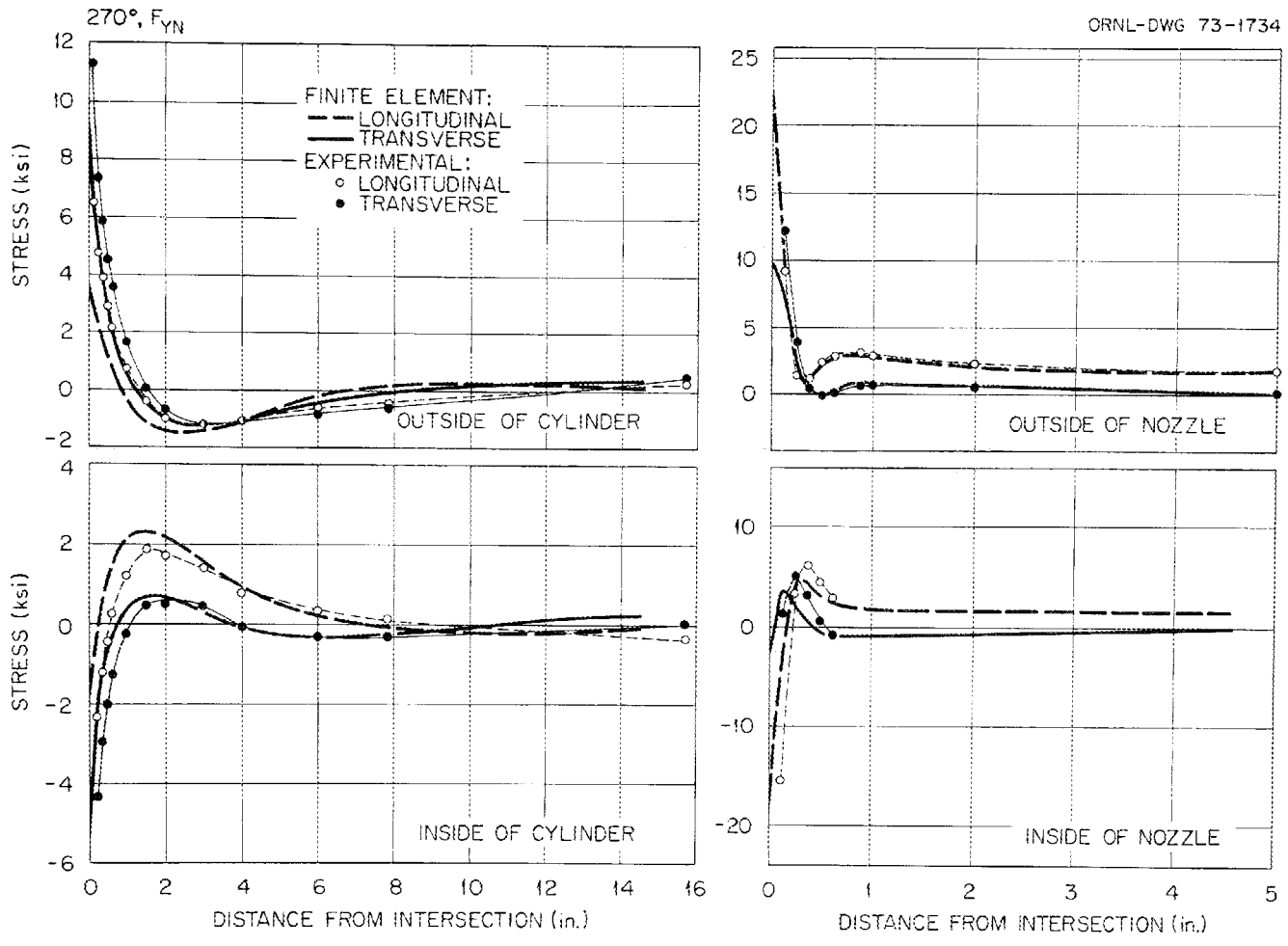

Fig. 53. Measured and predicted stress distributions at 270° for axial force, F_{YN}, on nozzle.

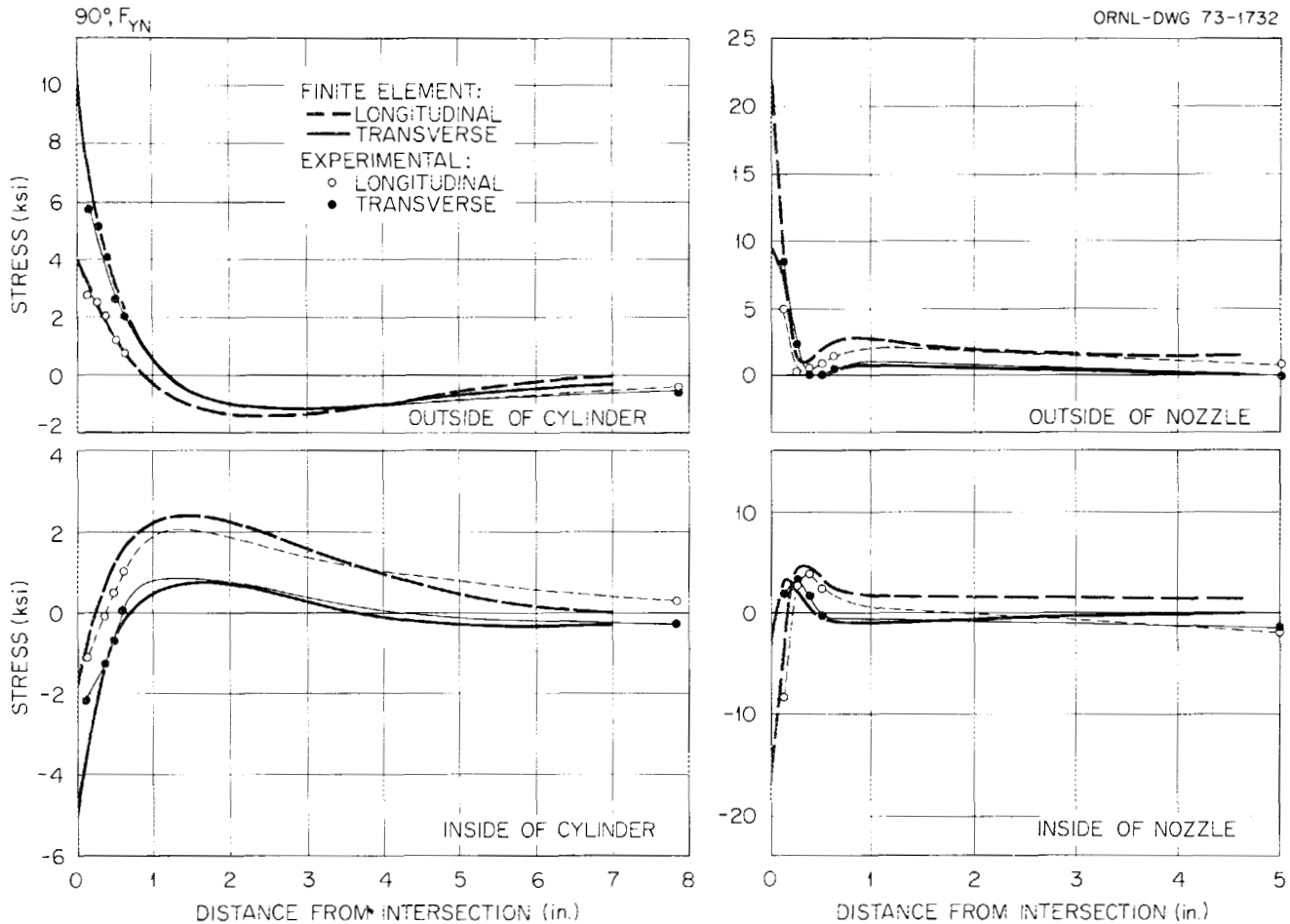

Fig. 54. Measured and predicted stress distributions at 90° for axial force, F_{YN}, on nozzle.

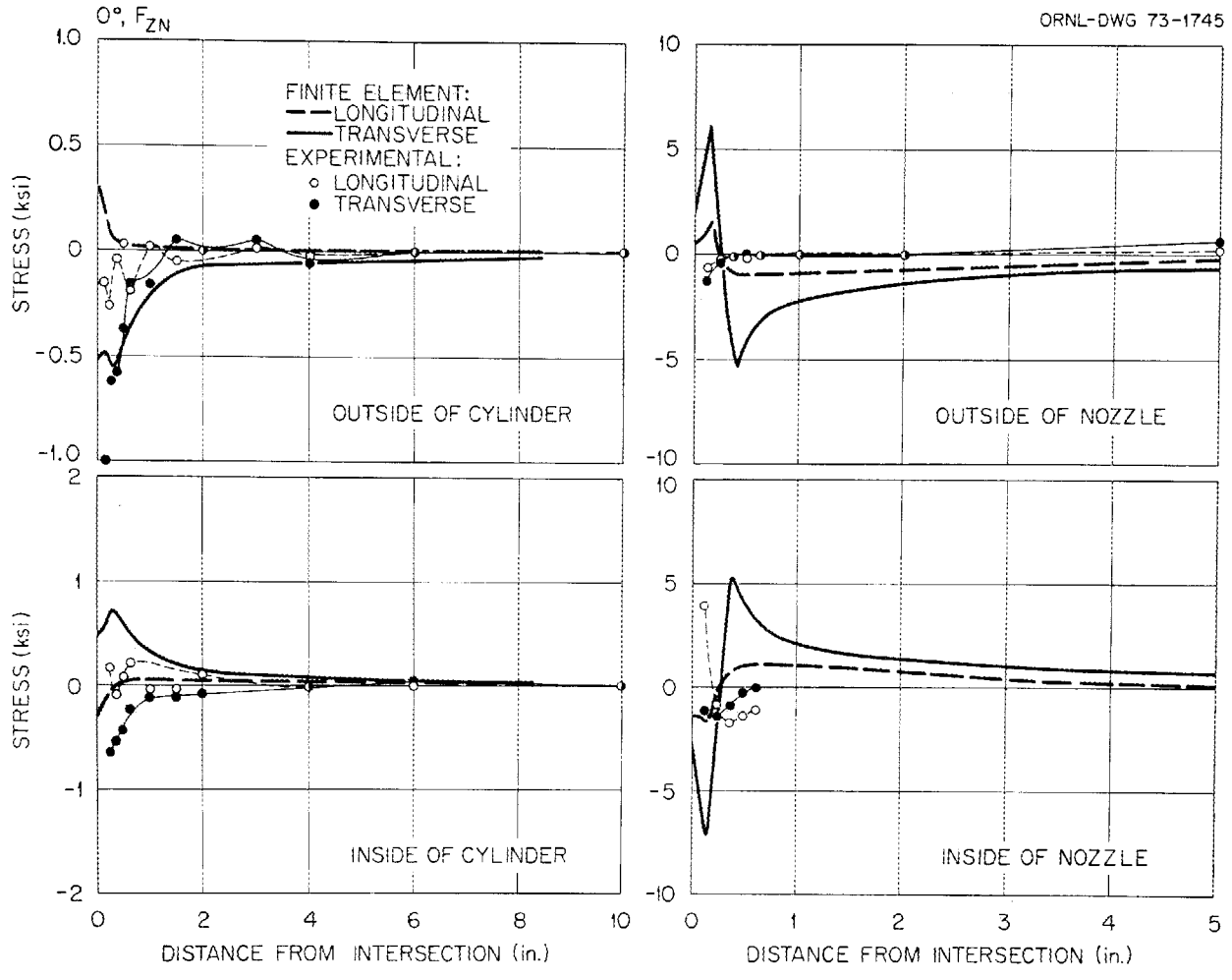

Fig. 55. Measured and predicted stress distributions at 0° for out-of-plane force, F_{ZN}, on nozzle.

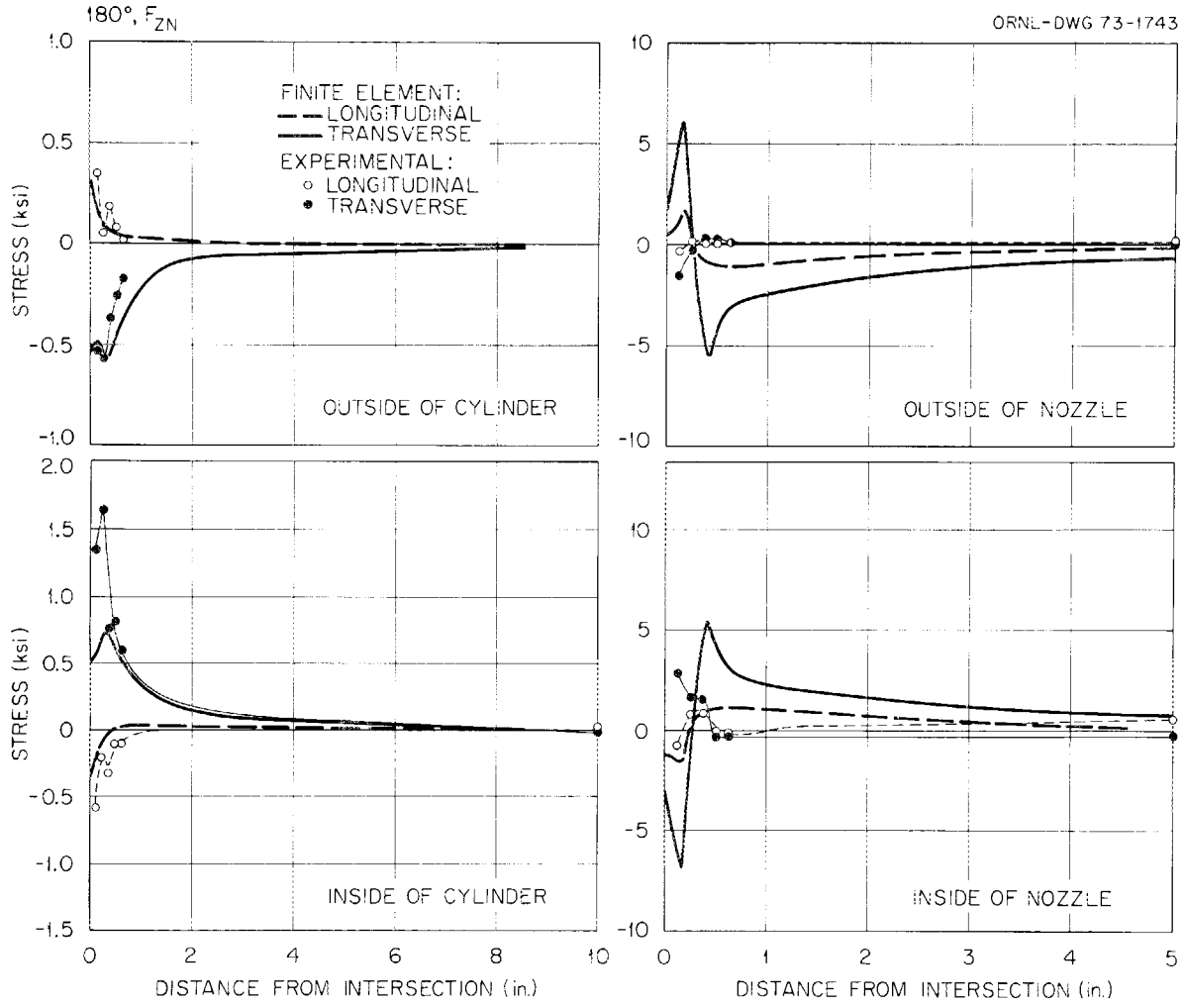

Fig. 56. Measured and predicted stress distributions at 180° for out-of-plane force, F_{ZN}, on nozzle.

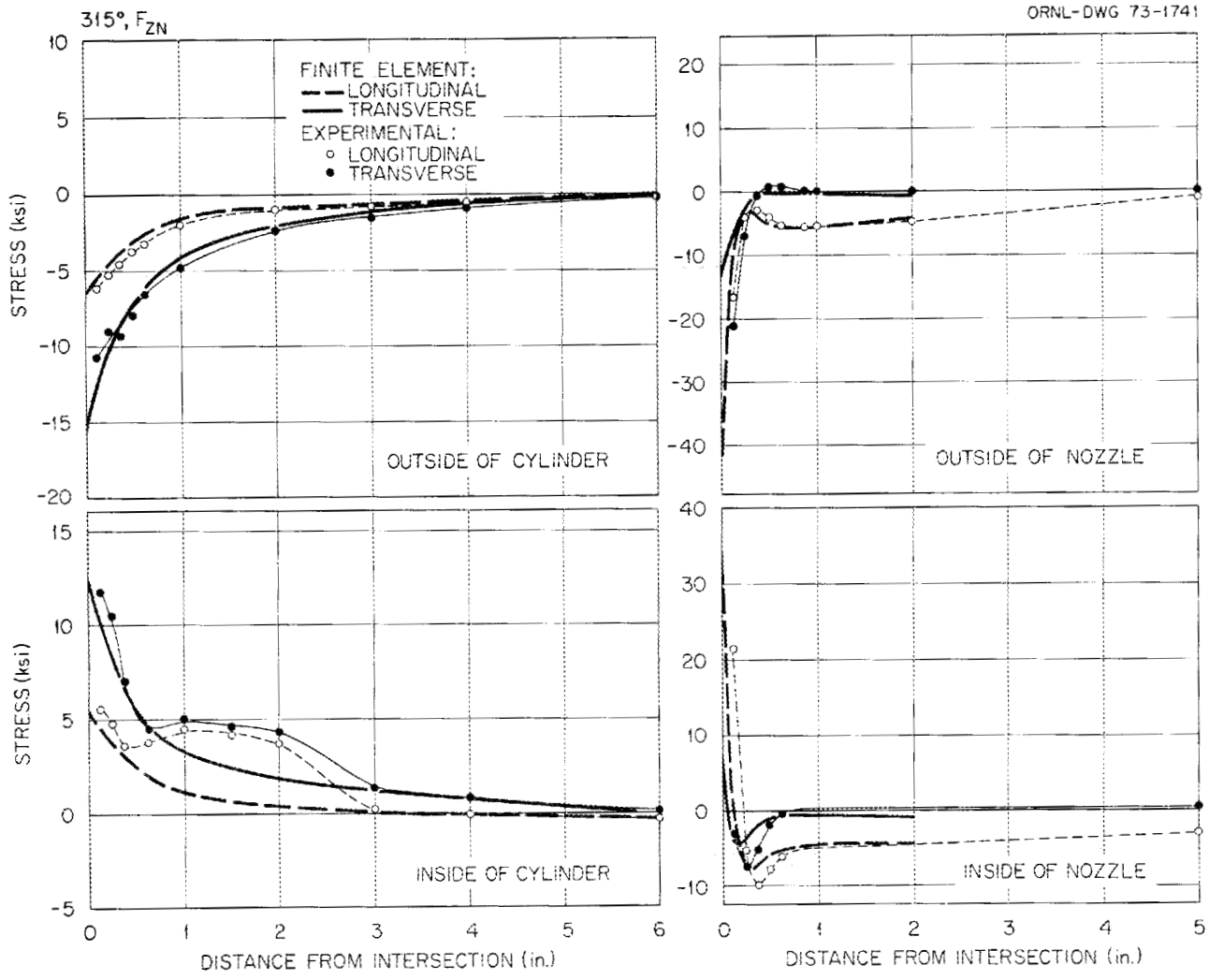

Fig. 57. Measured and predicted stress distributions at 315° for out-of-plane force, F_{ZN}, on nozzle.

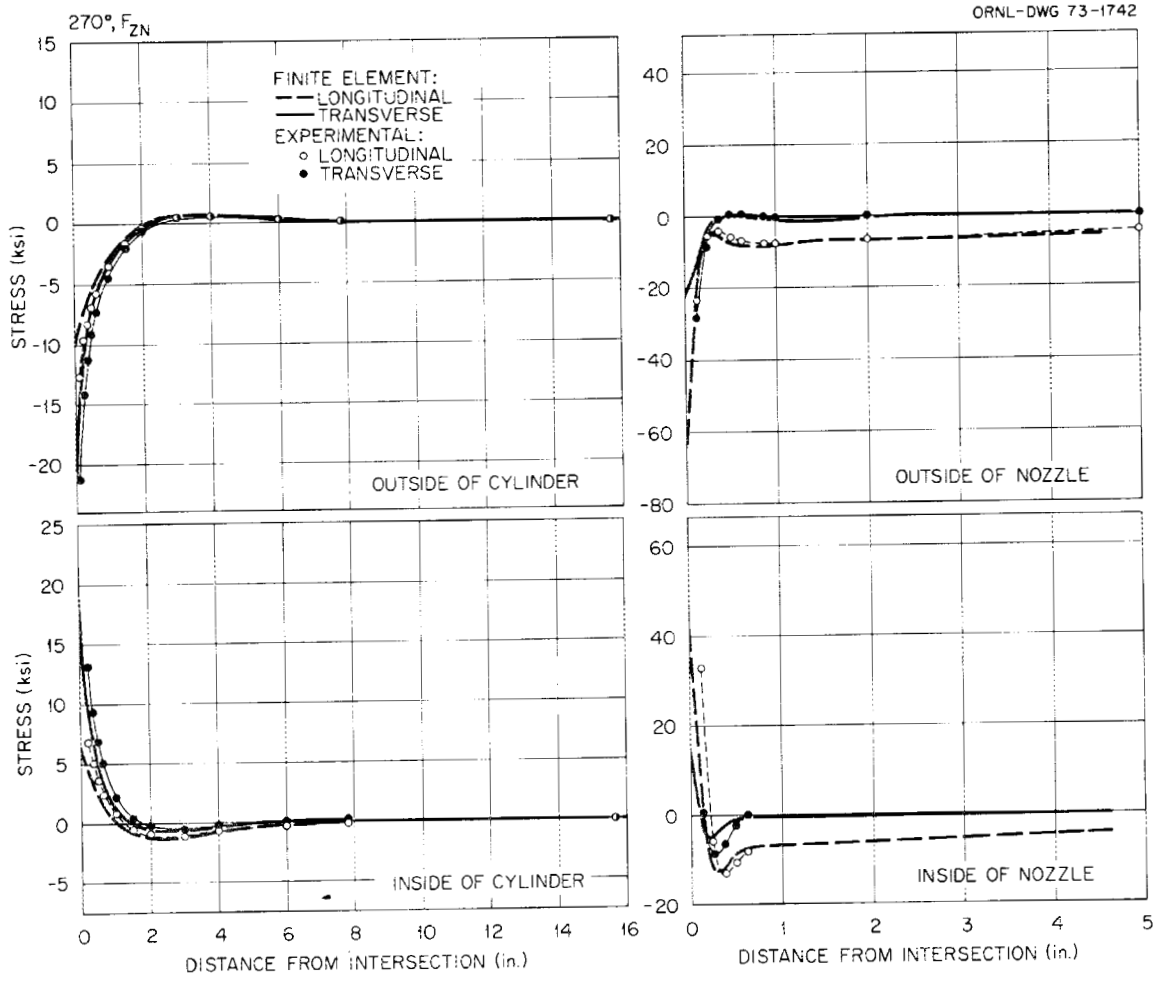

Fig. 58. Measured and predicted stress distributions at 270° for out-of-plane force, F_{ZN}, on nozzle.

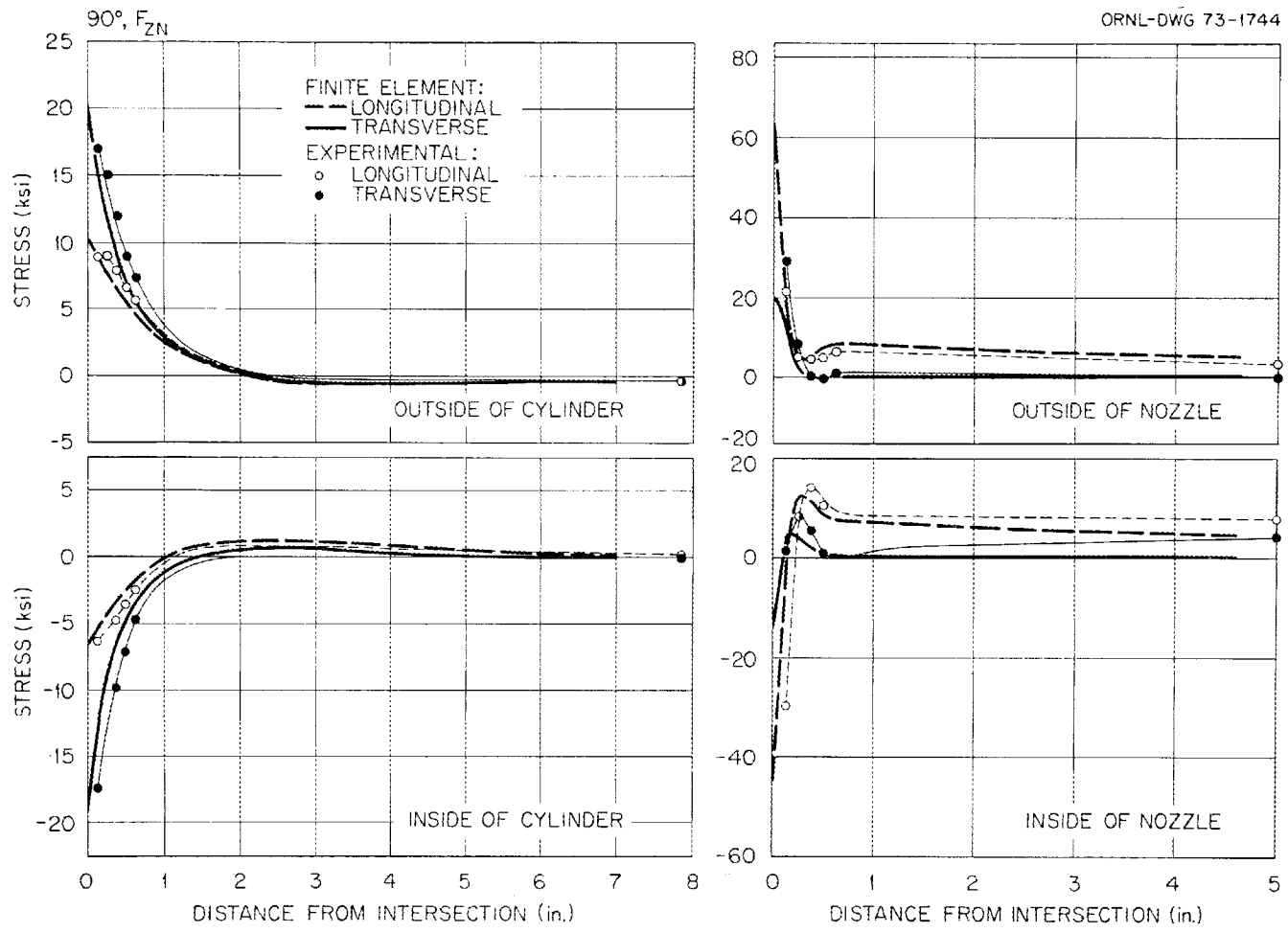

Fig. 59. Measured and predicted stress distributions at 90° for out-of-plane force, F_{ZN}, on nozzle.

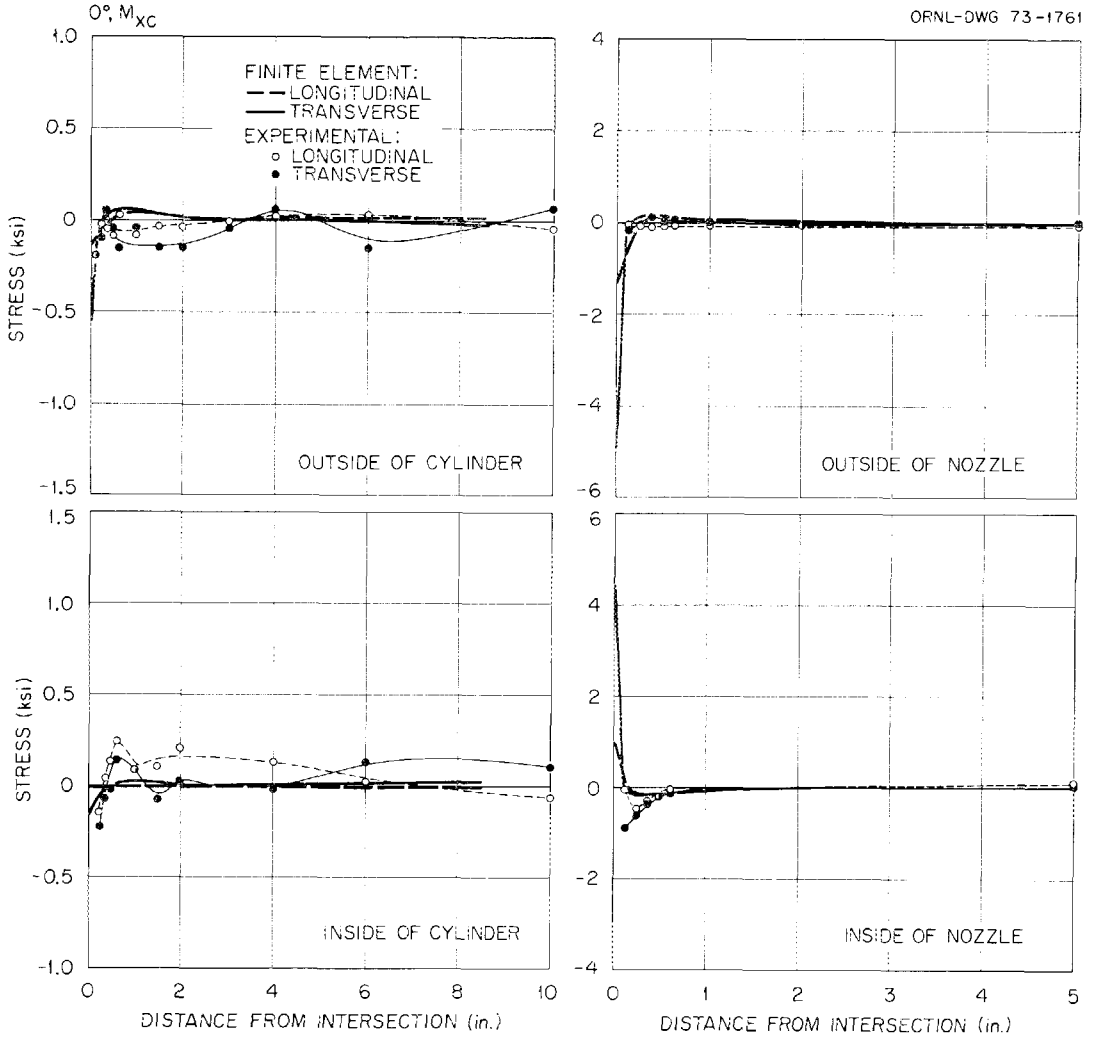

Fig. 60. Measured and predicted stress distributions at 0° for torsional moment, M_{XC}, on cylinder.

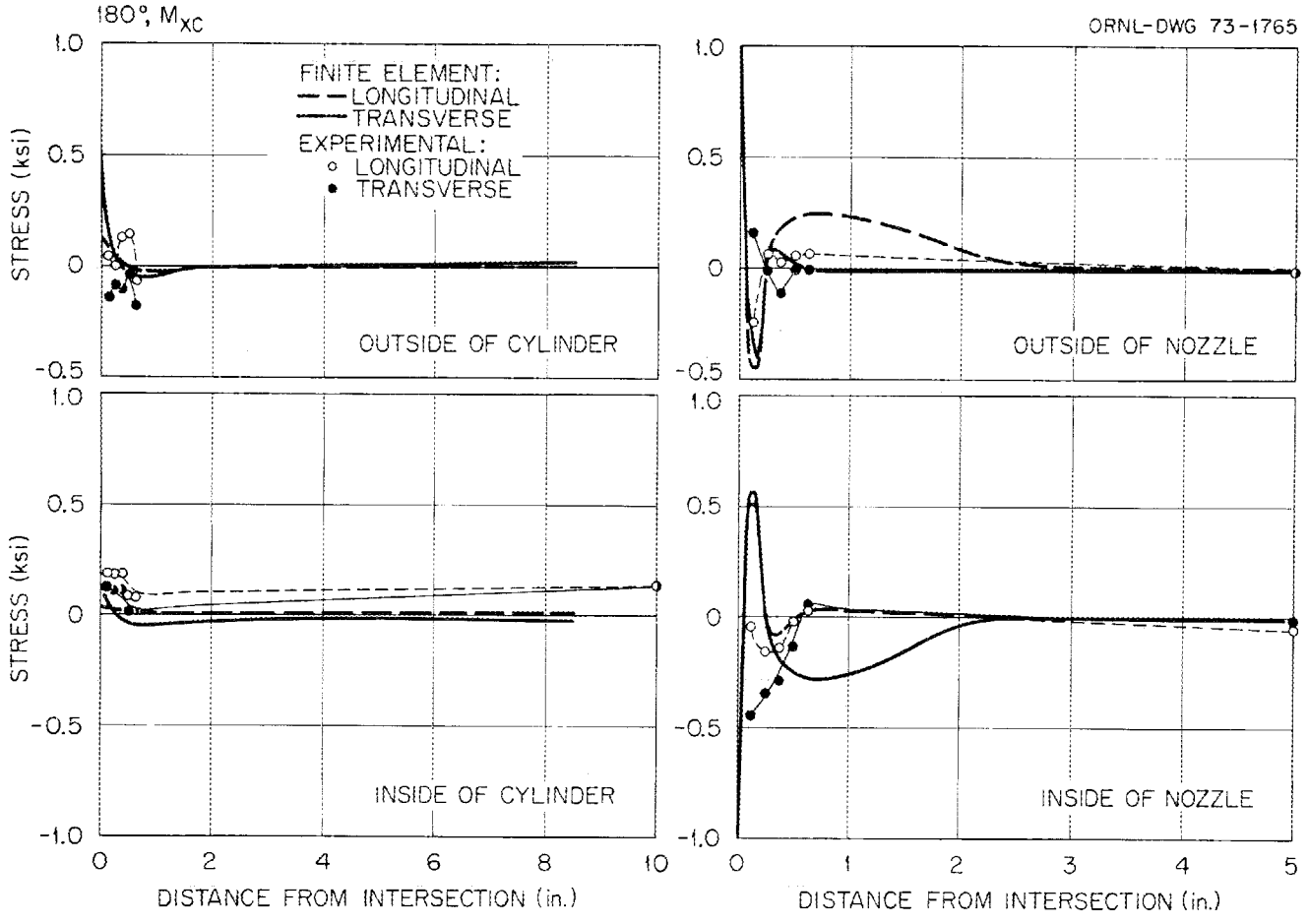

Fig. 61. Measured and predicted stress distributions at 180° for torsional moment, M_{XC}, on cylinder.

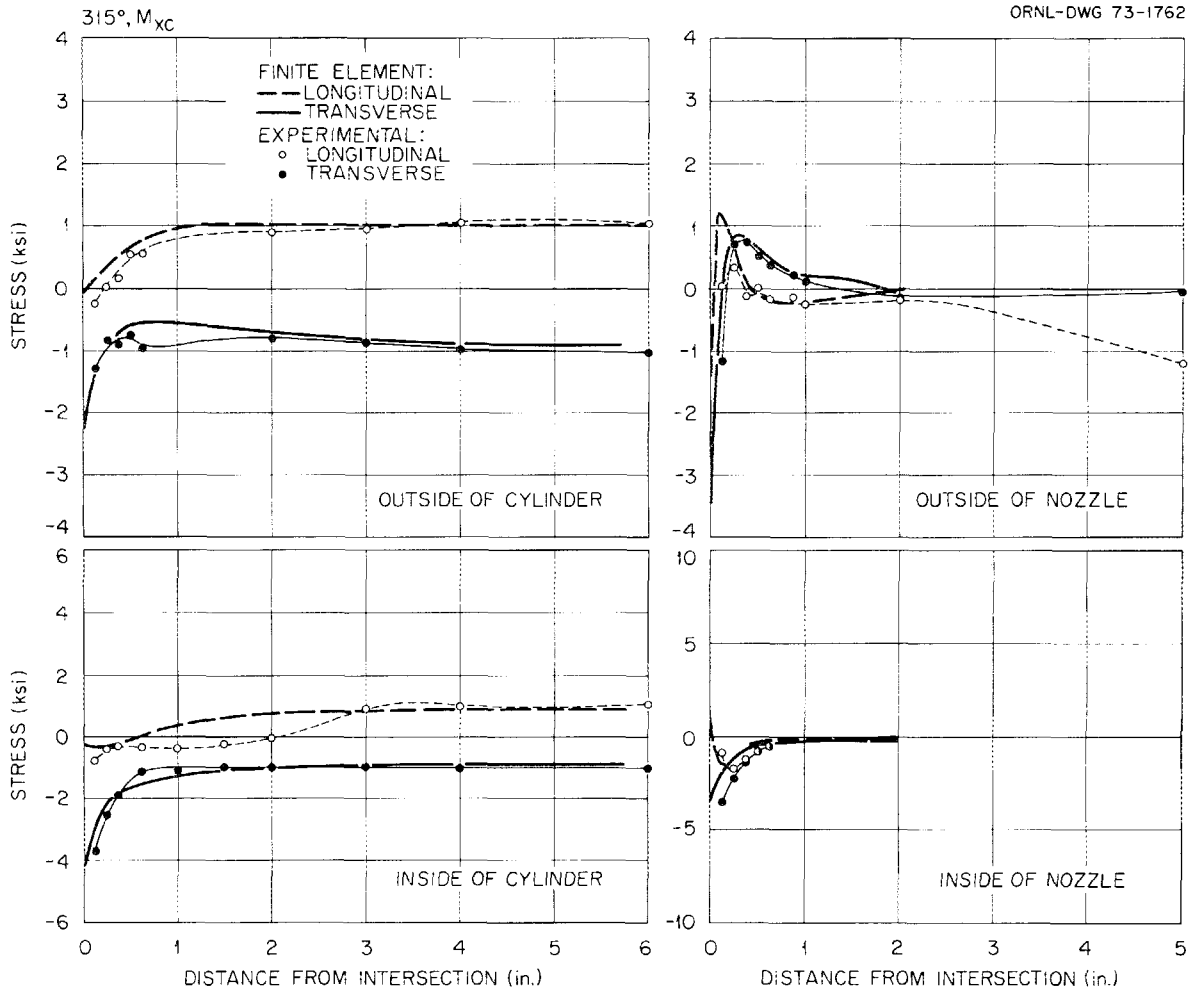

Fig. 62. Measured and predicted stress distributions at 315° for torsional moment, M_{XC}, on cylinder.

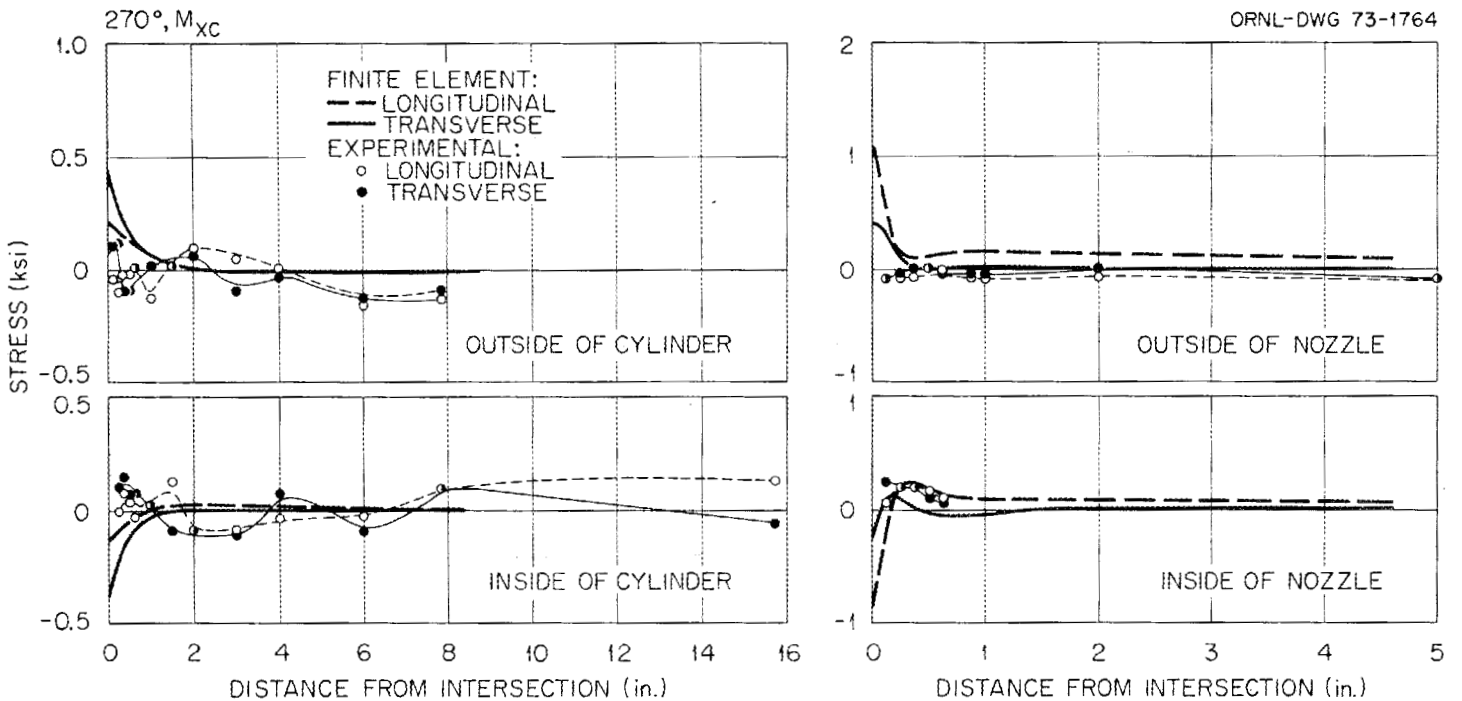

Fig. 63. Measured and predicted stress distributions at 270° for torsional moment, M_{XC}, on cylinder.

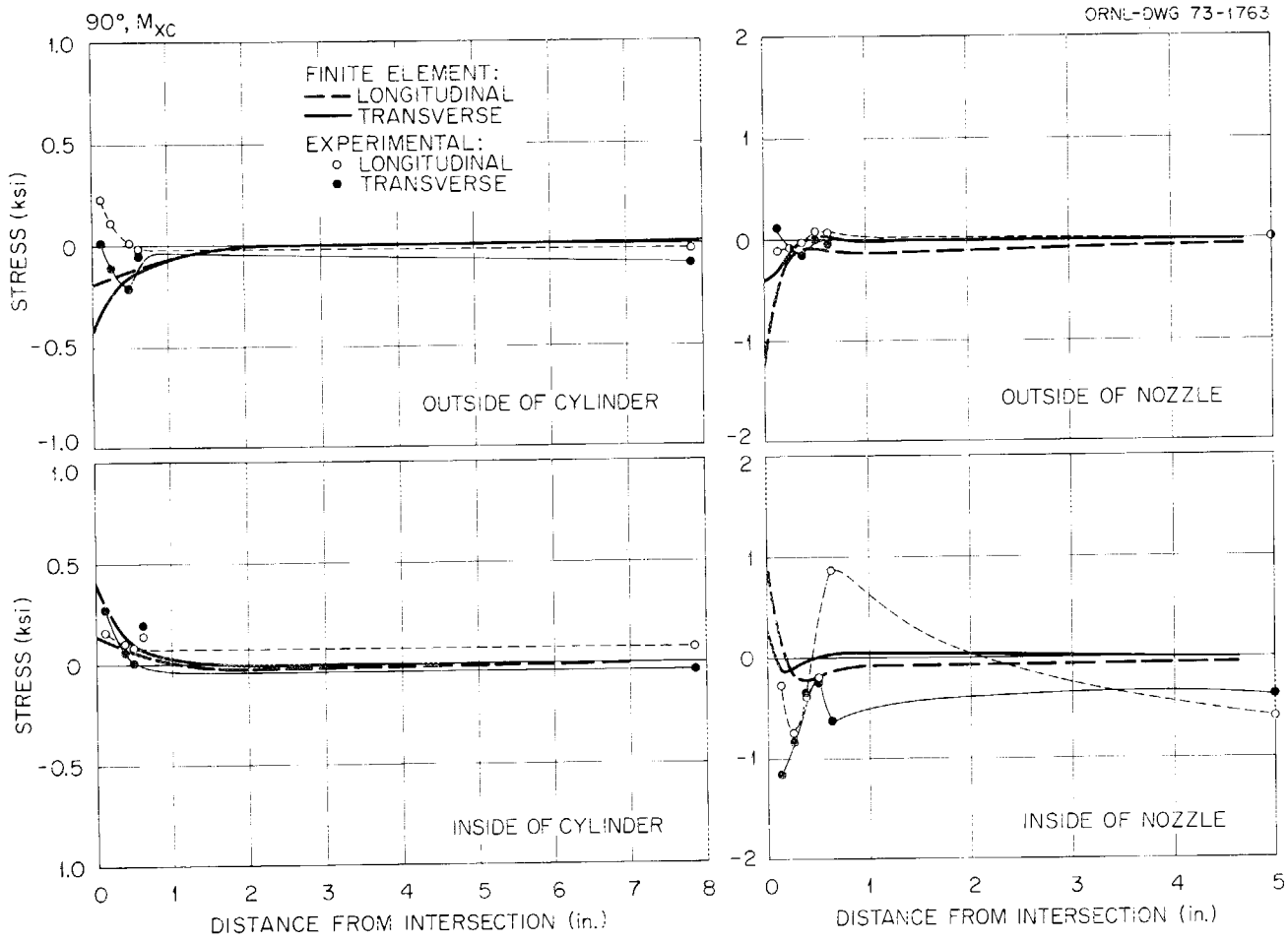

Fig. 64. Measured and predicted stress distributions at 90° for torsional moment, M_{XC}, on cylinder.

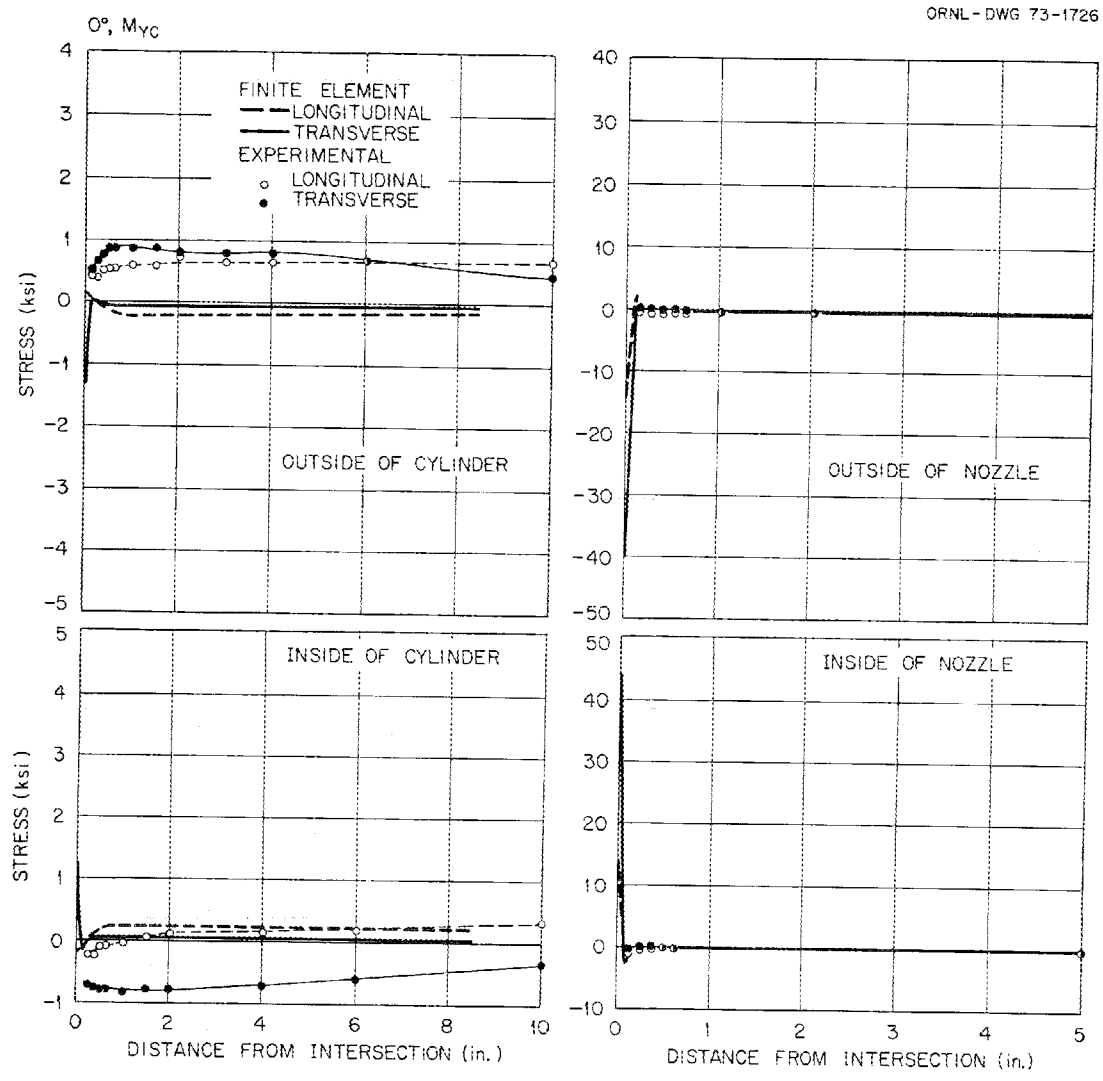

Fig. 65. Measured and predicted stress distributions at 0° for out-of-plane moment, M_{YC}, on cylinder.

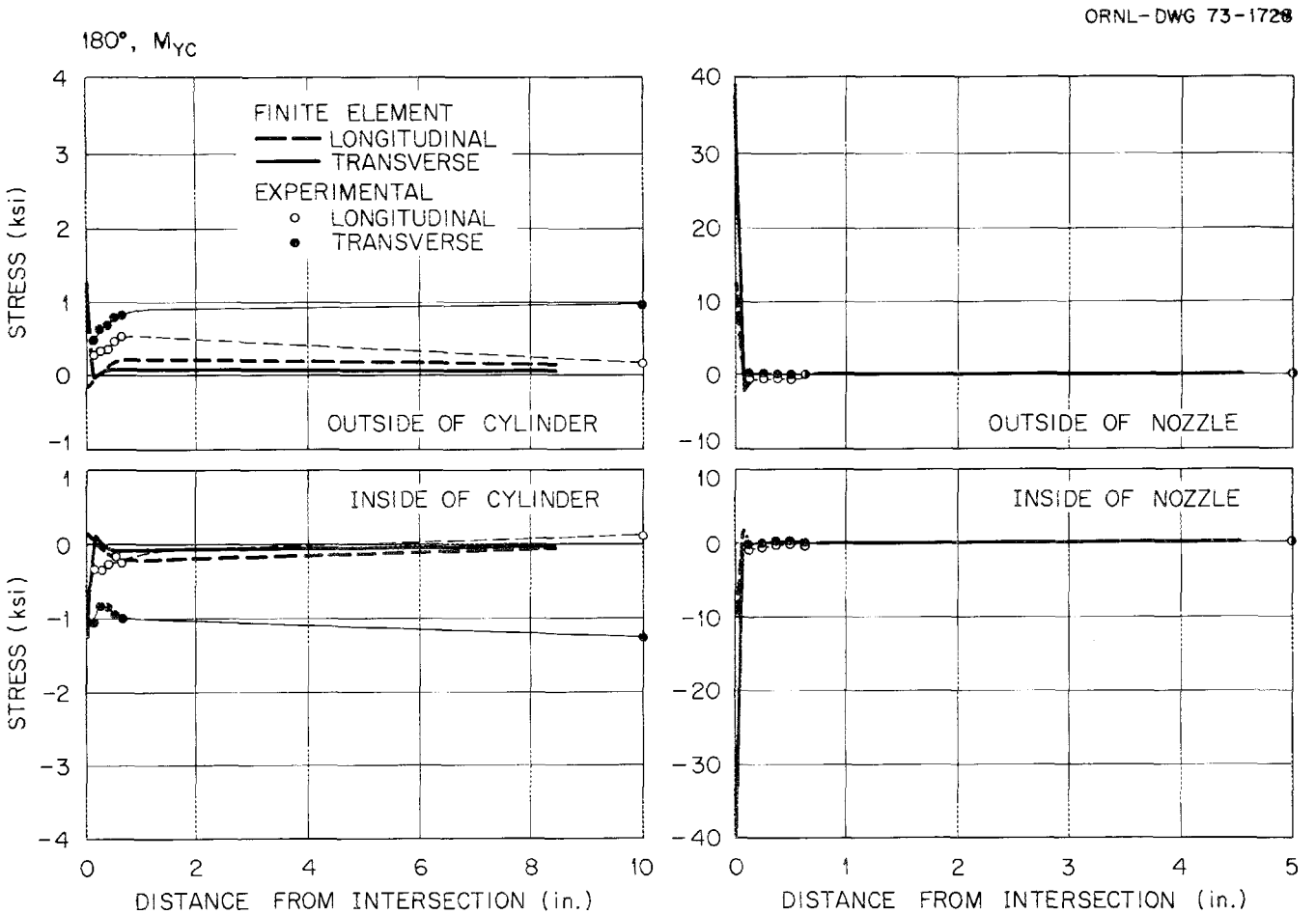

Fig. 66. Measured and predicted stress distributions at 180° for out-of-plane moment, M_{YC}, on cylinder.

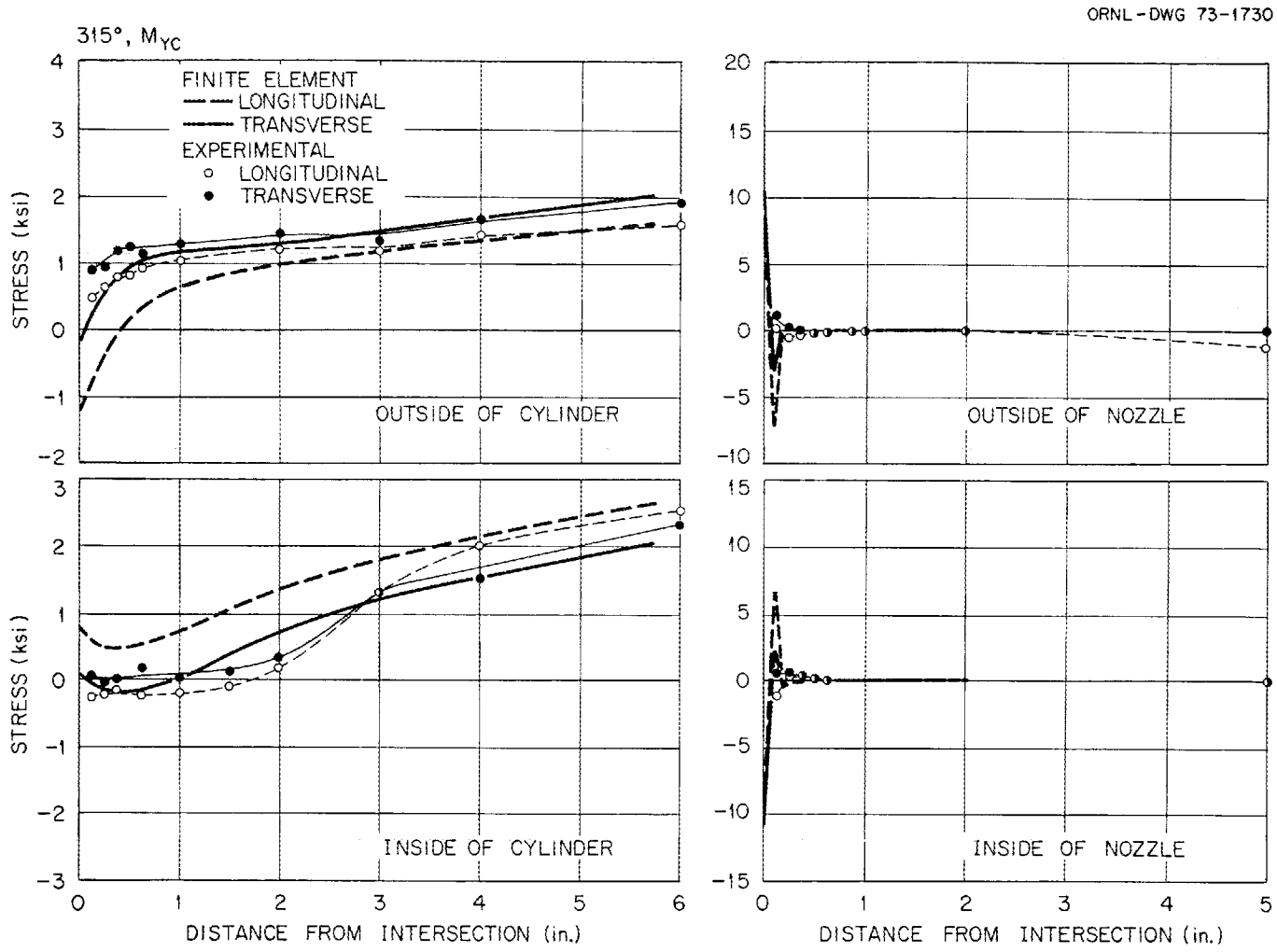

Fig. 67. Measured and predicted stress distributions at 315° for out-of-plane moment, M_{YC}, on cylinder.

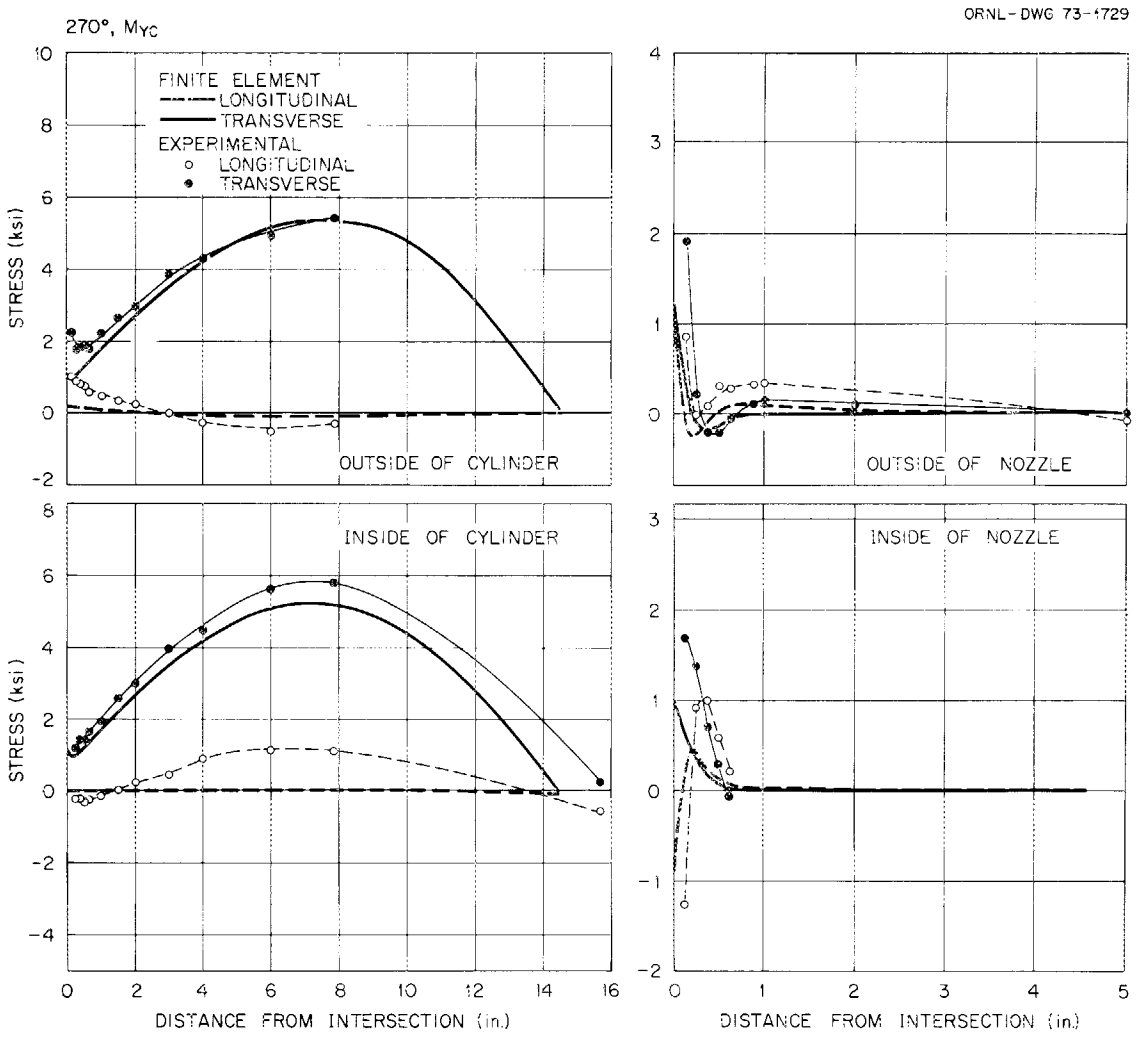

Fig. 68. Measured and predicted stress distributions at 270° for out-of-plane moment, M_{YC}, on cylinder.

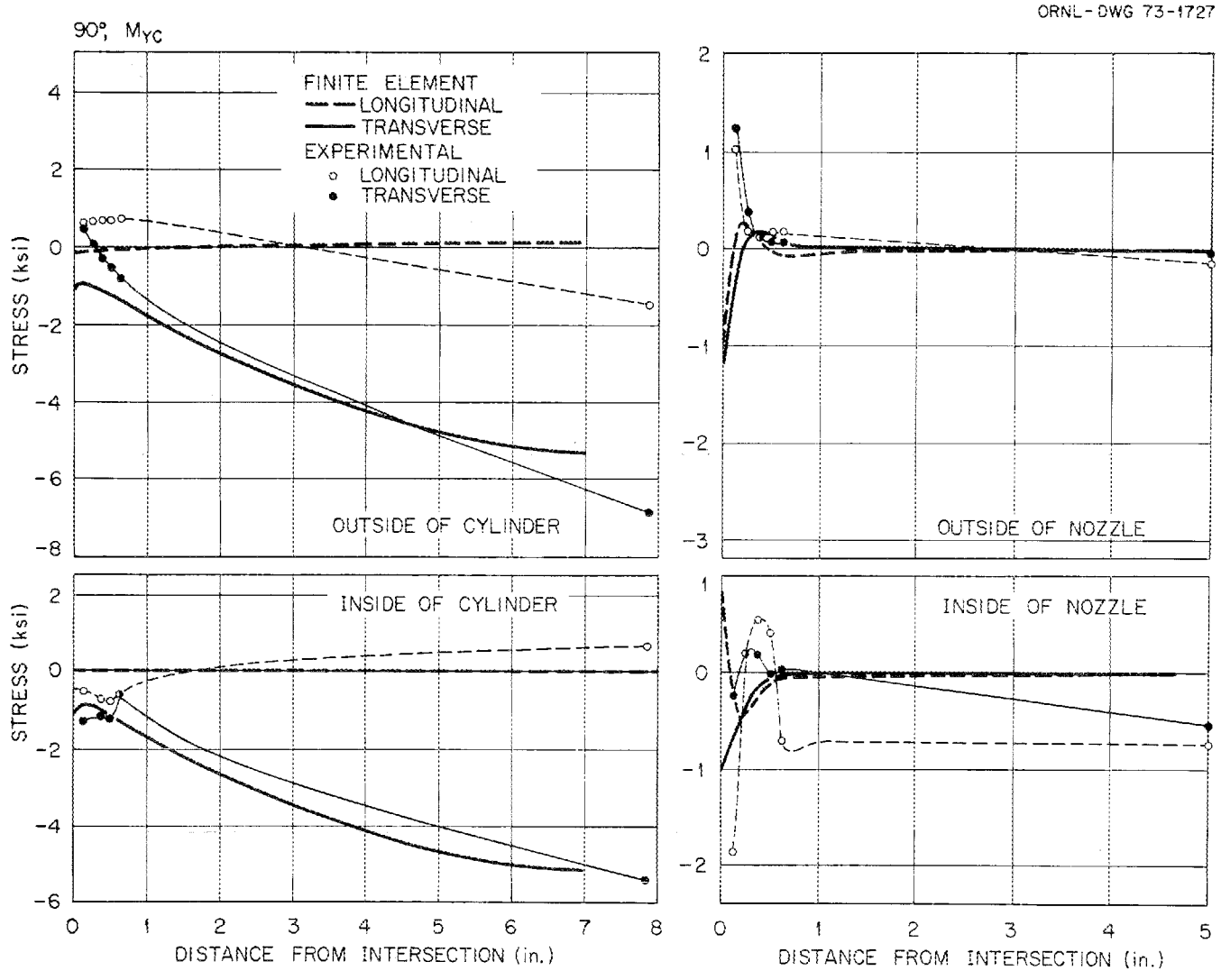

Fig. 69. Measured and predicted stress distributions at 90° for out-of-plane moment, M_{YC}, on cylinder.

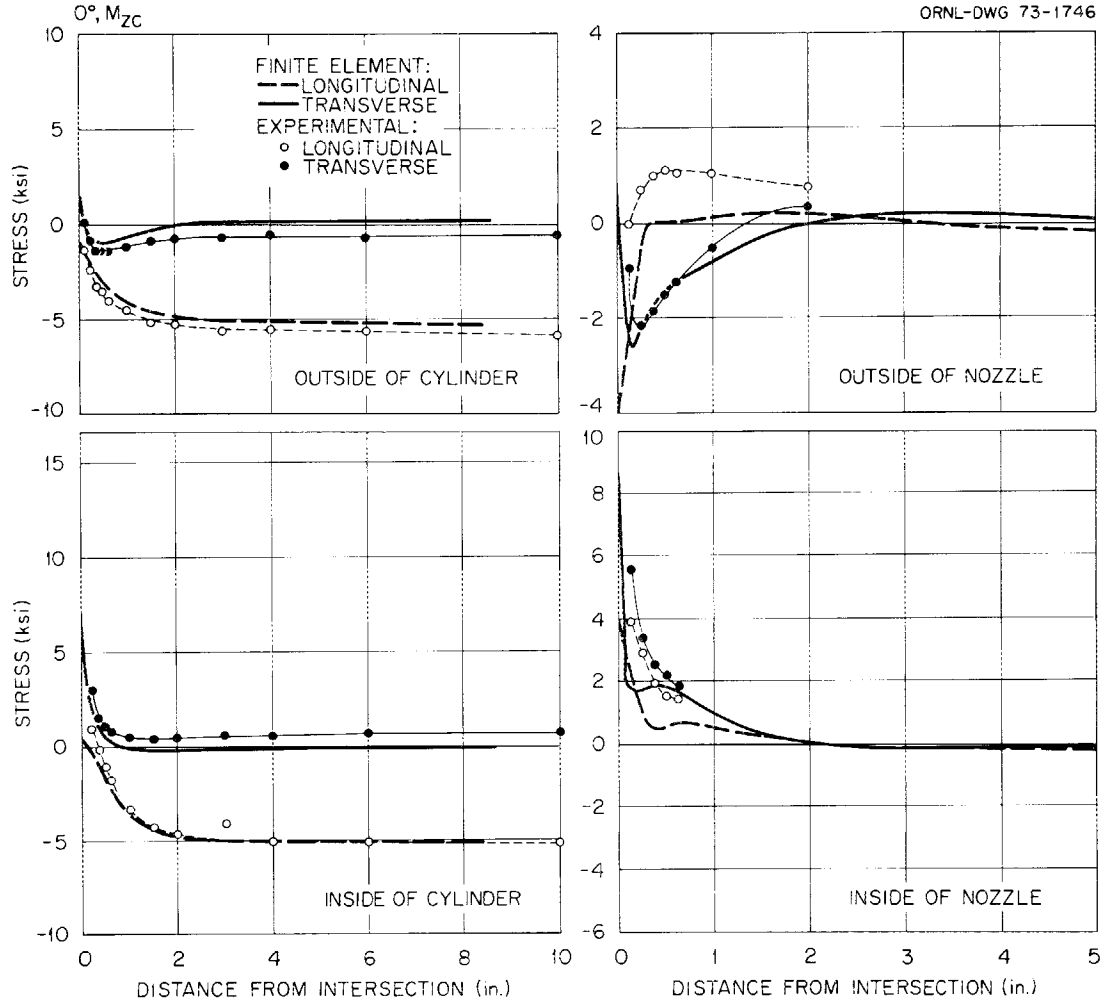

Fig. 70. Measured and predicted stress distributions at 0° for in-plane moment, M_{ZC}, on cylinder.

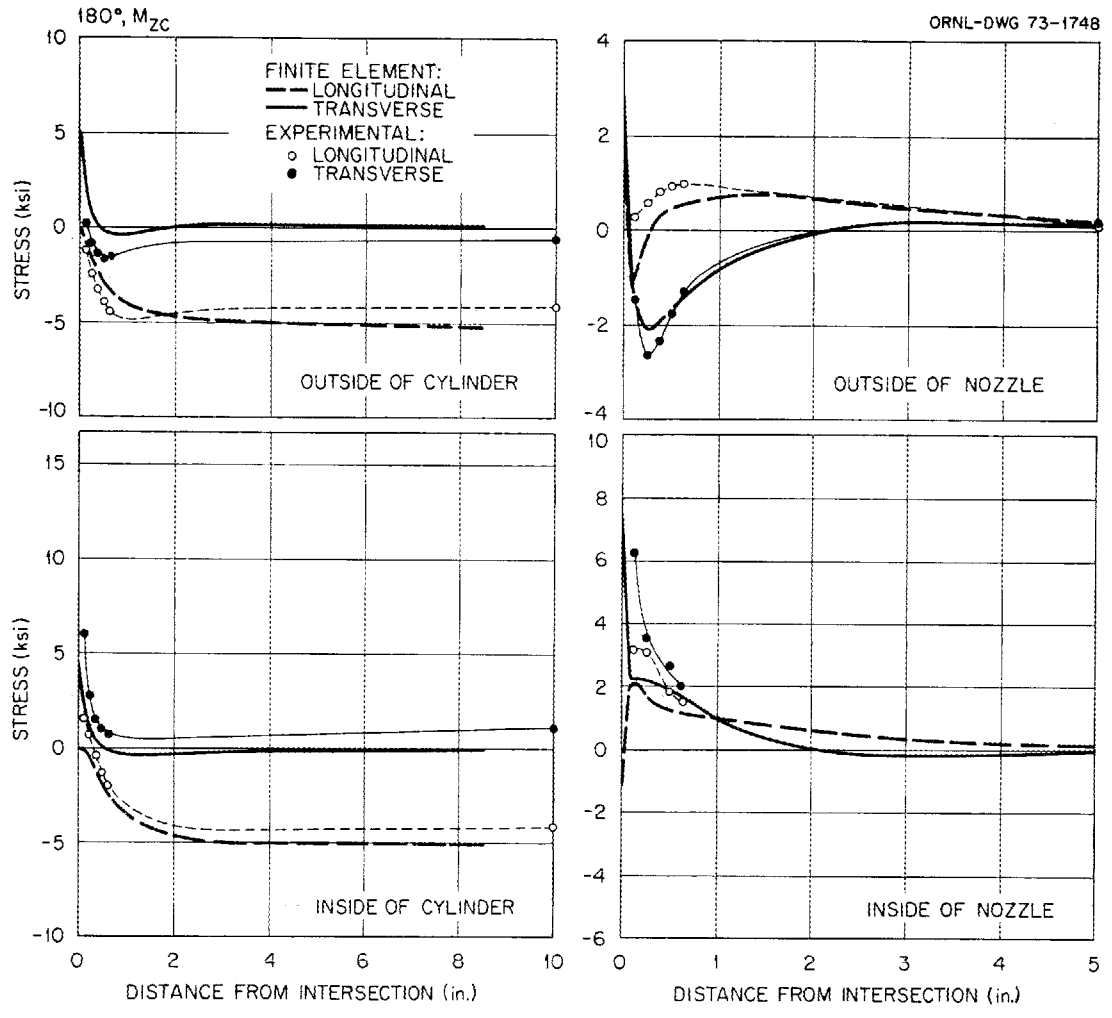

Fig. 71. Measured and predicted stress distributions at 180° for in-plane moment, M_{ZC}, on cylinder.

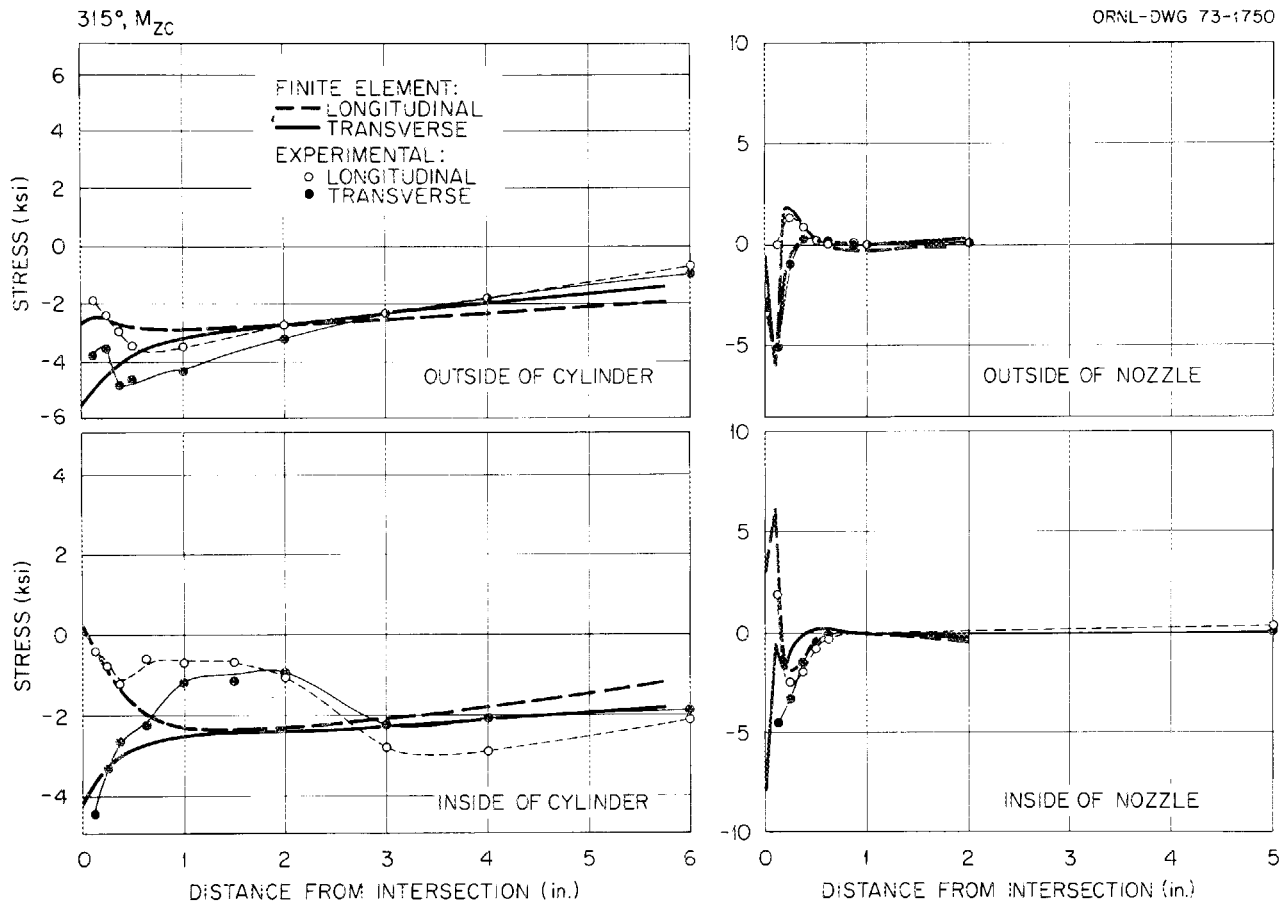

Fig. 72. Measured and predicted stress distributions at 315° for in-plane moment, M_{ZC}, on cylinder.

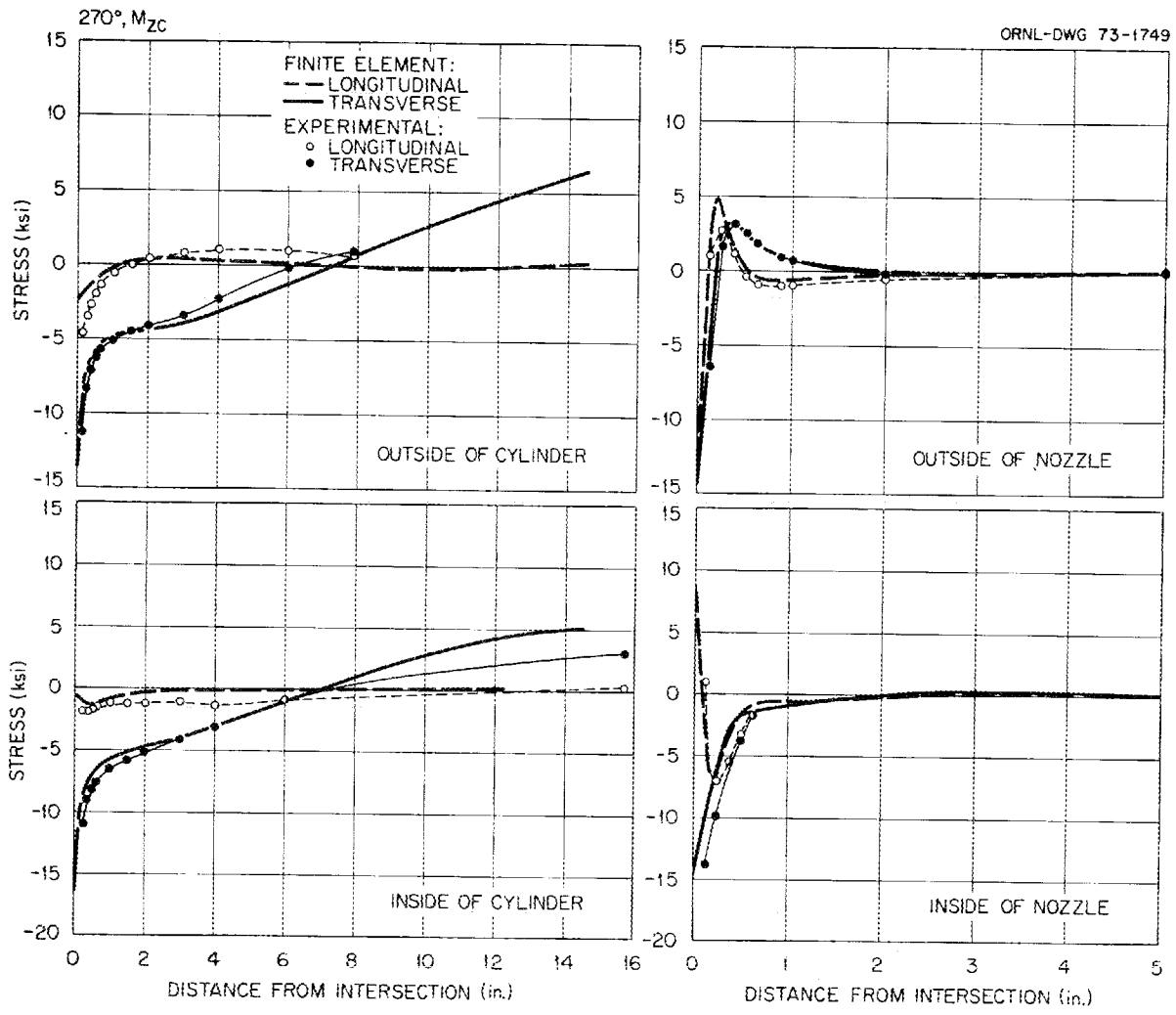

Fig. 73. Measured and predicted stress distributions at 270° for in-plane moment, M_{ZC}, on cylinder.

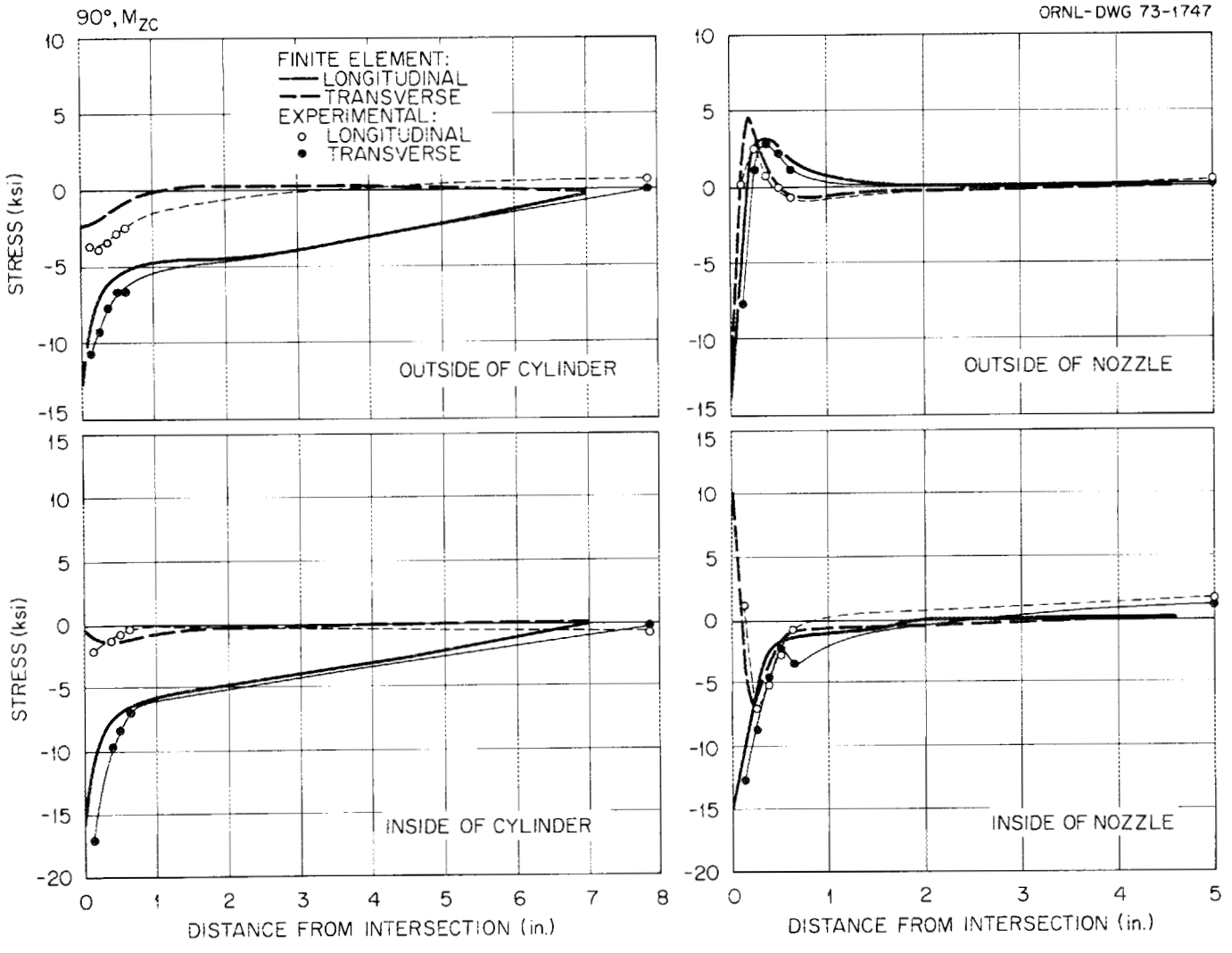

Fig. 74. Measured and predicted stress distributions at 90° for in-plane moment, M_{ZC}, on cylinder.

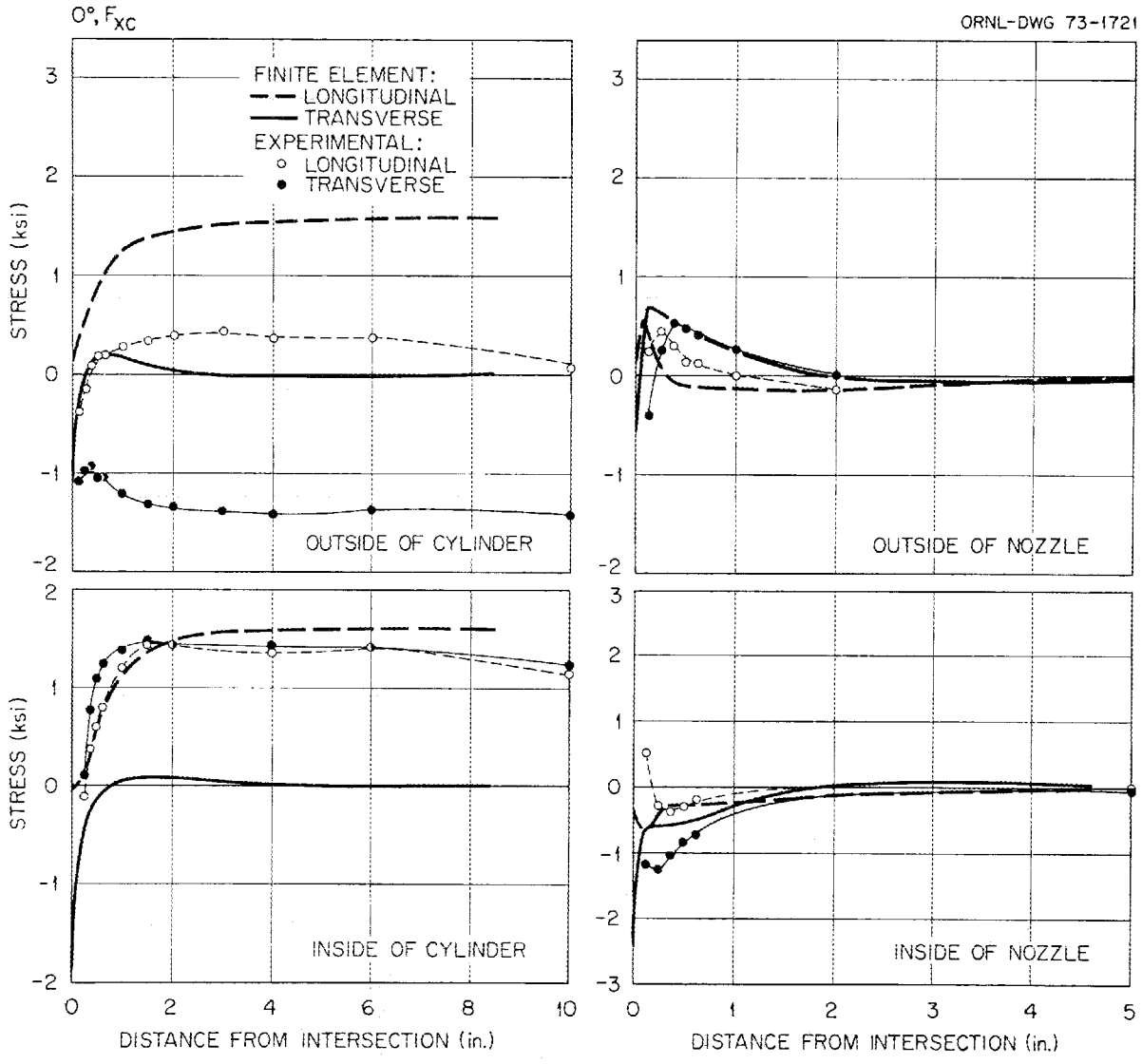

Fig. 75. Measured and predicted stress distributions at 0° for axial force, F_{XC}, on cylinder.

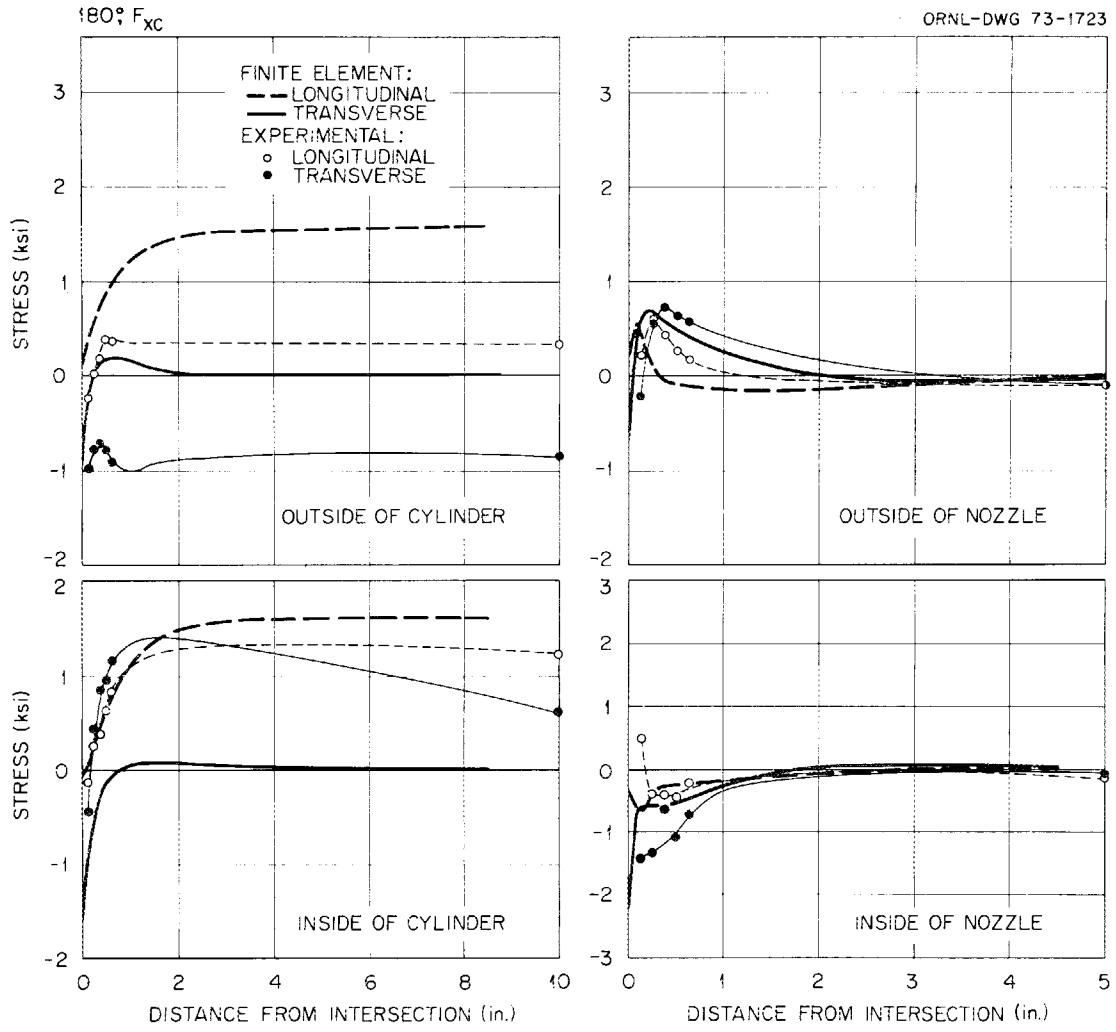

Fig. 76. Measured and predicted stress distributions at 180° for axial force, F_{XC}, on cylinder.

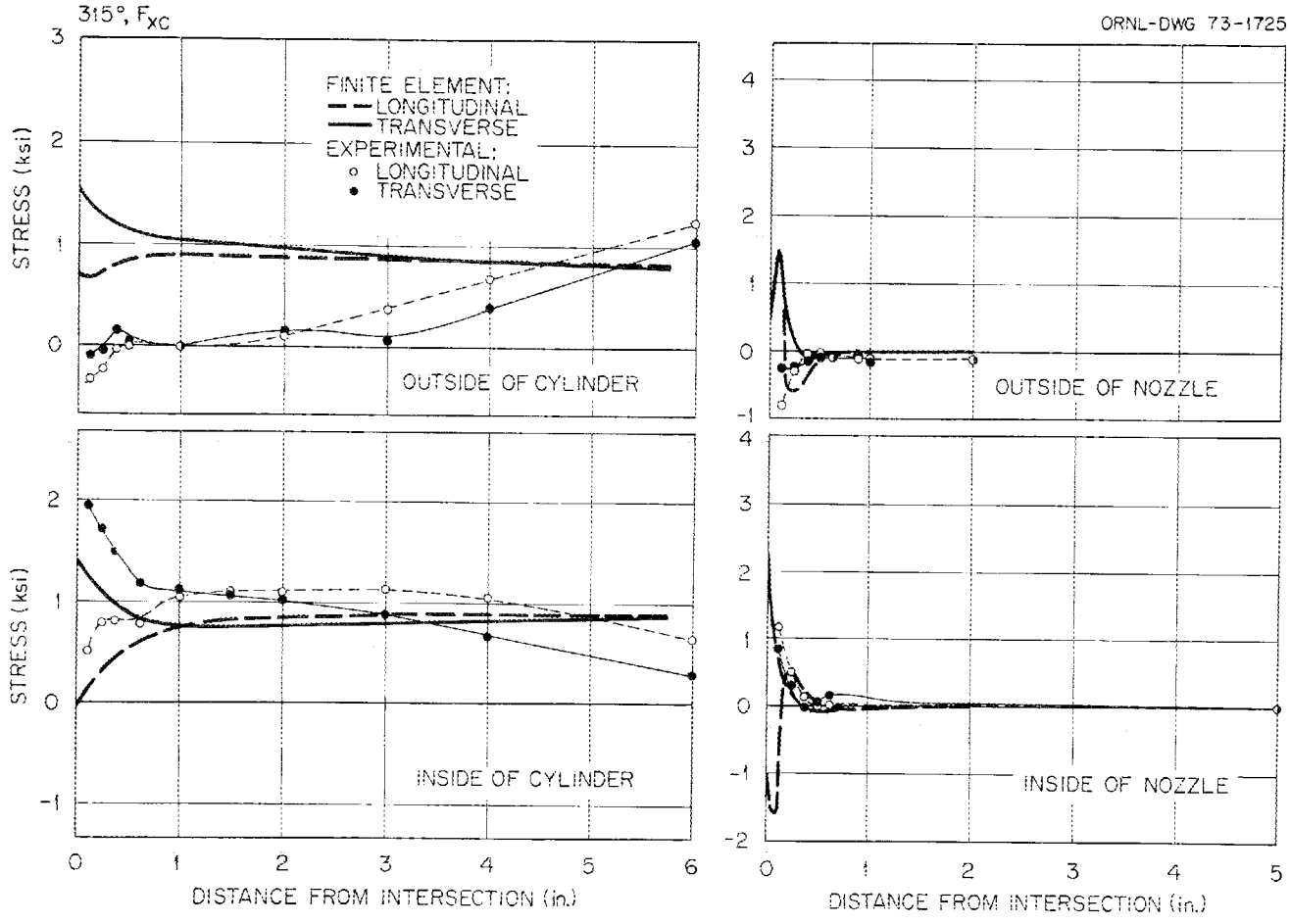

Fig. 77. Measured and predicted stress distributions at 315° for axial force, F_{XC}, on cylinder.

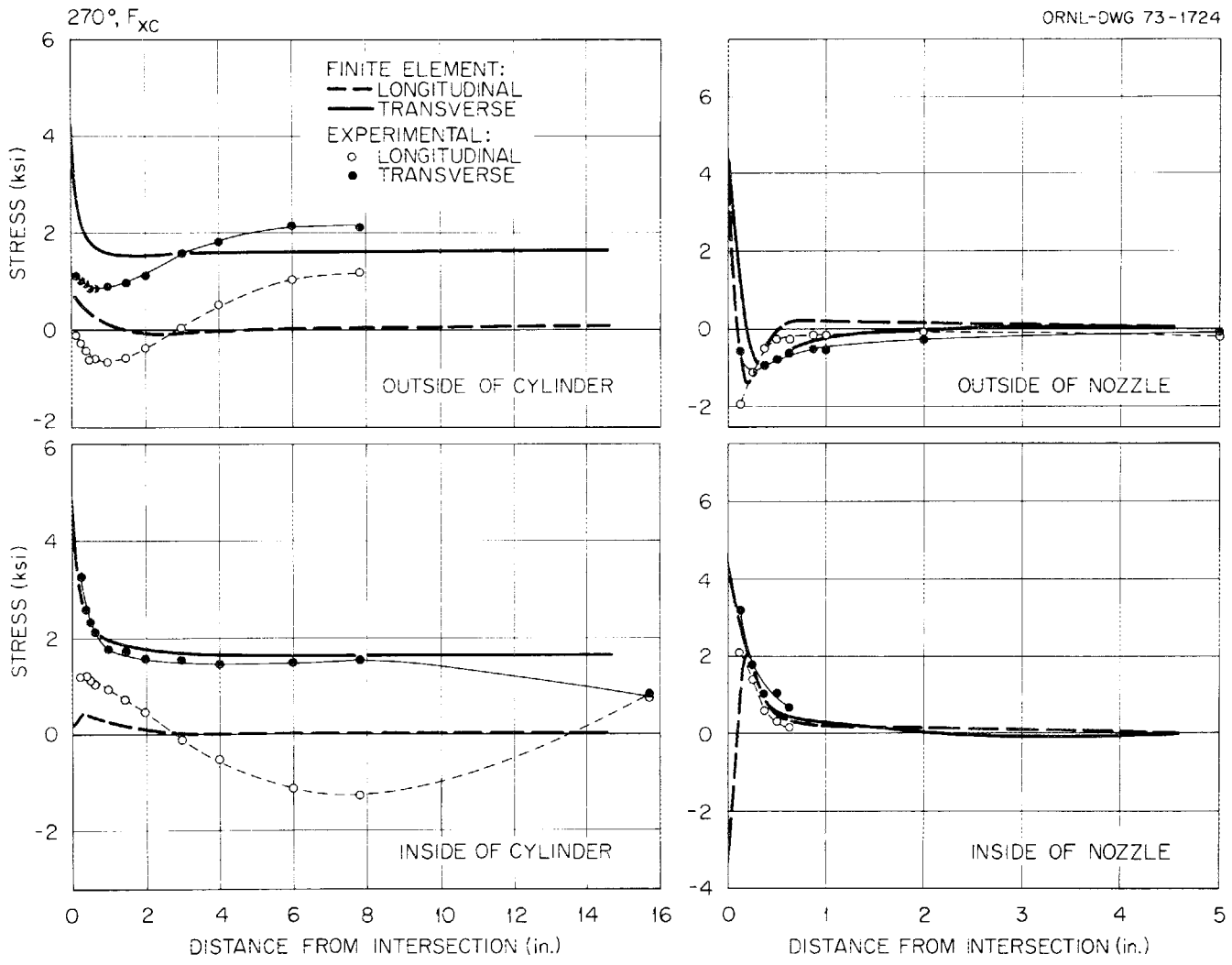

Fig. 78. Measured and predicted stress distributions at 270° for axial force, F_{XC}, on cylinder.

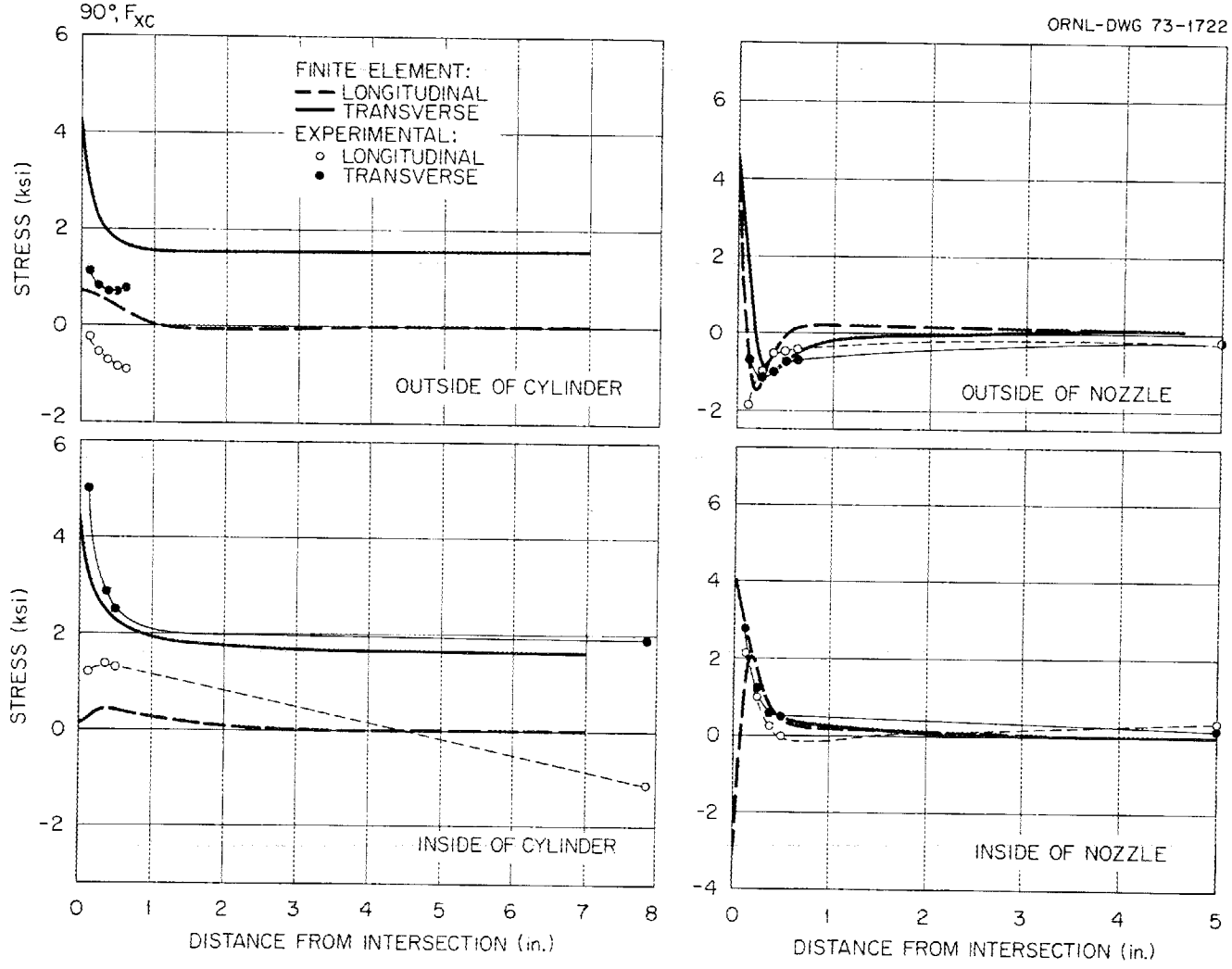

Fig. 79. Measured and predicted stress distributions at 90° for axial force, F_{XC}, on cylinder.

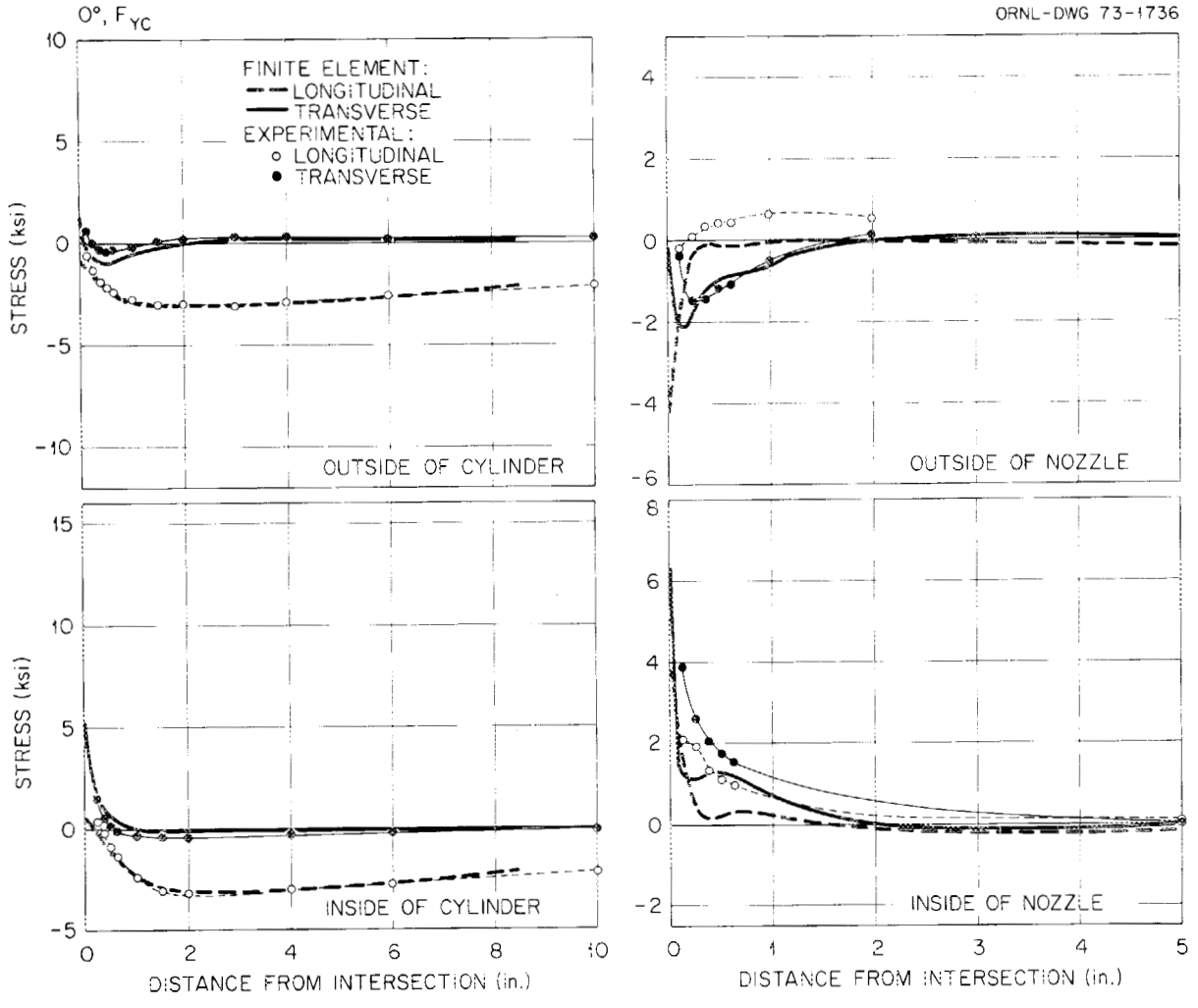

Fig. 80. Measured and predicted stress distributions at 0° for in-plane force, F_{YC}, on cylinder.

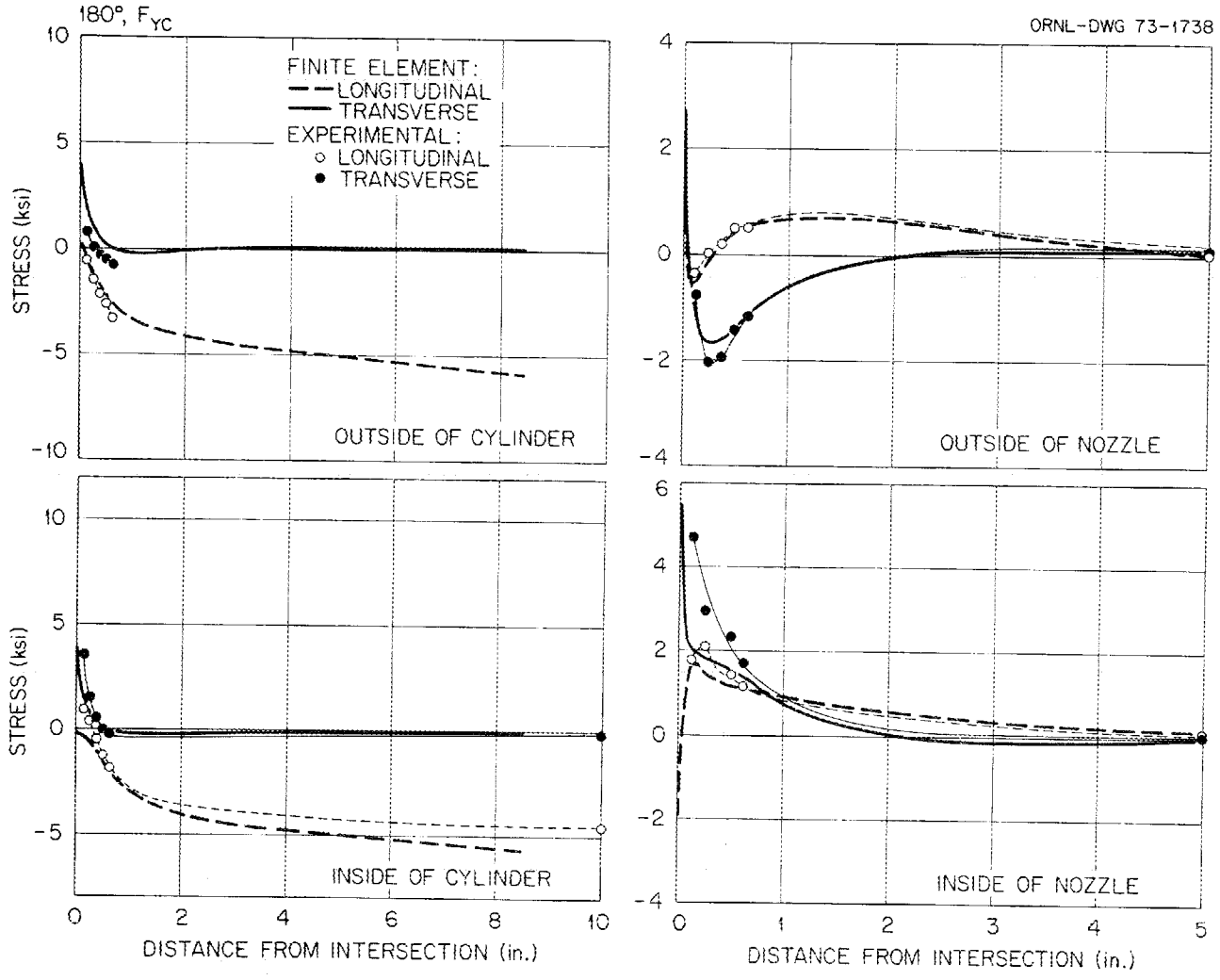

Fig. 81. Measured and predicted stress distributions at 180° for in-plane force, F_{YC}, on cylinder.

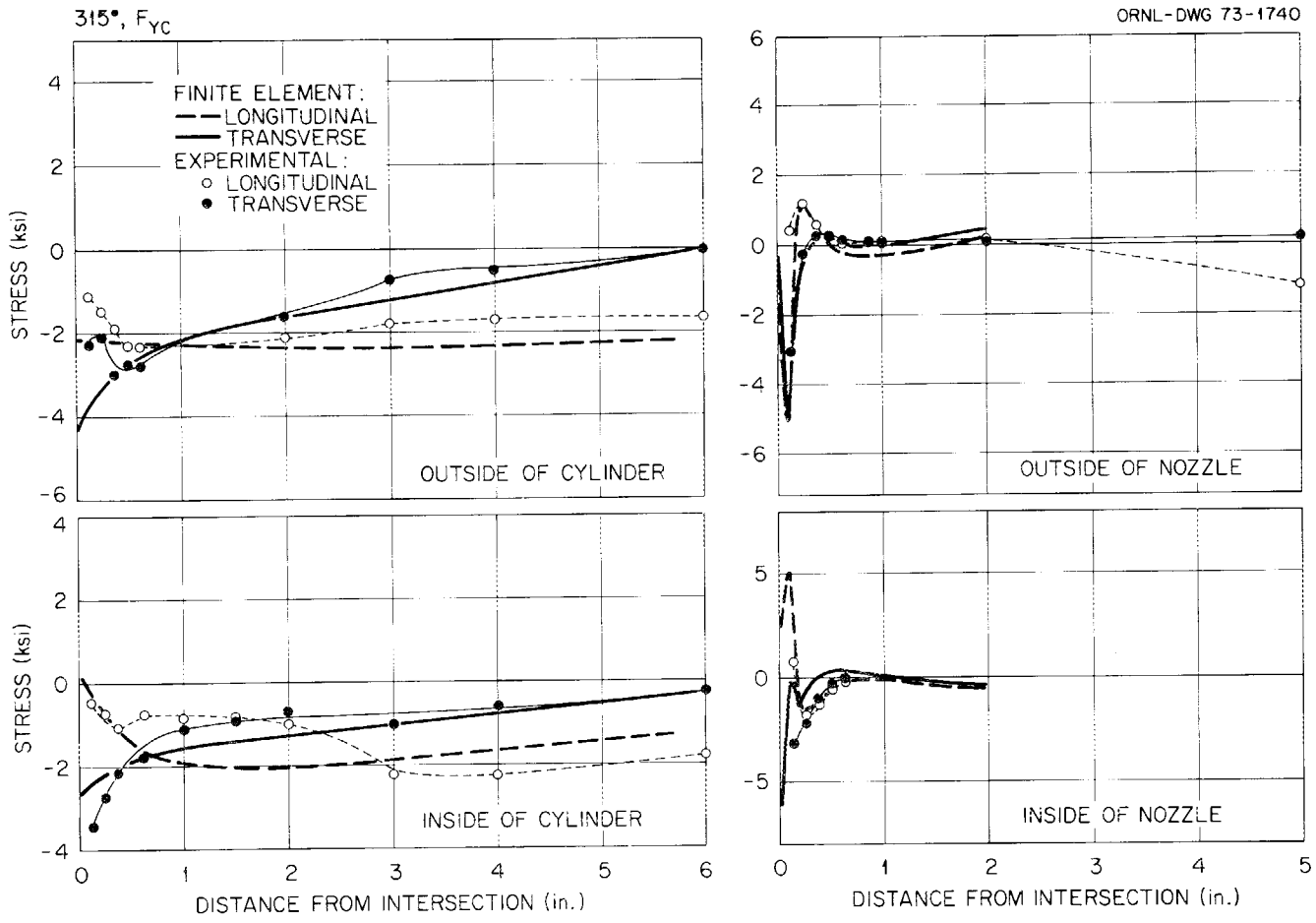

Fig. 82. Measured and predicted stress distributions at 315° for in-plane force, F_{YC}, on cylinder.

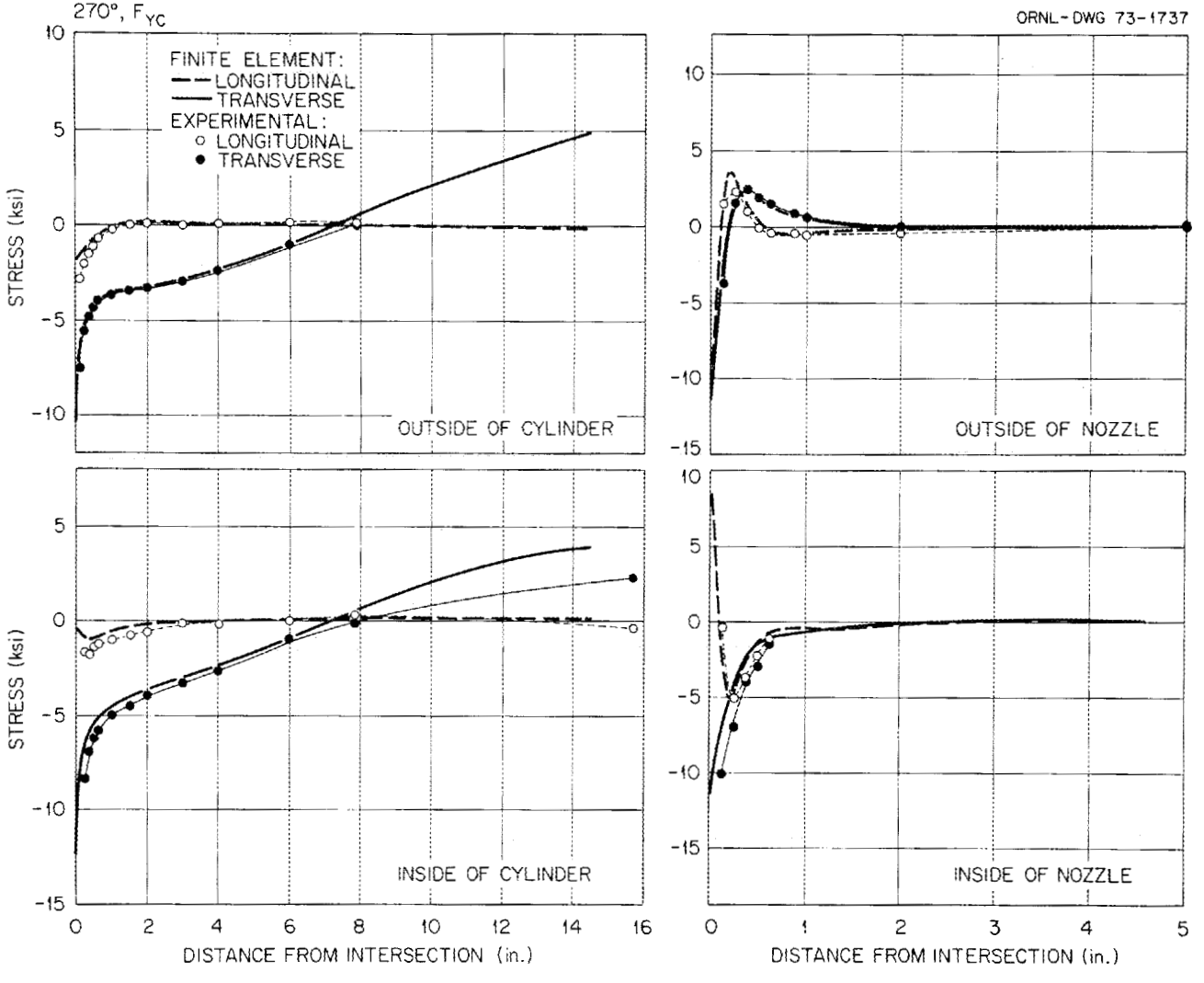

Fig. 83. Measured and predicted stress distributions at 270° for in-plane force, F_{YC}, on cylinder.

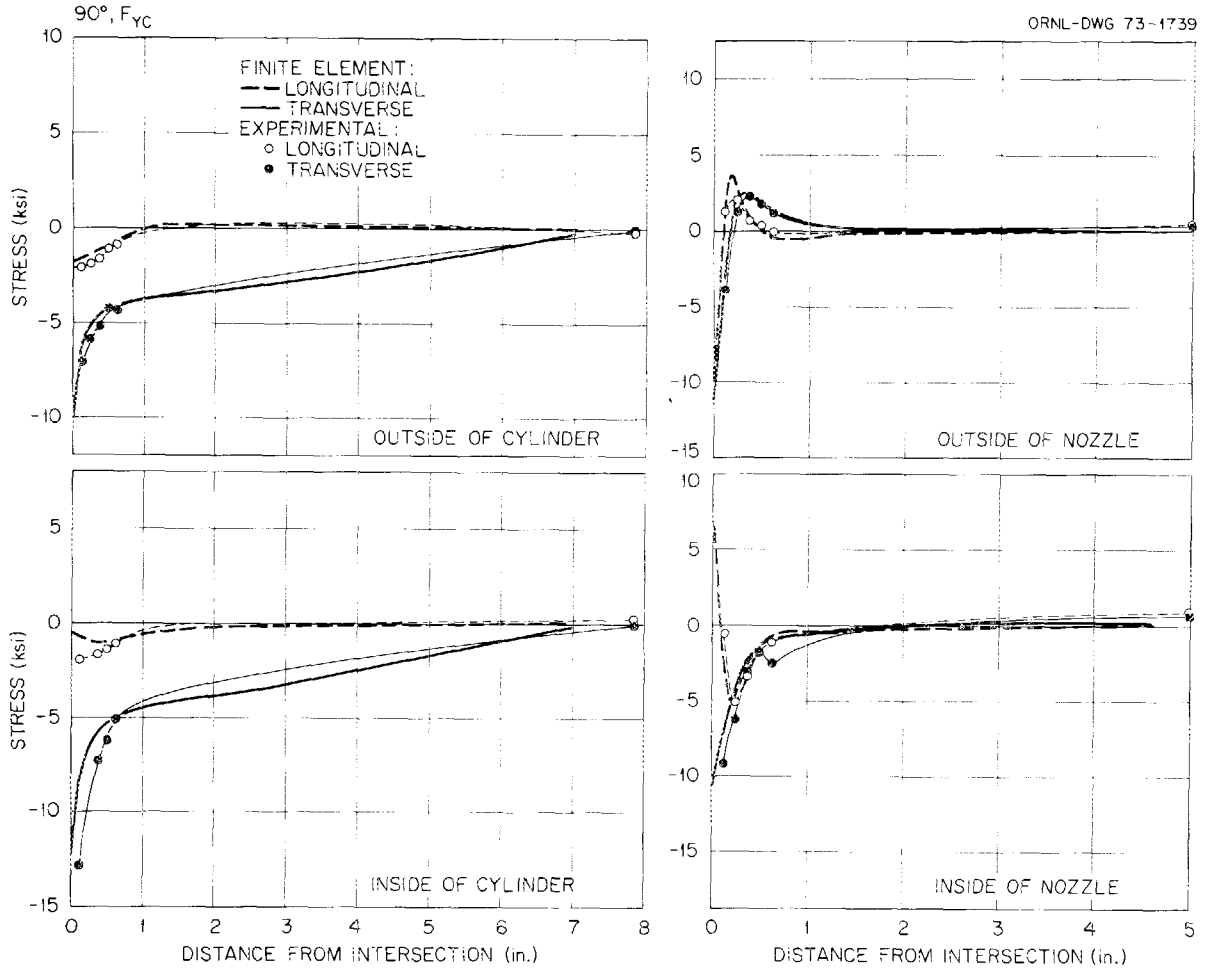

Fig. 84. Measured and predicted stress distributions at 90° for in-plane force, F_{YC}, on cylinder.

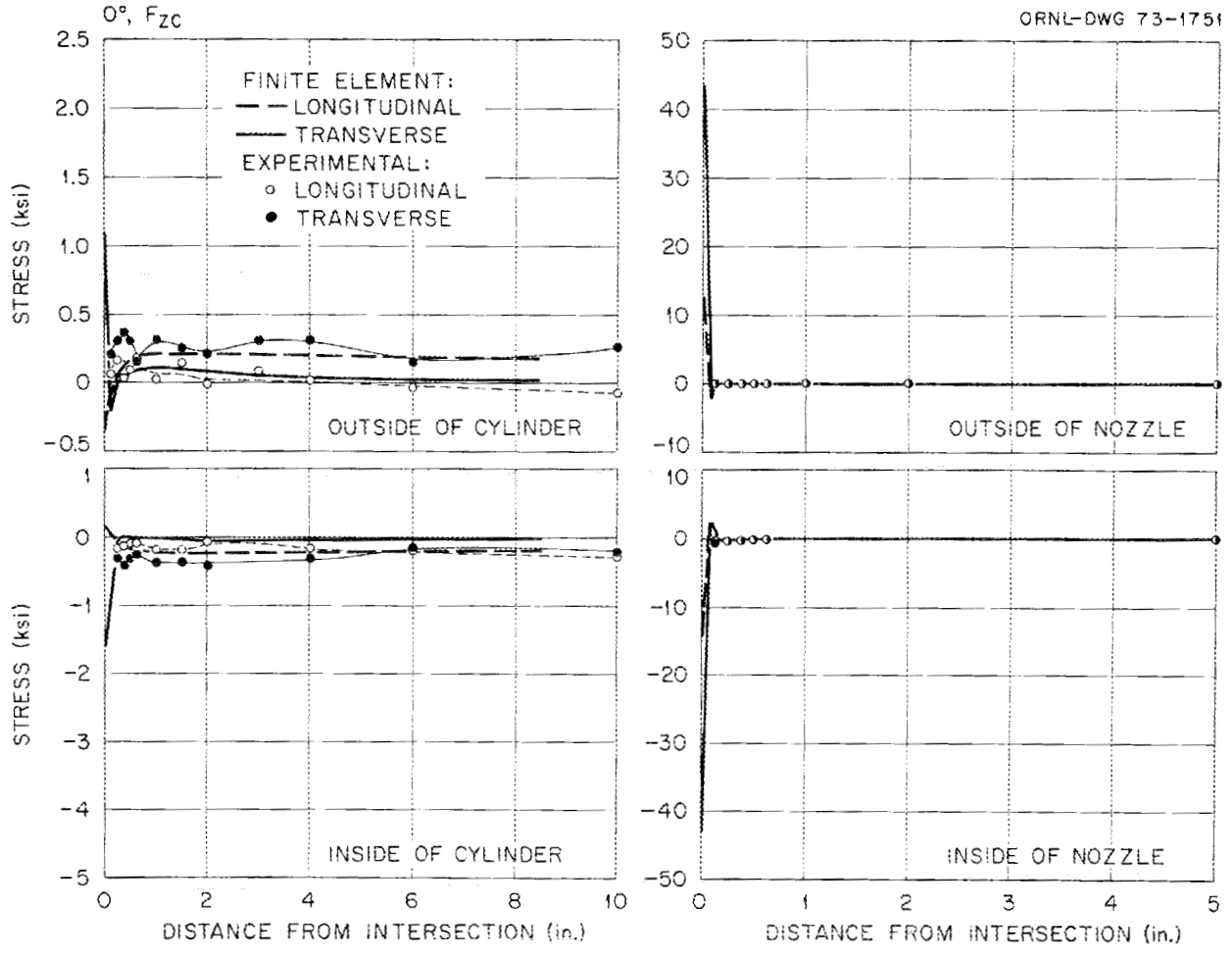

Fig. 85. Measured and predicted stress distributions at 0° for out-of-plane force, F_{ZC}, on cylinder.

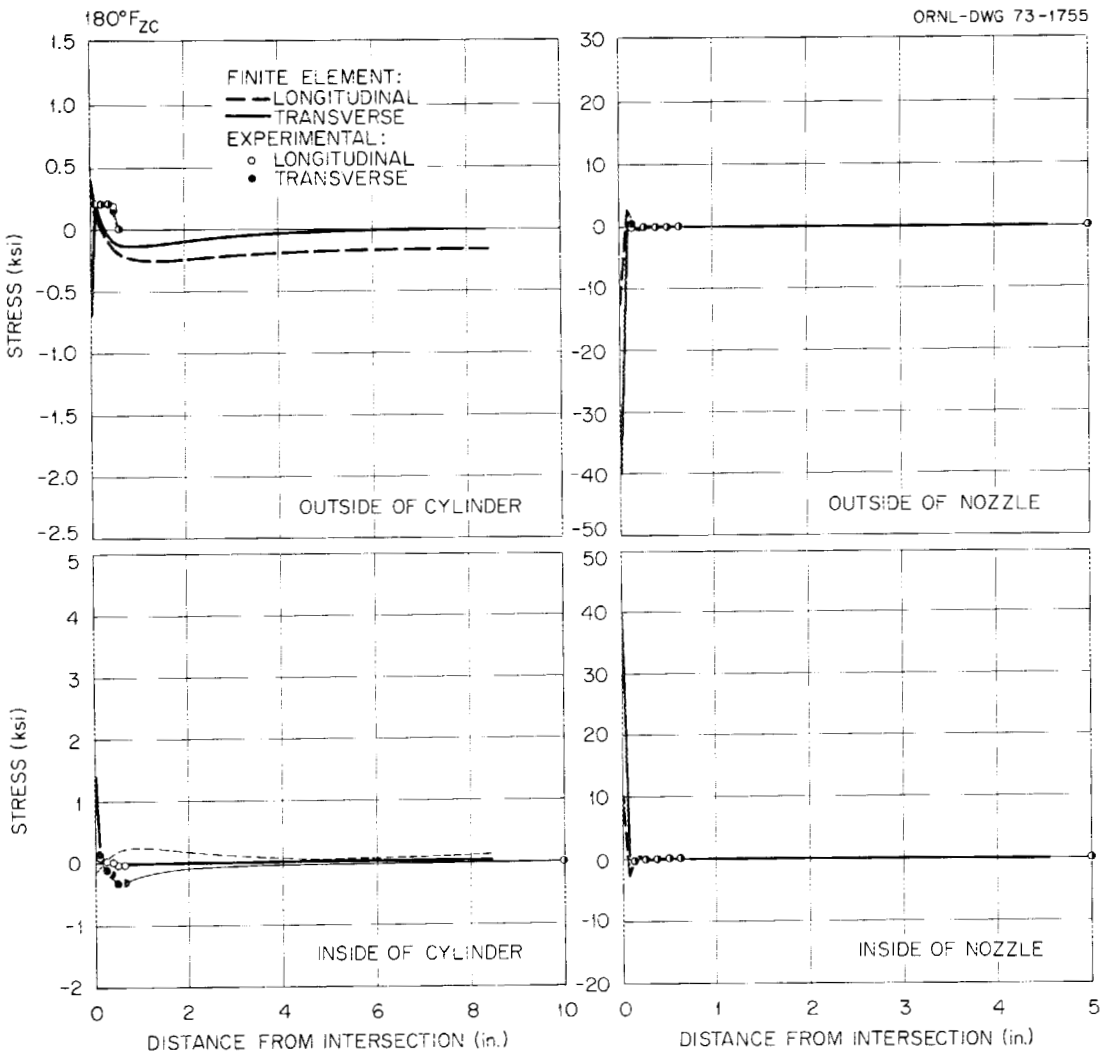

Fig. 86. Measured and predicted stress distributions at 180° for out-of-plane force, F_{ZC}, on cylinder.

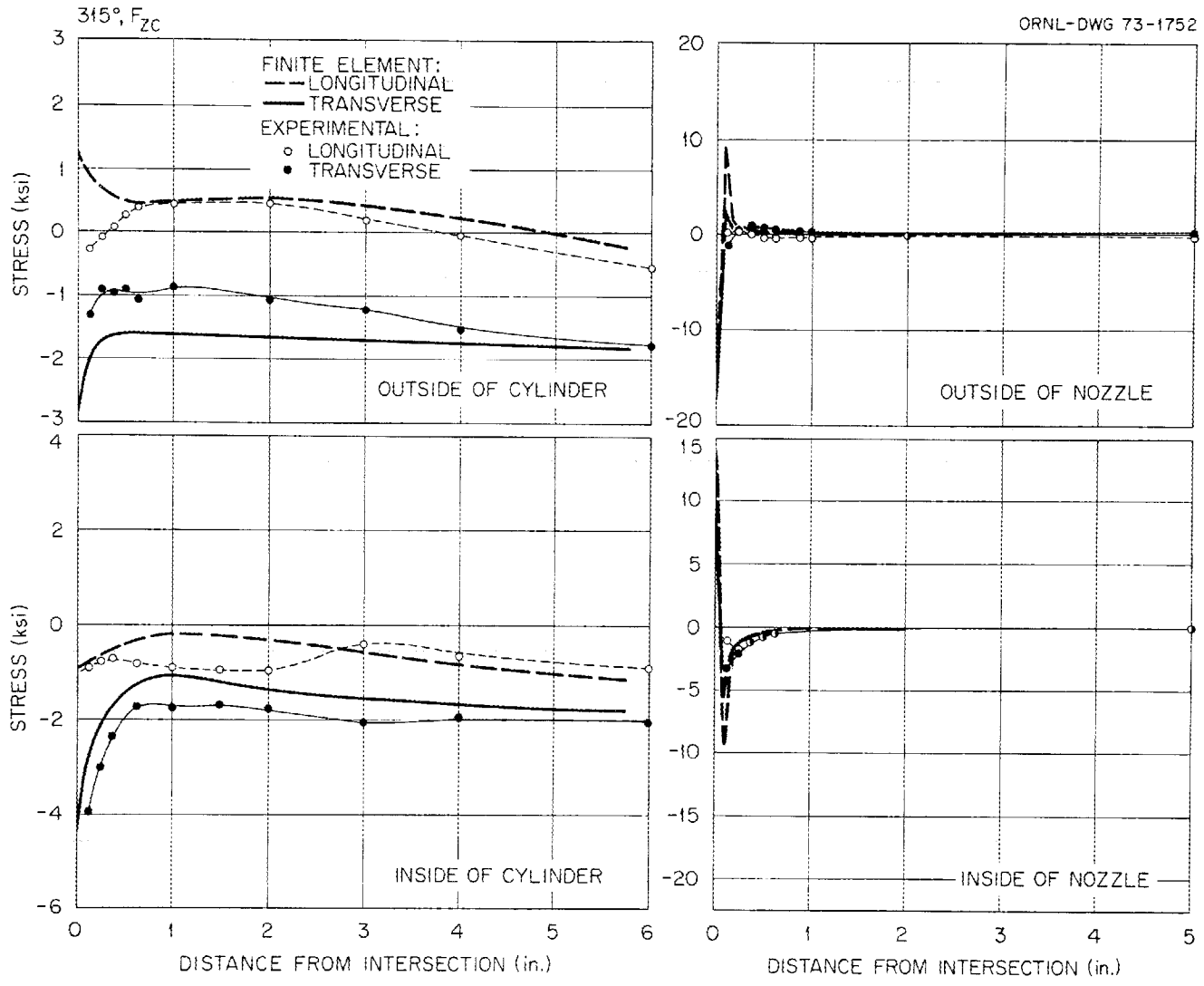

Fig. 87. Measured and predicted stress distributions at 315° for out-of-plane force, F_{ZC}, on cylinder.

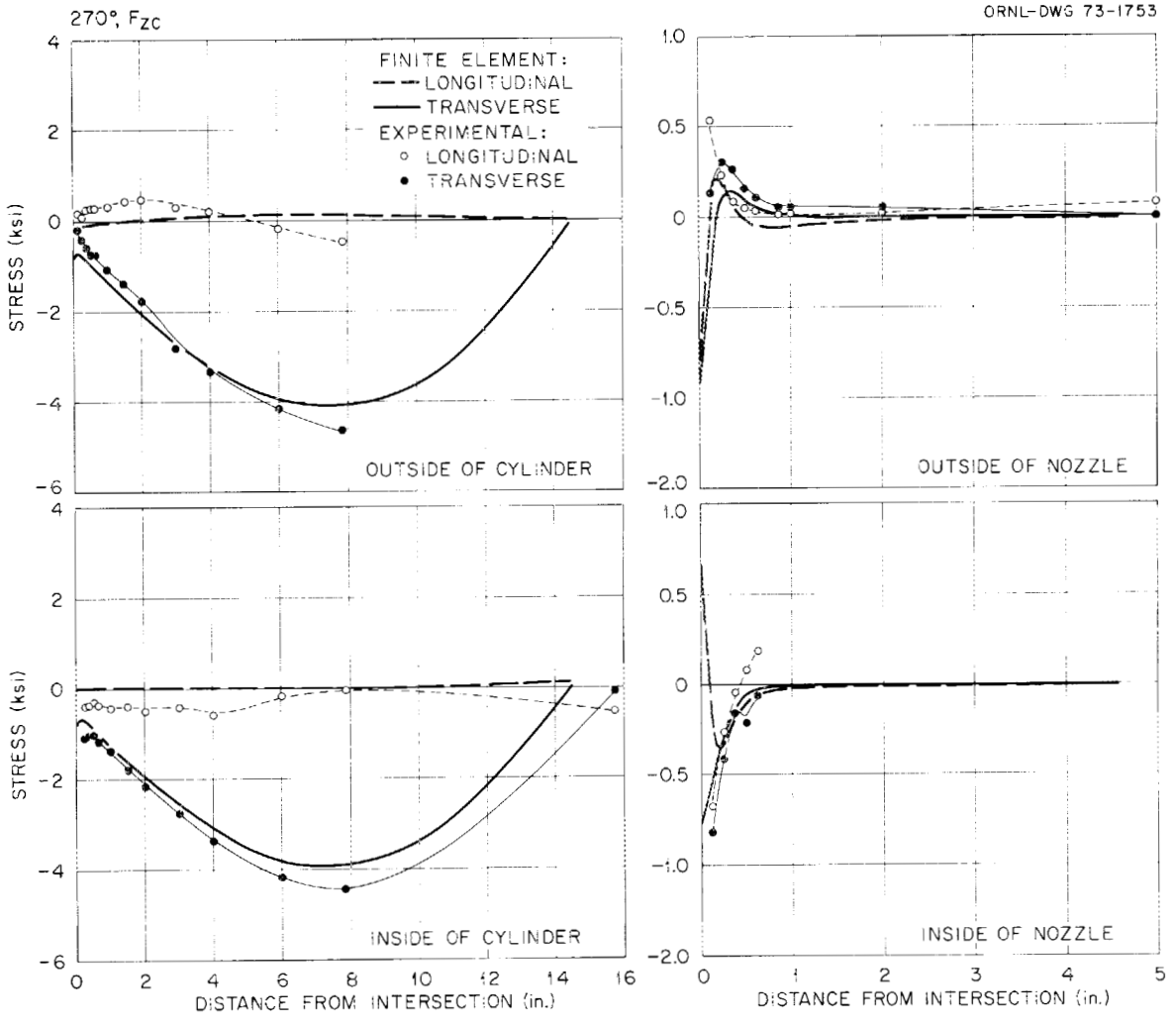

Fig. 88. Measured and predicted stress distributions at 270° for out-of-plane force, F_{ZC}, on cylinder.

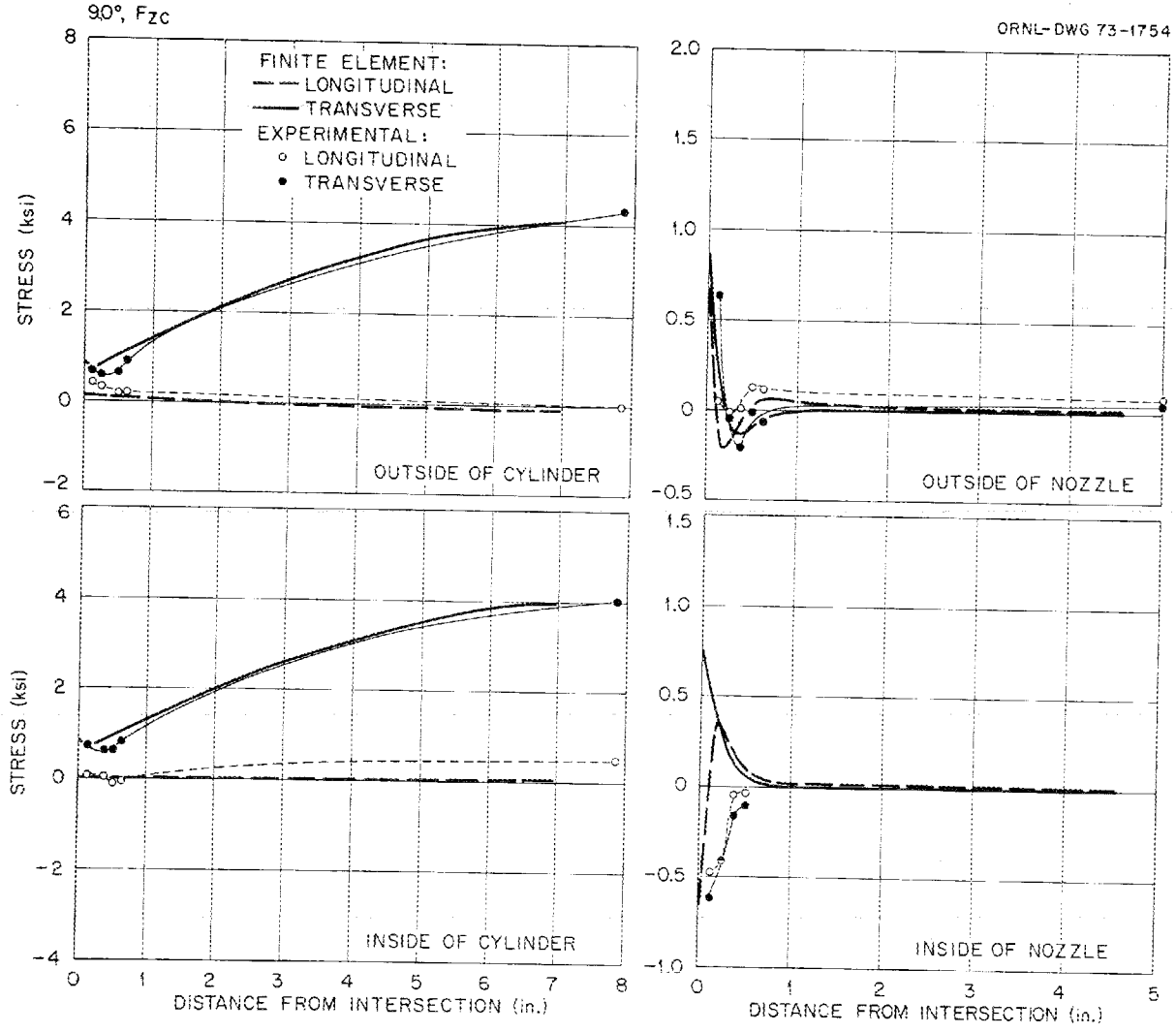

Fig. 89. Measured and predicted stress distributions at 90° for out-of-plane force, F_{ZC}, on cylinder.

REFERENCES

1. J. M. Corum et al., Theoretical and Experimental Stress Analysis of ORNL Thin-Shell Cylinder-to-Cylinder Model No. 1, ORNL-4553 (October 1972).

2. J. M. Corum and W. L. Greenstreet, "Experimental Elastic Stress Analyses of Cylinder-to-Cylinder Shell Models and Comparisons with Theoretical Predictions," paper No. G2/5, First International Conference on Structural Mechanics in Reactor Technology, Berlin, Sept. 20–24, 1971.

3. R. C. Gwaltney, J. W. Bryson, and S. E. Bolt, Theoretical and Experimental Stress Analysis of ORNL Thin-Shell Cylinder-to-Cylinder Model No. 3, ORNL-5020 (to be published).

4. D. E. Hardenbergh, S. Y. Zamrik, and A. J. Edmondson, "Experimental Investigation of Stresses in Nozzles in Cylindrical Pressure Vessels," Welding Research Council Bulletin 89, July 1963.

5. D. E. Hardenbergh and S. Y. Zamrik, "Effects of External Loadings on Large Outlets in a Cylindrical Pressure Vessel," Welding Research Council Bulletin 96, May 1964.

6. W. F. Riley, Experimental Determination of Stress Distributions in Thin Walled Cylindrical and Spherical Pressure Vessels with Circular Nozzles, IIT Research Institute Report No. M6053 (March 1965).

7. C. E. Taylor and N. C. Lind, "Photoelastic Study of the Stresses near Openings in Pressure Vessels," Welding Research Council Bulletin 113, April 1966.

8. M. M. Leven, "Photoelastic Determination of Stresses in Reinforced Openings in Pressure Vessels," Welding Research Council Bulletin 113, April 1966.

9. Ojars Greste, Finite Element Analysis of Tubular K Joints, Report UCSESM 70-11, University of California, Berkeley (June 1970).

10. W. Reidelbach, "The State of Stress at the Perpendicular Intersection of Two Right Circular Tubes," Ingenieur-Archiv. 30(5), 293–316 (1961).

11. A. C. Eringen, A. K. Naghdi, and C. C. Thiel, "State of Stress in a Circular Cylindrical Shell with a Circular Hole," Welding Research Council Bulletin 102, January 1965.

12. A. K. Naghdi and A. C. Eringen, "Stress Distribution in a Circular Cylindrical Shell with a Circular Cut-Out," Ingenieur-Archiv. 34(3), 161–72 (1965).

13. A. C. Eringen and E. S. Suhubi, "Stress Distribution at Two Normally Intersecting Shells," Nucl. Struct. Eng. 2(3), 253–70 (1965).

14. A. C. Eringen et al., "Stress Concentrations in Two Normally Intersecting Cylindrical Shells Subject to Internal Pressure," Welding Research Council Bulletin 139, April 1969.

15. J. W. Hansberry and N. Jones, "A Theoretical Study of the Elastic Behavior of Two Normally Intersecting Cylindrical Shells," Trans. ASME, J. Eng. Ind. 91B(3), 563–72 (1969).

16. R. F. Maye and A. C. Eringen, "Further Analysis of Two Normally Intersecting Cylindrical Shells Subjected to Internal Pressure," Nucl. Eng. Des. 12(3), 457–74 (1970).

17. J. W. Hansberry and N. Jones, "Elastic Stresses Due to Axial Loads on a Nozzle Which Intersects a Cylindrical Shell," Second International Conference on Pressure Vessel Technology, Part I, Design and Analysis, pp. 129–54, October 1973.

18. P. P. Bijlaard, R. J. Dohrmann, and I. C. Wang, "Stresses in Junction of Nozzle to Cylinder Pressure Vessel for Equal Diameter of Vessel and Nozzle," Nucl. Eng. Des. 5(3), 349–66 (1967).

19. K. C. Pan and R. E. Beckett, "Stress and Displacement Analysis of a Shell Intersection," Trans. ASME, J. Eng. Ind. 92B(3), 303–8 (May 1970).

20. L. R. Herrmann and D. M. Campbell, "A Finite-Element Analysis for Thin Shells," AIAA J. 6(10), 1842–47 (1968).

21. N. Prince and Y. R. Rashid, "Structural Analysis of Shell Intersections," presented at First International Conference on Pressure Vessels and Piping, Sept. 29–Oct. 2, 1969, Delft, The Netherlands.

22. C. P. Johnson, The Analysis of Thin Shells by a Finite Element Procedure, Report 67-22, Department of Civil Engineering, University of California, Berkeley (September 1967).

23. C. P. Johnson and P. G. Smith, A Computer Program for the Analysis of Thin Shells, Report 69-5, Department of Civil Engineering, University of California, Berkeley (August 1967).

24. Ojars Greste, A Computer Program for the Analysis of Tubular K Joints, Report 69-19, Department of Civil Engineering, University of California, Berkeley (November 1969).

25. R. W. Clough and J. L. Tocher, "Finite Element Stiffness Matrices for the Analysis of Plate Bending," Proceedings of Conference on Matrix Methods in Structural Mechanics, Report AFFDL-TR-66-80, Wright-Patterson Air Force Base (November 1966).

26. R. Bailey and R. Hicks, "Localized Loads Applied to a Spherical Pressure Vessel Through a Cylindrical Insert," J. Mech. Eng. Sci. 2(4), 302 (1964).

Appendix

TABULATION OF EXPERIMENTAL DATA

For the benefit of the reader who would like to use these experimental data to prepare comparisons with his own analysis techniques, the experimental data on which the various plots in this report were based are given in Tables A.1 to A.13. For each loading case, a set of data is tabulated for each operable rosette. These data were obtained from the several sets of data taken in each case by the procedures described in Sect. 2.4.

The rosette listings are grouped according to gage lines. For each rosette, the three strain readings are listed first, followed by the normal stress transverse (perpendicular) to the gage line, the normal stress parallel to the gage line, the shear stress (referred to the gage line as a coordinate axis), and the maximum and minimum principal stresses. The strains are given in microinches per inch, and the stresses are in pounds per square inch.

The nomenclature used to identify and locate each rosette can be explained by considering the following sample designation:

I 180 N-E .

The letter I designates that the rosette is located on the inner surface of nozzle or cylinder, an O in this position denotes an outside rosette. The number 180 indicates that the rosette is located on the 180° gage line (see Fig. 3 for the gage line designations). The letter N indicates that the rosette is on the nozzle; a C in this position designates a rosette on the cylinder; and E designates the location of the rosette along the gage line according to the following convention:

Rosette designation	Distance from nozzle-cylinder intersection (see Fig. 3) (in.)
A	≈0
B	1/8
C	1/4
D	3/8
E	1/2

Rosette designation	Distance from nozzle-cylinder intersection (see Fig. 3) (in.)
F	5/8
G	7/8
H	1
J	1 1/2
K	2
L	3
M	4
N	5
P	6
R	7.85
S	10
T	15.7

In every case, the rosettes were positioned on the gage lines so that the leg of the Y lay along the gage line and pointed away from the nozzle-cylinder junction. The convention used can be understood by referring to Fig. 7. The leg of the Y is designated as gage 1 in the tabulations, with gages 2 and 3 being numbered from 1 in the counterclockwise direction.

Finally, in those cases where nonlinearity or drift was excessive or where an individual gage or circuit was otherwise obviously malfunctioning, the rosette of which the gage was a part was not used in the final results plotted in this report for the specific loading under consideration. Nonetheless, these data are listed in the tabulations, but they are marked by an asterisk beside the rosette number.

Table A.1. Internal pressure

INTERNAL PRESSURE (300 PSI)

	MICRO-STRAIN			STRESSES			PRIN STRESSES	
ROSETTE	GAGE1	GAGE2	GAGE3	TRANS	LONG	SHEAR	SIGMX	SIGMN
I-0-C-C	-33	351	360	15658	3696	-127	15659	3695
I-0-C-D	45	286	305	12950	5245	-254	12959	5237
I-0-C-E	76	260	260	11344	5693	0	11344	5693
I-0-C-F	105	260	243	10945	6433	222	10956	6422
I-0-C-H	107	208	210	9056	5937	-32	9056	5937
I-0-C-J	88	186	184	8028	5056	32	8029	5056
I-0-C-K	62	172	184	7743	4184	-159	7750	4176
I-0-C-L*	-100	165	184	7767	-672	-254	7775	-680
I-0-C-M	50	174	177	7655	3800	-32	7655	3800
I-0-C-P	62	179	179	7799	4202	0	7799	4202
I-0-C-S	57	189	165	7704	4030	315	7731	4003
0-0-C-B	52	403	434	18336	7062	-410	18351	7047
0-0-C-C	45	296	310	13284	5334	-190	13289	5329
0-0-C-D	40	247	261	11103	4535	-189	11108	4530
0-0-C-E	19	228	223	9872	3525	65	9873	3524
0-0-C-F	21	206	194	8777	3267	158	8782	3263
0-0-C-H	21	161	175	7369	2845	-189	7377	2837
0-0-C-J	40	161	154	6879	3265	97	6882	3262
0-0-C-K	57	156	159	6860	3759	-31	6861	3758
0-0-C-L	61	166	168	7274	4024	-32	7274	4023
0-0-C-M	54	168	161	7177	3783	94	7180	3781
0-0-C-P	54	168	159	7126	3768	127	7130	3763
0-0-C-S	59	159	168	7120	3906	-126	7125	3901
I-0-N-B	-352	398	412	18176	-5108	-191	18178	-5110
I-0-N-C	158	304	297	13037	8654	96	13039	8651
I-0-N-D	184	184	201	8271	8014	-223	8400	7885
I-0-N-E	117	105	120	4819	4966	-191	5098	4687
I-0-N-F	69	77	91	3608	3166	-191	3679	3095
I-0-N-N	22	72	77	3240	1619	-64	3242	1616
0-0-N-B	-67	315	287	13305	1995	379	13318	1982
0-0-N-C	-67	68	64	2980	-1105	63	2981	-1106
0-0-N-D	19	14	12	545	726	30	731	540
0-0-N-E	69	19	24	857	2314	-64	2317	854
0-0-N-F	78	35	42	1626	2829	-94	2836	1619
0-0-N-H	64	59	62	2582	2690	-31	2699	2574
0-0-N-K	35	71	71	3083	1984	-1	3083	1984
0-0-N-N*	21	59	1616	36795	11675	-20749	48489	-19

Table A.1 (continued)

INTERNAL PRESSURE (300 PSI)

	MICRO-STRAIN			STRESSES			PRIN STRESSES	
ROSETTE	GAGE1	GAGE2	GAGE3	TRANS	LONG	SHEAR	SIGMX	SIGMN
I-90C-B	-31	14	7	508	-781	96	515	-788
I-90C-C*	5	48	0	1047	458	638	1455	50
I-90C-D	55	57	53	2359	2360	64	2423	2296
I-90C-E	91	60	57	2478	3472	32	3473	2477
I-90C-F	105	36	57	1948	3744	-280	3787	1905
I-90C-R	199	77	84	3306	6953	-96	6955	3304
O-90C-B	35	187	213	8757	3686	-349	8781	3662
O-90C-C	78	218	235	9879	5314	-221	9889	5303
O-90C-D	112	221	214	9425	6175	95	9427	6172
O-90C-E	135	190	197	8355	6566	-95	8360	6561
O-90C-F	157	183	183	7862	7059	0	7862	7059
O-90C-R	173	83	93	3670	6300	-127	6306	3664
I-90N-B	-291	95	38	3257	-7760	763	3310	-7812
I-90N-C	-5	114	86	4409	1180	381	4453	1135
I-90N-D	33	76	81	3421	2023	-65	3424	2020
I-90N-E	7	55	57	2454	946	-32	2455	945
I-90N-F*	184	172	62	4936	6991	1462	7750	4176
I-90N-N*	148	456	225	14798	8883	3087	16115	7565
O-90N-B	-47	221	228	9912	1550	-95	9913	1549
O-90N-C	-121	123	119	5454	-1996	63	5455	-1996
O-90N-D	-81	85	76	3636	-1330	127	3639	-1334
O-90N-E	-12	83	71	3403	665	158	3412	656
O-90N-F	-7	52	71	2720	602	-253	2750	573
O-90N-N	38	62	62	2670	1940	0	2670	1940

Table A.1 (continued)

INTERNAL PRESSURE (300 PSI)

	MICRO-STRAIN			STRESSES			PRIN STRESSES	
ROSETTE	GAGE1	GAGE2	GAGE3	TRANS	LONG	SHEAR	SIGMX	SIGMN
I180C-B	-85	465	495	21188	3810	-409	21198	3800
I180C-C	2	344	361	15495	4720	-220	15499	4715
I180C-D	57	302	292	12999	5598	126	13001	5596
I180C-E	71	271	262	11636	5614	126	11639	5611
I180C-F	99	250	238	10620	6158	157	10626	6153
I180C-S	26	170	163	7280	2962	94	7282	2960
O180C-B	29	374	376	16439	5789	-32	16439	5789
O180C-C	38	293	288	12716	4957	63	12717	4957
O180C-D	31	240	245	10632	4118	-63	10633	4117
O180C-E	21	205	205	8970	3334	0	8970	3334
O180C-F	14	193	183	8240	2900	127	8243	2897
O180C-S	10	171	162	7304	2477	127	7308	2474
I180N-B	-399	298	527	18563	-6389	-3053	18931	-6757
I180N-C	90	145	386	11580	6187	-3210	13076	4691
I180N-D	186	-182	203	257	5652	-5117	8739	-2830
I180N-E	114	117	98	4582	4802	253	4968	4416
I180N-F	83	92	99	4108	3709	-94	4129	3688
I180N-N	7	157	83	5274	1790	984	5533	1531
O180N-B	-78	230	271	11100	977	-545	11130	947
O180N-C	-64	52	52	2369	-1215	0	2369	-1215
O180N-D	33	10	5	277	1082	63	1087	272
O180N-E	76	29	21	1014	2587	95	2592	1008
O180N-F	76	50	38	1850	2837	158	2862	1825
O180N-N	19	64	64	2801	1411	0	2801	1411

Table A.1 (continued)

INTERNAL PRESSURE (300 PSI)

	MICRO-STRAIN			STRESSES			PRIN STRESSES	
ROSETTE	GAGE1	GAGE2	GAGE3	TRANS	LONG	SHEAR	SIGMX	SIGMN
I270C-C	4	47	52	2177	784	-64	2180	781
I270C-D	59	54	62	2483	2521	-97	2601	2403
I270C-E	97	59	64	2597	3700	-64	3704	2593
I270C-F	133	64	64	2664	4794	0	4794	2664
I270C-H	176	71	61	2719	6097	128	6102	2715
I270C-J	207	83	93	3636	7304	-128	7308	3631
I270C-K*	203	148	95	5111	7609	698	7791	4929
I270C-L	212	107	90	4097	7590	218	7603	4084
I270C-M	217	100	93	3987	7694	94	7696	3985
I270C-P	201	93	95	3913	7192	-29	7193	3912
I270C-R	197	105	89	4051	7115	222	7131	4035
I270C-T	153	19	55	1473	5042	-479	5105	1410
O270C-B	79	247	238	10578	5529	127	10581	5526
O270C-C	105	228	216	9657	6036	158	9664	6029
O270C-D	133	219	212	9312	6789	95	9315	6785
O270C-E	147	209	195	8721	7039	190	8743	7018
O270C-F	157	190	176	7875	7071	190	7918	7028
O270C-H	169	159	152	6660	7063	95	7084	6639
O270C-J	190	121	117	5017	7212	63	7214	5015
O270C-K	188	100	100	4183	6890	0	6890	4183
O270C-L	202	100	88	3906	7235	158	7243	3899
O270C-M	190	90	83	3608	6793	95	6795	3605
O270C-P	190	81	90	3556	6777	-127	6782	3551
O270C-R	195	86	90	3655	6950	-63	6951	3654
O270C-T*	183	102	0	2047	6110	1363	6525	1632
I270N-B	-305	60	36	2433	-8435	318	2443	-8444
I270N-C	-5	103	98	4411	1180	64	4412	1179
I270N-D	36	105	81	4052	2290	318	4107	2234
I270N-E	17	112	48	3496	1550	859	3820	1225
I270N-F	-7	43	41	1849	333	32	1850	332
O270N-B	-43	237	206	9787	1648	410	9807	1628
O270N-C	-123	111	114	5082	-2178	-31	5082	-2178
O270N-D	-93	71	81	3448	-1749	-127	3451	-1752
O270N-E	-55	59	67	2831	-792	-95	2833	-795
O270N-F	-36	64	67	2914	-196	-32	2915	-196
O270N-G	-26	62	62	2747	39	0	2747	39
O270N-H	-24	57	57	2535	47	0	2535	47
O270N-K	2	43	48	1984	667	-63	1987	664
O270N-N	19	55	57	2436	1302	-32	2437	1301

Table A.1 (continued)

INTERNAL PRESSURE (300 PSI)

	MICRO-STRAIN			STRESSES			PRIN STRESSES	
ROSETTE	GAGE1	GAGE2	GAGE3	TRANS	LONG	SHEAR	SIGMX	SIGMN
I315C-B	-74	167	315	10685	984	-1973	11071	598
I315C-C	-12	100	325	9357	2449	-2992	10472	1334
I315C-D	55	75	282	7790	3987	-2751	9233	2544
I315C-F	174	139	189	7000	7331	-668	7854	6477
I315C-H	179	134	210	7362	7583	-1018	8497	6448
I315C-J	184	143	198	7304	7709	-732	8266	6747
I315C-K	174	143	193	7210	7394	-668	7977	6627
I315C-L	132	72	191	5640	5639	-1592	7231	4048
I315C-M	108	83	203	6167	5079	-1607	7320	3927
I315C-P	124	65	194	5541	5394	-1720	7190	3746
O315C-B	64	311	171	10517	5078	1866	11095	4499
O315C-C	78	297	142	9563	5219	2055	10381	4400
O315C-D	78	320	123	9667	5250	2625	10889	4028
O315C-E	59	301	102	8801	4421	2656	10054	3168
O315C-F	83	278	74	7628	4780	2719	9274	3135
O315C-H	88	249	57	6632	4624	2561	8379	2877
O315C-K	109	206	50	5513	4929	2087	7328	3114
O315C-L	116	197	57	5453	5125	1866	7162	3416
O315C-M	126	199	62	5599	5453	1834	7362	3691
O315C-P	126	187	55	5182	5328	1771	7027	3483
I315N-B	-277	194	213	9240	-5551	-255	9245	-5556
I315N-C	69	201	225	9280	4865	-319	9303	4842
I315N-D	103	132	144	5932	4865	-159	5955	4842
I315N-E	48	62	72	2891	2303	-127	2917	2276
I315N-F	19	41	72	2449	1309	-414	2584	1174
I315N-N	24	35	87	2669	1508	-691	2992	1186
O315N-B	-33	325	211	11823	2551	1518	12065	2308
O315N-C	-112	104	97	4556	-1979	95	4557	-1981
O315N-D	-52	23	58	1854	-1001	-467	1929	-1075
O315N-E	-3	9	63	1599	404	-717	1935	68
O315N-F	18	19	73	1982	1148	-721	2397	732
O315N-G	21	33	75	2338	1326	-565	2590	1074
O315N-H	18	35	73	2345	1259	-500	2541	1063
O315N-K	16	49	61	2395	1204	-155	2415	1184
O315N-N	-43	61	58	2666	-478	31	2666	-479

Table A.2. Out-of-plane moment, M_{XN}, on nozzle

OUT-OF-PLANE MOMENT LOADING, MXN, ON NOZZLE (400 IN-LB)

	MICRO-STRAIN			STRESSES			PRIN STRESSES	
ROSETTE	GAGE1	GAGE2	GAGE3	TRANS	LONG	SHEAR	SIGMX	SIGMN
I-0-C-C	12	-190	179	-260	288	-4925	4947	-4919
I-0-C-D	0	-169	160	-197	-51	-4385	4262	-4510
I-0-C-E	7	-140	129	-257	143	-3591	3540	-3654
I-0-C-F	7	-114	108	-156	176	-2956	2971	-2951
I-0-C-H	0	62	-64	-39	1	1684	1665	-1704
I-0-C-J	0	39	-43	-88	-15	1080	1029	-1132
I-0-C-K	3	-28	24	-90	57	-703	690	-723
I-0-C-L*	0	-17	14	-52	-16	-413	380	-448
I-0-C-M	2	-10	10	-3	71	-254	291	-223
I-0-C-P	2	-5	5	-3	71	-127	166	-98
I-0-C-S	2	-2	5	50	87	-95	165	-29
0-0-C-B	5	-88	71	-366	37	-2118	1963	-2292
0-0-C-C	2	-97	88	-203	14	-2464	2372	-2561
0-0-C-D	3	-80	71	-204	17	-2023	1932	-2120
0-0-C-E	3	-66	60	-148	34	-1677	1622	-1736
0-0-C-F	-2	-50	52	62	-44	-1358	1368	-1351
0-0-C-H	3	-28	29	7	80	-759	803	-716
0-0-C-J	2	-14	19	102	102	-442	544	-341
0-0-C-K	0	-9	14	104	31	-316	386	-250
0-0-C-L	0	-7	7	0	0	-190	190	-190
0-0-C-M	0	-5	7	52	16	-158	193	-125
0-0-C-P	0	-2	2	0	0	-63	63	-63
0-0-C-S	2	0	0	-3	70	0	70	-3
I-0-N-B	79	-199	172	-666	2171	-4945	5897	-4392
I-0-N-C	-10	-34	-2	-779	-521	-415	-216	-1084
I-0-N-D	-26	7	-34	-550	-955	542	-174	-1332
I-0-N-E	-24	12	-17	-79	-742	383	96	-917
I-0-N-F	-22	5	-2	76	-624	96	89	-636
I-0-N-N*	-153	-5	0	63	-4579	-64	64	-4579
0-0-N-B	-2	64	-88	-519	-227	2022	1655	-2400
0-0-N-C	2	40	-45	-107	39	1138	1106	-1174
0-0-N-D*	2	749	-9	16252	4947	10108	22181	-981
0-0-N-E	0	2	0	52	16	32	70	-3
0-0-N-F	5	0	0	-5	141	0	141	-5
0-0-N-H	2	0	-2	-55	55	32	63	-63
0-0-N-K	-5	0	-5	-99	-172	63	-63	-208
0-0-N-N*	0	0	0	0	0	0	0	0

Table A.2 (continued)

OUT-OF-PLANE MOMENT LOADING, MXN, ON NOZZLE (400 IN-LB)

	MICRO-STRAIN			STRESSES			PRIN STRESSES	
ROSETTE	GAGE1	GAGE2	GAGE3	TRANS	LONG	SHEAR	SIGMX	SIGMN
I-90C-B	-17	-247	-227	-10402	-3635	-256	-3625	-10411
I-90C-C*	-46	-192	0	-4163	-2624	-2554	-726	-6061
I-90C-D	-34	-137	-132	-5866	-2774	-63	-2772	-5867
I-90C-E	-31	-98	-91	-4136	-2186	-96	-2181	-4141
I-90C-F	-22	-100	-67	-3652	-1754	-436	-1658	-3748
I-90C-R	7	2	2	81	226	1	226	81
O-90C-B	76	223	258	10493	5424	-474	10537	5380
O-90C-C	88	199	213	8971	5317	-191	8981	5307
O-90C-D*	85	168	0	3604	3636	2242	5862	1378
O-90C-E	80	123	130	5484	4058	-96	5491	4051
O-90C-F	71	102	102	4400	3450	-1	4400	3450
O-90C-R	-3	-5	1	-78	-104	-86	-4	-178
I-90N-B	-594	72	-74	600	-17645	1939	804	-17849
I-90N-C	127	122	122	5214	5364	0	5364	5214
I-90N-D	246	62	100	3294	8358	-508	8409	3244
I-90N-E	215	-5	45	655	6635	-667	6709	582
I-90N-F*	24	-28	3	-588	555	-415	690	-723
I-90N-N	170	84	48	2700	5895	477	5965	2630
O-90N-B	258	401	403	17388	12968	-31	17388	12967
O-90N-C	59	111	118	4983	3268	-94	4988	3263
O-90N-D	95	14	14	510	2991	1	2991	510
O-90N-E	107	-7	-2	-326	3105	-63	3106	-327
O-90N-F	130	38	5	795	4153	443	4210	738
O-90N-N	130	0	7	13	3918	-95	3921	11

Table A.2 (continued)

OUT-OF-PLANE MOMENT LOADING, MXN, ON NOZZLE (400 IN-LB)

	MICRO-STRAIN			STRESSES			PRIN STRESSES	
ROSETTE	GAGE1	GAGE2	GAGE3	TRANS	LONG	SHEAR	SIGMX	SIGMN
I180C-B	-19	162	-130	730	-357	3893	4118	-3744
I180C-C	-12	212	-165	1031	-55	5024	5541	-4565
I180C-D	-10	167	-142	562	-131	4115	4345	-3914
I180C-E	-3	141	-123	397	38	3519	3741	-3306
I180C-F	-3	115	-97	401	41	2827	3054	-2611
I180C-S	2	4	-1	71	66	63	131	6
O180C-B	9	85	-100	-340	167	2471	2397	-2570
O180C-C	2	90	-110	-441	-81	2664	2409	-2931
O180C-D	4	73	-86	-278	38	2122	2008	-2248
O180C-E	4	61	-65	-72	104	1679	1698	-1666
O180C-F	5	53	-53	-5	142	1402	1472	-1336
O180C-S	22	5	0	81	670	64	677	75
I180N-B	-33	246	-172	1662	-503	5561	6245	-5086
I180N-C	2	60	-14	993	370	985	1715	-352
I180N-D	5	24	17	886	409	95	904	391
I180N-E	0	-24	12	-262	-79	-477	315	-656
I180N-F	0	-7	4	-65	-30	-159	112	-207
I180N-N	10	2	-2	-10	283	64	296	-24
O180N-B	7	-77	33	-975	-77	-1478	1019	-2071
O180N-C	7	-36	31	-113	181	-892	938	-870
O180N-D	2	-5	12	155	118	-223	360	-87
O180N-E	2	5	0	102	102	64	166	39
O180N-F	0	7	-2	105	32	127	201	-64
O180N-N	2	2	2	102	102	0	102	102

Table A.2 (continued)

OUT-OF-PLANE MOMENT LOADING, MXN, ON NOZZLE (400 IN-LB)

	MICRO-STRAIN			STRESSES			PRIN STRESSES	
ROSETTE	GAGE1	GAGE2	GAGE3	TRANS	LONG	SHEAR	SIGMX	SIGMN
I270C-C	60	179	179	7797	4128	0	7797	4128
I270C-D	45	129	124	5506	3012	64	5508	3010
I270C-E	33	93	95	4105	2233	-32	4105	2233
I270C-F	21	69	69	3017	1549	0	3017	1549
I270C-H	5	31	29	1305	535	32	1307	533
I270C-J	-10	5	2	168	-236	32	170	-238
I270C-K	-17	-2	-7	-191	-558	64	-181	-569
I270C-L	-17	-10	-10	-401	-621	0	-401	-621
I270C-M	-12	-5	-7	-249	-433	32	-244	-438
I270C-P	-5	2	0	58	-126	32	63	-131
I270C-R*	101	5	0	-5	3016	64	3017	-7
I270C-T	2	7	2	208	134	64	245	97
O270C-B	-124	-281	-300	-12630	-7509	255	-7496	-12642
O270C-C	-112	-196	-193	-8416	-5894	-33	-5894	-8416
O270C-D	-100	-155	-158	-6757	-5039	35	-5039	-6757
O270C-E	-84	-127	-124	-5417	-4138	-31	-4137	-5418
O270C-F	-69	-103	-98	-4337	-3386	-64	-3381	-4341
O270C-H	-43	-62	-62	-2696	-2112	1	-2112	-2696
O270C-J	-20	-25	-27	-1108	-922	30	-918	-1113
O270C-K	-3	-5	-10	-332	-188	64	-163	-356
O270C-L	9	6	7	275	352	-1	352	275
O270C-M	11	9	9	384	454	2	454	384
O270C-P	6	4	7	229	261	-33	282	208
O270C-R	4	4	4	185	180	0	185	180
O270C-T	1	-3	2	-27	35	-64	75	-67
I270N-B	637	12	43	507	19268	-413	19277	498
I270N-C	-67	-126	-107	-5066	-3525	-254	-3484	-5107
I270N-D	-222	-88	-95	-3795	-7797	95	-3792	-7799
I270N-E	-203	-26	-48	-1403	-6507	286	-1387	-6523
I270N-F	-170	10	-12	131	-5051	287	146	-5067
O270N-B	-284	-344	-322	-14324	-12825	-283	-12773	-14375
O270N-C	-62	-109	-114	-4825	-3293	63	-3290	-4828
O270N-D	-83	-14	-17	-597	-2684	32	-596	-2684
O270N-E	-136	7	5	402	-3953	31	402	-3953
O270N-F	-153	2	7	362	-4468	-62	362	-4469
O270N-G	-162	0	-7	16	-4851	95	18	-4853
O270N-H	-164	0	-12	-91	-4959	158	-86	-4964
O270N-K	-164	-10	7	116	-4899	-223	126	-4909
O270N-N	-164	0	-10	-43	-4948	127	-40	-4951

Table A.2 (continued)

OUT-OF-PLANE MOMENT LOADING, MXN, ON NOZZLE (400 IN-LB)

	MICRO-STRAIN			STRESSES			PRIN STRESSES	
ROSETTE	GAGE1	GAGE2	GAGE3	TRANS	LONG	SHEAR	SIGMX	SIGMN
I315C-B	41	41	284	7091	3345	-3245	8965	1472
I315C-C	33	12	275	6260	2881	-3499	8456	684
I315C-D	31	5	191	4272	2213	-2479	5927	558
I315C-F	50	41	86	2726	2322	-604	3161	1887
I315C-H	62	41	100	3028	2771	-795	3705	2093
I315C-J	60	45	86	2820	2637	-541	3277	2180
I315C-K	53	48	76	2671	2377	-382	2933	2115
I315C-L	0	2	36	836	251	-441	1072	14
I315C-M	-5	8	21	657	45	-174	703	-1
I315C-P	-5	0	2	47	-147	-25	51	-150
O315C-B	-55	-228	-64	-6353	-3543	-2181	-2353	-7542
O315C-C	-50	-199	-47	-5367	-3105	-2023	-1918	-6554
O315C-D	-38	-209	-47	-5589	-2816	-2149	-1644	-6760
O315C-E	-26	-176	-45	-4820	-2229	-1738	-1356	-5693
O315C-F	-28	-145	-33	-3879	-2018	-1486	-1195	-4701
O315C-H	-14	-109	-31	-3060	-1345	-1043	-852	-3553
O315C-K	-7	-45	-21	-1452	-649	-316	-540	-1561
O315C-L	-7	-24	-17	-878	-477	-95	-456	-900
O315C-M	-7	-9	-12	-461	-352	32	-343	-470
O315C-P	-2	2	-2	3	-70	63	39	-107
I315N-B	440	-136	79	-1749	12664	-2865	13213	-2297
I315N-C	-62	-96	-108	-4408	-3195	160	-3175	-4428
I315N-D	-165	-51	-94	-2984	-5851	573	-2874	-5961
I315N-E	-149	-12	-43	-1059	-4774	412	-1014	-4819
I315N-F	-125	0	-17	-245	-3812	222	-231	-3826
I315N-N	-125	4	11	480	-3591	-96	482	-3593
O315N-B	-209	-218	-368	-12648	-10058	1991	-8977	-13728
O315N-C	-36	-57	-128	-4027	-2276	948	-1861	-4442
O315N-D	-56	5	-26	-393	-1801	404	-286	-1909
O315N-E	-91	16	3	516	-2586	185	527	-2597
O315N-F	-112	10	5	444	-3237	63	445	-3238
O315N-G	-122	3	-4	96	-3623	95	98	-3626
O315N-H	-117	3	-7	34	-3502	125	38	-3506
O315N-K	-117	3	-11	-65	-3533	186	-55	-3543
O315N-N*	-618	10	-11	640	-18353	281	644	-18357

Table A.3. Torsional moment loading, M_{YN}, on nozzle

TORSIONAL MOMENT LOADING, MYN, ON NOZZLE (1600 IN-LB)

	MICRO-STRAIN			STRESSES			PRIN STRESSES	
ROSETTE	GAGE1	GAGE2	GAGE3	TRANS	LONG	SHEAR	SIGMX	SIGMN
I-0-C-C	7	-24	47	499	354	-954	1383	-530
I-0-C-D	2	-27	47	454	198	-986	1320	-668
I-0-C-E	2	-22	35	297	154	-763	992	-540
I-0-C-F	0	-17	28	251	66	-603	768	-451
I-0-C-H	-3	19	-10	197	-27	381	483	-312
I-0-C-J	0	16	-10	137	28	350	437	-272
I-0-C-K	2	-5	11	134	98	-219	335	-104
I-0-C-L*	-112	-5	9	207	-3300	-190	217	-3311
I-0-C-M	2	-3	9	138	99	-160	280	-42
I-0-C-P	2	-1	4	76	79	-61	138	16
I-0-C-S	2	-1	3	40	61	-42	94	7
O-0-C-B	-9	192	-230	-813	-517	5619	4956	-6286
O-0-C-C	-2	50	-85	-759	-290	1801	1292	-2341
O-0-C-D	-2	31	-56	-554	-222	1166	790	-1566
O-0-C-E	-2	17	-40	-494	-203	753	419	-1116
O-0-C-F	1	8	-30	-504	-133	506	220	-857
O-0-C-H	-2	3	-16	-288	-142	252	47	-478
O-0-C-J	-2	0	-6	-129	-86	90	-15	-200
O-0-C-K	-2	-2	-4	-129	-90	31	-73	-146
O-0-C-L	-2	-2	-4	-132	-88	32	-71	-150
O-0-C-M	-2	1	-4	-80	-77	64	-14	-143
O-0-C-P	-2	-2	-2	-82	-77	-2	-76	-82
O-0-C-S	-2	-2	-2	-80	-70	0	-70	-80
I-0-N-B	57	-213	220	84	1740	-5775	6746	-4923
I-0-N-C	-22	-319	306	-246	-732	-8329	7844	-8821
I-0-N-D	-31	-335	309	-549	-1108	-8583	7759	-9416
I-0-N-E	-39	-326	337	300	-1069	-8836	8479	-9247
I-0-N-F	-34	-326	340	344	-909	-8872	8612	-9177
I-0-N-N	24	-348	335	-304	619	-9094	9263	-8948
O-0-N-B	5	403	-493	-1966	-434	11941	10765	-13165
O-0-N-C	20	394	-417	-511	432	10805	10776	-10855
O-0-N-D	8	373	-433	-1343	-173	10738	9996	-11512
O-0-N-E	10	375	-414	-882	35	10517	10103	-10950
O-0-N-F	15	387	-414	-623	256	10670	10496	-10862
O-0-N-H	-16	413	-395	395	-367	10766	10787	-10758
O-0-N-K	-9	403	-398	124	-225	10674	10624	-10726
O-0-N-N	-52	401	-370	734	-1331	10274	10028	-10625

Table A.3 (continued)

TORSIONAL MOMENT LOADING, MYN, ON NOZZLE (1600 IN-LB)

	MICRO-STRAIN			STRESSES			PRIN STRESSES	
ROSETTE	GAGE1	GAGE2	GAGE3	TRANS	LONG	SHEAR	SIGMX	SIGMN
I-90C-B	-7	-69	45	-518	-371	-1530	1088	-1976
I-90C-C*	-10	-115	0	-2513	-1041	-1530	-79	-3475
I-90C-D	-7	-96	91	-97	-245	-2487	2317	-2658
I-90C-E	-2	-74	72	-50	-87	-1945	1876	-2013
I-90C-F	-2	-29	55	581	103	-1116	1483	-799
I-90C-R	2	0	0	-3	71	0	71	-3
O-90C-B	-18	138	-85	1193	-189	2972	3553	-2549
O-90C-C	-4	74	-52	484	13	1677	1942	-1445
O-90C-D	-2	57	-40	383	54	1294	1523	-1086
O-90C-E	-4	50	-38	276	-49	1171	1296	-1068
O-90C-F	-2	48	-38	220	2	1138	1255	-1033
O-90C-R	-2	-4	-4	-172	-112	-10	-110	-174
I-90N-B	-92	-270	303	843	-2521	-7631	6975	-8654
I-90N-C	-48	-310	408	2194	-782	-9566	10387	-8975
I-90N-D	-62	-326	412	1957	-1259	-9846	10325	-9627
I-90N-E	-66	-338	400	1439	-1559	-9843	9897	-10017
I-90N-F	11	-5	2	-83	314	-94	335	-104
I-90N-N*	86	-176	117	-1386	2176	-3913	4694	-3904
O-90N-B	5	437	-420	370	265	11413	11730	-11095
O-90N-C	22	373	-398	-584	474	10274	10232	-10342
O-90N-D	24	385	-396	-273	641	10400	10594	-10225
O-90N-E*	89	394	-208	3992	3860	8029	11956	-4103
O-90N-F	91	212	-242	-753	2499	6039	7128	-5381
O-90N-N*	91	366	-251	2428	3450	8218	11173	-5295

Table A.3 (continued)

TORSIONAL MOMENT LOADING, MYN, ON NOZZLE (1600 IN-LB)

	MICRO-STRAIN			STRESSES			PRIN STRESSES	
ROSETTE	GAGE1	GAGE2	GAGE3	TRANS	LONG	SHEAR	SIGMX	SIGMN
I180C-B	0	-17	-24	-881	-264	94	-250	-895
I180C-C	0	-45	7	-829	-249	-691	211	-1288
I180C-D	5	-33	9	-523	-16	-565	350	-889
I180C-E	5	-28	7	-471	0	-471	291	-762
I180C-F	2	-21	5	-365	-39	-345	180	-584
I180C-S	0	-2	2	0	0	-63	63	-63
O180C-B	12	214	-202	250	434	5548	5890	-5206
O180C-C	2	93	-57	784	308	1997	2557	-1465
O180C-D	2	62	-36	574	246	1300	1720	-900
O180C-E	0	43	-24	420	128	887	1173	-625
O180C-F	2	33	-10	503	210	571	946	-232
O180C-S*	-8	2	2	97	-197	-2	97	-197
I180N-B	-21	-154	165	267	-541	-4252	4135	-4408
I180N-C	91	-355	268	-2012	2132	-8289	8604	-8484
I180N-D	101	-281	246	-868	2764	-7019	8198	-6303
I180N-E	98	-397	306	-2123	2313	-9369	9722	-9533
I180N-F	104	-415	325	-2082	2487	-9862	10325	-9921
I180N-N*	203	-438	218	-5061	4579	-8733	9734	-10216
O180N-B	-29	458	-293	3662	234	9997	12092	-8195
O180N-C	-22	463	-376	1946	-66	11182	12167	-10287
O180N-D	-5	435	-369	1458	285	10706	11593	-9851
O180N-E	-7	452	-402	1099	105	11371	11984	-10779
O180N-F	-17	437	-397	903	-233	11120	11470	-10799
O180N-N	16	409	-388	437	619	10613	11141	-10085

Table A.3 (continued)

TORSIONAL MOMENT LOADING, MYN, ON NOZZLE (1600 IN-LB)

	MICRO-STRAIN			STRESSES			PRIN STRESSES	
ROSETTE	GAGE1	GAGE2	GAGE3	TRANS	LONG	SHEAR	SIGMX	SIGMN
I270C-C	1	-75	82	160	85	-2096	2219	-1974
I270C-D	1	-61	66	109	69	-1679	1768	-1591
I270C-E	-1	-46	49	62	-17	-1270	1293	-1248
I270C-F	-1	-34	37	61	-16	-952	975	-931
I270C-H	-1	-18	18	13	-26	-477	471	-484
I270C-J	-1	-6	3	-58	-52	-125	70	-180
I270C-K	-2	1	-4	-63	-69	67	1	-133
I270C-L	-2	-2	-6	-183	-101	56	-72	-211
I270C-M	-1	4	-4	7	-27	98	90	-110
I270C-P	-3	0	1	27	-72	-6	27	-72
I270C-R*	-62	5	5	282	-1779	-1	282	-1779
I270C-T	2	0	3	58	90	-32	109	38
O270C-B	-2	155	-209	-1188	-419	4848	4060	-5666
O270C-C	1	79	-95	-345	-87	2314	2102	-2534
O270C-D	-7	62	-73	-232	-267	1803	1553	-2053
O270C-E	-4	53	-61	-182	-181	1520	1339	-1702
O270C-F	-4	46	-52	-129	-165	1299	1152	-1446
O270C-H	-4	31	-40	-178	-177	950	772	-1127
O270C-J	-2	20	-26	-123	-89	604	499	-710
O270C-K	-2	15	-16	-29	-63	412	366	-458
O270C-L	-2	5	-7	-23	-62	159	118	-203
O270C-M	-2	0	-2	-48	-84	31	-30	-102
O270C-P	-2	0	0	5	-67	0	5	-67
O270C-R	-2	-2	0	-48	-84	-32	-29	-103
O270C-T*	0	-2	0	-51	-13	-31	4	-68
I270N-B	7	-213	226	295	291	-5852	6145	-5559
I270N-C	-17	-313	339	588	-334	-8680	8819	-8565
I270N-D	-27	-322	346	548	-633	-8905	8882	-8966
I270N-E	-29	-315	344	655	-673	-8776	8792	-8810
I270N-F	-35	-304	354	1143	-717	-8767	9029	-8603
O270N-B	-16	358	-360	-19	-484	9573	9324	-9827
O270N-C	3	351	-341	219	146	9221	9404	-9039
O270N-D	-9	362	-361	19	-272	9635	9509	-9762
O270N-E	-36	369	-352	413	-941	9604	9364	-9892
O270N-F	-12	357	-354	79	-323	9476	9356	-9600
O270N-G	5	359	-373	-314	52	9762	9633	-9895
O270N-H	3	367	-385	-411	-44	10016	9790	-10245
O270N-K*	-31	398	-359	881	-653	10081	10224	-9996
O270N-N	17	355	-392	-841	258	9952	9676	-10259

Table A.3 (continued)

TORSIONAL MOMENT LOADING, MYN, ON NOZZLE (1600 IN-LB)

	MICRO-STRAIN			STRESSES			PRIN STRESSES	
ROSETTE	GAGE1	GAGE2	GAGE3	TRANS	LONG	SHEAR	SIGMX	SIGMN
I315C-B	0	31	101	2901	876	-925	3260	517
I315C-C	5	5	113	2582	926	-1431	3408	101
I315C-D	7	2	74	1679	718	-958	2270	127
I315C-F	43	29	41	1491	1748	-159	1824	1414
I315C-H	27	20	39	1253	1177	-256	1473	956
I315C-J	22	20	31	1098	987	-159	1211	874
I315C-K	17	17	24	890	783	-95	946	727
I315C-L	-5	-2	12	215	-79	-191	309	-173
I315C-M	-5	0	5	110	-110	-64	127	-127
I315C-P	-2	0	0	3	-71	0	3	-71
O315C-B	53	155	-47	2312	2279	2687	4983	-392
O315C-C	48	98	-4	2004	2041	1356	3379	666
O315C-D	55	17	-78	-1399	1232	1265	1742	-1908
O315C-E	-21	3	-66	-1366	-1042	917	-273	-2135
O315C-F	-21	3	-61	-1251	-1002	863	-255	-1998
O315C-H	-18	-11	-47	-1261	-927	474	-591	-1597
O315C-K	-14	-14	-23	-800	-650	124	-580	-870
O315C-L	-11	-6	-14	-428	-464	94	-350	-542
O315C-M	-7	-4	-9	-287	-286	65	-221	-352
O315C-P	-2	-2	-7	-181	-110	66	-70	-221
I315N-B	84	-220	280	1222	2877	-6657	8758	-4659
I315N-C	0	-316	311	-105	-32	-8345	8277	-8414
I315N-D	-17	-335	316	-402	-623	-8664	8152	-9177
I315N-E	-12	-332	316	-355	-465	-8632	8223	-9042
I315N-F	-24	-339	330	-184	-772	-8919	8446	-9402
I315N-N*	59	-264	299	712	1982	-7506	8880	-6186
O315N-B	52	340	-479	-3117	629	10909	9824	-12313
O315N-C	60	352	-389	-885	1528	9864	10259	-9617
O315N-D	87	357	-394	-918	2333	10008	10846	-9431
O315N-E	59	380	-371	144	1806	10008	11017	-9068
O315N-F	35	376	-380	-138	1018	10071	10528	-9648
O315N-G	26	373	-366	130	817	9852	10332	-9385
O315N-H	24	387	-366	442	840	10040	10682	-9401
O315N-K	21	371	-375	-122	600	9946	10191	-9714
O315N-N	-51	362	-387	-507	-1681	9977	8901	-11089

Table A.4. In-plane moment loading, M_{ZN}, on nozzle

IN-PLANE MOMENT LOADING, MZN, ON NOZZLE (400 IN-LB)

	MICRO-STRAIN			STRESSES			PRIN STRESSES	
ROSETTE	GAGE1	GAGE2	GAGE3	TRANS	LONG	SHEAR	SIGMX	SIGMN
I-0-C-C	-38	-110	-129	-5194	-2700	254	-2674	-5219
I-0-C-D	-7	-81	-102	-4023	-1419	286	-1388	-4054
I-0-C-E	10	-62	-79	-3098	-641	222	-621	-3118
I-0-C-F	22	-50	-64	-2536	-114	190	-99	-2551
I-0-C-H	34	-36	-31	-1499	557	-64	559	-1501
I-0-C-J	26	-26	-19	-1018	486	-96	492	-1024
I-0-C-K	17	-17	-21	-850	251	62	254	-853
I-0-C-L*	-162	-12	-17	-462	-5002	64	-461	-5003
I-0-C-M	0	-7	-10	-376	-120	31	-116	-379
I-0-C-P	0	-7	-5	-276	-91	-31	-86	-281
I-0-C-S	-3	-3	-4	-146	-127	18	-116	-157
O-0-C-B	66	256	261	11289	5381	-64	11290	5380
O-0-C-C	40	171	176	7568	3481	-63	7568	3480
O-0-C-D	19	130	133	5766	2302	-32	5767	2302
O-0-C-E	-2	109	102	4645	1325	94	4648	1323
O-0-C-F	-7	88	78	3659	888	126	3664	882
O-0-C-H	-14	45	45	2000	176	0	2000	176
O-0-C-J	-14	21	17	854	-166	62	858	-170
O-0-C-K	-5	12	10	479	5	32	481	3
O-0-C-L	0	5	5	212	68	0	212	68
O-0-C-M	0	5	5	212	67	0	212	67
O-0-C-P	-2	0	0	6	-66	0	6	-66
O-0-C-S	-2	0	0	7	-65	0	7	-65
I-0-N-B	-498	50	89	3602	-13857	-511	3617	-13872
I-0-N-C	70	110	117	4925	3565	-96	4932	3558
I-0-N-D	201	81	84	3411	7061	-32	7061	3411
I-0-N-E	192	24	31	1002	6050	-96	6052	1000
I-0-N-F	158	0	10	40	4755	-127	4759	37
I-0-N-N*	-19	-5	0	-79	-595	-64	-71	-603
O-0-N-B	197	287	285	12349	9613	32	12349	9613
O-0-N-C	64	83	81	3532	2984	32	3533	2982
O-0-N-D	100	5	5	102	3021	1	3021	102
O-0-N-E	140	-17	-7	-672	3997	-126	4001	-676
O-0-N-F	154	-17	-5	-635	4435	-158	4440	-640
O-0-N-H	164	5	0	-73	4888	63	4888	-74
O-0-N-K	161	5	-2	-123	4803	95	4805	-125
O-0-N-N*	168	14	-1761	-38572	-6521	23655	6026	-51119

Table A.4 (continued)

IN-PLANE MOMENT LOADING, MZN, ON NOZZLE (400 IN-LB)

	MICRO-STRAIN			STRESSES			PRIN STRESSES	
ROSETTE	GAGE1	GAGE2	GAGE3	TRANS	LONG	SHEAR	SIGMX	SIGMN
I-90C-B	12	112	-79	723	576	2550	3201	-1902
I-90C-C*	12	165	0	3615	1443	2200	4982	76
I-90C-D	10	136	-134	42	300	3602	3775	-3434
I-90C-E	2	112	-117	-108	39	3060	3027	-3095
I-90C-F	5	96	-98	-58	126	2582	2618	-2550
I-90C-R	-2	0	0	3	-71	0	3	-71
O-90C-B	-19	24	-66	-912	-839	1201	326	-2077
O-90C-C	-12	104	-93	266	-285	2623	2628	-2647
O-90C-D	-7	76	-69	152	-177	1930	1925	-1950
O-90C-E	-7	50	-50	0	-222	1327	1221	-1442
O-90C-F	-7	33	-40	-156	-266	979	770	-1192
O-90C-R	0	0	-3	-81	-33	40	-10	-104
I-90N-B	117	122	-146	-655	3303	3561	5398	-2750
I-90N-C	-31	-21	-19	-855	-1184	-32	-852	-1187
I-90N-D	-50	-36	24	-207	-1562	-794	160	-1929
I-90N-E	-38	-14	12	-10	-1146	-349	89	-1244
I-90N-F	-21	-17	17	29	-629	-446	254	-853
I-90N-N	21	12	12	484	779	0	779	484
O-90N-B	-3	-55	52	-58	-98	-1422	1345	-1500
O-90N-C	-5	-38	35	-58	-167	-979	868	-1093
O-90N-D	-5	-12	9	-58	-169	-283	175	-403
O-90N-E	0	0	-3	-62	-32	31	-12	-81
O-90N-F	-3	2	-3	-8	-83	62	27	-118
O-90N-N	-3	0	-3	-61	-97	31	-43	-115

Table A.4 (continued)

IN-PLANE MOMENT LOADING, MZN, ON NOZZLE (400 IN-LB)

	MICRO-STRAIN			STRESSES			PRIN STRESSES	
ROSETTE	GAGE1	GAGE2	GAGE3	TRANS	LONG	SHEAR	SIGMX	SIGMN
I180C-B	33	108	144	5507	2642	-471	5582	2567
I180C-C	21	94	130	4898	2106	-471	4975	2029
I180C-D	-2	68	94	3577	1002	-345	3622	957
I180C-E	-21	52	73	2769	194	-283	2799	164
I180C-F	-28	38	57	2103	-218	-251	2130	-244
I180C-S	0	2	2	104	31	0	104	31
O180C-B	-48	-238	-248	-10628	-4626	126	-4624	-10631
O180C-C	-34	-176	-165	-7455	-3247	-158	-3241	-7461
O180C-D	-15	-136	-126	-5745	-2164	-128	-2159	-5750
O180C-E	0	-105	-95	-4403	-1330	-127	-1325	-4408
O180C-F	7	-88	-78	-3660	-880	-127	-874	-3666
O180C-S	-17	-5	-5	-185	-571	1	-185	-571
I180N-B	449	-62	-131	-4732	12037	922	12088	-4782
I180N-C	-26	-57	-150	-4527	-2142	1240	-1614	-5055
I180N-D	-191	60	-60	214	-5657	1589	617	-6059
I180N-E	-203	-55	-2	-1030	-6388	-699	-941	-6478
I180N-F	-172	-31	5	-381	-5277	-471	-336	-5321
I180N-N	-129	-17	26	357	-3754	-571	435	-3832
O180N-B	-143	-209	-207	-8981	-6971	-28	-6971	-8981
O180N-C	-62	-71	-62	-2854	-2708	-126	-2635	-2927
O180N-D	-119	0	10	343	-3460	-126	347	-3464
O180N-E	-162	7	10	545	-4683	-31	545	-4683
O180N-F	-164	-5	7	233	-4850	-159	238	-4855
O180N-N	-178	-9	-7	-165	-5395	-32	-165	-5395

Table A.4 (continued)

IN-PLANE MOMENT LOADING, MZN, ON NOZZLE (400 IN-LB)

	MICRO-STRAIN			STRESSES			PRIN STRESSES	
ROSETTE	GAGE1	GAGE2	GAGE3	TRANS	LONG	SHEAR	SIGMX	SIGMN
I270C-C	-2	-172	153	-407	-187	-4322	4027	-4620
I270C-D	-5	-143	127	-351	-242	-3590	3294	-3887
I270C-E	-5	-124	108	-351	-242	-3083	2787	-3379
I270C-F	-5	-100	91	-194	-194	-2542	2348	-2737
I270C-H	-2	-67	65	-38	-75	-1748	1691	-1805
I270C-J	-2	-38	36	-42	-77	-985	925	-1044
I270C-K	-2	-19	17	-43	-80	-476	415	-538
I270C-L	0	-4	0	-88	-22	-57	11	-121
I270C-M	-2	3	-5	-39	-75	96	40	-155
I270C-P	-2	-2	-2	-98	-98	-1	-97	-99
I270C-R*	158	-2	0	-223	4682	-33	4683	-223
I270C-T	-2	-7	-2	-198	-130	-64	-92	-236
O270C-B	2	-77	109	708	267	-2470	2968	-1993
O270C-C	-1	-79	99	449	118	-2379	2668	-2101
O270C-D	7	-60	73	285	283	-1772	2056	-1488
O270C-E	4	-43	54	234	197	-1299	1515	-1083
O270C-F	4	-29	38	181	181	-888	1069	-707
O270C-H	2	-8	14	128	91	-284	394	-175
O270C-J	2	6	-3	71	73	125	197	-52
O270C-K	-1	11	-10	31	-7	286	298	-275
O270C-L	-1	11	-10	25	-9	284	292	-277
O270C-M	0	5	-5	-12	-14	128	115	-140
O270C-P	0	0	0	-13	-16	-1	-13	-16
O270C-R	0	0	0	-11	-13	0	-11	-13
O270C-T	0	0	0	-14	-18	0	-14	-19
I270N-B	-26	-162	165	75	-771	-4356	4029	-4725
I270N-C	-3	-12	12	-1	-76	-317	281	-358
I270N-D	0	19	-26	-160	-53	604	500	-713
I270N-E	-3	10	-19	-210	-140	382	209	-559
I270N-F	-1	2	-7	-104	-74	128	39	-217
O270N-B	14	74	-43	665	630	1549	2196	-902
O270N-C	2	52	-40	260	151	1232	1439	-1028
O270N-D	4	21	-17	84	155	508	629	-390
O270N-E	4	7	-5	33	141	157	253	-79
O270N-F	7	4	-3	19	202	97	244	-23
O270N-G	7	5	0	90	235	64	259	66
O270N-H	7	7	-3	79	223	127	297	5
O270N-K	4	4	-3	27	132	93	186	-27
O270N-N	-1	2	-1	27	-14	32	45	-31

Table A.4 (continued)

IN-PLANE MOMENT LOADING, MZN, ON NOZZLE (400 IN-LB)

	MICRO-STRAIN			STRESSES			PRIN STRESSES	
ROSETTE	GAGE1	GAGE2	GAGE3	TRANS	LONG	SHEAR	SIGMX	SIGMN
I315C-B	-41	-184	-3	-4060	-2440	-2415	-702	-5797
I315C-C	-19	-160	31	-2825	-1427	-2545	512	-4765
I315C-D	0	-115	38	-1695	-504	-2038	1024	-3222
I315C-F	21	-22	2	-457	498	-318	594	-553
I315C-H	26	0	21	424	904	-285	1037	291
I315C-J	28	9	21	634	1039	-159	1094	579
I315C-K	26	12	19	639	967	-96	993	614
I315C-L	7	0	7	150	260	-96	315	95
I315C-M	0	0	10	210	63	-127	284	-11
I315C-P	0	-2	5	53	16	-96	131	-63
O315C-B	40	85	140	4897	2670	-727	5113	2454
O315C-C	40	64	116	3907	2375	-694	4174	2107
O315C-D	28	59	111	3715	1962	-696	3957	1719
O315C-E	14	47	83	2843	1277	-474	2976	1144
O315C-F	9	38	62	2171	930	-317	2248	853
O315C-H	-3	16	23	879	183	-95	892	171
O315C-K	-7	-10	-7	-366	-331	-31	-313	-383
O315C-L	0	-15	-7	-482	-154	-94	-128	-507
O315C-M	-3	-10	-7	-370	-188	-33	-182	-376
O315C-P	-3	-5	-5	-217	-143	-1	-143	-217
I315N-B	-308	-100	122	811	-9008	-2962	1636	-9833
I315N-C	60	55	86	3034	2703	-414	3315	2423
I315N-D	139	60	43	2107	4792	223	4810	2088
I315N-E	124	19	14	599	3909	64	3910	598
I315N-F	105	0	7	42	3168	-96	3171	39
I315N-N	97	-9	-5	-417	2774	-63	2776	-418
O315N-B	201	268	197	9990	9014	946	10567	8437
O315N-C	52	118	40	3429	2588	1042	4132	1885
O315N-D	64	26	-4	421	2049	398	2141	329
O315N-E	92	-2	-9	-349	2659	86	2661	-351
O315N-F	111	-4	-6	-347	3237	34	3237	-348
O315N-G	123	3	1	-43	3678	36	3678	-44
O315N-H	118	3	3	-2	3547	-1	3547	-2
O315N-K	123	3	6	58	3703	-35	3703	58
O315N-N	-30	3	6	226	-821	-32	227	-822

Table A.5. In-plane force, F_{XN}, on nozzle

IN-PLANE FORCE LOADING, FXN, ON NOZZLE (80 LB)

	MICRO-STRAIN			STRESSES			PRIN STRESSES	
ROSETTE	GAGE1	GAGE2	GAGE3	TRANS	LONG	SHEAR	SIGMX	SIGMN
I-0-C-C	86	265	286	12018	6184	-286	12032	6170
I-0-C-D	17	196	229	9316	3297	-445	9349	3265
I-0-C-E	-33	150	174	7169	1151	-317	7186	1134
I-0-C-F	-57	124	141	5884	50	-222	5892	42
I-0-C-H	-88	76	74	3402	-1624	31	3403	-1624
I-0-C-J	-71	57	50	2442	-1411	95	2444	-1414
I-0-C-K	-45	41	48	1994	-759	-96	1997	-762
I-0-C-L*	-134	26	34	1462	-3574	-95	1464	-3576
I-0-C-M	-7	19	22	903	59	-32	904	58
I-0-C-P	-5	12	10	483	5	32	485	3
I-0-C-S	0	7	5	262	84	35	269	77
O-0-C-B	-168	-611	-640	-27311	-13232	376	-13222	-27321
O-0-C-C	-102	-400	-422	-17945	-8433	285	-8424	-17954
O-0-C-D	-52	-308	-324	-13835	-5700	219	-5695	-13841
O-0-C-E	-2	-258	-255	-11277	-3438	-36	-3438	-11277
O-0-C-F	8	-211	-196	-8950	-2454	-189	-2448	-8956
O-0-C-H	29	-111	-118	-5063	-650	94	-648	-5065
O-0-C-J	20	-59	-51	-2445	-141	-100	-136	-2449
O-0-C-K	3	-35	-33	-1488	-356	-32	-355	-1489
O-0-C-L	-9	-21	-21	-906	-534	1	-534	-906
O-0-C-M	-7	-16	-16	-700	-405	1	-405	-700
O-0-C-P	-4	-9	-9	-392	-241	-2	-241	-392
O-0-C-S	-2	-7	-7	-288	-132	0	-132	-288
I-0-N-B	1188	-115	-206	-8346	33146	1212	33181	-8381
I-0-N-C	-153	-273	-268	-11720	-8103	-63	-8102	-11721
I-0-N-D	-462	-206	-189	-8174	-16309	-224	-8168	-16315
I-0-N-E	-431	-67	-69	-2522	-13680	30	-2521	-13681
I-0-N-F	-352	-9	-17	-183	-10611	98	-182	-10611
I-0-N-N	19	-24	22	-58	566	-607	937	-428
O-0-N-B	-455	-678	-678	-29283	-22429	1	-22429	-29283
O-0-N-C	-139	-196	-196	-8464	-6718	2	-6718	-8464
O-0-N-D	-215	-11	-21	-473	-6595	130	-470	-6597
O-0-N-E	-303	38	5	1285	-8699	444	1304	-8719
O-0-N-F	-341	36	-2	1122	-9884	503	1145	-9907
O-0-N-H	-346	-9	-9	-24	-10375	-1	-24	-10375
O-0-N-K	-300	-7	-9	-25	-9014	33	-25	-9015
O-0-N-N*	-196	-16	1147	25060	1631	-15492	32768	-6077

Table A.5 (continued)

IN-PLANE FORCE LOADING, FXN, ON NOZZLE (80 LB)

	MICRO-STRAIN			STRESSES			PRIN STRESSES	
ROSETTE	GAGE1	GAGE2	GAGE3	TRANS	LONG	SHEAR	SIGMX	SIGMN
I-90C-B	-26	-242	201	-864	-1048	-5901	4946	-6858
I-90C-C*	-24	-364	0	-7970	-3107	-4848	-115	-10962
I-90C-D	-17	-304	323	442	-369	-8357	8404	-8331
I-90C-E	-5	-256	275	428	-12	-7081	7293	-6877
I-90C-F	-12	-180	230	1110	-24	-5461	6033	-4947
I-90C-R*	0	0	0	3	3	0	4	3
O-90C-B	34	-87	124	771	1248	-2806	3826	-1807
O-90C-C	22	-258	207	-1156	309	-6195	5815	-6662
O-90C-D	15	-192	150	-928	165	-4558	4210	-4972
O-90C-E	10	-132	107	-569	129	-3192	2991	-3431
O-90C-F	5	-85	83	-43	140	-2244	2294	-2197
O-90C-R	1	1	6	156	63	-78	200	18
I-90N-B	-224	-267	332	1668	-6214	-7981	6627	-11174
I-90N-C	64	57	10	1399	2354	635	2671	1082
I-90N-D	96	91	-60	580	3049	2004	4168	-539
I-90N-E	70	48	-60	-334	1986	1431	2668	-1017
I-90N-F	48	41	-45	-154	1389	1144	1997	-762
I-90N-N	-54	-21	-33	-1116	-1963	159	-1087	-1992
O-90N-B	-16	79	-137	-1270	-862	2877	1818	-3950
O-90N-C	3	62	-75	-296	-5	1832	1688	-1988
O-90N-D	1	5	-2	72	39	93	150	-39
O-90N-E	-6	-21	15	-122	-212	-474	309	-642
O-90N-F	-6	-13	20	142	-144	-439	461	-463
O-90N-N	-2	-18	13	-122	-87	-410	306	-515

Table A.5 (continued)

IN-PLANE FORCE LOADING, FXN, ON NOZZLE (80 LB)

	MICRO-STRAIN			STRESSES			PRIN STRESSES	
ROSETTE	GAGE1	GAGE2	GAGE3	TRANS	LONG	SHEAR	SIGMX	SIGMN
I180C-B	-75	-252	-316	-12409	-5987	849	-5877	-12519
I180C-C	-52	-231	-283	-11242	-4929	692	-4854	-11317
I180C-D	9	-170	-208	-8302	-2207	503	-2165	-8344
I180C-E	50	-127	-163	-6429	-442	471	-405	-6466
I180C-F	66	-94	-127	-4945	498	440	533	-4980
I180C-S	2	-5	-5	-207	11	0	11	-207
O180C-B	115	540	526	23297	10433	192	23300	10430
O180C-C	84	405	386	17275	7702	251	17282	7695
O180C-D	44	309	300	13338	5311	129	13340	5309
O180C-E	8	241	224	10196	3293	222	10203	3286
O180C-F	-17	195	176	8173	1955	253	8184	1945
O180C-S	-32	0	0	38	-951	1	38	-951
I180N-B	-1039	120	311	10607	-27982	-2537	10773	-28148
I180N-C	51	120	344	10137	4561	-2985	11434	3265
I180N-D	432	-152	129	-970	12676	-3747	13637	-1931
I180N-E	451	113	-4	1890	14105	1559	14301	1694
I180N-F	380	57	-9	620	11578	880	11649	550
I180N-N	144	20	-33	-438	4179	702	4283	-542
O180N-B	328	500	468	20925	16124	422	20961	16087
O180N-C	128	171	138	6655	5850	444	6851	5653
O180N-D	250	5	-31	-847	7239	475	7267	-875
O180N-E	345	-12	-31	-1318	9951	254	9956	-1324
O180N-F	347	14	-26	-642	10223	539	10250	-669
O180N-N	202	5	0	-115	6032	63	6032	-115

Table A.5 (continued)

IN-PLANE FORCE LOADING, FXN, ON NOZZLE (80 LB)

	MICRO-STRAIN			STRESSES			PRIN STRESSES	
ROSETTE	GAGE1	GAGE2	GAGE3	TRANS	LONG	SHEAR	SIGMX	SIGMN
I270C-C	-4	378	-361	374	5	9849	10040	-9661
I270C-D	-1	316	-302	321	61	8233	8424	-8043
I270C-E	6	276	-256	421	306	7085	7449	-6722
I270C-F	4	223	-220	56	126	5910	6001	-5819
I270C-H	-3	149	-151	-36	-113	4002	3928	-4077
I270C-J	1	80	-87	-166	-13	2226	2138	-2317
I270C-K	-4	39	-45	-113	-156	1115	981	-1250
I270C-L	-4	5	-4	30	-109	120	99	-178
I270C-M	-1	-3	6	60	-10	-123	153	-103
I270C-P	-3	-2	6	79	-56	-102	133	-111
I270C-R	11	2	2	82	361	3	361	82
I270C-T	0	-3	2	-32	-14	-64	42	-87
O270C-B	1	205	-246	-905	-243	6012	5447	-6595
O270C-C	5	195	-223	-606	-19	5572	5267	-5892
O270C-D	-9	150	-166	-331	-365	4206	3858	-4554
O270C-E	-4	112	-120	-177	-176	3101	2924	-3278
O270C-F	-2	79	-85	-127	-90	2184	2075	-2293
O270C-H	1	27	-30	-75	0	759	722	-797
O270C-J	3	-9	10	34	105	-251	322	-184
O270C-K	5	-18	24	125	200	-570	734	-409
O270C-L	3	-21	24	83	116	-600	699	-501
O270C-M	3	-9	13	74	115	-288	383	-194
O270C-P	1	3	3	133	66	1	133	66
O270C-R	1	1	1	23	29	0	29	23
O270C-T*	1	-2	0	-39	20	-23	28	-46
I270N-B	31	358	-370	-294	845	9700	9993	-9441
I270N-C	0	2	2	106	33	0	106	33
I270N-D	2	-74	91	366	183	-2194	2471	-1922
I270N-E	7	-52	76	518	372	-1718	2164	-1274
I270N-F	11	-34	50	356	441	-1117	1516	-719
O270N-B	-28	-132	74	-1256	-1210	-2745	1511	-3978
O270N-C	-7	-95	69	-553	-369	-2180	1721	-2643
O270N-D	-4	-18	13	-126	-159	-414	271	-556
O270N-E	-9	15	-16	-17	-272	413	288	-577
O270N-F	-6	22	-23	-2	-186	599	512	-701
O270N-G	-7	19	-23	-84	-229	570	418	-731
O270N-H	-9	17	-23	-118	-297	539	339	-754
O270N-K	-1	25	-18	139	1	574	648	-508
O270N-N	1	22	-23	-10	31	601	611	-590

Table A.5 (continued)

IN-PLANE FORCE LOADING, FXN, ON NOZZLE (80 LB)

	MICRO-STRAIN			STRESSES			PRIN STRESSES	
ROSETTE	GAGE1	GAGE2	GAGE3	TRANS	LONG	SHEAR	SIGMX	SIGMN
I315C-B	93	425	-4	9154	5548	5722	13350	1352
I315C-C	43	373	-83	6326	3200	6076	11037	-1511
I315C-D	-3	266	-97	3717	1036	4847	7405	-2652
I315C-F	-54	48	-9	925	-1353	763	1157	-1585
I315C-H	-64	1	-56	-1155	-2261	762	-767	-2649
I315C-J	-73	-26	-57	-1726	-2718	414	-1576	-2868
I315C-K	-59	-30	-47	-1641	-2260	223	-1569	-2332
I315C-L	-19	2	-24	-453	-711	348	-211	-953
I315C-M	-5	-1	-21	-488	-289	274	-98	-680
I315C-P	0	0	-12	-262	-75	157	14	-351
O315C-B	-94	-196	-334	-11544	-6286	1834	-5709	-12121
O315C-C	-89	-142	-274	-9047	-5399	1766	-4684	-9762
O315C-D	-63	-125	-258	-8355	-4409	1771	-3731	-9033
O315C-E	-33	-97	-189	-6249	-2861	1233	-2460	-6650
O315C-F	-18	-77	-140	-4743	-1975	831	-1744	-4974
O315C-H	12	-38	-54	-2029	-236	221	-209	-2055
O315C-K	15	26	17	938	722	125	995	665
O315C-L	3	19	17	801	329	31	803	327
O315C-M	0	19	12	693	218	97	712	199
O315C-P	5	8	5	276	238	34	296	218
I315N-B	715	227	-273	-1784	20923	6661	22733	-3594
I315N-C	-134	-155	-175	-7106	-6150	255	-6086	-7170
I315N-D	-313	-167	-69	-4858	-10858	-1307	-4586	-11130
I315N-E	-273	-72	-7	-1433	-8609	-860	-1332	-8711
I315N-F	-225	-24	10	-67	-6765	-446	-37	-6795
I315N-N	-106	-7	28	584	-3003	-471	645	-3064
O315N-B	-456	-612	-486	-23623	-20766	-1672	-19996	-24393
O315N-C	-106	-258	-116	-8108	-5624	-1894	-4601	-9131
O315N-D	-130	-42	-8	-960	-4176	-463	-894	-4241
O315N-E	-188	28	2	870	-5385	349	890	-5404
O315N-F	-231	28	-10	643	-6731	499	677	-6764
O315N-G	-250	13	-22	91	-7458	466	120	-7487
O315N-H	-240	14	-26	-11	-7205	533	28	-7244
O315N-K	-219	18	-29	7	-6564	628	67	-6623
O315N-N	-53	16	-26	-175	-1634	563	17	-1826

Table A.6. Axial force, F_{YN}, on nozzle

AXIAL FORCE LOADING, FYN, CN NOZZLE (400 LB)

	MICRO-STRAIN			STRESSES			PRIN STRESSES	
ROSETTE	GAGE1	GAGE2	GAGE3	TRANS	LONG	SHEAR	SIGMX	SIGMN
I-0-C-C	-15	-50	-115	-3616	-1523	858	-1216	-3923
I-0-C-D	24	-58	-117	-3865	-452	794	-276	-4041
I-0-C-E	43	-60	-110	-3782	148	667	258	-3892
I-0-C-F	50	-67	-110	-3943	311	573	387	-4019
I-0-C-H	54	-93	-72	-3690	526	-286	546	-3710
I-0-C-J	40	-81	-62	-3206	243	-253	261	-3225
I-0-C-K	28	-53	-74	-2827	-2	289	28	-2857
I-0-C-L*	69	-41	-58	-2245	1409	223	1423	-2258
I-0-C-M	9	-36	-46	-1808	-268	126	-258	-1818
I-0-C-P	2	-27	-29	-1232	-311	34	-310	-1233
I-0-C-S	2	-15	-14	-632	-138	-14	-137	-633
0-0-C-B	52	209	194	8792	4193	192	8800	4185
0-0-C-C	26	163	142	6676	2778	284	6696	2757
0-0-C-D	14	137	123	5702	2124	191	5712	2114
0-0-C-E	-3	125	106	5086	1441	257	5104	1423
0-0-C-F	-1	113	92	4518	1339	284	4543	1314
0-0-C-H	-3	78	75	3370	926	32	3371	926
0-0-C-J	2	66	54	2644	854	160	2659	840
0-0-C-K	7	52	47	2170	856	63	2173	853
0-0-C-L	7	42	38	1755	730	63	1759	726
0-0-C-M	4	35	31	1444	567	63	1449	563
0-0-C-P	0	26	23	1086	317	32	1087	316
0-0-C-S	-5	14	14	621	33	0	621	33
I-0-N-B	-386	103	31	3360	-10564	957	3425	-10629
I-0-N-C	7	117	105	4879	1670	159	4887	1662
I-0-N-D	98	77	81	3362	3945	-63	3951	3355
I-0-N-E	81	33	36	1432	2864	-30	2864	1432
I-0-N-F	57	17	17	666	1918	-2	1918	666
I-0-N-N	62	7	-3	24	1867	128	1876	15
0-0-N-B	21	168	187	7785	2971	-253	7799	2957
0-0-N-C	-60	26	45	1615	-1302	-254	1637	-1324
0-0-N-D	-24	-26	-14	-868	-979	-159	-755	-1092
0-0-N-E	14	-29	-21	-1116	85	-96	93	-1123
0-0-N-F	31	-24	-14	-875	654	-125	665	-885
0-0-N-H	42	-17	-10	-625	1087	-94	1092	-631
0-0-N-K	54	-14	-7	-532	1466	-95	1471	-537
0-0-N-N	57	0	77	1632	2191	-1033	2982	841

Table A.6 (continued)

AXIAL FORCE LOADING, FYN, CN NOZZLE (400 LB)

	MICRO-STRAIN			STRESSES			PRIN STRESSES	
ROSETTE	GAGE1	GAGE2	GAGE3	TRANS	LONG	SHEAR	SIGMX	SIGMN
I-90C-B	-17	-50	-50	-2190	-1159	0	-1159	-2190
I-90C-C*	-10	-41	0	-883	-552	-542	-151	-1284
I-90C-D	10	-24	-33	-1272	-95	127	-81	-1286
I-90C-E	24	-12	-19	-710	505	96	512	-717
I-90C-F	33	14	-10	68	1025	319	1122	-28
I-90C-R	12	-2	-10	-276	276	96	292	-292
O-90C-B	35	121	142	5731	2777	-286	5759	2749
O-90C-C	33	119	116	5129	2539	32	5129	2538
O-90C-D	29	97	88	4041	2070	126	4049	2062
O-90C-E	14	62	57	2595	1209	64	2597	1206
O-90C-F	5	48	43	1979	738	63	1982	735
O-90C-R	-9	-14	-14	-604	-462	-3	-462	-604
I-90N-B	-296	76	-10	1791	-8343	1145	1919	-8470
I-90N-C	59	79	69	3178	2735	128	3212	2701
I-90N-D	109	33	45	1608	3767	-160	3779	1596
I-90N-E	83	-12	5	-250	2423	-223	2442	-268
I-90N-F*	-74	-53	28	-458	-2372	-1079	28	-2857
I-90N-N	-43	-31	-36	-1432	-1725	64	-1419	-1738
O-90N-B	81	188	206	8570	4995	-253	8588	4977
O-90N-C	-12	43	64	2364	356	-285	2403	316
O-90N-D	19	-2	12	192	631	-190	702	121
O-90N-E	31	-2	10	126	968	-158	997	98
O-90N-F	45	17	12	580	1530	64	1534	576
O-90N-N	29	-5	7	25	865	-158	893	-3

Table A.6 (continued)

AXIAL FORCE LOADING, FYN, CN NOZZLE (400 LB)

	MICRO-STRAIN			STRESSES			PRIN STRESSES	
ROSETTE	GAGE1	GAGE2	GAGE3	TRANS	LONG	SHEAR	SIGMX	SIGMN
I180C-B	-7	-76	-31	-2335	-920	-598	-701	-2554
I180C-C	7	-104	-50	-3388	-812	-724	-622	-3577
I180C-D	33	-102	-62	-3624	-110	-534	-30	-3703
I180C-E	52	-102	-69	-3801	407	-439	452	-3846
I180C-F	52	-90	-73	-3643	456	-220	468	-3654
I180C-S	-1	-22	-24	-1008	-322	31	-320	-1009
O180C-B	35	142	190	7268	3237	-636	7366	3139
O180C-C	21	119	154	5973	2417	-473	6035	2355
O180C-D	9	107	133	5262	1846	-350	5298	1810
O180C-E	-1	92	112	4485	1330	-254	4505	1310
O180C-F	-7	86	95	3979	980	-127	3984	974
O180C-S*	33	17	19	747	1223	-32	1225	745
I180N-B	-287	0	117	2867	-7735	-1559	3091	-7960
I180N-C	-31	38	126	3638	154	-1176	3998	-206
I180N-D	64	-41	62	389	2039	-1367	2811	-383
I180N-E	62	43	26	1439	2284	221	2338	1385
I180N-F	37	28	9	778	1357	250	1450	685
I180N-N	36	12	-12	-55	1049	316	1133	-139
O180N-B	-26	115	124	5273	798	-115	5276	795
O180N-C	-71	21	21	1019	-1834	0	1019	-1834
O180N-D	-26	-31	-17	-1016	-1089	-190	-859	-1246
O180N-E	7	-31	-17	-1053	-102	-190	-65	-1089
O180N-F	19	-24	-14	-857	314	-127	327	-870
O180N-N	50	-5	2	-107	1466	-95	1471	-113

Table A.6 (continued)

AXIAL FORCE LOADING, FYN, CN NOZZLE (400 LB)

	MICRO-STRAIN			STRESSES			PRIN STRESSES	
ROSETTE	GAGE1	GAGE2	GAGE3	TRANS	LONG	SHEAR	SIGMX	SIGMN
I270C-C	-34	-110	-89	-4338	-2320	-286	-2280	-4378
I270C-D	-10	-77	-58	-2950	-1188	-256	-1151	-2987
I270C-E	7	-53	-39	-2027	-410	-191	-388	-2049
I270C-F	21	-34	-22	-1256	250	-159	267	-1272
I270C-H	42	-10	2	-233	1199	-159	1216	-250
I270C-J	57	9	16	494	1849	-97	1855	487
I270C-K	52	7	19	501	1715	-161	1736	480
I270C-L	43	14	9	451	1412	58	1415	448
I270C-M	28	-1	-1	-58	822	-1	822	-58
I270C-P	15	-7	-7	-341	334	3	334	-341
I270C-R	8	-7	-7	-316	145	-3	145	-316
I270C-T	-12	-2	3	37	-345	-64	48	-355
O270C-B	104	245	276	11329	6533	-411	11363	6498
O270C-C	85	166	173	7372	4774	-96	7376	4770
O270C-D	71	131	140	5872	3895	-125	5880	3887
O270C-E	52	104	104	4533	2923	0	4533	2923
O270C-F	38	81	83	3555	2201	-32	3556	2201
O270C-H	9	38	40	1703	788	-31	1704	787
O270C-J	-12	2	0	51	-350	31	53	-353
O270C-K	-26	-14	-19	-712	-1006	64	-699	-1019
O270C-L	-29	-26	-29	-1184	-1219	31	-1165	-1237
O270C-M	-27	-24	-27	-1089	-1128	34	-1069	-1147
O270C-P	-13	-17	-22	-845	-630	62	-613	-862
O270C-R	-10	-12	-17	-634	-492	64	-468	-659
O270C-T	4	11	9	443	251	32	448	246
I270N-B	-528	24	7	1250	-15456	222	1253	-15459
I270N-C	57	126	105	5018	3216	288	5063	3171
I270N-D	174	79	74	3160	6167	63	6168	3159
I270N-E	148	12	21	567	4600	-126	4604	563
I270N-F	106	-17	-12	-748	2967	-64	2968	-749
O270N-B	184	291	270	12132	9170	281	12158	9143
O270N-C	7	85	90	3837	1356	-63	3839	1355
O270N-D	33	9	14	479	1138	-63	1144	474
O270N-E	81	-5	2	-147	2378	-96	2382	-151
O270N-F	93	2	7	96	2805	-63	2807	94
O270N-G	95	9	21	573	3025	-158	3035	562
O270N-H	88	9	24	628	2823	-190	2840	611
O270N-K	71	9	12	383	2248	-33	2249	383
O270N-N	57	-7	4	-126	1666	-158	1680	-140

Table A.6 (continued)

AXIAL FORCE LOADING, FYN, CN NOZZLE (400 LB)

	MICRO-STRAIN			STRESSES			PRIN STRESSES	
ROSETTE	GAGE1	GAGE2	GAGE3	TRANS	LONG	SHEAR	SIGMX	SIGMN
I315C-B	-43	-43	-174	-4734	-2712	1751	-1701	-5745
I315C-C	-12	-36	-179	-4716	-1777	1908	-838	-5655
I315C-D	7	-31	-131	-3569	-849	1344	-298	-4121
I315C-F	-10	-31	-65	-2096	-921	445	-771	-2246
I315C-H	-17	-27	-79	-2301	-1198	700	-858	-2641
I315C-J	-19	-31	-67	-2140	-1221	477	-1019	-2343
I315C-K	-19	-34	-55	-1928	-1159	286	-1064	-2023
I315C-L	29	-4	-15	-450	726	136	741	-465
I315C-M	21	-1	7	102	668	-112	689	80
I315C-P	16	-5	19	291	574	-311	774	91
O315C-B	57	214	107	6979	3805	1422	7523	3261
O315C-C	52	183	90	5942	3351	1232	6434	2859
O315C-D	36	187	90	6063	2889	1296	6525	2427
O315C-E	24	161	78	5242	2286	1106	5610	1918
O315C-F	24	138	62	4356	2021	1012	4733	1644
O315C-H	5	85	38	2699	947	632	2903	743
O315C-K	2	12	19	670	268	-94	691	247
O315C-L	12	5	9	293	438	-63	462	269
O315C-M	2	-12	5	-164	19	-222	167	-312
O315C-P	-10	-22	-7	-622	-475	-191	-344	-753
I315N-B	-440	93	7	2686	-12396	1148	2773	-12483
I315N-C	57	115	124	5182	3269	-126	5190	3261
I315N-D	148	69	81	3136	5381	-159	5393	3125
I315N-E	119	16	26	803	3819	-129	3824	798
I315N-F	91	-5	5	-111	2685	-128	2691	-117
I315N-N	48	0	-10	-274	1357	125	1367	-283
O315N-B	154	275	287	12181	8260	-159	12188	8254
O315N-C	-24	95	81	3880	449	189	3890	439
O315N-D	0	9	-12	-48	-12	280	251	-311
O315N-E	42	-9	-23	-767	1040	187	1059	-786
O315N-F	68	-5	-19	-586	1870	188	1885	-601
O315N-G	73	2	-5	-126	2149	94	2153	-130
O315N-H	71	2	0	-23	2109	31	2110	-23
O315N-K	66	-5	5	-67	1955	-126	1962	-75
O315N-N*	503	-7	7	-547	14918	-188	14921	-549

Table A.7. Out-of-plane force, F_{ZN}, on nozzle

OUT-OF-PLANE FORCE LOADING, FZN, ON NOZZLE (60 LB)

	MICRO-STRAIN			STRESSES			PRIN STRESSES	
ROSETTE	GAGE1	GAGE2	GAGE3	TRANS	LONG	SHEAR	SIGMX	SIGMN
I-0-C-C	12	-322	293	-654	155	-8199	7960	-8459
I-0-C-D	2	-289	265	-531	-94	-7377	7068	-7693
I-0-C-E	7	-234	214	-437	79	-5975	5802	-6159
I-0-C-F	9	-189	179	-228	212	-4893	4890	-4906
I-0-C-H	0	102	-108	-115	-44	2797	2718	-2877
I-0-C-J	0	64	-69	-118	-44	1780	1700	-1862
I-0-C-K	4	-43	40	-72	112	-1110	1134	-1093
I-0-C-L*	-136	-27	21	30	-4065	-636	127	-4161
I-0-C-M	0	-17	16	-11	-12	-446	434	-457
I-0-C-P	0	-8	9	35	0	-221	239	-204
I-0-C-S	-1	-5	5	-1	-15	-137	130	-146
0-0-C-B	5	-164	119	-995	-156	-3758	3206	-4357
0-0-C-C	-2	-171	142	-622	-258	-4168	3732	-4612
0-0-C-D	5	-142	116	-578	-31	-3442	3148	-3757
0-0-C-E	5	-114	97	-370	31	-2810	2648	-2987
0-0-C-F	-5	-90	83	-151	-188	-2305	2136	-2475
0-0-C-H	2	-55	47	-159	23	-1358	1293	-1429
0-0-C-J	-2	-26	28	55	-55	-726	728	-728
0-0-C-K	0	-19	19	0	0	-505	505	-505
0-0-C-L	0	-9	12	52	16	-284	319	-251
0-0-C-M	0	-9	7	-52	-16	-221	188	-256
0-0-C-P	0	-5	5	0	0	-126	126	-126
0-0-C-S	0	-2	2	0	0	-63	63	-63
I-0-N-B	143	-319	275	-1112	3971	-7913	9740	-6882
I-0-N-C	-12	-41	-24	-1412	-790	-224	-718	-1484
I-0-N-D	-48	33	-77	-897	-1712	1468	219	-2828
I-0-N-E	-43	36	-50	-272	-1381	1150	451	-2103
I-0-N-F	-36	24	-26	-19	-1087	669	303	-1409
I-0-N-N*	-134	-5	2	85	-4003	-96	87	-4005
0-0-N-B	-9	78	-135	-1240	-656	2843	1909	-3806
0-0-N-C	-2	45	-62	-362	-180	1421	1153	-1695
0-0-N-D	-4	0	-5	-91	-162	65	-52	-200
0-0-N-E	-5	-16	17	11	-132	-441	386	-507
0-0-N-F	-2	-19	19	10	-61	-506	482	-532
0-0-N-H	0	-21	17	-99	-24	-506	446	-568
0-0-N-K	0	-21	17	-100	-20	-504	446	-566
0-0-N-N	0	-19	46	596	184	-861	1276	-495

Table A.7 (continued)

OUT-OF-PLANE FORCE LOADING, FZN, ON NOZZLE (60 LB)

	MICRO-STRAIN			STRESSES			PRIN STRESSES	
ROSETTE	GAGE1	GAGE2	GAGE3	TRANS	LONG	SHEAR	SIGMX	SIGMN
I-90C-B	-36	-416	-380	-17469	-6318	-478	-6298	-17490
I-90C-C*	-79	-328	0	-7117	-4504	-4367	-1252	-10369
I-90C-D	-60	-232	-218	-9819	-4740	-191	-4733	-9826
I-90C-E	-48	-167	-158	-7098	-3565	-128	-3561	-7103
I-90C-F	-36	-100	-117	-4745	-2500	223	-2478	-4767
I-90C-R	5	0	-2	-58	126	32	132	-63
O-90C-B	126	358	422	17006	8880	-851	17094	8792
O-90C-C	147	330	361	15012	8918	-411	15040	8890
O-90C-D	142	280	270	11941	7854	126	11945	7850
O-90C-E	128	199	214	8932	6524	-190	8947	6509
O-90C-F	116	166	171	7277	5671	-63	7279	5669
O-90C-R	-7	-7	-5	-253	-289	-32	-235	-308
I-90N-B	-1002	117	-119	1048	-29749	3147	1366	-30067
I-90N-C	203	193	203	8474	8619	-127	8692	8401
I-90N-D	413	107	167	5573	14051	-793	14125	5500
I-90N-E	348	-7	74	1086	10770	-1079	10889	967
I-90N-F*	40	-43	4	-895	936	-634	1134	-1093
I-90N-N	217	117	79	4064	7737	509	7806	3994
O-90N-B	432	669	672	28987	21652	-32	28987	21652
O-90N-C	97	185	202	8393	5437	-221	8409	5420
O-90N-D	152	19	24	772	4787	-63	4788	771
O-90N-E	171	-14	0	-500	4974	-190	4980	-507
O-90N-F	204	57	5	1131	6459	695	6549	1042
O-90N-N	114	-2	7	-21	3410	-126	3414	-25

Table A.7 (continued)

OUT-OF-PLANE FORCE LOADING, FZN, ON NOZZLE (60 LB)

	MICRO-STRAIN			STRESSES			PRIN STRESSES	
ROSETTE	GAGE1	GAGE2	GAGE3	TRANS	LONG	SHEAR	SIGMX	SIGMN
I180C-B	-33	271	-212	1343	-580	6440	6893	-6130
I180C-C	-23	352	-278	1645	-206	8388	9158	-7719
I180C-D	-18	271	-238	760	-325	6785	7023	-6589
I180C-E	-12	238	-202	804	-104	5873	6241	-5540
I180C-F	-9	189	-162	592	-99	4680	4939	-4446
I180C-S	1	1	-2	-28	11	32	28	-46
O180C-B	17	150	-173	-528	354	4309	4244	-4419
O180C-C	8	157	-183	-567	58	4529	4285	-4795
O180C-D	10	129	-145	-368	191	3645	3567	-3744
O180C-E	5	103	-114	-256	78	2884	2800	-2977
O180C-F	2	83	-91	-170	12	2313	2236	-2394
O180C-S*	-20	0	-7	-145	-643	94	-128	-660
I180N-B	-54	403	-279	2800	-795	9087	10265	-8260
I180N-C	10	86	-14	1573	766	1335	2564	-225
I180N-D	12	29	41	1519	822	-158	1553	788
I180N-E	3	-54	38	-357	-28	-1238	1056	-1441
I180N-F	-2	-35	21	-299	-153	-753	531	-982
I180N-N	22	-16	5	-270	571	-284	658	-357
O180N-B	5	-113	40	-1595	-342	-2039	1165	-3102
O180N-C	7	-48	36	-276	126	-1109	1052	-1202
O180N-D	0	5	7	255	70	-33	260	64
O180N-E	0	24	-14	205	55	505	641	-381
O180N-F	0	24	-19	102	28	571	637	-507
O180N-N	4	19	-17	37	146	475	570	-387

Table A.7 (continued)

OUT-OF-PLANE FORCE LOADING, FZN, ON NOZZLE (60 LB)

	MICRO-STRAIN			STRESSES			PRIN STRESSES	
ROSETTE	GAGE1	GAGE2	GAGE3	TRANS	LONG	SHEAR	SIGMX	SIGMN
I270C-C	98	306	296	13120	6885	127	13123	6883
I270C-D	77	218	210	9320	5102	97	9322	5099
I270C-E	54	159	159	6914	3681	1	6914	3681
I270C-F	32	118	113	5049	2479	64	5051	2477
I270C-H	4	54	49	2256	787	63	2258	784
I270C-J	-20	11	6	378	-496	66	383	-501
I270C-K	-30	-4	-9	-245	-984	67	-239	-990
I270C-L	-30	-17	-14	-647	-1101	-52	-641	-1107
I270C-M	-20	-6	-8	-291	-692	35	-288	-695
I270C-P	-10	0	1	32	-290	-6	32	-290
I270C-R	-7	2	3	119	-169	-2	119	-169
I270C-T	2	-4	0	-90	47	-64	72	-115
O270C-B	-211	-468	-513	-21328	-12733	600	-12691	-21370
O270C-C	-183	-332	-320	-14144	-9721	-157	-9715	-14150
O270C-D	-166	-261	-261	-11292	-8367	-2	-8367	-11292
O270C-E	-137	-216	-209	-9180	-6877	-96	-6873	-9184
O270C-F	-116	-171	-166	-7271	-5663	-63	-5660	-7274
O270C-H	-71	-104	-104	-4499	-3475	0	-3475	-4499
O270C-J	-33	-47	-47	-2030	-1592	2	-1592	-2030
O270C-K	-7	-14	-14	-602	-381	0	-381	-602
O270C-L	15	10	10	422	567	0	567	422
O270C-M	17	12	12	520	667	-2	667	520
O270C-P	8	5	8	271	312	-31	329	255
O270C-R	3	3	5	169	136	-32	188	117
O270C-T	-2	-2	0	-31	-62	-31	-11	-81
I270N-B	1090	24	64	735	32933	-541	32942	726
I270N-C	-105	-205	-186	-8491	-5703	-253	-5681	-8513
I270N-D	-368	-146	-162	-6366	-12942	223	-6358	-12949
I270N-E	-332	-38	-79	-2209	-10622	542	-2175	-10656
I270N-F	-269	12	-24	32	-8057	478	60	-8085
O270N-B	-491	-725	-585	-28263	-23197	-1863	-22586	-28875
O270N-C	-97	-192	-190	-8279	-5399	-32	-5399	-8279
O270N-D	-130	-28	-23	-994	-4211	-64	-993	-4212
O270N-E	-211	7	12	663	-6139	-63	663	-6140
O270N-F	-240	5	12	648	-6995	-96	649	-6997
O270N-G	-252	-5	-9	-30	-7563	63	-29	-7564
O270N-H	-249	-7	-16	-234	-7548	127	-232	-7550
O270N-K	-225	-19	7	1	-6762	-346	19	-6779
O270N-N	-147	-2	-11	-132	-4447	126	-128	-4450

Table A.7 (continued)

OUT-OF-PLANE FORCE LOADING, FZN, ON NOZZLE (60 LB)

	MICRO-STRAIN			STRESSES			PRIN STRESSES	
ROSETTE	GAGE1	GAGE2	GAGE3	TRANS	LONG	SHEAR	SIGMX	SIGMN
I315C-B	67	69	470	11784	5541	-5344	14851	2474
I315C-C	55	26	456	10538	4809	-5726	14076	1271
I315C-D	50	10	315	7083	3629	-4070	9777	935
I315C-F	81	67	141	4475	3778	-986	5173	3081
I315C-H	100	67	167	5032	4518	-1336	6135	3414
I315C-J	93	74	141	4620	4179	-891	5317	3482
I315C-K	81	76	122	4266	3715	-604	4654	3326
I315C-L	-7	4	58	1373	196	-709	1706	-137
I315C-M	-12	6	29	781	-117	-302	874	-209
I315C-P	-14	0	5	127	-376	-71	137	-386
O315C-B	-95	-384	-107	-10686	-6053	-3698	-4006	-12733
O315C-C	-85	-332	-81	-8977	-5255	-3350	-3284	-10948
O315C-D	-59	-346	-78	-9266	-4559	-3571	-2635	-11189
O315C-E	-40	-292	-71	-7931	-3589	-2939	-2106	-9414
O315C-F	-43	-244	-55	-6521	-3237	-2528	-1865	-7894
O315C-H	-19	-176	-47	-4879	-2033	-1707	-1234	-5678
O315C-K	-9	-76	-36	-2440	-1017	-537	-837	-2620
O315C-L	-12	-43	-31	-1603	-837	-158	-805	-1634
O315C-M	-9	-19	-24	-928	-563	63	-552	-939
O315C-P	-5	0	-12	-255	-219	158	-78	-396
I315N-B	749	-220	120	-3025	21548	-4524	22355	-3831
I315N-C	-103	-150	-201	-7602	-5359	668	-5175	-7786
I315N-D	-275	-76	-174	-5204	-9804	1306	-4859	-10149
I315N-E	-244	-12	-88	-1928	-7886	1021	-1758	-8056
I315N-F	-201	10	-45	-557	-6185	733	-463	-6279
I315N-N	-105	12	0	388	-3021	158	395	-3028
O315N-B	-346	-415	-572	-21305	-16782	2086	-15967	-22120
O315N-C	-64	-116	-202	-6915	-3996	1138	-3605	-7306
O315N-D	-91	-7	-30	-716	-2955	310	-674	-2997
O315N-E	-145	14	19	885	-4095	-65	886	-4096
O315N-F	-180	3	19	673	-5211	-218	681	-5219
O315N-G	-187	-9	5	116	-5590	-186	122	-5596
O315N-H	-178	-9	5	101	-5314	-188	107	-5320
O315N-K	-159	-7	3	85	-4756	-126	88	-4760
O315N-N	-33	-9	5	-55	-992	-188	-18	-1029

Table A.8. Torsional moment loading, M_{XC}, on cylinder

TORSIONAL MOMENT LOADING, MXC, ON CYLINDER (30000 IN-LB)

	MICRO-STRAIN			STRESSES			PRIN STRESSES	
ROSETTE	GAGE1	GAGE2	GAGE3	TRANS	LONG	SHEAR	SIGMX	SIGMN
I-0-C-C	-3	-51	40	-225	-149	-1208	1022	-1396
I-0-C-D	2	-60	57	-71	41	-1557	1543	-1573
I-0-C-E	5	-53	52	-21	130	-1398	1455	-1346
I-0-C-F	7	-46	52	138	247	-1302	1496	-1111
I-0-C-H	2	43	-39	87	83	1081	1166	-996
I-0-C-J	4	35	-39	-78	106	986	1005	-976
I-0-C-K	7	-34	35	23	207	-918	1037	-807
I-0-C-L*	0	-39	33	-127	-29	-954	877	-1033
I-0-C-M	4	-36	35	-21	123	-955	1009	-907
I-0-C-P	-1	-32	37	131	23	-920	999	-845
I-0-C-S	-3	-32	36	102	-64	-904	926	-888
O-0-C-B	-5	55	-64	-199	-197	1578	1380	-1776
O-0-C-C	0	52	-57	-97	-25	1453	1392	-1515
O-0-C-D	-2	57	-54	61	-47	1484	1491	-1478
O-0-C-E	-2	55	-57	-40	-77	1483	1424	-1541
O-0-C-F	3	50	-57	-152	32	1422	1365	-1485
O-0-C-H	-2	45	-47	-41	-78	1231	1172	-1291
O-0-C-J	0	40	-47	-147	-35	1167	1078	-1259
O-0-C-K	0	38	-45	-147	-37	1105	1015	-1198
O-0-C-L	0	36	-38	-44	-5	980	955	-1004
O-0-C-M	0	38	-35	61	25	980	1023	-937
O-0-C-P	3	33	-40	-151	33	979	924	-1042
O-0-C-S	-2	38	-35	63	-42	979	991	-970
I-0-N-B	7	-17	-24	-904	-57	96	-46	-915
I-0-N-C	-10	-7	-22	-622	-476	191	-344	-754
I-0-N-D	-7	-5	-12	-362	-325	96	-246	-441
I-0-N-E	-5	-7	-2	-206	-207	-63	-143	-270
I-0-N-F	0	-7	0	-159	-49	-96	7	-215
I-0-N-N	2	0	2	48	85	-32	104	30
O-0-N-B	0	17	-24	-149	-40	537	446	-634
O-0-N-C	-2	-2	0	-38	-76	-31	-20	-93
O-0-N-D	-4	-7	12	125	-91	-250	290	-255
O-0-N-E	-2	-9	10	14	-54	-251	233	-273
O-0-N-F	-2	-7	10	70	-36	-223	246	-212
O-0-N-H	-2	-7	7	14	-57	-190	171	-215
O-0-N-K	-2	-5	3	-42	-66	-93	40	-148
O-0-N-N	-2	0	-1	-1	-61	13	1	-64

Table A.8 (continued)

TORSIONAL MOMENT LOADING, MXC, ON CYLINDER (30000 IN-LB)

	MICRO-STRAIN			STRESSES			PRIN STRESSES	
ROSETTE	GAGE1	GAGE2	GAGE3	TRANS	LONG	SHEAR	SIGMX	SIGMN
I-90C-B	3	36	-24	268	161	798	1015	-585
I-90C-C*	3	55	0	1212	445	737	1659	-2
I-90C-D	3	55	-52	62	98	1434	1514	-1355
I-90C-E	3	53	-52	11	86	1403	1452	-1355
I-90C-F	3	57	-48	199	142	1391	1562	-1221
I-90C-R	3	29	-31	-41	71	796	813	-783
O-90C-B	8	-35	36	14	236	-944	1075	-826
O-90C-C	5	-55	50	-109	110	-1391	1395	-1395
O-90C-D*	2	-57	9	-1045	-242	-885	328	-1616
O-90C-E	2	-57	47	-211	8	-1391	1293	-1497
O-90C-F	0	-55	52	-52	-16	-1422	1389	-1456
O-90C-R	0	-38	33	-104	-31	-948	881	-1017
I-90N-B	3	-29	-24	-1153	-266	-64	-262	-1158
I-90N-C	-17	-26	-12	-828	-758	-190	-599	-986
I-90N-D	-9	-12	-5	-354	-380	-94	-272	-462
I-90N-E	-4	-5	-7	-254	-210	33	-192	-272
I-90N-F	35	-34	7	-633	864	-539	1037	-807
I-90N-N	-16	-12	-7	-384	-606	-64	-367	-623
O-90N-B	-5	-24	28	109	-110	-695	704	-704
O-90N-C	-2	-5	0	-102	-102	-63	-38	-165
O-90N-D	0	2	-9	-156	-47	158	66	-269
O-90N-E	2	7	-7	-3	70	190	227	-159
O-90N-F	2	5	-7	-55	55	158	167	-167
O-90N-N	0	0	0	0	0	0	0	0

Table A.8 (continued)

TORSIONAL MOMENT LOADING, MXC, ON CYLINDER (30000 IN-LB)

	MICRO-STRAIN			STRESSES			PRIN STRESSES	
ROSETTE	GAGE1	GAGE2	GAGE3	TRANS	LONG	SHEAR	SIGMX	SIGMN
I180C-B	5	-21	27	126	187	-636	793	-481
I180C-C	5	-44	50	111	182	-1255	1402	-1108
I180C-D	5	-49	55	112	188	-1382	1532	-1232
I180C-E	3	-52	52	12	83	-1382	1430	-1336
I180C-F	3	-47	47	9	80	-1256	1301	-1213
I180C-S	3	-28	34	125	128	-816	943	-690
O180C-B	3	50	-57	-145	42	1429	1381	-1483
O180C-C	1	53	-57	-87	-8	1457	1410	-1505
O180C-D	5	55	-59	-101	131	1524	1544	-1513
O180C-E	5	55	-57	-45	145	1491	1544	-1445
O180C-F	0	50	-57	-174	-64	1426	1308	-1546
O180C-S*	0	28	-41	-277	-83	917	741	-1102
I180N-B	3	-2	-19	-446	-44	226	58	-547
I180N-C	-2	1	-16	-342	-160	224	-10	-493
I180N-D	-2	-2	-11	-289	-142	128	-67	-363
I180N-E	0	-2	-4	-134	-25	34	-16	-144
I180N-F	0	-2	5	61	26	-93	138	-51
I180N-N	-2	1	-2	-21	-63	34	-2	-82
O180N-B	-10	14	-7	161	-245	284	307	-391
O180N-C	2	0	0	-14	60	-1	60	-14
O180N-D	2	-10	5	-117	25	-192	159	-251
O180N-E	2	-10	9	-8	58	-256	283	-233
O180N-F	2	-7	7	-6	65	-190	222	-163
O180N-N	0	0	0	-15	-16	0	-15	-16

Table A.8 (continued)

TORSIONAL MOMENT LOADING, MXC, ON CYLINDER (30000 IN-LB)

	MICRO-STRAIN			STRESSES			PRIN STRESSES	
ROSETTE	GAGE1	GAGE2	GAGE3	TRANS	LONG	SHEAR	SIGMX	SIGMN
I270C-C	-1	58	-54	100	-12	1493	1538	-1450
I270C-D	1	61	-54	151	75	1528	1642	-1416
I270C-E	0	58	-54	74	35	1493	1548	-1439
I270C-F	-2	53	-50	76	-35	1366	1388	-1347
I270C-H	1	46	-45	23	22	1207	1229	-1184
I270C-J	5	36	-40	-94	129	1017	1041	-1006
I270C-K	-2	31	-35	-88	-90	891	802	-980
I270C-L	-2	28	-33	-106	-94	815	715	-915
I270C-M	-2	34	-31	76	-34	859	882	-840
I270C-P	0	34	-38	-95	-30	951	889	-1014
I270C-R	2	41	-36	100	96	1022	1120	-924
I270C-T	5	17	-19	-66	123	479	516	-459
O270C-B	-2	-55	60	107	-39	-1522	1558	-1490
O270C-C	-5	-52	57	119	-100	-1458	1471	-1452
O270C-D	0	-57	53	-95	-21	-1460	1402	-1518
O270C-E	0	-57	53	-95	-21	-1458	1401	-1517
O270C-F	0	-52	53	10	10	-1395	1405	-1385
O270C-H	-4	-50	50	17	-129	-1332	1278	-1390
O270C-J	0	-47	48	14	13	-1267	1281	-1253
O270C-K	3	-40	43	59	96	-1110	1188	-1032
O270C-L	3	-43	38	-95	50	-1077	1058	-1102
O270C-M	1	-38	36	-33	6	-985	972	-999
O270C-P	-4	-40	34	-130	-162	-982	836	-1128
O270C-R	-2	-40	34	-137	-96	-984	867	-1101
O270C-T*	1	-42	0	-931	-255	-564	65	-1250
I270N-B	0	7	4	250	63	32	255	57
I270N-C	4	-2	12	198	193	-189	385	6
I270N-D	4	0	9	199	194	-127	324	69
I270N-E	4	2	2	93	161	1	161	93
I270N-F	3	5	-2	51	105	95	177	-21
O270N-B	-2	-28	24	-95	-92	-694	600	-787
O270N-C	-2	-5	3	-44	-80	-95	34	-159
O270N-D	-2	7	-7	3	-71	190	160	-228
O270N-E	0	10	-10	0	0	254	254	-254
O270N-F	0	7	-10	-52	-16	222	189	-257
O270N-G	-2	7	-10	-50	-86	222	155	-291
O270N-H	-2	7	-10	-50	-86	222	155	-291
O270N-K	-2	2	-2	3	-71	63	39	-107
O270N-N	-2	-2	-2	-102	-102	0	-102	-102

Table A.8 (continued)

TORSIONAL MOMENT LOADING, MXC, ON CYLINDER (30000 IN-LB)

	MICRO-STRAIN			STRESSES			PRIN STRESSES	
ROSETTE	GAGE1	GAGE2	GAGE3	TRANS	LONG	SHEAR	SIGMX	SIGMN
I315C-B	12	-91	-78	-3725	-755	-161	-747	-3734
I315C-C	12	-62	-52	-2517	-390	-127	-383	-2525
I315C-D	9	-49	-36	-1871	-278	-181	-257	-1891
I315C-F	0	-26	-26	-1140	-333	0	-333	-1140
I315C-H	-2	-21	-28	-1080	-384	94	-372	-1092
I315C-J	3	-19	-26	-983	-212	96	-200	-994
I315C-K	8	-21	-24	-991	-70	32	-69	-992
I315C-L	41	-19	-24	-988	923	58	924	-990
I315C-M	43	-28	-17	-1035	988	-157	1000	-1047
I315C-P	44	-22	-21	-985	1011	-7	1011	-985
O315C-B	5	-33	-26	-1308	-250	-95	-242	-1317
O315C-C	9	-21	-17	-844	31	-63	36	-849
O315C-D	14	-21	-19	-902	156	-32	157	-903
O315C-E	26	-19	-14	-758	555	-63	558	-761
O315C-F	28	-28	-14	-969	563	-190	586	-993
O315C-H*	0	-14	-16	-667	-200	32	-198	-669
O315C-K	38	-16	-19	-815	902	30	902	-815
O315C-L	41	-16	-21	-865	959	63	962	-868
O315C-M	45	-19	-24	-979	1064	64	1066	-981
O315C-P	45	-26	-19	-1028	1050	-93	1054	-1033
I315N-B	5	-79	-81	-3521	-907	31	-906	-3522
I315N-C	-36	-52	-52	-2263	-1748	-1	-1748	-2263
I315N-D	-28	-33	-31	-1376	-1267	-32	-1259	-1385
I315N-E	-19	-19	-19	-808	-808	1	-807	-809
I315N-F	-12	-12	-14	-554	-517	33	-498	-573
I315N-N*	-3	0	-282	-6190	-1953	3765	248	-8392
O315N-B	13	-31	-21	-1154	42	-124	55	-1167
O315N-C	5	14	19	731	368	-62	741	358
O315N-D	-11	14	19	752	-112	-66	757	-117
O315N-E	-4	12	12	531	31	-2	531	31
O315N-F	-9	8	10	392	-147	-30	394	-149
O315N-G	-6	5	5	238	-123	2	238	-123
O315N-H	-9	3	3	131	-226	0	131	-226
O315N-K	-4	-2	-4	-124	-164	29	-109	-179
O315N-N	-39	-2	-2	-34	-1187	0	-34	-1187

Table A.9. Out-of-plane moment loading, M_{YC}, on cylinder

OUT-OF-PLANE MOMENT LOADING, MYC, ON CYLINDER (80000 IN-LB)

	MICRO-STRAIN			STRESSES			PRIN STRESSES	
ROSETTE	GAGE1	GAGE2	GAGE3	TRANS	LONG	SHEAR	SIGMX	SIGMN
I-0-C-C	0	-19	-14	-734	-220	-64	-212	-742
I-0-C-D	0	-17	-19	-786	-236	32	-234	-788
I-0-C-E	5	-17	-19	-792	-94	32	-93	-793
I-0-C-F	5	-14	-21	-792	-94	95	-82	-804
I-0-C-H	7	-21	-17	-847	-39	-64	-34	-852
I-0-C-J	10	-24	-12	-797	47	-159	76	-826
I-0-C-K	12	-12	-24	-799	118	159	145	-826
I-0-C-L*	-122	-9	-21	-529	-3821	158	-522	-3828
I-0-C-M	12	-9	-24	-733	150	192	190	-773
I-0-C-P	12	-9	-18	-620	185	125	204	-639
I-0-C-S	15	-2	-12	-330	350	141	378	-358
0-0-C-B	9	12	12	505	430	1	505	430
0-0-C-C	7	14	16	659	406	-32	663	402
0-0-C-D	9	16	19	762	505	-30	765	501
0-0-C-E	9	19	21	862	534	-29	865	532
0-0-C-F	9	19	21	866	534	-32	869	531
0-0-C-H	12	16	23	861	605	-94	892	574
0-0-C-J	11	16	23	860	600	-92	889	571
0-0-C-K	16	16	21	802	728	-63	838	691
0-0-C-L	14	16	21	807	657	-64	830	633
0-0-C-M	14	16	21	806	659	-64	830	635
0-0-C-P	16	14	19	700	698	-62	761	637
0-0-C-S	19	7	16	488	702	-127	761	430
I-0-N-B	-29	-7	-10	-337	-963	32	-335	-965
I-0-N-C	-12	2	5	171	-308	-32	173	-310
I-0-N-D	-5	2	5	163	-95	-32	167	-99
I-0-N-E	-5	2	2	111	-111	0	111	-111
I-0-N-F	-5	2	2	111	-111	0	111	-111
I-0-N-N	0	0	0	0	0	0	0	0
0-0-N-B	-10	9	9	417	-167	-1	417	-167
0-0-N-C	-15	4	4	207	-375	-1	207	-375
0-0-N-D	-12	2	0	54	-349	30	56	-351
0-0-N-E	-10	2	0	54	-277	31	57	-280
0-0-N-F	-7	0	0	-3	-224	1	-3	-224
0-0-N-H	-5	0	0	-2	-150	1	-2	-150
0-0-N-K	2	0	0	-8	56	-1	56	-8
0-0-N-N*	2	2	-41	-868	-197	580	138	-1203

Table A.9 (continued)

OUT-OF-PLANE MOMENT LOADING, MYC, ON CYLINDER (80000 IN-LB)

	MICRO-STRAIN			STRESSES			PRIN STRESSES	
ROSETTE	GAGE1	GAGE2	GAGE3	TRANS	LONG	SHEAR	SIGMX	SIGMN
I-90C-B	-5	-34	-26	-1310	-537	-96	-525	-1322
I-90C-C*	-12	-34	0	-723	-576	-447	-197	-1102
I-90C-D	-12	-34	-22	-1197	-718	-159	-670	-1245
I-90C-E	-14	-36	-22	-1247	-805	-191	-734	-1318
I-90C-F	-14	-5	-24	-616	-616	255	-360	-871
I-90C-R	77	-122	-120	-5397	679	-32	679	-5397
O-90C-B	16	9	14	488	632	-66	658	463
O-90C-C	22	5	0	91	678	64	685	84
O-90C-D	26	-4	-9	-324	697	59	700	-327
O-90C-E	29	-9	-14	-543	702	64	705	-546
O-90C-F	33	-12	-24	-809	761	159	777	-825
O-90C-R	19	-151	-158	-6817	-1465	85	-1464	-6819
I-90N-B	-60	0	-14	-248	-1862	191	-226	-1884
I-90N-C	5	5	5	204	204	0	204	204
I-90N-D	16	2	7	189	550	-65	561	178
I-90N-E	14	-2	2	-18	417	-65	426	-27
I-90N-F	-24	-12	12	26	-708	-318	145	-826
I-90N-N	-19	-14	-11	-536	-721	-32	-531	-726
O-90N-B	22	29	29	1239	1024	0	1239	1024
O-90N-C	3	7	10	376	193	-33	381	187
O-90N-D	3	3	3	116	117	-2	118	115
O-90N-E	5	0	3	59	176	-31	184	52
O-90N-F	5	0	3	60	172	-30	179	52
O-90N-N	-4	-2	0	-33	-143	-31	-25	-151

Table A.9 (continued)

OUT-OF-PLANE MOMENT LOADING, MYC, ON CYLINDER (80000 IN-LB)

	MICRO-STRAIN			STRESSES			PRIN STRESSES	
ROSETTE	GAGE1	GAGE2	GAGE3	TRANS	LONG	SHEAR	SIGMX	SIGMN
I180C-B	0	-17	-31	-1037	-311	189	-265	-1083
I180C-C	-2	-9	-28	-827	-319	251	-215	-930
I180C-D	0	-12	-26	-829	-249	189	-193	-885
I180C-E	5	-14	-28	-938	-140	189	-98	-980
I180C-F	2	-17	-28	-987	-225	157	-194	-1018
I180C-S	17	-31	-26	-1262	117	-63	119	-1265
O180C-B	5	3	19	472	291	-221	620	142
O180C-C	5	7	22	630	339	-191	724	244
O180C-D	5	10	22	679	354	-158	743	290
O180C-E	7	12	24	782	455	-159	847	391
O180C-F	10	14	24	826	533	-127	873	486
O180C-S	-5	21	21	946	141	0	946	141
I180N-B	-24	-5	-3	-149	-773	-34	-148	-775
I180N-C	-12	2	9	260	-290	-96	277	-306
I180N-D	-3	4	9	302	8	-64	315	-6
I180N-E	-3	4	9	302	8	-65	316	-5
I180N-F	-9	2	2	114	-249	0	114	-249
I180N-N	2	2	2	83	86	-2	87	82
O180N-B	-14	2	12	329	-329	-127	352	-353
O180N-C	-17	5	5	227	-431	0	227	-431
O180N-D	-14	0	2	68	-408	-32	70	-410
O180N-E	-12	2	-2	13	-353	63	24	-363
O180N-F	-7	0	-2	-44	-227	32	-39	-233
O180N-N	2	2	2	102	102	0	102	102

Table A.9 (continued)

OUT-OF-PLANE MOMENT LOADING, MYC, ON CYLINDER (80000 IN-LB)

	MICRO-STRAIN			STRESSES			PRIN STRESSES	
ROSETTE	GAGE1	GAGE2	GAGE3	TRANS	LONG	SHEAR	SIGMX	SIGMN
I270C-C	-20	23	30	1197	-234	-96	1203	-240
I270C-D	-22	28	35	1409	-241	-98	1414	-247
I270C-E	-25	28	35	1409	-312	-96	1415	-318
I270C-F	-25	33	40	1620	-250	-96	1625	-255
I270C-H	-25	45	42	1932	-159	32	1932	-160
I270C-J	-25	61	54	2571	35	94	2575	32
I270C-K	-22	69	66	2991	242	30	2991	241
I270C-L	-24	91	88	3959	458	45	3960	458
I270C-M	-15	97	107	4492	895	-129	4497	890
I270C-P	-19	133	121	5617	1115	162	5623	1109
I270C-R	-22	132	132	5813	1097	0	5813	1097
I270C-T	-22	7	2	234	-576	64	239	-581
O270C-B	12	55	48	2233	1026	95	2241	1018
O270C-C	12	45	36	1772	894	127	1790	876
O270C-D	10	48	36	1826	839	157	1851	815
O270C-E	7	48	38	1882	785	126	1896	770
O270C-F	3	45	36	1782	612	127	1796	598
O270C-H	-5	55	45	2209	527	126	2218	517
O270C-J	-14	64	55	2639	371	128	2647	364
O270C-K	-21	69	64	2958	252	63	2960	250
O270C-L	-38	83	91	3867	25	-94	3869	22
O270C-M	-52	98	95	4301	-273	31	4301	-273
O270C-P	-66	114	107	4945	-507	95	4946	-508
O270C-R	-64	122	122	5412	-297	0	5412	-297
O270C-T*	15	14	0	303	529	193	639	192
I270N-B	-59	41	34	1702	-1269	96	1705	-1272
I270N-C	17	33	31	1404	930	30	1406	928
I270N-D	27	17	17	710	1008	0	1008	710
I270N-E	17	7	7	301	600	-1	600	301
I270N-F	8	-2	0	-61	215	-32	219	-65
O270N-B	9	50	38	1909	847	156	1932	824
O270N-C	-3	5	5	204	-16	0	204	-16
O270N-D	5	-5	-5	-215	77	0	77	-215
O270N-E	12	-5	-5	-222	290	0	290	-222
O270N-F	9	-2	0	-65	265	-31	268	-68
O270N-G	10	2	2	95	314	0	314	95
O270N-H	9	2	5	146	328	-32	334	140
O270N-K	2	2	2	100	100	0	100	100
O270N-N	-2	0	0	1	-73	0	1	-73

Table A.9 (continued)

OUT-OF-PLANE MOMENT LOADING, MYC, ON CYLINDER (80000 IN-LB)

	MICRO-STRAIN			STRESSES			PRIN STRESSES	
ROSETTE	GAGE1	GAGE2	GAGE3	TRANS	LONG	SHEAR	SIGMX	SIGMN
I315C-B	-9	26	-23	78	-258	665	596	-776
I315C-C	-7	31	-33	-28	-215	859	742	-986
I315C-D	-5	34	-33	16	-139	888	830	-953
I315C-F	-9	12	-4	185	-220	223	283	-319
I315C-H	-7	15	-14	30	-193	380	315	-478
I315C-J	-4	20	-14	129	-91	445	478	-440
I315C-K	3	29	-14	329	186	572	834	-319
I315C-L	31	82	-19	1334	1333	1346	2680	-13
I315C-M	52	94	-22	1539	2033	1545	3351	221
I315C-P	62	125	-15	2343	2553	1856	4307	589
O315C-B	7	15	26	891	492	-158	946	437
O315C-C	12	14	29	938	646	-191	1032	552
O315C-D	15	12	43	1192	793	-411	1449	536
O315C-E	14	12	45	1245	805	-443	1520	531
O315C-F	19	3	50	1139	919	-629	1667	391
O315C-H	21	7	52	1282	1027	-601	1768	540
O315C-K	26	-2	69	1433	1214	-949	2279	369
O315C-L	26	-26	88	1330	1184	-1517	2776	-262
O315C-M	31	-26	102	1636	1418	-1707	3237	-183
O315C-P	33	-35	123	1895	1566	-2117	3854	-393
I315N-B	-43	21	5	622	-1111	224	650	-1140
I315N-C	7	12	14	562	378	-31	567	373
I315N-D	12	5	7	239	425	-32	430	234
I315N-E	7	0	0	-19	201	-1	202	-19
I315N-F	2	0	0	-14	61	-1	61	-14
I315N-N	0	-2	0	-52	-16	-31	3	-70
O315N-B	-5	19	33	1154	209	-189	1191	173
O315N-C	-17	5	2	177	-444	32	178	-445
O315N-D	-9	3	-9	-124	-302	150	-39	-388
O315N-E	-4	2	-9	-142	-170	151	-4	-308
O315N-F	1	1	-9	-182	-31	127	41	-254
O315N-G	-2	3	-9	-122	-85	160	57	-264
O315N-H	-2	3	-7	-81	-75	124	46	-202
O315N-K	-2	1	-2	-20	-59	29	-4	-74
O315N-N	-41	-2	-4	-80	-1252	31	-79	-1253

Table A.10. In-plane moment loading, M_{ZC}, on cylinder

IN-PLANE MOMENT LOADING, MZC, ON CYLINDER (80000 IN-LB)

	MICRO-STRAIN			STRESSES			PRIN STRESSES	
ROSETTE	GAGE1	GAGE2	GAGE3	TRANS	LONG	SHEAR	SIGMX	SIGMN
I-0-C-C	1	80	58	3025	928	287	3063	889
I-0-C-D	-21	44	25	1523	-169	255	1560	-206
I-0-C-E	-47	32	15	1079	-1093	222	1102	-1116
I-0-C-F	-69	22	10	780	-1821	157	790	-1831
I-0-C-H	-118	1	15	477	-3405	-191	487	-3415
I-0-C-J	-149	3	6	363	-4372	-34	363	-4372
I-0-C-K	-161	3	8	431	-4708	-71	432	-4709
I-0-C-L	-144	1	18	569	-4146	-224	580	-4157
I-0-C-M	-173	3	13	539	-5036	-125	542	-5039
I-0-C-P	-178	18	4	671	-5137	186	677	-5143
I-0-C-S	-180	18	4	677	-5191	189	683	-5197
O-0-C-B	-45	5	-2	101	-1321	94	107	-1327
O-0-C-C	-71	-17	-26	-859	-2392	126	-849	-2402
O-0-C-D	-97	-33	-36	-1404	-3337	32	-1403	-3338
O-0-C-E	-104	-36	-33	-1395	-3548	-32	-1394	-3548
O-0-C-F	-121	-31	-38	-1378	-4040	95	-1375	-4044
O-0-C-H	-140	-33	-28	-1200	-4557	-63	-1199	-4558
O-0-C-J	-164	-19	-31	-913	-5182	157	-907	-5188
O-0-C-K	-168	-24	-19	-752	-5276	-63	-751	-5277
O-0-C-L	-183	-17	-24	-684	-5682	95	-683	-5684
O-0-C-M	-180	-19	-17	-582	-5581	-31	-582	-5581
O-0-C-P	-183	-19	-24	-737	-5699	63	-736	-5699
O-0-C-S	-192	-24	-14	-622	-5948	-126	-619	-5951
I-0-N-B	74	134	122	5554	3897	159	5569	3882
I-0-N-C	62	84	74	3407	2894	128	3438	2864
I-0-N-D	38	60	55	2485	1899	64	2492	1892
I-0-N-E	29	50	50	2181	1520	-1	2181	1520
I-0-N-F	29	38	46	1813	1408	-95	1835	1387
I-0-N-N*	0	3	3	110	36	0	110	36
O-0-N-B	7	-21	-21	-945	-69	0	-69	-945
O-0-N-C	45	-52	-45	-2184	698	-94	701	-2188
O-0-N-D	52	-43	-40	-1880	1002	-32	1002	-1880
O-0-N-E	52	-36	-31	-1516	1111	-63	1113	-1517
O-0-N-F	47	-28	-26	-1250	1049	-32	1049	-1250
O-0-N-H	40	-9	-12	-512	1056	32	1057	-513
O-0-N-K	21	7	9	341	744	-32	747	339
O-0-N-N*	2	2	244	5422	1698	-3225	7284	-164

Table A.10 (continued)

IN-PLANE MOMENT LOADING, MZC, ON CYLINDER (80000 IN-LB)

	MICRO-STRAIN			STRESSES			PRIN STRESSES	
ROSETTE	GAGE1	GAGE2	GAGE3	TRANS	LONG	SHEAR	SIGMX	SIGMN
I-90C-B	98	-387	-385	-17083	-2175	-31	-2175	-17083
I-90C-C*	58	-275	0	-6105	-102	-3663	1632	-7839
I-90C-D	50	-232	-203	-9614	-1372	-383	-1354	-9632
I-90C-E	53	-198	-174	-8248	-887	-319	-873	-8262
I-90C-F	55	-159	-155	-6976	-434	-54	-434	-6977
I-90C-R	-21	0	-19	-387	-753	255	-256	-883
O-90C-B	-17	-244	-242	-10661	-3695	-31	-3695	-10661
O-90C-C	-38	-213	-206	-9178	-3882	-94	-3881	-9179
O-90C-D	-35	-182	-168	-7660	-3355	-193	-3347	-7669
O-90C-E	-26	-147	-156	-6635	-2763	128	-2759	-6639
O-90C-F	-16	-149	-152	-6595	-2470	32	-2470	-6595
O-90C-R	22	-4	8	63	670	-168	714	20
I-90N-B	168	-334	-236	-12708	1215	-1304	1336	-12829
I-90N-C	-147	-191	-212	-8682	-7024	285	-6977	-8730
I-90N-D	-126	-100	-112	-4527	-5150	159	-4489	-5188
I-90N-E	-69	-50	-57	-2283	-2759	96	-2264	-2777
I-90N-F	8	3	-161	-3485	-792	2189	432	-4708
I-90N-N	41	27	24	1077	1554	31	1556	1075
O-90N-B	83	-178	-163	-7589	226	-190	231	-7594
O-90N-C	74	24	31	1132	2555	-96	2561	1125
O-90N-D	-4	69	62	2886	735	94	2890	731
O-90N-E	-21	50	45	2121	12	64	2123	10
O-90N-F	-33	17	33	1144	-641	-220	1171	-668
O-90N-N	10	5	5	212	357	0	357	212

Table A.10 (continued)

IN-PLANE MOMENT LOADING, MZC, ON CYLINDER (80000 IN-LB)

	MICRO-STRAIN			STRESSES			PRIN STRESSES	
ROSETTE	GAGE1	GAGE2	GAGE3	TRANS	LONG	SHEAR	SIGMX	SIGMN
I180C-B	-7	144	130	6028	1603	190	6036	1595
I180C-C	-4	80	45	2763	694	473	2865	592
I180C-D	-28	52	14	1494	-389	503	1619	-515
I180C-E	-54	38	5	1006	-1317	439	1086	-1397
I180C-F	-73	26	3	713	-1972	314	750	-2008
I180C-S	-150	36	5	1068	-4188	408	1099	-4219
O180C-B	-43	0	10	262	-1200	-126	273	-1210
O180C-C	-71	-31	-12	-855	-2391	-254	-814	-2432
O180C-D	-95	-43	-28	-1460	-3285	-190	-1441	-3305
O180C-E	-114	-45	-36	-1647	-3914	-127	-1639	-3921
O180C-F	-130	-47	-32	-1599	-4379	-191	-1586	-4392
O180C-S	-132	-16	-16	-554	-4116	5	-554	-4116
I180N-B	43	131	155	6247	3164	-317	6279	3132
I180N-C	67	69	95	3546	3069	-349	3730	2884
I180N-D*	43	7	69	1633	1780	-826	2536	877
I180N-E	36	50	72	2637	1866	-286	2731	1772
I180N-F	31	43	50	1996	1526	-93	2013	1508
I180N-N*	2	0	0	0	73	0	73	0
O180N-B	24	-33	-33	-1475	288	3	288	-1475
O180N-C	46	-59	-59	-2639	579	2	579	-2639
O180N-D	51	-40	-64	-2333	820	320	852	-2365
O180N-E	48	-33	-45	-1766	920	164	930	-1776
O180N-F	45	-21	-35	-1297	975	189	991	-1313
O180N-N	1	3	3	135	65	0	135	65

Table A.10 (continued)

IN-PLANE MOMENT LOADING, MZC, ON CYLINDER (80000 IN-LB)

	MICRO-STRAIN			STRESSES			PRIN STRESSES	
ROSETTE	GAGE1	GAGE2	GAGE3	TRANS	LONG	SHEAR	SIGMX	SIGMN
I270C-C	48	-265	-236	-11055	-1882	-381	-1866	-11071
I270C-D	26	-217	-193	-9039	-1921	-317	-1907	-9053
I270C-E	26	-193	-181	-8254	-1686	-159	-1682	-8258
I270C-F	26	-181	-164	-7624	-1496	-222	-1488	-7633
I270C-H	24	-164	-131	-6521	-1236	-445	-1199	-6558
I270C-J	17	-148	-119	-5886	-1261	-381	-1230	-5917
I270C-K	12	-122	-112	-5147	-1184	-127	-1180	-5151
I270C-L	5	-96	-91	-4116	-1089	-79	-1087	-4118
I270C-M	-14	-67	-74	-3072	-1346	96	-1341	-3077
I270C-P	-19	-17	-26	-921	-854	126	-757	-1018
I270C-R*	168	14	5	237	5100	128	5104	234
I270C-T	-22	77	60	3024	261	223	3041	243
O270C-B	-43	-252	-264	-11288	-4665	157	-4661	-11292
O270C-C	-33	-185	-192	-8264	-3472	96	-3470	-8266
O270C-D	-21	-154	-169	-7075	-2758	189	-2750	-7084
O270C-E	-5	-135	-147	-6205	-1998	158	-1992	-6211
O270C-F	10	-126	-133	-5697	-1418	95	-1416	-5700
O270C-H	31	-109	-121	-5093	-593	158	-588	-5099
O270C-J	45	-97	-107	-4532	3	127	6	-4536
O270C-K	55	-88	-97	-4128	408	127	412	-4131
O270C-L	60	-69	-85	-3452	753	222	765	-3464
O270C-M	57	-50	-52	-2303	1029	31	1029	-2303
O270C-P	34	-7	0	-185	952	-95	960	-193
O270C-R	12	19	24	935	644	-64	948	631
O270C-T*	-62	122	0	2739	-1025	1620	3340	-1626
I270N-B	168	-338	-283	-13847	882	-731	918	-13884
I270N-C	-140	-231	-224	-9849	-7161	-99	-7157	-9853
I270N-D	-131	-131	-131	-5614	-5604	0	-5604	-5614
I270N-E	-71	-107	-71	-3843	-3281	-479	-3006	-4118
I270N-F	-40	-41	-45	-1846	-1755	64	-1723	-1879
O270N-B	97	-152	-138	-6464	979	-189	984	-6469
O270N-C	76	38	38	1585	2752	0	2752	1585
O270N-D	5	64	76	3085	1073	-159	3097	1061
O270N-E	-40	50	60	2454	-472	-126	2460	-478
O270N-F	-50	38	43	1841	-940	-64	1843	-941
O270N-G	-43	17	21	887	-1016	-63	889	-1018
O270N-H	-38	14	14	675	-934	0	675	-934
O270N-K	-16	-7	-5	-236	-564	-31	-233	-566
O270N-N	3	0	-2	-45	65	31	74	-53

Table A.10 (continued)

IN-PLANE MOMENT LOADING, MZC, ON CYLINDER (80000 IN-LB)

	MICRO-STRAIN			STRESSES			PRIN STRESSES	
ROSETTE	GAGE1	GAGE2	GAGE3	TRANS	LONG	SHEAR	SIGMX	SIGMN
I315C-B	31	-203	3	-4426	-391	-2738	992	-5810
I315C-C	7	-219	70	-3296	-766	-3848	2020	-6082
I315C-D	-14	-203	84	-2601	-1213	-3822	1977	-5792
I315C-F	3	-83	-19	-2242	-590	-859	-224	-2607
I315C-H	-12	-81	27	-1171	-696	-1433	518	-2386
I315C-J	-12	-76	24	-1122	-682	-1336	452	-2255
I315C-K	-26	-66	22	-951	-1058	-1177	173	-2182
I315C-L	-72	-129	24	-2236	-2822	-2046	-462	-4596
I315C-M	-76	-114	14	-2100	-2918	-1709	-751	-4267
I315C-P	-52	-79	-9	-1882	-2131	-930	-1068	-2944
O315C-B	-26	24	-199	-3816	-1917	2971	253	-5986
O315C-C	-45	29	-194	-3586	-2419	2969	23	-6028
O315C-D	-52	38	-261	-4834	-3007	3982	165	-8006
O315C-E	-71	33	-249	-4655	-3527	3761	-288	-7894
O315C-F*	-73	-151	-247	-8662	-4796	1269	-4417	-9041
O315C-H	-73	24	-227	-4379	-3500	3350	-561	-7318
O315C-K	-59	29	-180	-3251	-2738	2779	-204	-5785
O315C-L	-56	39	-149	-2359	-2395	2496	119	-4873
O315C-M	-42	43	-130	-1863	-1826	2309	465	-4154
O315C-P	-14	39	-85	-1002	-712	1646	796	-2510
I315N-B	108	-100	-103	-4580	1859	31	1859	-4580
I315N-C	-50	-55	-100	-3353	-2507	604	-2192	-3667
I315N-D	-50	-28	-43	-1512	-1955	191	-1441	-2026
I315N-E	-21	-19	-5	-492	-787	-190	-399	-880
I315N-F	-9	-19	10	-190	-338	-382	125	-653
I315N-N	8	3	-2	3	253	64	268	-12
O315N-B	50	-33	-197	-5095	-35	2185	778	-5908
O315N-C	57	-14	-28	-986	1425	193	1441	-1001
O315N-D	26	-12	26	284	862	-501	1151	-5
O315N-E	5	-19	31	254	219	-657	894	-421
O315N-F	0	-21	28	158	51	-657	763	-554
O315N-G	2	-21	19	-50	58	-532	539	-530
O315N-H	0	-19	17	-48	-12	-469	440	-500
O315N-K	0	-7	9	56	19	-219	257	-182
O315N-N*	-51	0	-5	-43	-1541	63	-40	-1544

Table A.11. Axial force, F_{XC}, on cylinder

AXIAL FORCE LOADING, FXC, ON CYLINDER (10000 LB)

	MICRO-STRAIN			STRESSES			PRIN STRESSES	
ROSETTE	GAGE1	GAGE2	GAGE3	TRANS	LONG	SHEAR	SIGMX	SIGMN
I-0-C-C	-5	2	2	104	-115	0	104	-115
I-0-C-D	5	14	21	776	373	-95	797	351
I-0-C-E	9	26	24	1085	609	32	1087	607
I-0-C-F	14	31	26	1239	798	64	1248	789
I-0-C-H	26	31	33	1381	1197	-32	1387	1191
I-0-C-J	33	33	36	1477	1440	-31	1495	1422
I-0-C-K	33	33	33	1424	1424	1	1425	1423
I-0-C-L*	-79	31	33	1495	-1914	-32	1496	-1914
I-0-C-M	31	33	33	1429	1355	0	1429	1355
I-0-C-P	33	33	33	1423	1424	1	1424	1422
I-0-C-S	26	28	29	1225	1147	-3	1226	1147
0-0-C-B	-2	-26	-24	-1090	-396	-32	-394	-1091
0-0-C-C	5	-24	-21	-991	-153	-31	-152	-992
0-0-C-D	12	-21	-21	-948	74	-1	74	-948
0-0-C-E	17	-24	-24	-1056	184	-1	184	-1056
0-0-C-F	17	-26	-21	-1057	184	-63	188	-1060
0-0-C-H	21	-26	-28	-1218	278	32	279	-1219
0-0-C-J	24	-31	-28	-1325	319	-32	319	-1325
0-0-C-K	26	-28	-31	-1327	389	32	389	-1327
0-0-C-L	29	-31	-31	-1382	443	0	443	-1382
0-0-C-M	26	-31	-33	-1432	356	32	357	-1433
0-0-C-P	26	-31	-31	-1380	372	0	372	-1380
0-0-C-S	17	-28	-35	-1422	77	95	82	-1428
I-0-N-B	29	-31	-21	-1184	512	-128	522	-1193
I-0-N-C	3	-31	-26	-1262	-301	-64	-297	-1266
I-0-N-D	-2	-24	-24	-1048	-381	0	-381	-1048
I-0-N-E	-2	-19	-19	-837	-318	-1	-318	-837
I-0-N-F	0	-14	-19	-732	-216	65	-208	-740
I-0-N-N	0	0	-2	-45	-9	32	9	-63
0-0-N-B	12	-12	-7	-426	230	-63	236	-432
0-0-N-C	12	5	7	254	436	-31	441	248
0-0-N-D	5	12	12	511	291	-1	511	291
0-0-N-E	0	12	9	466	136	31	469	133
0-0-N-F	0	9	9	413	120	1	413	120
0-0-N-H	-2	7	5	261	4	32	265	0
0-0-N-K	-5	0	0	4	-147	0	4	-147
0-0-N-N*	-5	-5	-88	-2043	-758	1113	-116	-2685

Table A.11 (continued)

AXIAL FORCE LOADING, FXC, ON CYLINDER (10000 LB)

	MICRO-STRAIN			STRESSES			PRIN STRESSES	
ROSETTE	GAGE1	GAGE2	GAGE3	TRANS	LONG	SHEAR	SIGMX	SIGMN
I-90C-B	-10	112	115	4998	1201	-33	4999	1201
I-90C-C*	12	81	0	1769	878	1080	2492	155
I-90C-D	16	64	67	2860	1352	-32	2861	1351
I-90C-E	19	55	59	2487	1309	-64	2490	1305
I-90C-F*	21	116	52	3674	1737	846	3992	1420
I-90C-R	-56	43	40	1886	-1100	33	1886	-1100
O-90C-B	-19	31	19	1108	-242	157	1126	-260
O-90C-C	-26	19	17	808	-544	31	808	-545
O-90C-D	-31	17	14	706	-717	33	707	-718
O-90C-E	-36	14	17	714	-857	-32	715	-858
O-90C-F	-38	17	17	769	-911	0	769	-911
O-90C-R*	14	64	66	2841	1276	-28	2841	1275
I-90N-B	45	62	67	2778	2182	-63	2784	2176
I-90N-C	21	26	31	1232	1011	-63	1249	994
I-90N-D	2	17	10	575	247	96	601	221
I-90N-E	-5	14	10	529	13	63	537	6
I-90N-F*	33	33	33	1425	1423	1	1425	1423
I-90N-N	9	5	5	193	340	0	340	193
O-90N-B	-55	-14	-19	-673	-1843	63	-670	-1846
O-90N-C	-21	-24	-29	-1128	-982	64	-958	-1152
O-90N-D	-7	-24	-21	-987	-514	-31	-512	-989
O-90N-E	-7	-17	-17	-726	-437	0	-437	-726
O-90N-F	-7	-14	-17	-674	-419	31	-416	-678
O-90N-N	-5	-5	-5	-208	-208	0	-208	-208

Table A.11 (continued)

AXIAL FORCE LOADING, FXC, ON CYLINDER (10000 LB)

	MICRO-STRAIN			STRESSES			PRIN STRESSES	
ROSETTE	GAGE1	GAGE2	GAGE3	TRANS	LONG	SHEAR	SIGMX	SIGMN
I180C-B	0	-10	-10	-431	-139	-2	-139	-431
I180C-C	4	9	11	444	265	-33	450	258
I180C-D	4	18	21	858	383	-32	860	381
I180C-E	11	21	23	953	629	-31	956	626
I180C-F	16	26	28	1158	834	-31	1161	831
I180C-S	35	16	13	604	1217	32	1219	602
O180C-B	2	-20	-24	-968	-243	61	-238	-973
O180C-C	9	-17	-17	-772	26	3	26	-772
O180C-D	13	-15	-17	-712	185	29	186	-713
O180C-E	21	-17	-17	-777	385	-1	385	-777
O180C-F	21	-22	-19	-917	363	-32	363	-918
O180C-S	20	-22	-17	-863	328	-64	332	-866
I180N-B	29	-26	-38	-1441	431	160	444	-1454
I180N-C	0	-21	-40	-1358	-404	254	-340	-1421
I180N-D	-7	0	-31	-668	-412	414	-107	-973
I180N-E	-5	-19	-31	-1090	-466	160	-428	-1129
I180N-F	0	-15	-19	-739	-232	61	-225	-746
I180N-N	-5	-2	-2	-93	-167	1	-93	-167
O180N-B	9	0	-10	-220	216	127	251	-254
O180N-C	14	17	9	555	592	95	670	477
O180N-D	7	17	17	720	426	-1	720	426
O180N-E	2	14	14	623	254	-1	623	254
O180N-F	0	12	14	574	171	-32	576	168
O180N-N	-3	-2	-2	-107	-107	0	-107	-107

Table A.11 (continued)

AXIAL FORCE LOADING, FXC, ON CYLINDER (10000 LB)

	MICRO-STRAIN			STRESSES			PRIN STRESSES	
ROSETTE	GAGE1	GAGE2	GAGE3	TRANS	LONG	SHEAR	SIGMX	SIGMN
I270C-C	7	77	72	3252	1197	64	3254	1195
I270C-D	15	60	57	2563	1204	33	2563	1204
I270C-E	14	54	52	2326	1117	31	2327	1116
I270C-F	14	50	47	2117	1054	32	2118	1054
I270C-H	14	45	35	1749	943	127	1769	923
I270C-J	7	45	33	1710	718	158	1734	693
I270C-K	0	40	31	1562	463	126	1576	449
I270C-L	-19	41	28	1546	-115	168	1563	-132
I270C-M	-31	33	31	1434	-512	31	1434	-513
I270C-P	-52	40	24	1467	-1132	224	1487	-1151
I270C-R	-58	33	33	1528	-1283	2	1528	-1283
I270C-T	19	14	21	744	794	-96	868	670
O270C-B	-15	24	26	1102	-108	-30	1103	-108
O270C-C	-19	21	24	1002	-279	-32	1003	-280
O270C-D	-24	19	23	956	-436	-61	958	-439
O270C-E	-29	16	21	856	-609	-63	858	-611
O270C-F	-29	19	19	856	-609	0	856	-609
O270C-H	-31	19	21	908	-666	-31	909	-666
O270C-J	-29	21	21	955	-581	-1	955	-581
O270C-K	-24	24	26	1112	-389	-31	1113	-390
O270C-L	-15	31	40	1569	33	-128	1579	23
O270C-M	-1	40	42	1800	514	-29	1801	513
O270C-P	13	49	49	2147	1041	-2	2147	1041
O270C-R	18	49	47	2096	1174	32	2097	1173
O270C-T*	-49	21	0	506	-1316	274	546	-1356
I270N-B	38	76	69	3153	2088	95	3162	2079
I270N-C	29	41	40	1750	1381	1	1750	1381
I270N-D	9	24	24	1037	594	0	1037	594
I270N-E	0	31	17	1047	311	191	1094	264
I270N-F	-2	17	14	683	130	32	685	129
O270N-B	-59	-17	-12	-557	-1942	-63	-554	-1945
O270N-C	-26	-26	-26	-1115	-1115	0	-1115	-1115
O270N-D	-7	-22	-22	-942	-504	1	-504	-942
O270N-E	0	-17	-19	-793	-244	31	-243	-795
O270N-F	-3	-15	-15	-639	-273	1	-273	-639
O270N-G	0	-12	-12	-527	-162	0	-162	-527
O270N-H	0	-12	-12	-533	-168	0	-168	-533
O270N-K	0	-5	-7	-273	-92	31	-87	-278
O270N-N	-5	-3	-3	-114	-188	0	-114	-188

Table A.11 (continued)

AXIAL FORCE LOADING, FXC, ON CYLINDER (10000 LB)

	MICRO-STRAIN			STRESSES			PRIN STRESSES	
ROSETTE	GAGE1	GAGE2	GAGE3	TRANS	LONG	SHEAR	SIGMX	SIGMN
I315C-B	-2	45	43	1939	508	33	1940	508
I315C-C	9	48	31	1715	798	223	1767	747
I315C-D	12	47	21	1492	806	343	1634	664
I315C-F	14	29	26	1186	782	32	1188	779
I315C-H	24	31	21	1120	1048	128	1217	951
I315C-J	26	31	19	1066	1103	159	1245	925
I315C-K	26	31	17	1015	1087	191	1245	857
I315C-L	29	38	2	860	1119	485	1492	487
I315C-M	28	41	-10	650	1046	672	1549	147
I315C-P	19	46	-32	285	641	1028	1506	-580
O315C-B	-10	-43	38	-98	-318	-1075	872	-1288
O315C-C	-7	-40	38	-48	-231	-1042	907	-1186
O315C-D	-2	-45	52	156	-27	-1296	1364	-1235
O315C-E	0	-45	47	49	13	-1233	1264	-1202
O315C-F*	-2	-119	47	-1565	-543	-2213	1217	-3326
O315C-H	0	-41	40	-14	-17	-1075	1059	-1090
O315C-K	2	-31	38	142	103	-915	1038	-793
O315C-L	11	-31	35	74	365	-885	1116	-677
O315C-M	19	-19	38	385	676	-760	1304	-243
O315C-P	31	0	50	1045	1229	-666	1809	465
I315N-B	31	5	36	854	1181	-413	1462	574
I315N-C	14	0	14	289	510	-190	619	180
I315N-D	5	0	0	-18	131	0	131	-18
I315N-E	0	4	-3	39	2	94	116	-75
I315N-F	0	9	-3	144	34	158	257	-79
I315N-N	0	0	0	-20	7	-1	7	-20
O315N-B	-25	-31	19	-242	-830	-667	192	-1264
O315N-C	-7	-15	2	-262	-300	-223	-57	-505
O315N-D	0	-7	0	-158	-50	-93	3	-212
O315N-E	0	-2	-2	-105	-34	1	-34	-105
O315N-F	-2	-2	-2	-105	-106	0	-105	-106
O315N-G	-2	0	-2	-54	-91	31	-37	-108
O315N-H	-2	-2	-5	-155	-121	31	-102	-174
O315N-K	-2	0	-5	-106	-105	63	-42	-168
O315N-N*	-36	0	0	35	-1078	0	35	-1078

Table A.12. In-plane force, F_{YC}, on cylinder

IN-PLANE FORCE LOADING, FYC, ON CYLINDER (3000 LB)

	MICRO-STRAIN			STRESSES			PRIN STRESSES	
ROSETTE	GAGE1	GAGE2	GAGE3	TRANS	LONG	SHEAR	SIGMX	SIGMN
I-0-C-C	-2	33	33	1470	370	0	1470	370
I-0-C-D	-12	10	10	432	-228	0	432	-228
I-0-C-E	-31	2	0	86	-904	32	87	-905
I-0-C-F	-45	-5	-5	-160	-1408	0	-160	-1408
I-0-C-H	-79	-12	-10	-385	-2477	-32	-385	-2478
I-0-C-J	-98	-12	-14	-469	-3075	32	-469	-3075
I-0-C-K	-103	-17	-12	-516	-3232	-64	-515	-3234
I-0-C-L*	-177	-14	-5	-226	-5367	-127	-223	-5370
I-0-C-M	-98	-12	-7	-312	-3030	-64	-311	-3031
I-0-C-P	-91	-2	-12	-215	-2786	127	-209	-2792
I-0-C-S	-72	-2	-7	-131	-2188	64	-129	-2190
0-0-C-B	-26	14	12	597	-610	33	598	-611
0-0-C-C	-45	0	-5	-66	-1377	63	-63	-1380
0-0-C-D	-62	-10	-10	-358	-1966	1	-358	-1966
0-0-C-E	-69	-12	-10	-407	-2195	-29	-407	-2195
0-0-C-F	-79	-7	-12	-341	-2461	63	-339	-2463
0-0-C-H	-90	-10	-5	-226	-2780	-63	-225	-2782
0-0-C-J	-102	2	-5	46	-3059	97	49	-3062
0-0-C-K	-102	0	2	151	-3025	-31	151	-3025
0-0-C-L	-107	4	2	262	-3136	31	262	-3136
0-0-C-M	-100	2	4	253	-2923	-32	254	-2923
0-0-C-P	-88	2	0	137	-2603	33	137	-2603
0-0-C-S	-72	0	7	222	-2082	-95	226	-2086
I-0-N-B	31	91	86	3861	2093	64	3863	2090
I-0-N-C	38	65	55	2590	1927	128	2614	1903
I-0-N-D	24	48	46	2027	1327	32	2028	1325
I-0-N-E	19	41	38	1716	1090	32	1718	1088
I-0-N-F	17	31	38	1508	955	-96	1524	939
I-0-N-N	2	0	0	-3	71	0	71	-3
0-0-N-B	-3	-5	-12	-373	-190	94	-150	-413
0-0-N-C	19	-34	-34	-1497	110	-1	110	-1497
0-0-N-D	26	-33	-31	-1446	339	-33	340	-1447
0-0-N-E	26	-29	-24	-1183	419	-64	421	-1186
0-0-N-F	26	-26	-22	-1081	449	-62	451	-1084
0-0-N-H	26	-10	-12	-505	624	32	625	-506
0-0-N-K	16	5	2	132	526	31	528	130
0-0-N-N*	2	4	87	1998	663	-1094	2612	49

Table A.12 (continued)

IN-PLANE FORCE LOADING, FYC, ON CYLINDER (3000 LB)

	MICRO-STRAIN			STRESSES			PRIN STRESSES	
ROSETTE	GAGE1	GAGE2	GAGE3	TRANS	LONG	SHEAR	SIGMX	SIGMN
I-90C-B	65	-287	-297	-12901	-1933	128	-1931	-12902
I-90C-C*	26	-199	0	-4393	-529	-2646	816	-5737
I-90C-D	17	-163	-167	-7275	-1680	64	-1679	-7275
I-90C-E	14	-139	-146	-6273	-1451	96	-1450	-6275
I-90C-F	14	-100	-132	-5116	-1104	414	-1062	-5159
I-90C-R	10	31	-33	-63	268	861	979	-774
O-90C-B	2	-171	-150	-7052	-2057	-286	-2040	-7068
O-90C-C	-5	-142	-123	-5835	-1893	-253	-1877	-5851
O-90C-D	-2	-123	-112	-5160	-1619	-158	-1612	-5167
O-90C-E	7	-102	-93	-4284	-1072	-126	-1067	-4289
O-90C-F	14	-104	-90	-4291	-860	-190	-850	-4302
O-90C-R	-5	-38	31	-151	-188	-917	748	-1087
I-90N-B	74	-234	-184	-9256	-558	-668	-507	-9307
I-90N-C	-107	-138	-153	-6277	-5104	191	-5073	-6308
I-90N-D	-79	-69	-79	-3166	-3320	126	-3095	-3391
I-90N-E	-38	-41	-43	-1795	-1690	31	-1682	-1804
I-90N-F	-12	-17	-103	-2608	-1140	1144	-515	-3233
I-90N-N	24	17	14	656	913	32	917	652
O-90N-B	81	-97	-78	-3947	1236	-253	1248	-3960
O-90N-C	57	28	31	1241	2081	-32	2082	1240
O-90N-D	0	55	50	2294	688	63	2297	686
O-90N-E	-7	43	38	1780	321	63	1783	318
O-90N-F	-14	21	28	1110	-94	-95	1118	-101
O-90N-N	12	7	7	300	446	0	446	300

Table A.12 (continued)

IN-PLANE FORCE LOADING, FYC, ON CYLINDER (3000 LB)

	MICRO-STRAIN			STRESSES			PRIN STRESSES	
ROSETTE	GAGE1	GAGE2	GAGE3	TRANS	LONG	SHEAR	SIGMX	SIGMN
I180C-B	-5	92	68	3528	917	314	3566	880
I180C-C	-2	42	26	1505	381	220	1547	339
I180C-D	-21	19	2	490	-490	220	537	-537
I180C-E	-42	5	-7	-5	-1275	157	14	-1294
I180C-F	-59	-2	-12	-246	-1842	126	-236	-1852
I180C-S	-151	-2	-12	-145	-4570	126	-142	-4574
O180C-B	-26	12	22	768	-548	-126	780	-560
O180C-C	-50	-5	3	11	-1487	-96	18	-1493
O180C-D	-69	-14	-7	-390	-2178	-94	-385	-2183
O180C-E	-83	-16	-12	-530	-2650	-63	-528	-2652
O180C-F	-105	-24	-17	-773	-3371	-95	-770	-3374
O180C-S*	0	12	-10	52	16	285	320	-252
I180N-B	12	97	117	4686	1751	-257	4709	1729
I180N-C	40	54	81	2929	2086	-350	3056	1959
I180N-D*	28	2	59	1316	1243	-764	2044	515
I180N-E	24	43	64	2317	1401	-288	2400	1318
I180N-F	21	35	42	1686	1143	-94	1702	1127
I180N-N	2	-1	0	-22	55	-2	55	-22
O180N-B	-5	-19	-17	-774	-375	-29	-373	-776
O180N-C	21	-50	-43	-2061	24	-95	28	-2066
O180N-D	26	-38	-50	-1962	196	158	208	-1974
O180N-E	31	-31	-33	-1445	494	32	494	-1445
O180N-F	29	-21	-31	-1181	502	127	511	-1190
O180N-N	0	2	2	105	31	0	105	31

Table A.12 (continued)

IN-PLANE FORCE LOADING, FYC, ON CYLINDER (3000 LB)

	MICRO-STRAIN			STRESSES			PRIN STRESSES	
ROSETTE	GAGE1	GAGE2	GAGE3	TRANS	LONG	SHEAR	SIGMX	SIGMN
I270C-C	28	-201	-177	-8345	-1665	-319	-1650	-8360
I270C-D	11	-168	-146	-6912	-1735	-289	-1719	-6928
I270C-E	15	-149	-133	-6212	-1399	-224	-1388	-6222
I270C-F	15	-142	-121	-5792	-1274	-287	-1256	-5810
I270C-H	15	-133	-92	-4957	-1028	-539	-956	-5029
I270C-J	18	-123	-82	-4521	-822	-543	-744	-4599
I270C-K	18	-108	-70	-3941	-631	-512	-554	-4018
I270C-L	28	-96	-53	-3308	-159	-566	-60	-3407
I270C-M	20	-83	-37	-2650	-194	-607	-52	-2792
I270C-P	10	-55	11	-978	1	-883	521	-1498
I270C-R	12	-38	31	-171	308	-926	1024	-888
I270C-T	-36	57	46	2303	-387	160	2312	-396
O270C-B	-19	-162	-183	-7560	-2839	285	-2822	-7577
O270C-C	-12	-117	-138	-5578	-2030	285	-2008	-5601
O270C-D	-2	-97	-124	-4857	-1529	349	-1493	-4893
O270C-E	7	-86	-112	-4345	-1090	349	-1053	-4382
O270C-F	17	-81	-100	-3990	-698	253	-678	-4009
O270C-H	31	-71	-95	-3692	-180	317	-152	-3720
O270C-J	36	-64	-90	-3436	39	349	74	-3471
O270C-K	38	-57	-93	-3334	141	475	205	-3398
O270C-L	31	-38	-95	-2960	39	760	221	-3142
O270C-M	26	-28	-78	-2373	81	665	250	-2541
O270C-P	15	10	-55	-999	139	857	598	-1458
O270C-R	0	36	-33	61	27	919	963	-876
O270C-T*	-26	112	0	2492	-25	1494	3187	-720
I270N-B	88	-246	-212	-10168	-401	-445	-381	-10189
I270N-C	-100	-165	-160	-7024	-5115	-64	-5113	-7026
I270N-D	-88	-93	-93	-3995	-3848	0	-3848	-3995
I270N-E	-45	-88	-53	-3045	-2274	-477	-2046	-3273
I270N-F	-23	-33	-36	-1500	-1140	32	-1137	-1502
O270N-B	87	-83	-83	-3754	1495	-2	1495	-3754
O270N-C	59	35	38	1544	2236	-31	2237	1542
O270N-D	10	52	57	2395	1004	-63	2397	1001
O270N-E	-21	40	45	1906	-71	-63	1908	-73
O270N-F	-29	31	36	1495	-408	-63	1497	-410
O270N-G	-24	19	19	863	-455	0	863	-455
O270N-H	-24	12	14	601	-533	-32	602	-534
O270N-K	-14	0	2	68	-408	-32	70	-410
O270N-N	2	2	2	102	102	0	102	102

Table A.12 (continued)

IN-PLANE FORCE LOADING, FYC, ON CYLINDER (3000 LB)

	MICRO-STRAIN			STRESSES			PRIN STRESSES	
ROSETTE	GAGE1	GAGE2	GAGE3	TRANS	LONG	SHEAR	SIGMX	SIGMN
I315C-B	19	-141	-14	-3431	-457	-1686	304	-4192
I315C-C	2	-155	31	-2731	-748	-2481	933	-4411
I315C-D	-14	-144	45	-2143	-1073	-2517	966	-4181
I315C-F	-7	-62	-21	-1828	-763	-541	-537	-2055
I315C-H	-17	-62	10	-1136	-842	-954	-23	-1955
I315C-J	-19	-55	12	-923	-850	-891	5	-1778
I315C-K	-26	-48	14	-706	-1000	-827	-13	-1693
I315C-L	-65	-81	31	-1032	-2246	-1497	-24	-3255
I315C-M	-69	-60	29	-607	-2262	-1179	6	-2875
I315C-P	-57	-41	26	-252	-1797	-892	155	-2205
O315C-B	-14	33	-138	-2278	-1110	2276	655	-4043
O315C-C	-28	36	-133	-2106	-1486	2244	469	-4061
O315C-D	-33	45	-183	-2987	-1892	3034	643	-5523
O315C-E	-50	43	-171	-2760	-2323	2844	311	-5394
O315C-F	-50	38	-168	-2812	-2338	2750	185	-5335
O315C-H*	0	33	-154	-2658	-798	2497	936	-4392
O315C-K	-55	33	-109	-1608	-2119	1896	50	-3777
O315C-L	-52	50	-85	-725	-1783	1801	624	-3131
O315C-M	-52	43	-69	-516	-1720	1485	485	-2721
O315C-P	-55	36	-40	-44	-1650	1011	444	-2138
I315N-B	57	-62	-79	-3163	772	223	785	-3175
I315N-C	-38	-33	-67	-2165	-1797	446	-1499	-2463
I315N-D	-33	-19	-26	-962	-1293	96	-936	-1318
I315N-E	-14	-12	-2	-299	-520	-127	-241	-578
I315N-F	-5	-12	7	-100	-173	-255	121	-394
I315N-N*	-2	2	-469	-10256	-3148	6283	516	-13920
O315N-B	45	-5	-133	-3073	430	1707	1124	-3767
O315N-C	43	5	-14	-255	1204	253	1247	-298
O315N-D	17	-4	17	257	584	-287	751	91
O315N-E	5	-9	21	259	230	-412	656	-167
O315N-F	1	-11	17	124	58	-374	466	-284
O315N-G	3	-11	15	75	112	-341	435	-248
O315N-H	3	-9	12	65	107	-282	369	-197
O315N-K	3	-4	8	74	108	-159	251	-69
O315N-N	-42	3	3	174	-1193	0	174	-1193

Table A.13. Out-of-plane force, F_{ZC}, on cylinder

OUT-OF-PLANE FORCE LOADING, FZC, ON CYLINDER (3000 LB)

	MICRO-STRAIN			STRESSES			PRIN STRESSES	
ROSETTE	GAGE1	GAGE2	GAGE3	TRANS	LONG	SHEAR	SIGMX	SIGMN
I-0-C-C	-2	-45	31	-312	-165	-1017	781	-1258
I-0-C-D	0	-60	41	-419	-126	-1335	1070	-1615
I-0-C-E	0	-52	38	-315	-94	-1208	1008	-1417
I-0-C-F	0	-50	38	-262	-79	-1176	1009	-1350
I-0-C-H	-2	29	-45	-364	-181	985	717	-1262
I-0-C-J	-2	26	-43	-364	-181	922	654	-1199
I-0-C-K	2	-41	21	-422	-55	-826	608	-1085
I-0-C-L*	-138	-43	21	-320	-4249	-859	-141	-4428
I-0-C-M	-2	-41	26	-312	-165	-890	655	-1132
I-0-C-P	-5	-36	29	-152	-189	-859	688	-1029
I-0-C-S	-7	-36	26	-202	-275	-827	589	-1066
O-0-C-B	0	54	-45	204	57	1328	1460	-1199
O-0-C-C	2	54	-40	303	158	1264	1497	-1035
O-0-C-D	-3	59	-43	361	31	1359	1566	-1173
O-0-C-E	0	57	-43	304	85	1329	1527	-1139
O-0-C-F	5	52	-45	144	178	1295	1457	-1134
O-0-C-H	-3	50	-36	307	15	1138	1308	-986
O-0-C-J	2	45	-33	249	137	1045	1239	-853
O-0-C-K	-3	42	-33	202	-18	1011	1109	-925
O-0-C-L	0	42	-29	305	83	948	1148	-760
O-0-C-M	-3	40	-26	307	14	884	1057	-736
O-0-C-P	-3	38	-31	151	-33	917	981	-863
O-0-C-S	-5	40	-29	257	-74	917	1023	-840
I-0-N-B	-5	-12	-19	-679	-347	96	-322	-705
I-0-N-C	-12	0	-17	-355	-466	223	-180	-641
I-0-N-D	-10	0	-10	-200	-347	128	-126	-421
I-0-N-E	-7	-5	-2	-150	-261	-32	-141	-269
I-0-N-F	-5	-5	0	-100	-174	-64	-63	-211
I-0-N-N	0	0	0	0	0	0	0	0
O-0-N-B	0	19	-17	45	8	474	500	-447
O-0-N-C	-3	2	2	96	-49	-1	96	-49
O-0-N-D	-3	-5	9	100	-48	-191	230	-178
O-0-N-E	-3	-7	7	-3	-78	-190	153	-234
O-0-N-F	-3	-3	7	100	-47	-126	172	-120
O-0-N-H	0	-7	7	-5	-6	-189	184	-195
O-0-N-K	2	-5	2	-59	46	-95	102	-115
O-0-N-N	0	0	-1	-21	-12	8	-7	-26

Table A.13 (continued)

OUT-OF-PLANE FORCE LOADING, FZC, ON CYLINDER (3000 LB)

	MICRO-STRAIN			STRESSES			PRIN STRESSES	
ROSETTE	GAGE1	GAGE2	GAGE3	TRANS	LONG	SHEAR	SIGMX	SIGMN
I-90C-B	-5	43	-10	735	70	701	1178	-373
I-90C-C*	-3	62	0	1366	331	826	1823	-127
I-90C-D	-5	64	-36	627	39	1339	1704	-1038
I-90C-E	-10	62	-34	631	-106	1275	1590	-1065
I-90C-F	-10	65	-29	812	-51	1257	1710	-949
I-90C-R	-24	98	83	4013	477	192	4023	466
O-90C-B	7	-17	47	660	403	-854	1395	-333
O-90C-C	5	-36	62	568	313	-1296	1743	-862
O-90C-D*	2	-33	-147	-3965	-1119	1517	-461	-4622
O-90C-E	0	-33	62	626	188	-1265	1690	-877
O-90C-F	-2	-28	69	889	196	-1296	1884	-799
O-90C-R	-43	93	102	4322	16	-126	4326	12
I-90N-B	-10	-12	-17	-619	-472	64	-448	-642
I-90N-C	-10	-17	-2	-409	-409	-191	-218	-600
I-90N-D	0	-7	0	-158	-47	-95	8	-212
I-90N-E	0	0	-5	-107	-36	63	1	-144
I-90N-F*	21	-41	2	-862	385	-572	608	-1085
I-90N-N*	-22	-12	-12	-518	-811	0	-518	-811
O-90N-B	-5	-9	38	631	47	-632	1035	-358
O-90N-C	0	-2	0	-52	-16	-32	3	-70
O-90N-D	2	2	-12	-211	8	190	117	-321
O-90N-E	4	7	-7	-15	124	189	256	-147
O-90N-F	4	4	-7	-68	112	157	203	-159
O-90N-N	2	0	2	38	75	-32	93	20

Table A.13 (continued)

OUT-OF-PLANE FORCE LOADING, FZC, ON CYLINDER (3000 LB)

	MICRO-STRAIN			STRESSES			PRIN STRESSES	
ROSETTE	GAGE1	GAGE2	GAGE3	TRANS	LONG	SHEAR	SIGMX	SIGMN
I180C-B	2	-26	33	142	106	-787	911	-663
I180C-C	2	-52	47	-119	28	-1321	1278	-1368
I180C-D	2	-55	47	-171	8	-1351	1273	-1435
I180C-E	2	-57	42	-327	-35	-1319	1146	-1509
I180C-F	2	-52	37	-325	-33	-1194	1024	-1382
I180C-S	-1	-29	28	-22	-24	-754	732	-777
O180C-B	5	55	-45	198	196	1331	1529	-1134
O180C-C	5	55	-45	196	195	1333	1528	-1137
O180C-D	5	59	-50	200	196	1458	1656	-1261
O180C-E	5	55	-48	146	180	1364	1527	-1200
O180C-F	0	50	-50	0	0	1330	1330	-1330
O180C-S*	0	26	-36	-209	-63	824	691	-963
I180N-B	-2	-2	-12	-309	-163	128	-89	-383
I180N-C	-2	0	-7	-153	-116	95	-37	-232
I180N-D	0	-2	-7	-208	-61	64	-37	-231
I180N-E	2	2	2	104	104	0	104	104
I180N-F	2	0	7	144	106	-96	222	28
I180N-N	0	0	0	3	2	0	3	2
O180N-B	-10	16	-5	265	-206	281	397	-337
O180N-C	-5	-5	2	-47	-157	-95	8	-212
O180N-D	-5	-14	2	-256	-219	-222	-15	-460
O180N-E	-2	-14	7	-154	-118	-285	150	-422
O180N-F	0	-12	7	-104	-31	-253	188	-324
O180N-N	0	0	0	0	0	0	0	0

Table A.13 (continued)

OUT-OF-PLANE FORCE LOADING, FZC, ON CYLINDER (3000 LB)

	MICRO-STRAIN			STRESSES			PRIN STRESSES	
ROSETTE	GAGE1	GAGE2	GAGE3	TRANS	LONG	SHEAR	SIGMX	SIGMN
I270C-C	-2	26	-76	-1093	-396	1367	666	-2155
I270C-D	-2	29	-76	-1040	-380	1399	727	-2147
I270C-E	0	28	-74	-1017	-318	1366	743	-2078
I270C-F	0	21	-74	-1175	-366	1271	564	-2104
I270C-H	0	7	-70	-1385	-430	1017	216	-2031
I270C-J	4	-10	-72	-1804	-411	825	-28	-2187
I270C-K	4	-22	-77	-2169	-516	730	-240	-2446
I270C-L	14	-39	-86	-2777	-413	623	-259	-2931
I270C-M	14	-53	-101	-3392	-604	634	-466	-3529
I270C-P	36	-88	-100	-4190	-179	161	-173	-4196
I270C-R	43	-96	-105	-4468	-47	128	-44	-4472
I270C-T	-17	-26	22	-87	-529	-638	367	-983
O270C-B	7	-57	48	-216	151	-1396	1375	-1440
O270C-C	7	-60	40	-433	78	-1332	1179	-1534
O270C-D	14	-62	35	-598	243	-1299	1187	-1543
O270C-E	16	-67	33	-759	266	-1331	1180	-1673
O270C-F	16	-64	31	-759	266	-1268	1121	-1614
O270C-H	21	-67	19	-1079	312	-1141	953	-1719
O270C-J	28	-72	9	-1402	429	-1079	928	-1901
O270C-K	33	-74	-5	-1770	462	-919	791	-2100
O270C-L	38	-88	-38	-2823	289	-666	426	-2960
O270C-M	40	-98	-53	-3348	203	-602	302	-3447
O270C-P	35	-107	-81	-4181	-191	-350	-161	-4211
O270C-R	31	-105	-105	-4645	-472	0	-472	-4645
O270C-T*	7	43	0	929	483	568	1316	96
I270N-B	-14	-19	-19	-823	-677	0	-677	-823
I270N-C	-5	-17	-2	-414	-268	-191	-137	-545
I270N-D	0	-7	0	-157	-47	-95	8	-212
I270N-E	5	-7	-2	-215	79	-64	92	-228
I270N-F	7	2	-5	-63	183	96	216	-96
O270N-B	16	-22	28	132	530	-665	1025	-363
O270N-C	5	5	9	302	229	-63	339	193
O270N-D	0	12	0	263	80	159	354	-12
O270N-E	0	14	-7	157	47	286	393	-189
O270N-F	0	12	-7	107	33	253	326	-186
O270N-G	0	10	-7	52	15	222	256	-189
O270N-H	0	7	-5	53	17	159	195	-125
O270N-K	0	5	-2	54	18	95	133	-61
O270N-N	2	0	0	-1	73	0	73	-1

Table A.13 (continued)

OUT-OF-PLANE FORCE LOADING, FZC, ON CYLINDER (3000 LB)

	MICRO-STRAIN			STRESSES			PRIN STRESSES	
ROSETTE	GAGE1	GAGE2	GAGE3	TRANS	LONG	SHEAR	SIGMX	SIGMN
I315C-B	9	-96	-84	-3957	-905	-157	-897	-3965
I315C-C	5	-74	-62	-3009	-766	-159	-755	-3020
I315C-D	0	-63	-43	-2333	-695	-262	-654	-2374
I315C-F	-10	-41	-39	-1734	-816	-32	-815	-1735
I315C-H	-12	-41	-39	-1737	-890	-31	-889	-1739
I315C-J	-15	-43	-34	-1679	-945	-127	-923	-1701
I315C-K	-15	-50	-31	-1782	-977	-255	-903	-1856
I315C-L	7	-69	-24	-2058	-402	-600	-208	-2253
I315C-M	-3	-79	-10	-1943	-661	-922	-179	-2425
I315C-P	-10	-91	-3	-2045	-912	-1174	-175	-2782
0315C-B	4	-19	-41	-1319	-262	284	-191	-1391
0315C-C	7	-10	-31	-904	-65	286	23	-993
0315C-D	12	-5	-38	-958	61	442	226	-1123
0315C-E	19	-3	-38	-915	291	474	455	-1079
0315C-F	24	-10	-38	-1079	381	376	472	-1170
0315C-H	24	2	-40	-860	454	569	666	-1072
0315C-K	26	5	-52	-1071	461	758	773	-1383
0315C-L	19	14	-69	-1220	203	1106	807	-1823
0315C-M	14	12	-81	-1527	-31	1233	662	-2221
0315C-P	0	7	-88	-1772	-532	1264	256	-2560
I315N-B	-7	-69	-81	-3307	-1213	160	-1201	-3319
I315N-C	-38	-48	-48	-2068	-1774	1	-1774	-2068
I315N-D	-29	-29	-27	-1186	-1222	-32	-1167	-1241
I315N-E	-17	-19	-19	-831	-758	-1	-758	-831
I315N-F	-12	-15	-15	-627	-553	-1	-553	-627
I315N-N	-1	0	0	-12	-44	-1	-12	-44
0315N-B	19	-21	-24	-1011	266	32	267	-1012
0315N-C	7	17	12	618	399	63	635	382
0315N-D	-6	20	23	961	104	-39	963	103
0315N-E	-14	16	19	788	-177	-35	789	-178
0315N-F	-14	13	12	583	-243	12	584	-243
0315N-G	-12	10	8	408	-236	21	409	-237
0315N-H	-10	7	8	335	-199	-6	335	-199
0315N-K	-3	-1	2	31	-94	-48	47	-110
0315N-N	-9	4	4	192	-221	-2	192	-221

ORNL-5019
UC-79, -79h, -79k

INTERNAL DISTRIBUTION

1. R. L. Battiste
2. M. Bender
3. J. J. Blass
4-6. S. E. Bolt
7. R. H. Bryan
8-10. J. W. Bryson
11. J. H. Butler
12. J. P. Callahan
13. R. D. Cheverton
14. C. J. Claffey
15. J. A. Clinard
16. C. W. Collins
17-19. J. M. Corum
20. W. B. Cottrell
21. J. S. Crowell
22. F. L. Culler
23. R. W. Derby
24. W. G. Dodge
25. D. N. Fanning
26. G. G. Fee
27. M. H. Fontana
28. A. P. Fraas
29. W. R. Gall
30. R. H. Gallagher (consultant)
31. W. L. Greenstreet
32-41. R. C. Gwaltney
42. W. O. Harms
43. R. F. Hibbs
44. H. W. Hoffman
45. P. P. Holz
46. S. K. Iskander
47. P. R. Kasten
48. K. C. Liu
49. R. N. Lyon
50. R. E. MacPherson
51. W. J. McAfee
52. H. C. McCurdy
53. J. G. Merkle
54-68. S. E. Moore
69. D. J. Naus
70. F. M. O'Hara (consultant)
71. T. W. Pickel
72. H. Postma
73. C. E. Pugh
74. M. Raftenberg
75. M. Richardson
76. D. N. Robinson
77. W. K. Sartory
78. R. A. Schmidt
79. M. R. Sheldon
80. J. E. Smith
81. I. Spiewak
82. W. C. T. Stoddart
83. D. B. Trauger
84. G. D. Whitman
85. G. T. Yahr
86. ORNL Patent Office
87-89. Central Research Library
90. ORNL — Y-12 Technical Library
Document Reference Section
91-96. Laboratory Records Department
97. Laboratory Records, ORNL R.C.

Subcontractors

98. Auburn University, Auburn, AL 36830
99. Battelle-Columbus Laboratories, Columbus, OH 43201
100. Combustion Engineering, Chattanooga, TN 37401
101. University of Tennessee, Knoxville, TN 37916

EXTERNAL DISTRIBUTION

102-103. Director, Division of Reactor Research and Development, ERDA, Washington, D.C. 20545
104-105. Director, Office of Nuclear Regulatory Research, NRC, Washington, D.C. 20555
106. Director, Reactor Division, ERDA, ORO
107. Research and Technical Support Division, ERDA, Oak Ridge Operations Office, Oak Ridge, TN 37830
108-184. Nozzle Analysis and Nuclear Design Criteria — Piping-Pumps-Valves Programs Distribution
185-458. Given distribution as shown in TID-4500 under categories UC-79, -79h, and -79k (25 copies — NTIS)